New HCR Technologies: 10-Plex Quantitative Spectral Imaging of RNAs and Proteins; Multiplexed Quantitative Imaging of Protein:Protein Complexes; and Sensitive, Instrument-Free, At-Home Pathogen Detection

Thesis by
Samuel Jordan Schulte

In Partial Fulfillment of the Requirements for the
Degree of
Doctor of Philosophy

CALIFORNIA INSTITUTE OF TECHNOLOGY
Pasadena, California

2023
Defended June 6, 2023

Samuel Jordan Schulte
ORCID: 0000-0001-9982-6504

ACKNOWLEDGEMENTS

I would like to first thank my advisor, Niles Pierce. Thank you, Niles, for providing me with the opportunity to pursue such rewarding projects in your lab. It has been a joy to learn from you and to grow as a researcher, and I greatly appreciate the tireless time and effort you have given to help me succeed in graduate school. I would also like to thank Barbara Wold, Marianne Bronner, and Lulu Qian for serving as my thesis committee members, and for your insightful questions and guidance at pivotal points during my studies.

Thank you to everyone who set me on the path to graduate school. I am grateful to my undergraduate research advisor Reuben Peters, who was beyond generous with his time as I conducted research in his lab and applied to graduate programs. Thank you to my research advisors Susanne Dreisigacker, Emily-Jean Fuerst, and Bil Clemons, each of whom inspired me to pursue graduate research. Thank you to the many mentors I have had along the way, including Kevin Neal, Karen Downing, Keegan Kautzky, Miguel Santillán Martínez, Kevin Potter, Shyam Saladi, Don Beitz, and Dana Schumacher.

I would like to thank the UCLA-Caltech Medical Scientist Training Program for the wonderful opportunity to pursue joint degrees at UCLA and Caltech. Thank you to Olujimi Ajijola and Carlos Portera-Cailliau for serving as my MSTP advisors and for co-directing the program, and to Susie Esquivel and the program administration for their assistance. Thank you to Liz Ayala and Raina Beaven for helping to coordinate the program at Caltech. Thank you to my MSTP classmates, who have accompanied me on the journey through medical school and graduate school; I look forward to seeing you much more often over the next two years.

Thank you to the many people at Caltech who have supported me. Maayan, thank you for teaching me so much of what I know about research in the Pierce lab and for continuing to field my questions to this day. Grace, thank you for your daily help, support, and conversation. Jining, thank you for weathering the pandemic with me as we embarked on the COVID-19 project and for your abundant help on nucleic acid design and analysis. Mark, thank you for your keen insights on my projects. Thank you to Giada of the Biological Imaging Facility for your frequent assistance with microscopy. Thank you to Sheldon, John, Katelyn, Duo, Lisa, Heyun, Sarah,

Zhewei, Eric, Mikhail, Nikhil, Avinash, Melinda, and all other Pierce lab members for creating a fantastic environment in which to conduct research.

Lastly, I would like to express my deepest gratitude to those who have personally supported me before and during graduate school. Alex, Brent, Cameron, Chelsea, Ryan, Sarah, and Scott: thank you for too many laughs and good times to count, and thank you to Chelsea for making my time in Southern California feel like home.

Thank you to Michael, my sister (Kelli), and my parents (Rich and Kari) for your constant support, encouragement, and love. I could not have done it without you.

ABSTRACT

Signal amplification based on the mechanism of hybridization chain reaction (HCR) enables researchers to quantitatively image RNA and protein expression in highly autofluorescent biological samples. This thesis extends the capabilities of HCR to three new domains: spectral HCR imaging for quantitative 10-plex immunofluorescence and in situ hybridization in highly autofluorescent samples; imaging of protein:protein complexes using cooperative probes for logical control over HCR signal amplification; and HCR lateral flow tests for sensitive, instrument-free, at-home testing for infectious diseases.

While 4- or 5-plex imaging is readily achieved using orthogonal HCR systems labeled with spectrally distinct fluorophores, higher levels of multiplexing are challenging due to overlap in the broad excitation and emission spectra of commonly used fluorophores. In Chapter 2, we simultaneously image a combination of 10 protein and RNA targets via spectral imaging with linear unmixing. A combination of 10 reference spectra for 10 fluorophores chosen for optimal unmixing, 10 orthogonal HCR systems, and 11 optimized excitation and emission settings enable robust, user-friendly performance, which is demonstrated in whole-mount zebrafish embryos and mouse brain sections. We validate that unmixed subcellular voxel intensities enable accurate and precise relative target quantitation with subcellular resolution across all 10 channels and demonstrate single-molecule sensitivity and resolution for absolute RNA quantitation.

In Chapter 3, we introduce an enzyme-free method for multiplexed imaging of protein:protein complexes using split-initiator HCR signal amplification. Antibodies specific to each protein of the complex carry fractional initiators that become colocalized upon introduction of a DNA ruler strand to form a full HCR initiator and trigger growth of a tethered amplification polymer. Automatic background suppression is present throughout the protocol, as split-initiator antibody probes that bind to the sample nonspecifically or to isolated protein targets are too far apart to become colocalized by the ruler strand, precluding colocalization of a full initiator and preventing HCR signal amplification. We demonstrate the technique with high signal-to-background in adherent mammalian cells, pro-T cells, and highly autofluorescent formalin-fixed paraffin-embedded human breast tissue sections. Leveraging existing orthogonal HCR amplifiers, we design three orthogonal cooperative junctions for simultaneous 3-plex detection of protein:protein complexes. We validate

that quantitative subcellular voxel intensities are generated, allowing for built-in relative quantitation of protein:protein complexes within the spatial context of the sample. Lastly, we demonstrate simultaneous detection of protein targets, RNA targets, and protein:protein complexes via a unified protocol for HCR immunofluorescence, in situ hybridization, and protein:protein complex imaging.

In Chapter 4, we enhance the sensitivity of conventional unamplified lateral flow tests for at-home infectious disease testing by developing an amplified assay with isothermal, enzyme-free signal amplification based on the mechanism of HCR. Traditional lateral flow tests are amenable to at-home testing and return a result within 10–15 minutes but demonstrate a high false-negative rate (e.g., 25-50% for SARS-CoV-2) due to the absence of signal amplification. The HCR lateral flow assay we develop maintains the simplicity of the conventional lateral flow assay user experience via a disposable 3-channel lateral flow device to automatically deliver reagents to the test region in three successive stages without user interaction. To perform a test, the user loads the sample, closes the device, and reads the result by eye after 60 minutes. Detecting gamma-irradiated SARS-CoV-2 virions in a mixture of saliva and extraction buffer, the current amplified HCR lateral flow assay achieves a limit of detection of 200 copies/μL using available antibodies to target the SARS-CoV-2 nucleocapsid protein. By comparison, five commercial unamplified lateral flow assays that use proprietary antibodies exhibit limits of detection of 500 copies/μL, 1000 copies/μL, 2000 copies/μL, 2000 copies/μL, and 20,000 copies/μL. By swapping out antibody probes to target different pathogens, amplified HCR lateral flow assays offer a platform for simple, rapid, and sensitive at-home testing for infectious diseases.

PUBLISHED CONTENT AND CONTRIBUTIONS

(*1*) Schulte, S. J., Huang, J., and Pierce, N. A. (2023). Hybridization chain reaction lateral flow assays for amplified instrument-free at-home SARS-CoV-2 testing. *ACS Infectious Diseases*, DOI: 10.1021/acsinfecdis.2c00472.

S.J.S. developed and validated the methodology for viral protein detection, collected the data for viral protein detection, and wrote the original draft.

TABLE OF CONTENTS

LIST OF ILLUSTRATIONS

LIST OF TABLES

Chapter 1

INTRODUCTION

Cells alter the production, localization, activity, and interaction of RNAs and proteins to assert biological state (*1–3*). As such, researchers have long been interested in surveying the presence and function of nucleic acids and proteins within biological specimens by binding them with probes that generate a detectable signal. The earliest example of protein imaging in mammalian tissue dates to 1942, when Coons et al. labeled an anti-pneumococcal antibody with a fluorescent molecule and demonstrated staining of a pneumococcal antigen in a mouse liver (*4*). Nearly three decades later, several research groups successfully imaged repetitive DNA sequences (*5–7*), while Harrison et al. achieved in situ RNA imaging in fetal liver cells in 1973 (*8*). Both methods for imaging nucleic acids relied on complementary DNA or RNA directly labeled with a detectable radioisotope to bind the target of interest.

These earliest examples of protein imaging and nucleic acid imaging (coined immunostaining and in situ hybridization [ISH], respectively) opened new opportunities for querying biological processes. In each case, probes that bound the target of interest were directly labeled with a signal-generating moiety. This strategy necessarily limits the number of signals generated to the number of signal-generating molecules that can be attached to the probe without disrupting the probe's binding activity, which in many cases results in a low signal-to-background ratio (*9–13*). To overcome the low signal generated by direct-labeled probes, methods that amplify the signal have become the mainstay of RNA and protein imaging. One method that remains in widespread use today is catalyzed reporter deposition (CARD), which uses enzyme-labeled probes to convert a substrate small molecule into a colorimetric or fluorescent molecule that then deposits nearby in the sample (*14*). For protein imaging, the antibody specific to the target of interest can be directly labeled with an enzyme that mediates CARD (*15*), while for nucleic acid imaging, DNA or RNA probes are labeled with a small molecule hapten (such as digoxigenin), which is in turn detected by an enzyme-labeled antibody (*16*, *17*). While CARD amplifies the signal to a level above that of direct-labeled probes, because the generated signal does not remain tethered to the probe, the signal becomes distributed over a wider area and results in non-quantitative staining with lower resolution (*10*, *16*). Another

consideration when imaging biomolecules is the frequent desire to image as many targets as possible to gain a more holistic view of the biological state of the sample, yet CARD complicates multiplexed imaging due to the paucity of orthogonal enzymes and deposition chemistries, necessitating serial signal amplification for one target after another (*10*, *18–20*).

To further increase signal intensity, a variety of in situ amplification methods have been developed to generate large nucleic acid scaffolds that then mediate production of additional signal. For example, branched DNA techniques use a dendritic nucleic acid structure, which is generated over multiple stages, to bind to a target of interest, and subsequent hybridization of many short enzyme- or fluorophore-labeled strands to the branched structure leads to signal generation (*21–26*). In the rolling circle amplification method, a polymerase enzyme generates a long single-stranded DNA scaffold that is in turn hybridized with short readout strands (*27–29*). While these methods generate additional signal above direct-labeled probes, they lack background suppression, resulting in the generation of amplified background in the case of off-target binding of one or more of the components of the method. For example, in branched DNA methods, if the dendritic DNA structure binds to an off-target location, the readout strands will nevertheless bind to the dendrimer, resulting in amplified background of equal brightness to dendrimers that bind to the target of interest.

In parallel, a suite of methods focusing on genome-wide study of RNA expression have been developed. Single-cell RNA sequencing enables extremely high levels of multiplexed quantitation of RNA expression but poorly retains anatomical context due to the requirement to dissociate the cells from one another before capturing single cells and performing sequencing (*30*). As an alternative, barcode-based imaging methods use several rounds of imaging to assign a unique series of fluorophores to each detected target (*31–34*). This approach requires image alignment between imaging rounds, making imaging of delicate samples and samples not affixed to a slide (such as whole-mount vertebrate embryos) impractical. Moreover, to enable decoding of the barcode sequence, researchers are limited to detecting non-overlapping, spatially-separated target molecules.

The mechanism of hybridization chain reaction (HCR) overcomes these concerns, enabling multiplexed, high-resolution, amplified biomolecule imaging with automatic background suppression. HCR, introduced nearly two decades ago, consists of two nucleic acid strands that each remain kinetically trapped in a metastable

hairpin structure when together in solution (Figure 1.1A) (*35*). Upon exposure to an initiator sequence (i1), hairpin h1 binds to i1 and opens via toehold-mediated strand displacement, exposing an output domain that then binds to and opens hairpin h2. The exposed output domain on hairpin h2 is identical in sequence to initiator i1, thereby allowing another h1 to bind and propagating a chain reaction of alternating h1 and h2 polymerization steps. Together, hairpins h1 and h2 comprise an HCR amplifier that generates long, double-stranded polymers.

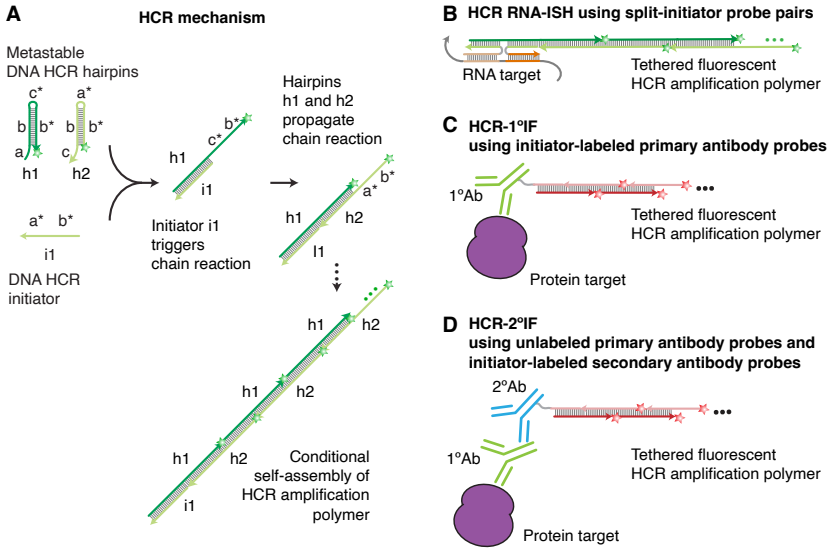

Figure 1.1: A unified framework for multiplexed quantitative protein and RNA imaging using HCR 1°IF + HCR RNA-FISH or HCR 2°IF + RNA-FISH. (A) 1-step, isothermal, enzyme-free signal amplification via hybridization chain reaction (HCR) (*35*). Kinetically trapped hairpins h1 and h2 co-exist metastably in solution on lab time scales, storing the energy to drive a conditional self-assembly cascade upon exposure to a cognate initiator sequence i1. Stars denote fluorophores. (B) HCR RNA-FISH using split-initiator probe pairs that hybridize to adjacent binding sites on the target RNA to colocalize a full HCR initiator and trigger HCR. (C) HCR 1°IF using unlabeled primary antibody probes. (D) HCR 2°IF using unlabeled primary antibody probes and initiator-labeled secondary antibody probes. Figure adapted from (*36*).

Amplified imaging of RNA and protein targets with HCR signal amplification is achieved by a two-stage protocol (*36–39*). In the detection stage, probes specific to a target of interest are labeled with initiator i1 and added to the sample. For detection of RNA targets, HCR RNA fluorescence ISH (RNA-FISH) v3.0 introduced split-initiator probes, wherein each probe consists of a target-binding region and half of an HCR initiator (Figure 1.1B) (*39*). As a result, only pairs of probes that bind adjacent sites on the RNA target form a full initiator; individual probes that bind

non-specifically in the sample only carry half of an HCR initiator and therefore cannot trigger hairpin polymerization. For detection of protein targets, initiator i1 is appended to a primary antibody raised against the protein target (or to a secondary antibody specific to an unlabeled primary antibody against the protein target) (Figure 1.1CD) (*36*). Washes at the end of the first stage remove any unbound initiator-labeled probes. In the amplification stage, hairpins h1 and h2 labeled with small molecule fluorophores are added to the sample and polymerize upon encountering a full-length initiator in the sample, forming tethered amplification polymers decorated with many fluorophores. Washes at the end of the second stage remove unpolymerized HCR hairpins.

Target detection based on the mechanism of HCR offers several advantages. First, automatic background suppression is present throughout the protocol (*39*). For both RNA and protein detection, individual HCR hairpins that bind nonspecifically in the sample do not polymerize, as the hairpins remain kinetically trapped in the hairpin structure unless exposed to an HCR initiator. For RNA detection, split-initiator probes ensure that nonspecific binding of individual probes does not trigger signal amplification (*39*). For protein targets, because the initiator is always present in its full-length form, it is important to use validated antibodies that are selective for the protein target of interest, as off-target binding of the antibody will trigger amplified background. Second, by employing orthogonal HCR systems designed with the NUPACK software suite (*40–42*), straightforward multiplexed imaging is achieved by labeling the probes for each target with a different HCR initiator and utilizing spectrally distinct fluorophores on the HCR hairpins for each system (*36*, *39*). Unified detection of protein and RNA targets further allows for one-step signal amplification for both target types, allowing users to query gene expression at multiple levels (*36*). Third, as a built-in feature, HCR generates quantitative subcellular voxel intensities that scale with the number of targets per imaging voxel (qHCR imaging) (*43*). Furthermore, absolute quantitation of RNA targets is possible via digital HCR imaging, with single-molecule sensitivity for RNA targets even in highly autofluorescent whole-mount vertebrate embryos (dHCR imaging) (*39*, *44*). Fourth, the signal amplification mechanism is isothermal, operating at room temperature, and is enzyme-free, eliminating concerns about enzyme cost and stability. Fifth, the probes and hairpins used in HCR signal amplification are small in size, permitting access to regions deep within thick specimens. With these favorable properties, HCR has enabled laboratory researchers to study RNA and protein expression in multiplex in a panoply of biological sample types (*36*, *45*). This thesis seeks to further extend

the capabilities of HCR to higher levels of simultaneous multiplexing (Chapter 2), quantitative imaging of protein:protein complexes (Chapter 3), and at-home testing for infectious disease (Chapter 4).

With orthogonal HCR amplifiers labeled with spectrally distinct fluorophores, researchers have the option of detecting multiple RNA and protein targets simultaneously within biological samples. Each fluorophore has a characteristic excitation spectrum, which defines the degree to which the fluorophore is excited across a range of wavelengths, as well as a characteristic emission spectrum, which defines the degree to which the fluorophore emits photons across a range of wavelengths. Because commonly used small molecule organic fluorophores absorb and emit photons over a wide range of wavelengths, to conduct multiplexed experiments, it is necessary to use fluorophores with maximally disparate excitation and emission spectra. By exciting each fluorophore with a different wavelength of light, as well as employing bandpass filters that only allow certain wavelengths of light to reach the detector(s), researchers can image 4–5 targets in a sample without crosstalk between the fluorescence channels (*38*, *39*). Above 5 targets, increasing overlap in the excitation and emission spectra between fluorophores leads to crosstalk, preventing attribution of the fluorescence to one target in the sample. Therefore, we aimed to develop a method for simultaneous signal amplification and imaging of 10 targets, effectively doubling the number of targets researchers can detect in a single imaging round. In Chapter 2, we pursue a robust, user-friendly method for imaging 10 targets regardless of expression level or anatomical location, allowing for detection of spatially-overlapping, high-expression, and low-expression targets of interest. We employ spectral imaging with linear unmixing to achieve 10-plex imaging. Spectral imaging applies light from multiple wavelengths to excite fluorophores labeling targets in the sample, while linear unmixing uses a reference spectrum for each fluorophore to determine the concentration of each fluorophore in every pixel of the image.

In addition to exploring the expression of RNA and protein targets, to better understand the actions executed by these biological macromolecules, it is necessary to query their interactions (*2*, *3*). Multi-channel imaging of two targets with spectrally distinct fluorophores allows some measure of the proximity of two targets, yet the resolution of fluorescence microscopy is limited to the diffraction limit of light, preventing inquiry of proximity on the scale most relevant to molecular interactions. In contrast, generating one signal upon the physical interaction of two

probes can assess proximity at a sub-diffraction limit level. We hypothesized that the split-initiator principle of HCR v3.0 would be amenable to detecting molecular interactions, and as one implementation of this strategy, in Chapter 3 we pursue the detection of protein:protein complexes (*39*). Antibodies specific to each protein of the complex carry oligonucleotide strands harboring half of an HCR initiator, and a third oligonucleotide strand functions as a molecular ruler, colocalizing the two fractional initiators to form a full HCR initiator if the two antibodies bind proximally to one another in the sample.

While the aforementioned techniques are applicable to the sensitive detection of RNA targets, protein targets, and protein:protein complexes in a laboratory setting, we also hypothesized that the mechanism of HCR would be well-suited for at-home testing for infectious disease. PCR tests remain the gold standard for detecting infectious diseases such as SARS-CoV-2, yet they take hours to return a result and require laboratory instrumentation (*46*, *47*). In contrast, conventional lateral flow assay tests allow users to test themselves for infectious disease at home, but the unamplified nature of the lateral flow format leads to an unacceptably high false-negative rate (e.g., 25%–50%) (*48–50*). In Chapter 4, motivated by the ongoing COVID-19 pandemic, we employ HCR signal amplification for at-home testing for infectious disease, partially bridging the sensitivity gap between commercial unamplified lateral flow assays and laboratory-based PCR tests.

Chapter 2

HCR SPECTRAL IMAGING: 10-PLEX QUANTITATIVE RNA FLUORESCENCE IN SITU HYBRIDIZATION AND IMMUNOFLUORESCENCE IN HIGHLY AUTOFLUORESCENT SAMPLES

2.1 Introduction

Visualizing RNA and protein expression provides researchers with a spatial view of the biological components that execute cellular processes. Immunohistochemistry (IHC) (*51*, *52*) and in situ hybridization (ISH) (*8*, *53*) use antibody or DNA probes to selectively bind a protein or RNA target of interest and produce an output signal in the vicinity of that target. To gain a more complete view of the biomolecules present in a specimen, researchers would ideally image as many target molecules as possible. However, multiplexing has historically been compromised by reliance on enzymatic signal-generating methods, such as catalyzed reporter deposition (CARD), which lack robust orthogonal chemistries for simultaneous multiplexing (*10*, *18–20*) and provide poor spatial resolution due to diffusion of the reporter molecules (*10*, *16*). To address these shortcomings, immunofluorescence (IF) and fluorescence in situ hybridization (FISH) exploit fluorophores that remain tethered to the target-binding probes, greatly improving spatial resolution (*9*, *10*, *13*). Imaging up to 4–5 targets is achievable by employing fluorophores with well-separated excitation and emission spectra, allowing for selective excitation of each fluorophore and collection of emitted fluorescence via bandpass filters that only allow certain wavelengths of light to reach the microscope detector (*12*). However, increasing overlap of the excitation and emission spectra leads to crosstalk between fluorescence channels as the number of fluorophores increases, prohibiting higher levels of multiplexing.

Fluorescence-based methods relying on unamplified approaches, such as direct-labeled probes, further suffer from low signal-to-background and prevent detection of low-expression targets (*54*, *55*). In contrast, sensitive detection of protein and RNA targets is enabled by the mechanism of hybridization chain reaction (HCR), an enzyme-free signal amplification method in which two fluorophore-labeled nucleic acid hairpins (h1 & h2) comprising an HCR amplifier undergo a self-assembly cascade upon exposure to a target initiator (i1) (*35–39*). With HCR v3.0 for RNA-FISH,

probe pairs in which each probe harbors half of an HCR initiator provide automatic background suppression, requiring a pair of probes to bind adjacent locations on the target RNA to generate a full HCR initiator and trigger amplification (*39*). More recently, we also demonstrated that HCR IF with initiator-labeled antibodies achieves amplified detection of protein targets (*36*). Both HCR IF and HCR RNA-FISH provide sensitive, high-resolution, quantitative imaging paradigms, allowing researchers to perform relative and absolute quantitation of high- and low-expression targets of interest (*36*, *43*).

By utilizing orthogonal HCR systems that polymerize independently of one another, straightforward multiplexing is achieved by labeling the hairpins of each system with a different fluorophore, yet simultaneous signal amplification for more than five targets has been of limited use due to fluorescence crosstalk. We aimed to develop a method for simultaneous signal amplification and imaging of 10 targets, effectively doubling the number of targets researchers can detect in a single imaging round. We set the goal of enabling robust, user-friendly, one-step imaging of all 10 targets regardless of the expression level or anatomical location of the target, allowing for detection of spatially overlapping high- and low-expression targets of interest. While dramatically higher levels of multiplexing can be achieved using temporal barcoding methods, these approaches require low target expression levels in order to spatially separate the signal for each target molecule as a distinct dot and require repeated imaging that is unfavorable for whole-mount embryos and delicate specimens (*31*, *32*, *56*, *57*). In contrast, spectral imaging (*58–60*) offers the conceptual promise of exceeding 5-plex without the need for re-imaging samples and without constraints on target expression level or pattern. However, in practice, it has proven difficult to realize this conceptual promise in the challenging imaging environment of whole-mount vertebrate embryos (*60*).

Here, we demonstrate simultaneous imaging of a combination of 10 protein and RNA targets in highly autofluorescent samples via spectral imaging of 10 orthogonal HCR systems and linear unmixing of the fluorescence signal. We show robust separation of 10 target fluorophore channels, plus an additional 11^{th} autofluorescence channel, and validate that unmixed subcellular voxel intensities enable accurate and precise relative target quantitation with subcellular resolution across all 10 channels, as well as absolute digital RNA quantitation.

2.2 Results

10-plex spectral imaging and linear unmixing

We utilize spectral imaging with linear unmixing to image 10 targets, each of which is bound by probes triggering amplification of an orthogonal HCR system labeled with a different fluorophore. With spectral imaging, light from across the visible and near-IR spectrum is applied to the sample to excite the 10 fluorophores labeling all 10 targets (*58*). Here, 10 laser lines excite each of the 10 target fluorophores near their excitation peaks, and an 11^{th} laser line excites the autofluorescence in the sample at its peak excitation wavelength. Light emitted upon applying each laser line is then collected via one or more fluorescence detectors. Because the 10 fluorophores (and autofluorescence) overlap in their excitation and emission spectra (see Figure 2.1A), light collected in the detectors will consist of a combination of fluorescence from different fluorophores in the sample. Therefore, to determine the contribution of each fluorophore to every pixel in the image, linear unmixing is applied. Linear unmixing assumes the total fluorescence in each pixel at a given wavelength is a linear combination of the abundance of each fluorophore multiplied by the intensity of the fluorophore reference spectrum at that wavelength (*61*). By determining the reference spectrum of each fluorophore, linear unmixing can solve for the unknown concentration of each fluorophore in every pixel in the image. The output is 11 unmixed channels: one for each of the 10 target fluorophores, and one for autofluorescence.

The steps to conduct a 10-plex experiment are summarized in Figure 2.1B. The user first determines the wavelength that maximally excites the autofluorescence of the sample by conducting an excitation-emission scan of an unlabeled sample (note: this step need not be repeated for future experiments in the same sample type). Next, the user spectrally images the 10-plex sample and 1-plex samples for each of the 10 target fluorophores, as well as an unlabeled sample. The reference spectra are generated from the 1-plex and unlabeled sample images by evaluating the fluorescence intensity across all channels in a region of maximal expression of a given target (or maximal autofluorescence for the unlabeled sample), generating a linear unmixing matrix (Figure 2.1C). Lastly, the linear unmixing matrix is applied to the 10-plex image to solve for the concentration of each fluorophore in every pixel of the image, generating 11 output channels (including autofluorescence).

As an example, consider Figure 2.1D, which depicts the raw spectral fluorescence intensity for a single pixel in the notochord region of a 10-plex whole-mount ze-

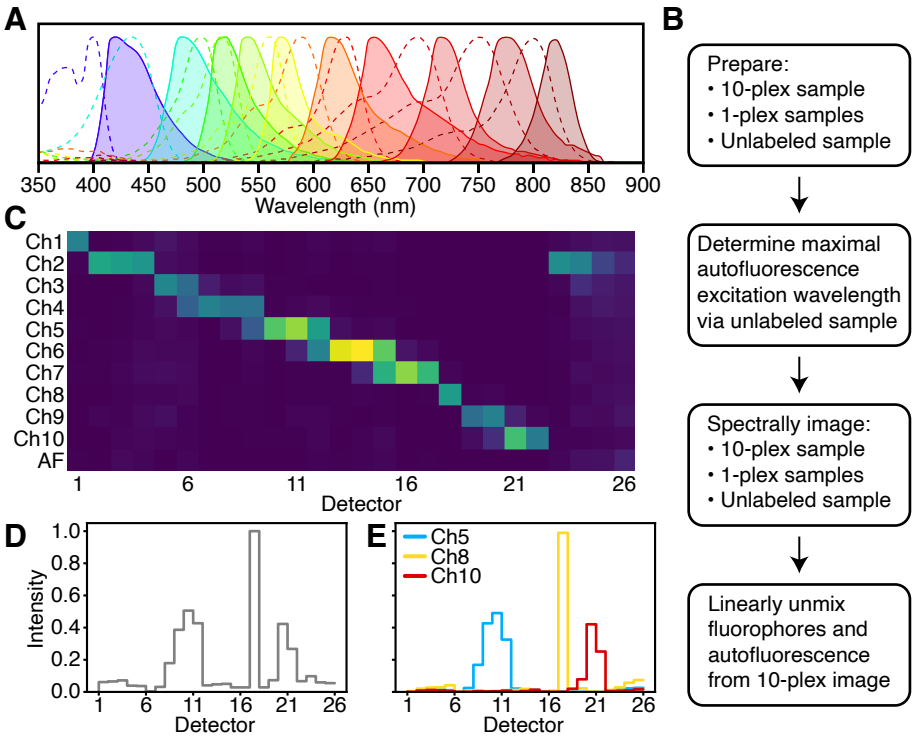

Figure 2.1: Overview of 10-plex imaging using spectral imaging and linear unmixing. (A) Excitation (dashed lines) and emission (solid lines) spectra for the 10 fluorophores utilized for HCR spectral imaging. Commercially available fluorophores were chosen for maximal separation between spectra to enable robust linear unmixing. Spectra from left to right: Alexa405, Atto425, Alexa488, Alexa514, Alexa546, Alexa594, Atto633, Alexa700, Alexa750, iFluor800. Spectra obtained from FluoroFinder. (B) Protocol summary for performing a 10-plex spectral imaging and linear unmixing experiment. (C) Linear unmixing matrix of reference fluorophore spectrum intensity gathered via spectral imaging of 10 fluorophores in 1-plex samples. Autofluorescence (AF) spectrum gathered from an unlabeled sample. (D) Spectral fluorescence intensity of a single pixel in the notochord of a 27 hpf zebrafish embryo. (E) Linear unmixing determines the fluorescence contribution from each fluorophore to the pixel in panel D. Linear unmixing utilizing the reference spectra from panel C correctly identifies that the pixel in the notochord is labeled by Ch5, Ch8, and Ch10 fluorophores, comprising the bulk of the spectral fluorescence intensity in panel D.

brafish embryo. By applying linear unmixing, we determine the amounts of each of the 10 fluorophores and autofluorescence that combine to create the spectral fluorescence intensity curve. Here, linear unmixing determines that the preponderance of the fluorescence intensity was contributed by Channels 5, 8, and 10, generating the three peaks seen in the spectral fluorescence intensity curve (Figure 2.1E).

We demonstrate 10-plex spectral imaging with linear unmixing on the Leica Stellaris 8 microscope, which is equipped with a fixed 405 nm laser, as well as a tunable white light laser capable of generating laser lines in 1 nm increments between 440 nm to 790 nm. The tunability of the white light laser affords optimal excitation wavelengths for each target fluorophore, as well as autofluorescence, minimizing cross-excitation of other fluorophores. The Leica LAS X software is capable of performing the linear unmixing, allowing users to complete both the spectral imaging and linear unmixing on the Stellaris 8 microscope. As an alternative, we present a novel linear unmixing algorithm, which we have released as the LinearUnmixing 1.0 notebook (available for download at www.moleculartechnologies.org).

10-plex RNA imaging using spectral HCR RNA-FISH in a whole-mount vertebrate embryo

To validate our approach to spectral imaging with linear unmixing, we performed 10-plex HCR RNA-FISH in a fixed 27 hours post-fertilization (hpf) whole-mount zebrafish embryo. The RNA targets represent a variety of expression levels, and each target has a distinct expression pattern corresponding to a certain anatomical region of the zebrafish, allowing for visual confirmation of unmixing fidelity.

Generating samples for 10-plex HCR RNA-FISH has the same protocol timeline as that of a single-plex or lower-level multiplexed experiment. Targets are detected via two overnight steps consisting of a detection stage and amplification stage (Figure 2.2A). In the detection stage, all HCR probe sets, each of which consists of split-initiator probes, are added simultaneously to the sample and bind to the 10 RNA targets. In the subsequent overnight amplification stage, all HCR amplifiers are added. Because the 10 HCR systems operate independently of one another, concurrent signal amplification occurs for all 10 targets, each of which becomes labeled with tethered amplification polymers decorated with a different fluorophore. To gather the fluorophore reference spectra, 1-plex zebrafish embryos were labeled with the probe set and HCR amplifier corresponding to 1 of the 10 targets and imaged with the same imaging settings as the 10-plex sample. The autofluorescence

reference spectrum was gathered from an unlabeled zebrafish embryo (no probes and no hairpins added).

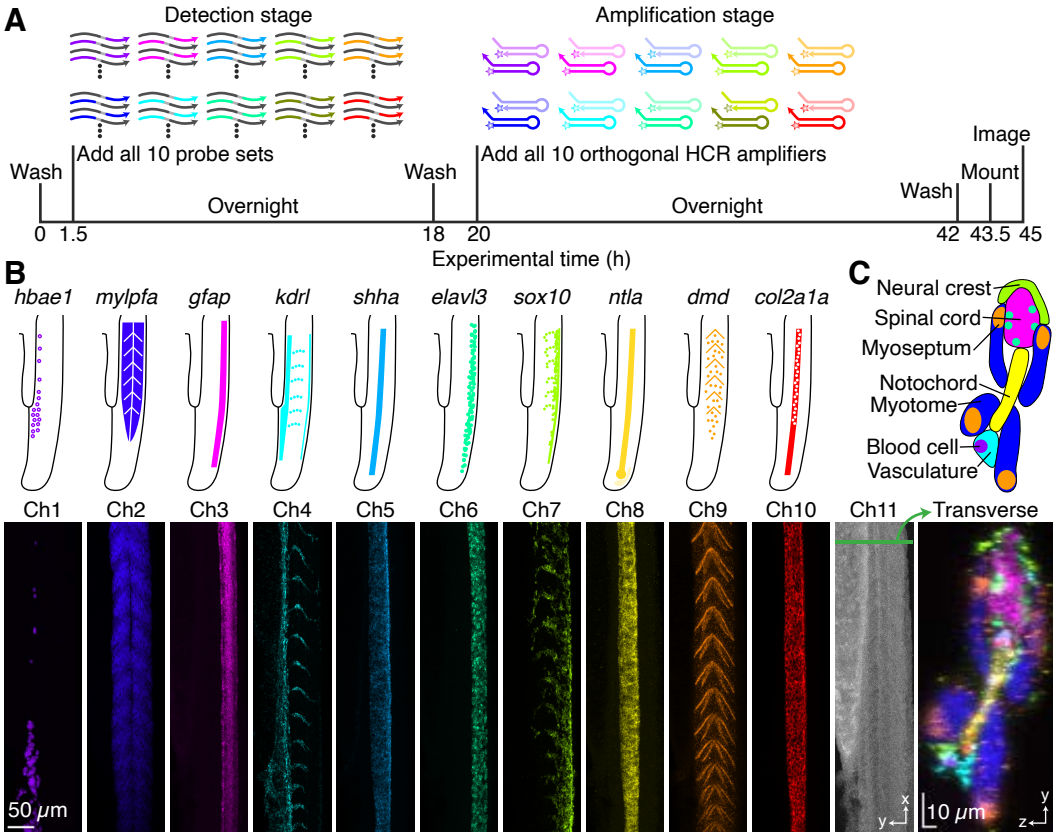

Figure 2.2: 10-plex RNA imaging in a 27 hours post-fertilization (hpf) whole-mount zebrafish embryo. (A) 2-stage 10-plex HCR RNA-FISH protocol. Detection stage: 10 split-initiator DNA probe sets bind to 10 RNA targets; wash. Amplification stage: split-initiator probes trigger self-assembly of 10 fluorophore-labeled HCR amplifiers into tethered fluorescent amplification polymers; wash. Amplification occurs simultaneously for all 10 targets. (B) Top: expression atlas for 10 RNA targets in the tail region of a 27 hpf zebrafish embryo. Bottom: Confocal single-channel images of 10-plex RNA imaging in the tail region of a 27 hpf zebrafish embryo; 0.568×0.568×4.0 μm pixels; maximum intensity z-projection of 77 z-dimension sections (103 μm total). Ch1: *hbae1* (Alexa405). Ch2: *mylpfa* (Atto425). Ch3: *gfap* (Alexa488). Ch4: *kdrl* (Alexa514). Ch5: *shha* (Alexa546). Ch6: *elavl3* (Alexa594). Ch7: *sox10* (Atto633). Ch8: *ntla* (Alexa700). Ch9: *dmd* (Alexa750). Ch10: *col2a1a* (iFluor800). Ch11: autofluorescence (AF). Channels unmixed with the Leica LAS X software. (C) Top: anatomical schematic of a transverse view 27 hpf zebrafish embryo tail region. Bottom: Composite transverse view image of Ch1 to Ch10 reveals anatomical structures labeled by the 10-plex RNA targets; maximum intensity x-projection of 11 x-dimension sections (6.25 μm total) within the green rectangle region depicted on the Ch11 image of panel B. See Section A.3.1 and Supplementary Movie 1 for additional data.

Visual inspection of the 11 unmixed channels reveals robust separation of each of the 10 targets, as well as of the autofluorescence channel (Figure 2.2B). Of note, the linear unmixing algorithm is able to separate targets with overlapping expression patterns, including *shha*, *ntla*, and *col2a1a*, all of which label the notochord of the zebrafish embryo (*62*). A composite transverse view of the embryo reveals several of the anatomical structures labeled by the RNA targets, including the neural crest (labeled by *sox10*) (*63*), spinal cord (labeled throughout by *gfap* (*64*) and around the perimeter by *elavl3* (*65*)), myotome (labeled by *mylpfa*) (*66*), myoseptum (labeled by *dmd*) (*67*), vasculature (labeled by *kdrl*) (*68*), hematopoietic blood cells (labeled by *hbae1*) (*69*), and notochord (labeled by *shha*, *ntla*, and *col2a1a*) (Figure 2.2C). The estimated signal-to-background ratios range from 17 to 100 (median: 45) across the 10 RNA targets (mean signal-to-background for $N = 3$ replicate embryos; see Table A.7).

qHCR imaging: 10-plex relative quantitation with subcellular resolution in an anatomical context

As a built-in feature, HCR signal amplification generates quantitative subcellular voxel intensities for both RNA (*39*) and protein (*36*) targets (qHCR), permitting multidimensional quantitative analysis of target expression in highly autofluorescent tissues (*43*). To verify whether spectral imaging with linear unmixing generates quantitative voxel intensities, five target RNAs in a 27 hpf whole-mount zebrafish embryo were each redundantly detected in two fluorescence channels via a single 10-plex experiment. Target RNAs are redundantly detected by designing two HCR probe sets with orthogonal HCR initiators that bind interleaving sites along the target RNA (Figure 2.3A). If HCR signal scales approximately linearly with the number of target RNAs per voxel, a scatter plot of normalized voxel intensities for each pair of redundant channels will yield a tight linear distribution with approximately zero intercept (*43*), after first ruling out potential systematic crowding effects that could permit pairwise voxel intensities to slide undetected along a line (*36*, *39*).

A 10-plex zebrafish embryo sample was spectrally imaged and linearly unmixed via reference spectra for the 10 target fluorophores and autofluorescence (Figure 2.3B). For each pair of redundant channels, subcellular 2×2×1.2 μm voxels were compared within a region of the sample with varying signal intensity. Plots of the normalized subcellular voxel intensities for each of the redundant channel pairs reveal high precision (scatter around the line) and high accuracy (linearity with zero intercept), indicating spectral unmixing with linear unmixing generates quantitative

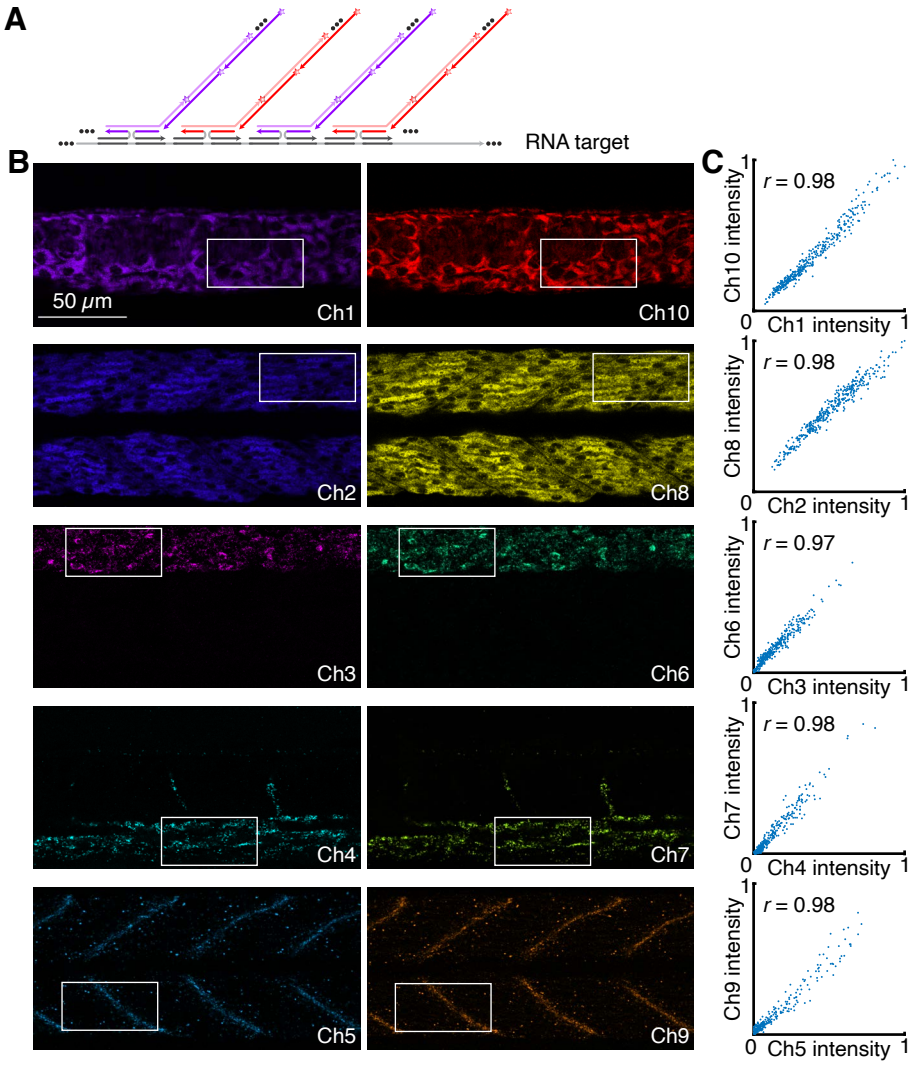

Figure 2.3: qHCR imaging: relative quantitation with subcellular resolution in an anatomical context using 10-plex spectral imaging with linear unmixing. (A) Redundant detection of an RNA target using two split-initiator DNA probe sets labeled with orthogonal HCR initiators. (B) 10-channel confocal images of 5 redundantly detected RNA targets; 0.180×0.180×1.2 μm pixels; single optical sections. Ch1: *col2a1a* (Alexa405). Ch2: *mylpfa* (Atto425). Ch3: *elavl3* (Alexa488). Ch4: *kdrl* (Alexa514). Ch5: *dmd* (Alexa546). Ch6: *elavl3* (Alexa594). Ch7: *kdrl* (Atto633). Ch8: *mylpfa* (Alexa700). Ch9: *dmd* (Alexa750). Ch10: *col2a1a* (iFluor800). Sample: 27 hpf whole-mount zebrafish embryo. Chromatic aberration corrected with Huygens software. Channels unmixed with the Leica LAS X software. Solid boxes: region analyzed in panel C. (C) High precision (scatter around the line) and high accuracy (linearity with zero intercept) for RNA relative quantitation in an anatomical context across all 10 channels. Highly correlated normalized signal (Pearson correlation coefficient, r) for subcellular voxels (2.0×2.0×1.2 μm) in the depicted region of panel B above mean background fluorescence. See Section A.3.2 for additional data.

voxel intensities across all 10 channels (Figure 2.3C). Each channel displays a high estimated signal-to-background ratio (median: 60), ranging from 27 to 130 (mean signal-to-background for $N = 3$ replicate embryos; see Table A.10).

dHCR imaging: absolute quantitation of RNA targets in a 10-plex sample

We previously demonstrated that HCR provides single-molecule sensitivity for digital RNA quantitation (dHCR) (*39*, *44*). We were curious to see whether a single-molecule target RNA could be spectrally imaged and linearly unmixed within the context of a 10-plex imaging experiment. Toward that end, we performed the same 10-plex experiment as for Figure 2.3, but imaged the dorsal posterior region of the zebrafish tail, where the RNA target *kdrl* is expressed as single-molecule punctae. Alongside redundant detection of 4 other RNA targets, the *kdrl* RNA was redundantly detected with two HCR probe sets configured to bind interleaving portions of the *kdrl* target, and the 10-plex sample was spectrally imaged and linearly unmixed.

To determine the fidelity with which single-molecule targets can be detected with spectral HCR imaging, we performed dot detection on the redundant *kdrl* channels (Channels 4 and 7) using a novel dot detection algorithm (Figure 2.4). We observe a colocalization rate of 0.80 ± 0.003 for Channel 4 and 0.82 ± 0.009 for Channel 7, consistent with previous colocalization rates for dHCR imaging with HCR RNA-FISH v3.0 (*39*), indicating spectral imaging with linear unmixing is compatible with absolute quantitation of low-expression, single-molecule targets. The dot detection algorithm is available for download as the DotDetection 2.0 notebook at www.moleculartechnologies.org.

10-plex protein and RNA imaging using spectral HCR IF + HCR RNA-FISH in a mouse brain section

To illustrate the versatility of HCR spectral imaging with linear unmixing for detection of diverse target types in a different sample setting, we also performed 10-plex HCR IF + HCR RNA-FISH in a 5 μm fresh-frozen coronal mouse brain section. For HCR IF + HCR RNA-FISH, targets are detected via three overnight steps consisting of a protein detection stage, an RNA detection stage, and an amplification stage (Figure 2.5A). In the first overnight of the detection stage, all HCR IF unlabeled primary antibodies are added simultaneously, after which the initiator-labeled secondary antibodies are incubated to bind to the primary antibodies. In the second overnight of the detection stage, all HCR RNA-FISH probe sets are added simultaneously. Lastly, in the final overnight amplification stage, all orthogonal HCR hairpins are

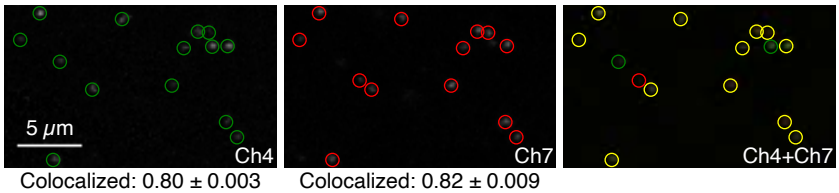

Figure 2.4: dHCR imaging: absolute quantitation of RNA targets within the context of 10-plex spectral imaging with linear unmixing. Alongside four other redundantly detected targets, target RNA *kdrl* was redundantly detected using two split-initiator DNA probe sets labeled with orthogonal HCR initiators that bind interleaving locations along the target RNA. The 10-plex zebrafish embryo was spectrally imaged in the dorsal posterior tail, where *kdrl* is expressed as single molecule punctae, and linearly unmixed. Left: Ch4 (*kdrl*; Alexa514). Middle: Ch7 (*kdrl*; Atto633). Right: Ch4+Ch7 merge. Green circles denote dots detected in Ch4, red circles denote dots detected in Ch7, and yellow circles denote dots detected in both channels. Colocalization rate indicates the fraction of dots in each channel that are detected in both channels (mean ± estimated standard error of the mean via uncertainty propagation for $N = 3$ replicate embryos). Dots were detected using the DotDetection 2.0 notebook (available for download from www.moleculartechnologies.org). Maximum intensity z-projection of 5 z-dimension sections (2.7 μm total); 0.180×0.180×1.2 μm pixels. Sample: 27 hpf whole-mount zebrafish embryo. Channels unmixed with the Leica LAS X software. See Section A.3.3 for additional data.

added. One-time signal amplification is achieved for the combination of all 10 RNA and protein targets, each of which becomes labeled with a tethered amplification polymer with a different fluorophore. Reference spectra for the fluorophores were gathered from 1-plex samples, and a reference spectrum for the autofluorescence was gathered from an unlabeled sample.

Each protein and RNA target has a characteristic expression pattern corresponding to certain cells and/or cellular compartments within the cerebral cortex, enabling confirmation of the linear unmixing success (Figure 2.5B). The protein targets label various components of the cerebral cortex: NFH labels the intermediate filaments in large myelinated axons (*70*), CD31 labels endothelial cells (*71*), and RBFOX3 labels neuronal nuclei (*72*). Among the RNA targets, *Actb* is expressed in several cell types (*73*), while *Slc17a7* labels excitatory neurons and *Gad1* labels inhibitory neurons (*74*). Subtypes of inhibitory neurons are labeled by *Sst* and *Vip*, and expression of these two RNA targets overlaps as expected with *Gad1*-expressing neurons, again confirming the ability to distinguish overlapping targets with linear unmixing (*74*). Lastly, as expected, *Lamp5* expression is most pronounced in the upper layers of the

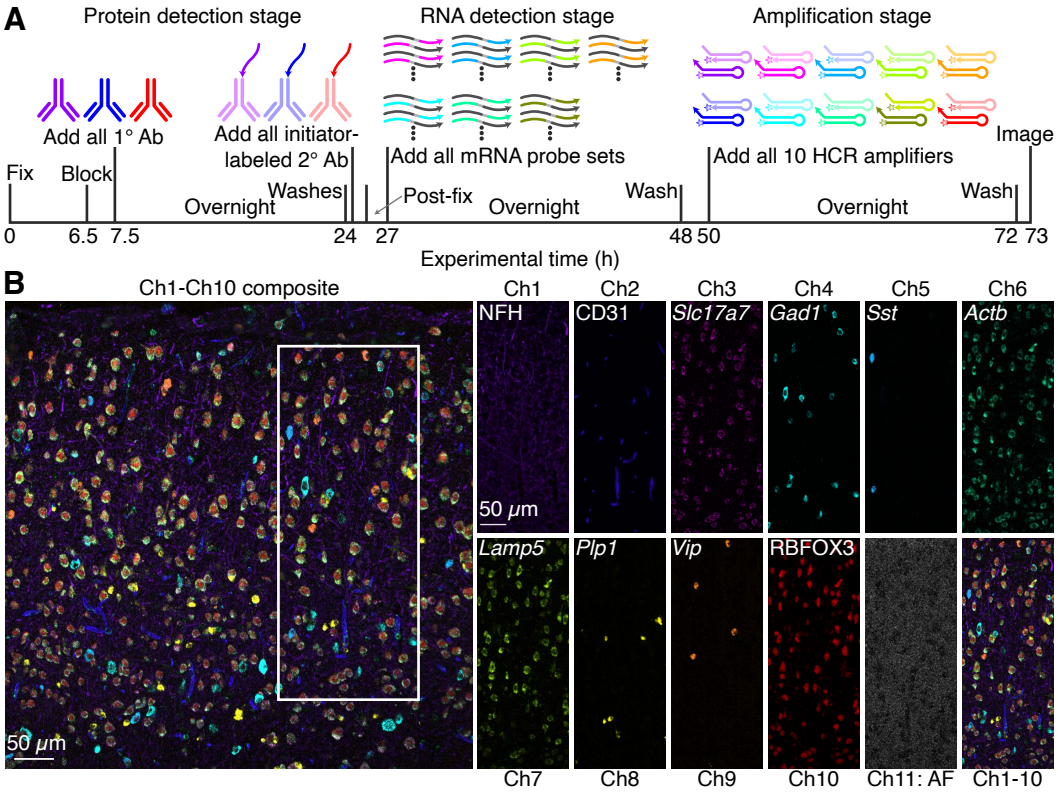

Figure 2.5: 10-plex protein and RNA imaging in a fresh-frozen mouse brain section. (A) 3-stage 10-plex HCR IF + RNA-FISH protocol. Protein detection stage: primary antibodies bind to protein targets; wash. Initiator-labeled secondary antibodies bind to primary antibodies; wash. Post-fix. RNA detection stage: split-initiator DNA probe sets bind to RNA targets; wash. Amplification stage: initiator-labeled secondary antibodies and split-initiator DNA probes trigger concurrent self-assembly of 10 fluorophore-labeled HCR amplifiers into tethered fluorescent amplification polymers; wash. Amplification occurs simultaneously for all 10 targets, regardless of target type. (B) 10-plex confocal images of 3 protein and 7 RNA targets in the cerebral cortex of a 5 μm fresh-fixed mouse brain section; 0.568×0.568×4.0 μm pixels; single optical section. Ch1: target protein NFH (Alexa405). Ch2: target protein CD31 (Atto425). Ch3: target RNA *Slc17a7* (Alexa488). Ch4: target RNA *Gad1* (Alexa514). Ch5: target RNA *Sst* (Alexa546). Ch6: target RNA *Actb* (Alexa594). Ch7: target RNA *Lamp5* (Atto633). Ch8: target RNA *Plp1* (Alexa700). Ch9: target RNA *Vip* (Alexa750). Ch10: target protein RBFOX3 (iFluor800). Ch11: autofluorescence (AF). Left: composite image of Ch1-Ch10. Right: Confocal single-channel images of Ch1-Ch11 and composite image of Ch1-Ch10 for the region depicted in the left image. Channels unmixed with the Leica LAS X software. Sample: coronal fresh-frozen mouse brain section (thickness: 5 μm; region: interaural 0.88 mm ± 0.2 mm; age: 8 weeks old). See Section A.3.4 for additional data.

cortex (*75*), and *Plp1* labels oligodendrocytes, which are non-overlapping with the neuronal cells (*76*). The estimated signal-to-background ratios range from 25 to 140 (median: 70) across the 10 protein and RNA targets (mean signal-to-background for $N = 3$ replicate sections; see Table A.12).

2.3 Discussion

Spectral imaging with linear unmixing enables researchers to simultaneously image a combination of 10 RNA and protein targets by harnessing the robust signal amplification mechanism of HCR. While other multiplexed methods utilize repeated imaging rounds with signal removal between rounds to enable dramatically higher levels of multiplexing, these methods require image alignment between imaging rounds, making imaging of delicate samples and samples not affixed to a slide (such as whole-mount vertebrate embryos) particularly onerous (*31–34*). Moreover, many methods place constraints on the expression location of the target, only allowing researchers to detect non-overlapping, spatially-separated target molecules in the case of barcode-based methods (*31*, *32*, *34*). In contrast, HCR spectral imaging with linear unmixing allows for detection of high-expression spatially-overlapping targets, as well as low-expression single-molecule targets, in highly autofluorescent samples not affixed to slides, such as whole-mount vertebrate embryos. To that end, we demonstrate detection of the single-molecule *kdrl* target RNA in whole-mount vertebrate embryos, as well as detection of the overlapping *Gad1*, *Actb*, and *Sst* RNA targets in an inhibitory neuron subtype in mouse brain sections. HCR spectral imaging of 10 targets further benefits from a quick, user-friendly protocol, as all probes of the same type are added simultaneously in the detection stage, and all HCR hairpins are added simultaneously in the amplification stage. This results in a two-overnight protocol for HCR RNA-FISH and a three-overnight protocol for HCR RNA-FISH + HCR IF.

HCR applies fluorescence-based signal amplification to generate high signal-to-background across the visible and near-IR spectrum, even in highly autofluorescent samples such as whole-mount vertebrate embryos and brain sections. In addition to amplified signal, low background is achieved by the automatic background suppression of split-initiator DNA probe pairs, as well as the kinetically trapped HCR hairpins, which do not polymerize unless exposed to a full HCR initiator (*39*). Spectral imaging with linear unmixing further preserves the high spatial resolution and quantitative subcellular voxel intensities of normal bandpass imaging HCR. We demonstrate that the unmixed fluorescence channels generate quantitative voxel

intensities, allowing for researchers to harness the built-in benefit of relative target quantitation.

En route to 10-plex imaging, we optimized several method parameters. First, we leveraged 10 orthogonal HCR systems, wherein the initiator of each system does not trigger polymerization of hairpins of other systems; the orthogonality of this signal amplification mechanism means amplification can occur simultaneously across all 10 targets. Second, we chose fluorophores that enable high signal-to-background, also seeking to use fluorophores that are as spectrally distinct as possible. Using fluorophores with disparate spectra ensures that linear unmixing performs well even if noise or other fluorophores in the sample perturb the spectra. Third, we optimized the laser line wavelengths to excite the fluorophores and autofluorescence as selectively as possible, helping to reduce crosstalk between channels prior to unmixing. Fourth, we determined the optimal wavelengths for the microscope detectors, finding that for many channels it was beneficial to line up several detectors back to back across different wavelengths, allowing for collection of more detailed spectral information than if a single detector were used for each channel. The Leica Stellaris 8 microscope allowed us to perform these discriminate optimizations of the excitation and collection wavelengths, providing laser lines in 1 nm increments and five detectors. Fifth, we gathered reference spectra for each of the 10 fluorophores, as well as for the autofluorescence, using the same imaging conditions as for the 10-plex sample. Sixth, we used robust linear unmixing algorithms via the Leica LAS X software and via a novel unmixing method we developed, which has been released as the LinearUnmixing 1.0 notebook (available at moleculartechnologies.org).

The work presented here is designed to be plug-and-play for researchers looking to image more than five targets in biological samples. To image 10 targets of interest, a user need only obtain the reference spectrum for each target fluorophore in 1-plex samples (and an unlabeled sample for autofluorescence) in order to linearly unmix the spectral fluorescence of a 10-plex sample. As an added benefit, unified 10-plex HCR IF + HCR RNA-ISH allows researchers to query gene expression at multiple levels. For example, researchers can interrogate expression of both the RNA and protein for a given gene, which may be expressed in vastly different quantities and in different spatial compartments (*77*, *78*). This opens the door to new multiplexed studies of protein and RNA spatial expression in historically difficult-to-image biological samples, enabling researchers to gain a more holistic view of the biomolecules that guide cellular activity.

2.4 Methods Summary

Probes, amplifiers, and buffers

Details regarding the probes, amplifiers, and buffers for each experiment are displayed in Table A.1.1 for HCR RNA-FISH and Table A.1.2 for HCR IF.

HCR RNA-FISH in whole-mount zebrafish embryos

HCR RNA-FISH in whole-mount zebrafish embryos was performed using the protocols detailed in Section A.2.2. Experiments were performed in AB wild-type whole-mount zebrafish embryos (fixed 27 hpf) from the Zebrafish Facility of the Beckman Institute at Caltech. Procedures for the care and use of zebrafish embryos were approved by the Caltech IACUC.

HCR IF + HCR RNA-FISH in fresh-frozen mouse brain sections

HCR IF + HCR RNA-FISH in fresh-frozen mouse brain sections was performed using the protocols detailed in Section A.2.3. Experiments were performed in C57BL/6 fresh-frozen coronal mouse brain sections (thickness: 5 μm; region: interaural 0.88 mm ± 0.2 mm; age: 8 weeks old; sex: male) from Acepix Biosciences (Cat. # A2203-0561).

Confocal microscopy

Microscopy was performed using a Leica Stellaris 8 inverted confocal microscope with an HC PL APO 20×/0.75 IMM CORR CS2 (Cat. # 11506343) objective or HC PL APO 63×/1.40 OIL CS2 (Cat. # 11506350) objective. Detailed information on the objectives, excitation wavelengths, detectors, and detection wavelengths used for each experiment is displayed in Tables A.3 and A.4.

Spectral imaging and linear unmixing

Spectral imaging and linear unmixing was performed using the protocol detailed in Section A.2.1. Alternatively, linear unmixing was performed using the LinearUnmixing 1.0 notebook for Figures A.2 and A.20–A.22. The LinearUnmixing 1.0 notebook is available for download at www.moleculartechnologies.org.

Image analysis

Image analysis was performed as detailed in Section A.1.4 of the supplementary material, including: definition of raw pixel intensities; measurement of signal, background, and signal-to-background; calculation of normalized subcellular voxel intensities for qHCR imaging; and dot detection for dHCR imaging. For qHCR

imaging, Huygens software was used to correct for chromatic aberration. For enhanced visualization, images are displayed with 0.1% of pixels saturated across three replicates, with the exception of Figures 2.4 and A.15, which are displayed between the minimum and maximum pixel intensities across three replicates. All images are displayed without background subtraction.

Chapter 3

MULTIPLEXED QUANTITATIVE IMAGING OF PROTEIN:PROTEIN COMPLEXES USING COOPERATIVE PROBES FOR LOGICAL CONTROL OVER HCR SIGNAL AMPLIFICATION

3.1 Introduction

Proteins undergo novel interactions to steer cellular activity in new directions during processes such as transcription, signal transduction, development, and disease (*2*, *3*). While immunofluorescence methods querying multi-channel protein expression provide some measure of the proximity of two or more proteins, this readout of protein:protein proximity is maximally resolved to the diffraction limit of light. In contrast, generating one signal upon physical interaction of probes targeting proximal proteins provides a sub-diffraction limit indication of proximity.

The proximity ligation assay is one such method, utilizing antibodies labeled with oligonucleotides that interact only if the antibodies bind to nearby locations in the sample (*79–82*). If the oligonucleotides are close enough to interact, they hybridize with one another and are enzymatically ligated prior to rolling circle amplification with a polymerase enzyme, creating a long DNA strand that is in turn hybridized with fluorescent readout probes to generate a signal. The reliance on multiple enzymes creates experimental difficulties: enzyme stocks are costly, have strict cold storage conditions, and have variable activity over time (requiring frequent re-assaying for activity). Moreover, the proximity ligation assay exhibits a low reaction efficiency owing to the frequent generation of noncircular ligation products during the enzymatic ligase step, reducing sensitivity (*83*). Specificity is also hampered due to high background, which is displayed for technical controls in which one reaction component is omitted (*82*).

To avoid the experimental shortcomings associated with using enzymes, the prox-HCR method employs nonenzymatic hybridization chain reaction (HCR) signal amplification (*83*, *84*). Two antibodies labeled with oligonucleotides configured to adopt a hairpin secondary structure bind proximally in a sample, and a third oligonucleotide strand hybridizes with one of the hairpins to free a sequence that hybridizes with the other hairpin, de-sequestering a full-length HCR initiator that

triggers polymerization of an HCR amplifier. This multi-stage reaction pathway, which is sequence-dependent on the initiator, has thus far been limited to 1-plex applications.

In addition to proxHCR, the mechanism of HCR (*35*) has previously been applied for amplified detection of both RNA (*37–39*) and protein (*36*) targets. The split-initiator concept was introduced by HCR RNA fluorescence in situ hybridization (RNA-FISH) v3.0, in which a target RNA is detected by probes harboring one half of an HCR initiator (*39*). When both probes in a probe pair bind adjacent locations on the target RNA, a full HCR initiator is colocalized, triggering alternating polymerization of HCR hairpins h1 and h2. Splitting the initiator across two probes achieves automatic background suppression, as off-target binding of one probe is insufficient to generate amplified background due to the absence of a full-length initiator. We also recently demonstrated HCR immunofluorescence (IF) for the sensitive detection of target proteins in highly autofluorescent samples by employing initiator-labeled antibodies that trigger growth of tethered HCR amplification polymers (*36*).

Drawing on the principles of HCR RNA-FISH v3.0 and HCR IF, we hypothesized that a split-initiator approach would be well-suited for the detection of protein:protein complexes. We set the goal of developing a robust split-initiator technology for imaging protein:protein complexes that is multiplexed, quantitative, compatible with HCR RNA-FISH and HCR IF for simultaneous imaging of RNA and protein targets, and provides high signal-to-background in highly autofluorescent samples, including FFPE tissue sections.

To achieve that goal, we designed split-initiator probes to generate a full-length HCR initiator only when two proteins are proximal to one another in the sample (Figure 3.1A). To perform an experiment, primary antibodies are first bound to the interacting proteins. The primary antibodies are then bound by P1 and P2 interaction probes, each of which consists of two components: 1) a secondary antibody configured to bind to one of the primary antibodies, and 2) a P1 or P2 oligonucleotide comprising a fractional initiator domain (18 nt) and a ruler-binding domain (24 nt). The P1 oligonucleotide fractional initiator domain consists of the 5' half of the initiator, while the P2 oligonucleotide fractional initiator domain consists of the 3' half of the initiator. If the P1 and P2 interaction probes are close enough to one another, a ruler strand (50 nt) hybridizes with the ruler-binding domains of the P1 and P2 oligonucleotides, colocalizing the fractional initiator halves to form a full HCR initiator capable of triggering HCR upon addition of an HCR amplifier. For

scenarios in which two target proteins are not interacting, the ruler strand is incapable of binding to both the P1 and P2 oligonucleotides, preventing formation of a colocalized HCR initiator, and because individual fractional initiators cannot trigger HCR, signal amplification does not occur if the ruler strand does not colocalize the two initiator halves. This scheme provides automatic background suppression, generating a full-length initiator and triggering HCR signal amplification only when two proteins are proximal, and suppressing HCR signal amplification when the ruler strand cannot bridge the gap between spatially-distant P1 and P2 oligonucleotides.

3.2 Results

Protein:protein complex imaging in adherent mammalian cells, mouse pro-T cells, and human breast tissue sections

To evaluate our approach for HCR imaging of protein:protein complexes, we compared the fluorescence intensity between pairs of biological samples, where one sample is expected to form the protein:protein complex of interest, and the other sample is expected to not form the protein:protein complex of interest and therefore not trigger HCR signal amplification. For each case, we calculate an estimated signal-to-background ratio between the two sample types. This provides a conservative estimate of the method's performance, as the protein:protein complex may nevertheless be present at a low level in the biological sample expected to not form the protein:protein complex. First, we compared the fluorescence intensity for the β-catenin:E-cadherin complex in the human adherent A-431 and HeLa cell lines. While A-431 cells form the β-catenin:E-cadherin complex at the cell membrane of intercellular junctions (*85*), HeLa cells express N-cadherin rather than E-cadherin (*86*, *87*) and therefore do not form the β-catenin:E-cadherin complex. As expected, A-431 cells (Figure 3.2A) display much higher fluorescence than HeLa cells (Figure 3.2B), with a signal-to-background ratio of 26 ± 5 between the two cell lines (mean ± estimated standard error of the mean via uncertainty propagation for $N = 3$ replicate wells on a coverslip).

We also examined the RUNX1:PU.1 complex in the Scid.adh.2C2 mouse pro-T cell line (*88*). The Scid.adh.2C2 cell line has emerged as a useful pro-T cell line for studying T cell development, with exogenous introduction of PU.1 protein capable of reverting the cell line to an earlier developmental time point, in part via the interaction of PU.1 with other proteins such as RUNX1 (*89–91*). Because the Scid.adh.2C2 cell line does not endogenously express the PU.1 protein (*88*), we do not expect the Scid.adh.2C2 cells to natively form the RUNX1:PU.1 complex.

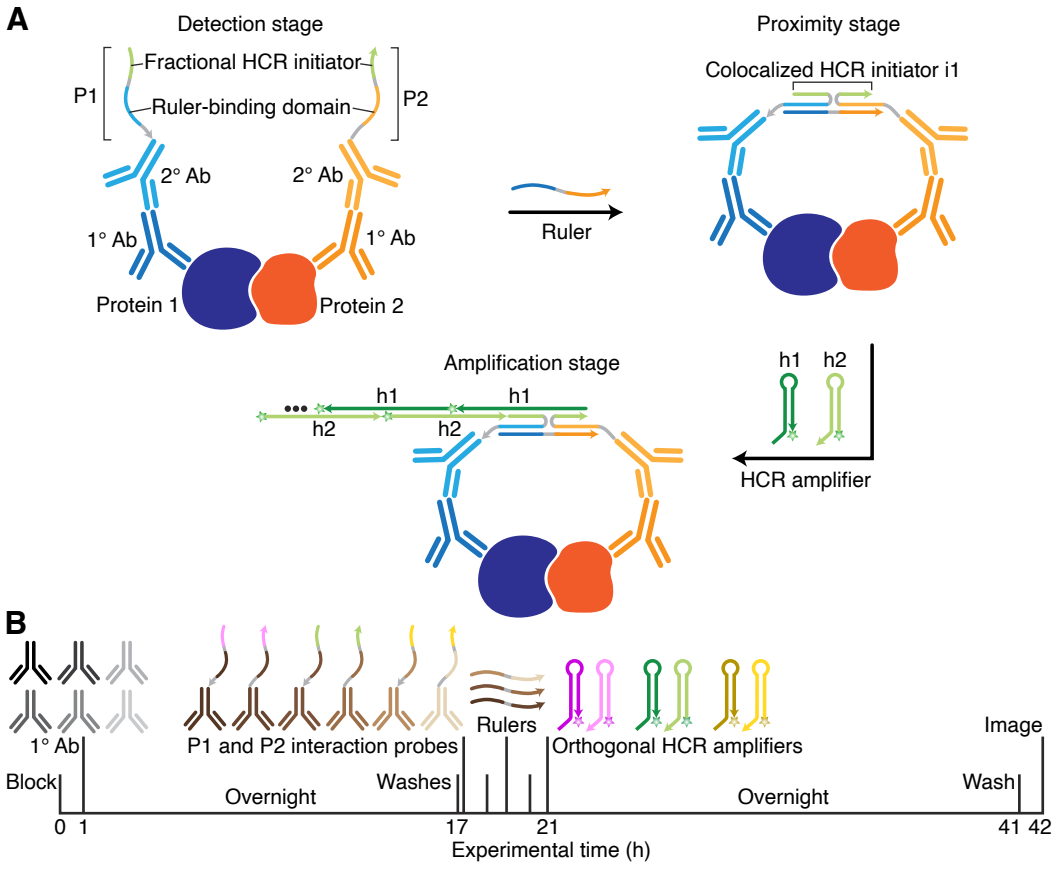

Figure 3.1: Detection of protein:protein complexes using HCR. (A) Protocol for detecting protein:protein complexes. Detection stage: primary antibodies first bind to complexed proteins 1 and 2. The secondary antibody component of the P1 and P2 interaction probes then binds to the primary antibodies labeling the complexed proteins. Proximity stage: if the P1 and P2 oligonucleotides are close enough to one another, a ruler DNA strand binds to the ruler-binding domains of the P1 and P2 oligonucleotides, colocalizing HCR initiator i1. Amplification stage: initiator i1 triggers alternating polymerization of an HCR amplifier consisting of fluorescently-labeled HCR hairpins h1 and h2, generating an amplification polymer that remains tethered to the initiator. Washes between each step remove unbound reagents. (B) Protocol timeline.

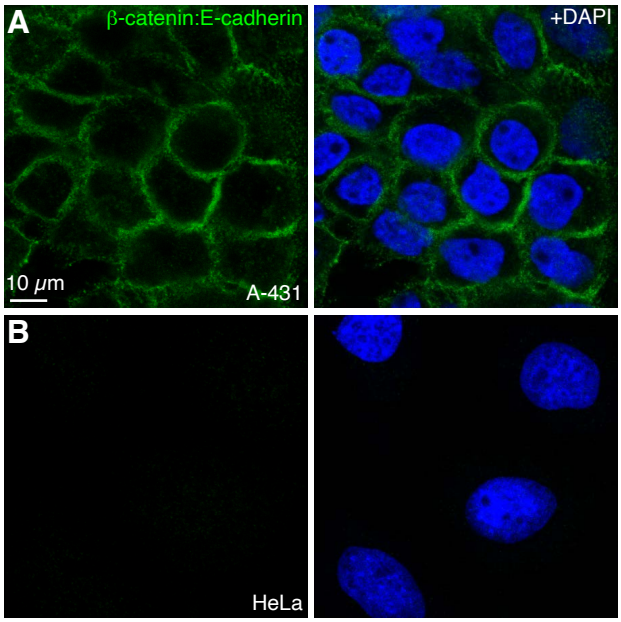

Figure 3.2: Detection of the β-catenin:E-cadherin complex in adherent mammalian cells. A) A-431 cells. (B) HeLa cells. (A,B) Adherent A-431 and HeLa cell lines were processed according to the protocol of Section B.2.1 and imaged under identical conditions. Left: β-catenin:E-cadherin complex (Alexa647). Right: composite image with DAPI. Single optical sections shown ($0.180 \times 0.180 \times 0.8$ μm pixels). See Section B.3.1 for additional data.

In contrast, when the Scid.adh.2C2 cell line is retrovirally transduced with the PU.1 protein, we expect the expressed PU.1 protein to form a complex with the RUNX1 protein, its typical binding partner at earlier developmental time points. Indeed, we observe higher fluorescence for cells retrovirally transduced with a PU.1-containing vector (Figure 3.3A) than for cells retrovirally transduced with an empty vector (Figure 3.3B), with a signal-to-background ratio of 15 ± 4 between the two experiment types (mean $\pm$ estimated standard error of the mean via uncertainty propagation for $N = 3$ replicate wells on a coverslip).

To validate the method in highly autofluorescent human FFPE tissue sections, we detected the β-catenin:E-cadherin complex in FFPE human breast tissue sections (5 μm thickness). The β-catenin:E-cadherin complex is robustly formed in normal breast epithelial cells, but the expression of and interaction between the β-catenin and E-cadherin proteins is interrupted when breast epithelial cells become cancerous in the invasive lobular carcinoma disease process (*92*, *93*). We obtained paired normal and invasive lobular carcinoma 5 μm FFPE breast tissue sections from the same patient and evaluated them for the β-catenin:E-cadherin complex, observing much

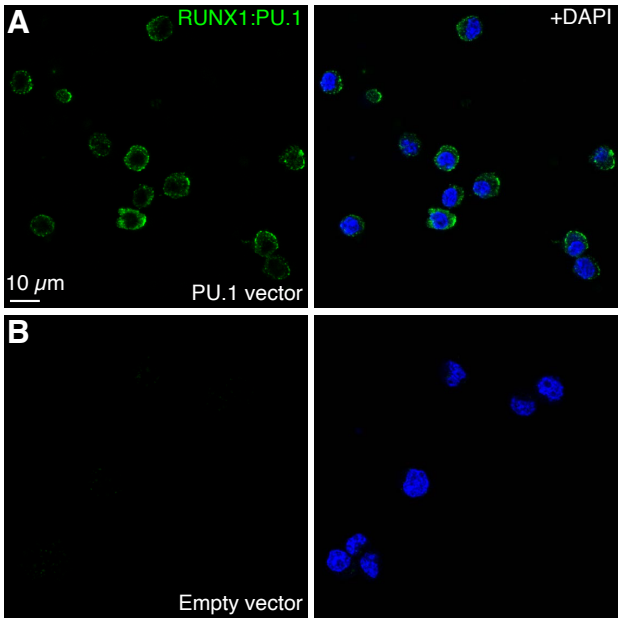

Figure 3.3: Detection of the RUNX1:PU.1 complex in mouse pro-T cells. A) Scid.adh.2C2 cells retrovirally transduced with a PU.1-expressing vector. (B) Scid.adh.2C2 cells retrovirally transduced with an empty vector. (A,B) Mouse Scid.adh.2C2 pro-T cells with and without exogenous expression of the PU.1 protein were processed according to the protocol of Section B.2.3 and imaged under identical conditions. Left: RUNX1:PU.1 complex (Alexa647). Right: composite image with DAPI. Single optical sections shown ($0.180 \times 0.180 \times 0.8$ μm pixels). See Section B.3.2 for additional data.

higher fluorescence in sections from a normal breast tissue region (Figure 3.4A) than in sections from an invasive lobular carcinoma region (Figure 3.4B), with a signal-to-background ratio of 30 ± 5 between the two section types (mean $\pm$ estimated standard error of the mean via uncertainty propagation for $N = 3$ replicate sections).

In summary, we observe high signal-to-background ratios for detection of different protein:protein complexes across three different sample types, including highly autofluorescent FFPE tissue sections, validating that the split-initiator approach for detecting protein:protein complexes performs well in a variety of sample and biological settings.

Multiplexed protein:protein complex imaging

With HCR IF and HCR RNA-FISH, researchers can perform multiplexed detection of protein and RNA targets (including a combination of both target types), allowing for multidimensional examination of gene expression (*36*, *39*, *43*). Similarly, we sought to enable users to perform multiplexed detection of protein:protein com-

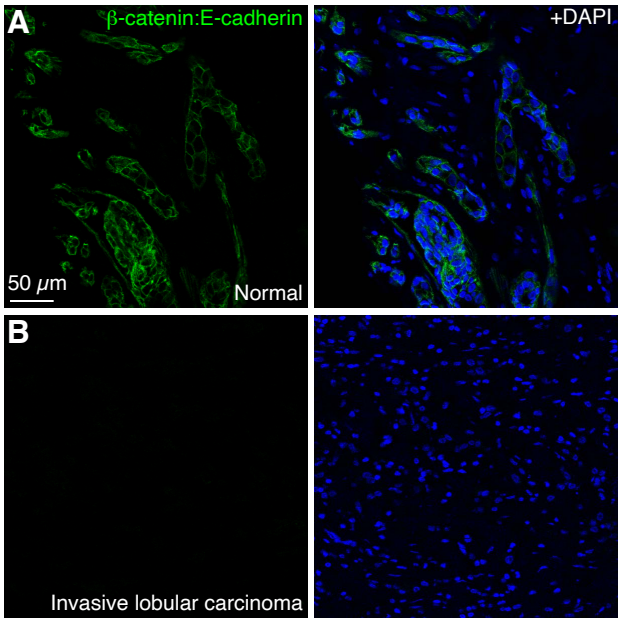

Figure 3.4: Detection of the β-catenin:E-cadherin complex in FFPE human breast tissue. A) Normal FFPE human breast tissue. (B) Invasive lobular carcinoma FFPE human breast tissue. (A,B) Normal and invasive lobular carcinoma FFPE breast tissue sections from the same patient were processed according to the protocol of Section B.2.2 and imaged under identical conditions. Left: β-catenin:E-cadherin complex (Alexa647). Right: composite image with DAPI. Single optical sections shown ($0.568 \times 0.568 \times 3.3$ μm pixels). See Section B.3.3 for additional data.

plexes. We used NUPACK 4.0 (*42*) to design three sets of P1-P2-ruler sequences, which are orthogonal to each other at two levels: 1) the ruler strands each have a unique sequence and are designed to not interact with one another, and 2) each design employs a split initiator from a different HCR system. Using distinct ruler sequences avoids a scenario wherein the ruler strand colocalizes a P1 oligonucleotide from one HCR system with the P2 oligonucleotide from a different HCR system. Therefore, users can detect multiple complexes within the same region of the sample without concern of cross-reactivity between designs. The split-initiator designs we employed come from existing HCR systems verified for their orthogonality (B1, B6, and B9), allowing users to conduct multiplexed experiments by using spectrally distinct amplifiers for each HCR system.

For each P1-P2-ruler junction, sequence design was performed using the reaction pathway designer within NUPACK (*40*, *41*, *94*). Sequence design was formulated as a multistate optimization problem using target test tubes to represent reactant, intermediate, and product states of hybridization between P1, P2, ruler, and hair-

pin strands, as well as to model crosstalk between orthogonal systems (Figure 3.5) (*41*). Each tube contains a set of desired on-target complexes (each with a target secondary structure and target concentration), corresponding to the on-pathway hybridization products for a given step, and a set of undesired off-target complexes (each with a target concentration of 0 nM), corresponding to on-pathway reactants and off-pathway hybridization crosstalk for a given step. To simultaneously design N orthogonal systems, elementary step tubes are specified for each system. Furthermore, to design against off-pathway interactions between systems, a single global crosstalk tube is specified. In the global crosstalk tube, the on-target complexes correspond to all reactive species generated during all elementary steps for all systems ($n = 1, ..., N$); the off-target complexes correspond to noncognate interactions between these reactive species. Crucially, the global crosstalk tube ensemble omits the cognate products that the reactive species are intended to form (they appear as neither on-targets nor off-targets). Hence, all reactive species in the global crosstalk tube are forced to either perform no reaction (remaining as desired on-targets) or undergo a crosstalk reaction (forming undesired off-targets), providing the basis for minimization of global crosstalk during sequence optimization. Note that, for design of a library of N P1-P2-ruler junctions, all N junctions have the same on-target structure; within a library, the only difference between orthogonal junctions is the designed sequence.

We demonstrated the capacity for multiplexed protein:protein complex imaging by detecting three complexes that label different compartments of human adherent A-431 cells: the cytoskeletal α-tubulin:β-tubulin complex, membranous β-catenin:E-cadherin complex, and nuclear speckle SC35:SON complex (Figure 3.6). A high signal-to-background ratio was observed for each complex via technical control experiments in which the primary antibody and interaction probe corresponding to one protein of the complex were omitted (see Table B.14 for additional details).

qHCR imaging: relative quantitation of protein:protein complexes with subcellular resolution

We have previously demonstrated that HCR imaging enables relative quantitation of both RNA and protein targets with subcellular resolution (*36*, *39*, *43*). To determine whether the same applies for imaging protein:protein complexes, we redundantly detected a protein:protein complex with two orthogonal HCR systems (Figure 3.7A). The two primary antibodies targeting the proteins of the complex were each detected by two batches of P1 or P2 interaction probes corresponding to two different HCR

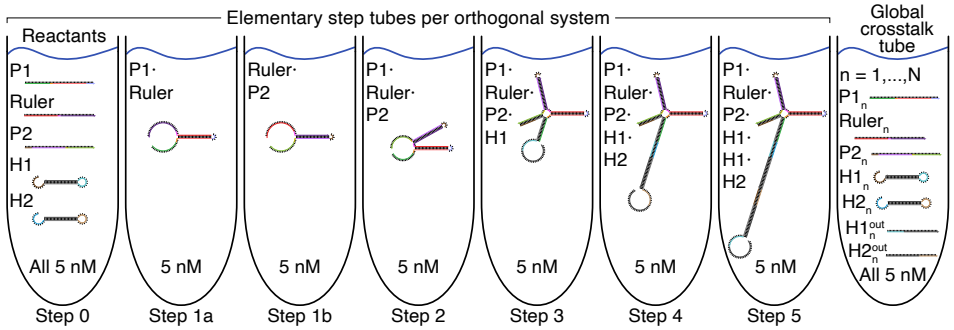

Figure 3.5: Computational P1-P2-ruler junction sequence design using NUPACK. Target test tubes for design of N orthogonal P1-P2-ruler junctions. Left: elementary step tubes. Each target test tube contains a set of desired on-target complexes (each with the depicted target secondary structure and a target concentration of 5 nM) corresponding to the on-pathway hybridization products for a given step and a set of undesired off-target complexes (each with a target concentration of 0 nM; not depicted) corresponding to on-pathway reactants and off-pathway hybridization crosstalk for a given step. To design N orthogonal systems, there are elementary step tubes for each orthogonal system. Right: global crosstalk tube. Contains the depicted on-target complexes corresponding to reactive species generated during Steps 0–5 (each with the depicted target secondary structure and a target concentration of 5 nM) as well as off-target complexes (each with a target concentration of 0 nM; not depicted) corresponding to off-pathway interactions between these reactive species. To design 3 orthogonal systems, the global crosstalk tube contains a set of on-targets and off-targets for each orthogonal system ($n = 1, \ldots, N$). Figure and description adapted from (*94*).

systems. The ruler strand designed for each HCR system was then hybridized to the P1 and P2 oligonucleotides, colocalizing the full initiator for both HCR systems and triggering signal amplification of orthogonal HCR amplifiers labeled with spectrally distinct fluorophores. To check whether quantitative voxel intensities are produced, we plot the subcellular voxel intensities of the two independent HCR channels against one another, expecting a tight linear correlation and an intercept of zero. For the β-catenin:E-cadherin complex in the human adherent A-431 cell line (Figure 3.7B, top), we observe high precision (tight scatter around the diagonal) and high accuracy (linearity and an intercept of zero) for subcellular 2 μm $\times$ 2 μm voxels (Figure 3.7C, top), consistent with quantitative voxel intensities. We also queried the β-catenin:E-cadherin complex in human FFPE breast tissue sections (5 μm thickness) (Figure 3.7B, bottom), again observing high precision and accuracy for the subcellular 2 μm $\times$ 2 μm voxel intensities between the two channels (Figure 3.7C, bottom). The B1 and B6 HCR system designs were used for the A-431

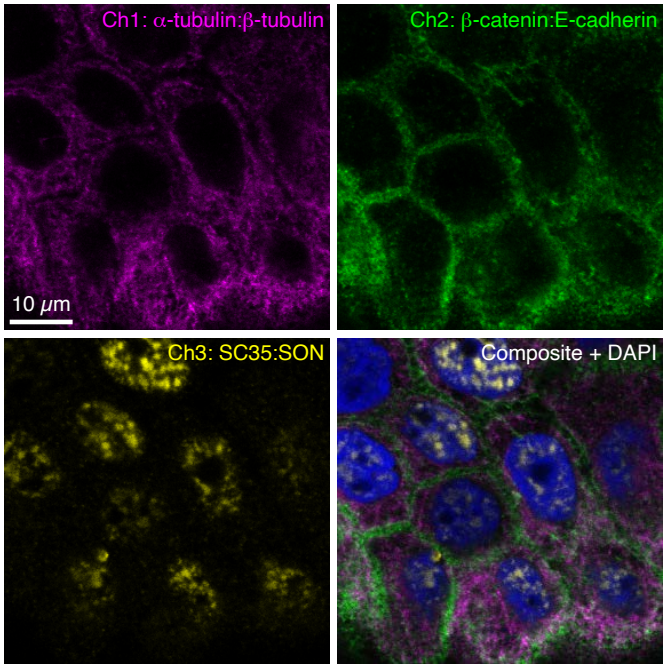

Figure 3.6: Multiplexed imaging of protein:protein complexes. 3-plex detection of protein:protein complexes. Ch1: cytoskeletal α-tubulin:β-tubulin complex (Alexa488). Ch2: membranous β-catenin:E-cadherin complex (Alexa546). Ch3: nuclear speckle SC35:SON complex (Alexa647). Right: composite with DAPI. Single optical section shown ($0.180 \times 0.180 \times 0.8$ μm pixels). Sample: A-431 cells on a coverslip. The same protocol (see Section B.2.1) is used independent of the number of protein:protein complexes imaged. See Section B.3.4 for additional data.

cell experiment, while the B1 and B9 HCR system designs were used for the human FFPE breast tissue section experiment, verifying that quantitative voxel intensities are generated across all three HCR systems for which we have designed P1, P2, and ruler strand sequences.

Simultaneous detection of protein targets, RNA targets, and protein:protein complexes

Building on our recent work illustrating the unified detection of protein and RNA targets using HCR IF + HCR RNA-FISH (*36*), we demonstrate co-detection of a protein target, an RNA target, and a protein:protein complex. For co-detection of protein targets, the primary antibody and initiator-labeled secondary antibody for protein detection are added concurrently with the primary and secondary antibodies for protein:protein complex detection. Co-detection of an RNA involves an additional overnight incubation with split-initiator DNA probes (Figure 3.8A).

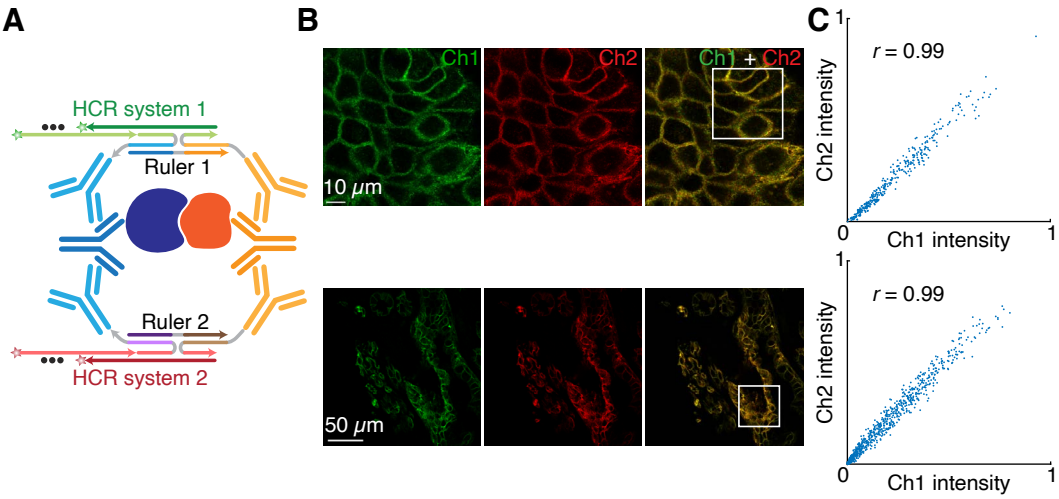

Figure 3.7: qHCR imaging: relative quantitation of protein:protein complexes with subcellular resolution in an anatomical context. (A) Scheme for redundant detection of a protein:protein interaction. Two batches of P1 and P2 interaction probes redundantly detect each primary antibody, and orthogonal ruler strands colocalize a full HCR initiator for both HCR systems, triggering polymerization of two spectrally distinct HCR amplifiers (Ch1: Alexa546; Ch2: Alexa647). (B) Confocal images. Solid box: region of varying voxel intensity. Top: β-catenin:E-cadherin complex in fixed adherent A-431 cells ($0.180 \times 0.180 \times 0.8$ μm pixels). Bottom: β-catenin:E-cadherin complex in normal 5 μm FFPE human breast tissue ($0.568 \times 0.568 \times 3.3$ μm pixels). (C) Normalized subcellular (2×2 μm) voxel intensities from the solid boxes depicted in B are highly correlated (Pearson correlation coefficient, r), displaying high precision (tight scatter around the line) and high accuracy (linearity and zero intercept). See Section B.3.5 for additional data.

Signal amplification occurs simultaneously for all target and complex types via orthogonal HCR amplifiers labeled with spectrally distinct fluorophores. The mitochondrial HSP60 protein target, cytoskeletal α-tubulin:β-tubulin protein:protein complex, and nuclear *U6* RNA were simultaneously detected in human adherent A-431 cells (Figure 3.8B), with high signal-to-background observed via technical control experiments for each of the target and complex types (see Table B.19 for additional details).

3.3 Discussion

Methods for imaging molecular complexes have been comparatively less explored than methods for imaging protein and RNA targets, yet represent an important frontier for spatial exploration of the interactome (*95*, *96*). Leveraging the split-initiator concept of HCR RNA-FISH v3.0 (*39*) and sensitive detection of protein targets from

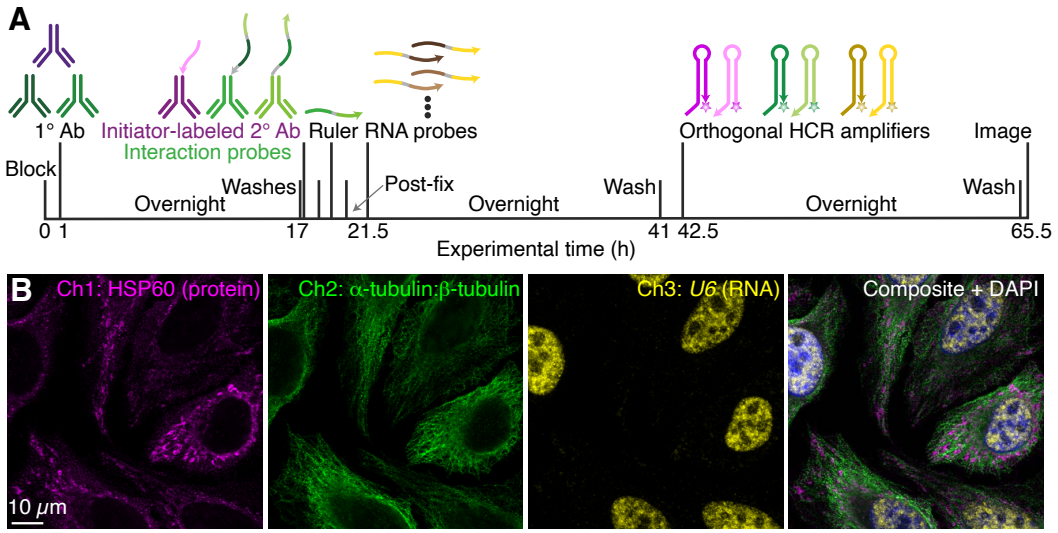

Figure 3.8: Simultaneous detection of protein targets, RNA targets, and protein:protein complexes with a unified protocol for HCR IF + RNA-FISH + protein:protein complex imaging. (A) Protocol timeline. Primary antibodies against protein targets and protein:protein complexes are added concurrently and incubated overnight. Initiator-labeled secondary antibody probes, as well as P1 and P2 interaction probes, are added concurrently and bind to the primary antibodies. Ruler strands colocalize fractional initiators on the P1 and P2 interaction probes. Following post-fixation, RNA targets are detected by split-initiator DNA probes. HCR signal amplification occurs simultaneously for all target and complex types via spectrally distinct HCR amplifiers. Washes between each step remove unbound reagents. (B) Simultaneous detection of a protein target, RNA target, and protein:protein complex. Ch1: mitochondrial HSP60 protein (Alexa488). Ch2: cytoskeletal α-tubulin:β-tubulin complex (Alexa546). Ch3: nuclear *U6* RNA (Alexa647). Right: composite with DAPI. Single optical section shown ($0.180 \times 0.180 \times 0.8$ μm pixels). Sample: HeLa cells on a coverslip. See Section B.3.6 for additional data.

HCR IF, HCR imaging of protein:protein complexes is multiplexed, quantitative, spatially-resolved, and enzyme-free. Split-initiator P1 and P2 interaction probes recapitulate the junction formed in HCR RNA-FISH v3.0, in which a target RNA colocalizes a probe pair where each probe harbors either the 5' or 3' half of an HCR initiator (*39*). For protein:protein complex imaging, the ruler strand serves the same structural function as the target RNA in HCR RNA-FISH v3.0, hybridizing to the P1 and P2 oligonucleotides to colocalize the two halves of the HCR initiator. If the distance between the P1 and P2 interaction probes is greater than the length of the ruler strand, the ruler strand cannot bind to both the P1 and P2 interaction probes, precluding formation of the P1-P2-ruler junction and preventing colocalization of a

full HCR initiator. Thus, for cases in which the two target proteins are not proximal, P1 and P2 interaction probes are not colocalized in a junction with a ruler strand and do not generate signal, as the fractional initiator of each interaction probe is insufficient to trigger HCR.

The work presented here employs unlabeled primary antibodies and P1 and P2 oligonucleotide-labeled secondary antibodies to detect protein:protein complexes, thereby requiring that each primary antibody be of a different isotype or raised in a different species. With the large library of primary antibodies commercially available to users, this requirement is often not an impediment. Moreover, using labeled secondary antibodies has several benefits. First, labeled secondary antibodies can be re-used for primary antibodies against other targets, whereas labeled primary antibodies would only be applicable for one protein target, highlighting the cost-effectiveness and versatility of the labeled secondary antibody approach. Second, in some cases, conjugating an oligonucleotide to an antibody can disrupt the epitope-binding site; by using validated secondary antibodies already conjugated to oligonucleotides, users can plug-and-play with their primary antibodies of choice without concerns of diminished antibody activity. Third, because multiple secondary antibodies can bind to each primary antibody, there are likely more P1-P2-ruler junctions formed when using labeled secondary antibodies, increasing signal strength. Despite these advantages, for cases where it is not desirable to use secondary antibodies, labeled primary antibodies represent an alternative strategy for protein:protein complex imaging.

With HCR imaging of protein:protein complexes, researchers gain the benefit of an enzyme-free method, avoiding the sensitivity, specificity, and storage concerns associated with using enzymes. HCR imaging of protein:protein complexes achieves automatic background suppression throughout the entire protocol, as HCR signal amplification is only triggered if the P1 and P2 interaction probes bind to adjacent locations in the sample. Furthermore, the HCR hairpins themselves incorporate automatic background suppression during the amplification stage, as nonspecific binding of individual HCR hairpins to the sample is insufficient to trigger polymerization. The combination of HCR signal amplification alongside automatic background suppression achieves high signal-to-background ratios in a variety of cell and tissue types, including highly autofluorescent FFPE tissue sections.

Because HCR imaging of protein:protein complexes uses uncomplicated molecular choreography for colocalizing an HCR initiator and can take advantage of the same

HCR systems developed for RNA and protein imaging, designing high-performance orthogonal P1-P2-ruler junctions for multiplexed complex detection is straightforward, and we demonstrate 3-plex detection of protein:protein complexes. Of note, the ruler strand used to assess proximity is independent of the sequence used by the split HCR initiator, freeing up the sequence space for designing P1-P2-ruler junctions and obviating concerns of cross-reactivity between the ruler sequence and HCR initiator sequence. Utilizing these orthogonal systems for redundant detection of protein:protein complexes, we further illustrate that all 3 designs allow for relative quantitation of protein:protein complex abundance, as the HCR signal scales linearly with the number of protein:protein complexes present in each imaging voxel. In addition to multiplexed imaging of protein:protein complexes, users can take advantage of co-detection of protein and RNA targets with HCR IF and HCR RNA-FISH, enabling multi-level spatial interrogation of biomolecules and complexes thereof.

3.4 Methods Summary

Probes, amplifiers, and buffers

Probes, amplifiers, and buffers were obtained from Molecular Technologies, a non-profit academic resource within the Beckman Institute at Caltech. Detailed information for the probes, amplifiers, and buffers for each experiment is displayed in Tables B.1–B.3 for HCR imaging of protein:protein complexes, in Table B.4 for HCR RNA-ISH, and in Table B.5 for HCR IF.

HCR imaging of protein:protein complexes

HCR imaging of protein:protein complexes, with optional co-detection of protein and RNA targets, was performed in human adherent cell lines using the protocol detailed in Section B.2.1. Experiments were performed in A-431 cells (ATCC, CRL-1555) cultured in Dulbecco's Modified Eagle Medium (DMEM) with high glucose and pyruvate (Gibco, 11995-073) supplemented with 10% fetal bovine serum (FBS) (Sigma-Aldrich, F4135), as well as in HeLa cells (ATCC, CRM-CCL-2) cultured in Eagle's Minimum Essential Medium (EMEM) (ATCC, 30-2003) supplemented with 10% FBS (Sigma-Aldrich, F4135). HCR imaging of protein:protein complexes was performed in Scid.adh.2C2 mouse pro-T cells (*88*) cultured in RPMI1640 media (Gibco, 31800022) supplemented with 10% FBS (Sigma-Aldrich, F2442), 1× Penicillin-Streptomycin-Glutamine (Gibco, 10378-016), 0.1 mM sodium pyruvate (Gibco, 11360-070), 1× MEM non-essential amino acids (Gibco, 11140-050), and 50 μM β-mercaptoethanol (Gibco, 21985-023) using the protocol detailed in Section

B.2.3. HCR imaging of protein:protein complexes was performed in 5 μm normal FFPE human breast tissue sections (Acepix Biosciences, HuN-06-0027) and invasive lobular carcinoma FFPE human breast tissue sections (Acepix Biosciences, HuC-06-0101) from the same patient using the protocol details in Section B.2.2.

Microscopy

Microscopy was performed using a Leica Stellaris 8 inverted confocal microscope. For enhanced visualization, all non-DAPI images are displayed with 0.01% of pixels saturated across three replicates. All images are displayed without background subtraction. Detailed information on the objectives, excitation wavelengths, detectors, and detection wavelengths used for each experiment is displayed in Table B.7.

Image analysis

Image analysis was performed as detailed in Section B.1.6 of the supplementary material, including: definition of raw pixel intensities; measurement of signal, background, and signal-to-background; and calculation of normalized subcellular voxel intensities for qHCR imaging.

Chapter 4

HCR LATERAL FLOW TESTS FOR SENSITIVE, INSTRUMENT-FREE, AT-HOME PATHOGEN DETECTION

Schulte, S. J., Huang, J., and Pierce, N. A. (2023). Hybridization chain reaction lateral flow assays for amplified instrument-free at-home SARS-CoV-2 testing. *ACS Infectious Diseases*, DOI: 10.1021/acsinfecdis.2c00472.

4.1 Introduction

In March of 2020, the COVID-19 pandemic revealed that lab-based testing could address the technical requirements for detecting the SARS-CoV-2 virus, but could not readily scale to meet the needs of the global population during a pandemic. To address this shortfall in testing capacity, we wondered whether it would be possible to engineer a simple disposable test that could be used at home without special expertise. For inspiration, we looked to disposable at-home pregnancy tests, which had already been in wide use for decades. At-home pregnancy tests employ a lateral flow assay format in which a target protein abundant in urine during early pregnancy moves via capillary forces through a porous substrate, binding in a sandwich between a first antibody carrying a colored label and a second immobilized antibody that concentrates the label within a test region visible to the naked eye (*97*). The resulting signal is unamplified (i.e., one labeled antibody generates signal for one detected target protein), placing limits on sensitivity, but the striking simplicity of lateral flow assays makes them ideal for home use. To take a test, the user simply adds the sample to the disposable device and then checks by eye for a colored signal in the test region after a prescribed number of minutes.

One challenge to developing a lateral flow assay for detection of SARS-CoV-2 virions is their relative scarcity in readily sampled biological fluids. The protein that serves as a pregnancy marker in urine rises to $\approx 10^{10}$ copies/μL during the first month of pregnancy (*98*, *99*), with unamplified commercial lateral flow assays typically providing limits of detection of $\approx 10^{7}$ copies/μL (*99*, *100*). By comparison, in March 2020, two SARS-CoV-2 studies revealed median viral loads of 158 and 3300 virions/μL in saliva (*101*, *102*), and lab-based tests using reverse transcription quantitative PCR (PCR tests) achieved limits of detection of 0.1–6 copies/μL (*46*, *47*, *103*). Based on these numbers, we set the goal of developing an amplified

lateral flow assay that would enable detection of 1000 SARS-CoV-2 virions/μL, representing an increase in sensitivity of approximately four orders of magnitude relative to at-home pregnancy tests. Due to widely reported patient discomfort during nasopharyngeal swabbing (i.e., the deep nasal swabbing that was prevalent at PCR testing sites at the beginning of the pandemic), we decided to focus on saliva samples as they are readily obtainable without discomfort or medical expertise.

To boost sensitivity while maintaining simplicity, we hypothesized that signal amplification based on the mechanism of hybridization chain reaction (HCR) (*35*) would be well-suited for adaptation to the lateral flow assay format. HCR has been previously used to provide in situ signal amplification for RNA and protein imaging within fixed biological specimens (*36–39*). In that context, target molecules are detected by probes carrying HCR initiators that trigger chain reactions in which fluorophore-labeled HCR hairpins self-assemble into tethered fluorescent HCR amplification polymers (*36–39*), generating amplified signals in situ at the locations of target molecules within cells, tissue sections, or whole-mount embryos; the specimen is then imaged with a fluorescence microscope to map the expression patterns of target molecules in an anatomical context (*36–39*, *44*, *45*). HCR signal amplification has critical properties that make it attractive for use in an at-home testing platform: HCR polymerization is isothermal and operates efficiently at room temperature, the resulting amplification polymers are tethered to their initiating probes to concentrate the amplified signal at the target location, and HCR is enzyme-free, employing robust reagents that do not require cold-storage. However, some aspects of HCR imaging protocols presented us with challenges when contemplating at-home use: multiple hands-on steps (probe addition, probe incubation, and probe removal via washing, followed by amplifier addition, amplifier incubation, and amplifier removal via washing), protocol duration (typically overnight probe incubation and overnight amplifier incubation), and the need for a fluorescence microscope to image the results. To eliminate the need for hands-on steps, we planned to attempt the use of multi-channel lateral flow devices to automatically deliver reagents to the test region in successive stages (*104*, *105*). To dramatically speed up signal amplification, we planned to work at higher reagent concentrations than are typical for HCR imaging experiments. And to eliminate the need for a fluorescence microscope, we planned to switch to colored rather than fluorescent reporters, which are bulky by comparison (potentially even larger than the HCR hairpins themselves), but can be seen by the human eye if concentrated in the test region in sufficient abundance.

As a precursor reality check, we verified that by increasing the HCR hairpin concentration, HCR amplification polymers can grow to a length of over 500 hairpins within 10 minutes (Figure C.14), matching the two orders of magnitude of signal amplification achieved in situ using overnight amplification for HCR imaging (*36*, *38*). We then set out to pursue developing an amplified HCR lateral flow assay for detecting SARS-CoV-2 viral protein.

Seeking to maintain the attractive properties of existing pregnancy tests while addressing the more demanding challenge of SARS-CoV-2 detection, we set firm design criteria:

- *Simple*: from the user's perspective, the test should be as simple to use as a pregnancy test, enabling routine at-home use by a non-expert.
- *Inexpensive*: the test device should be disposable and not require at-home instrumentation.
- *Robust*: the test should avoid reagents (e.g., enzymes) that require cold storage.
- *Rapid*: the test should return results in 1 hour or less.
- *Sensitive*: the test should have a limit of detection of 1000 virions/μL or lower.

During the two years that we have been working to achieve these goals, the testing landscape has evolved. While lab-based PCR tests remain the gold standard for SARS-CoV-2 testing, a number of unamplified lateral flow assays have been commercialized for at-home testing. These tests are simple, inexpensive, robust, and rapid, and are highly reliable when they return a positive result (e.g., 96%–100%) (*48*, *49*), but sensitivity limitations can lead to a high false-negative rate ($\approx$25% for symptomatic COVID-19 patients and $\approx$50% for asymptomatic COVID-19 patients) (*48–50*). With this work we seek to partially bridge the sensitivity gap between commercial unamplified lateral flow assays and lab-based PCR tests so as to reduce the false-negative rate for at-home testing. Other efforts to enhance sensitivity by introducing amplification into SARS-CoV-2 lateral flow assays, including use of loop-mediated isothermal amplification (LAMP) (*106*, *107*) and CRISPR/Cas (*108*, *109*), have led to compromises on simplicity, cost, and/or robustness, requiring multiple user steps, dedicated instrumentation, and/or enzymes with strict storage requirements.

Here, we have developed an amplified HCR lateral flow assay for SARS-CoV-2 protein detection that is simple, disposable, enzyme-free, returns a result in 1 hour, and achieves a limit of detection lower than all five commercial SARS-CoV-2

rapid antigen tests that we evaluated. Amplified HCR lateral flow assays fill an important sensitivity gap between current commercial lateral flow assays and PCR tests. High false-negative rates using commercial unamplified SARS-CoV-2 lateral flow tests (*48*, *49*) indicate that their limits of detection fall not in the lower tail of the distribution of clinical viral loads, but near the middle of the distribution where further reductions of the limit of detection will be maximally impactful in reducing the false-negative rate.

4.2 Results

To detect viral protein, we target the same SARS-CoV-2 nucleocapsid protein (N) that is targeted by numerous commercial SARS-CoV-2 lateral flow assays. The protein target N decorates the RNA genome within the viral envelope with $\approx 10^3$ copies/virion (*110*) (enhancing sensitivity) and is strongly immunogenic (*111*, *112*) (facilitating development of high-affinity anti-N antibodies). In a conventional lateral flow assay (Figure 4.1A), the target protein is detected in a sandwich between a reporter-labeled signal antibody that binds a first target epitope and a capture antibody that binds a second target epitope, immobilizing the signal in the test region when the target is present in the sample (*97*). If the target is sufficiently abundant, the signal in the test region is visible to the naked eye. To incorporate HCR into an amplified lateral flow assay for SARS-CoV-2 (Figure 4.1B), the anti-N signal antibody is instead labeled with one or more HCR initiators. After the antibody/target sandwich is immobilized in the test region, the HCR initiators labeling the anti-N signal antibody trigger the self-assembly of HCR hairpins into tethered HCR amplification polymers. For fluorescence imaging applications, HCR hairpins are fluorophore-labeled for imaging with a fluorescence microscope (*36–39*), but for lateral flow assays, a colored label is required to enable detection by the human eye. In order to maximize the signal per HCR hairpin while avoiding impeding polymerization kinetics by labeling hairpins with bulky colored reporters, we instead label HCR hairpins with a hapten (digoxigenin; DIG), which in turn is detected by an anti-DIG reporter antibody carrying carbon black (CB). The anti-N capture antibody is biotinylated and is itself captured in the test region by pre-immobilized polystreptavidin R (PR) (*113*, *114*).

For conventional unamplified lateral flow assays, the protein target and anti-target signal antibodies flow to the test region along a single membrane channel. For our amplified HCR lateral flow assay, we leverage prior work that explored the use of multi-channel lateral flow assays (*104*, *105*). Reagents are automatically

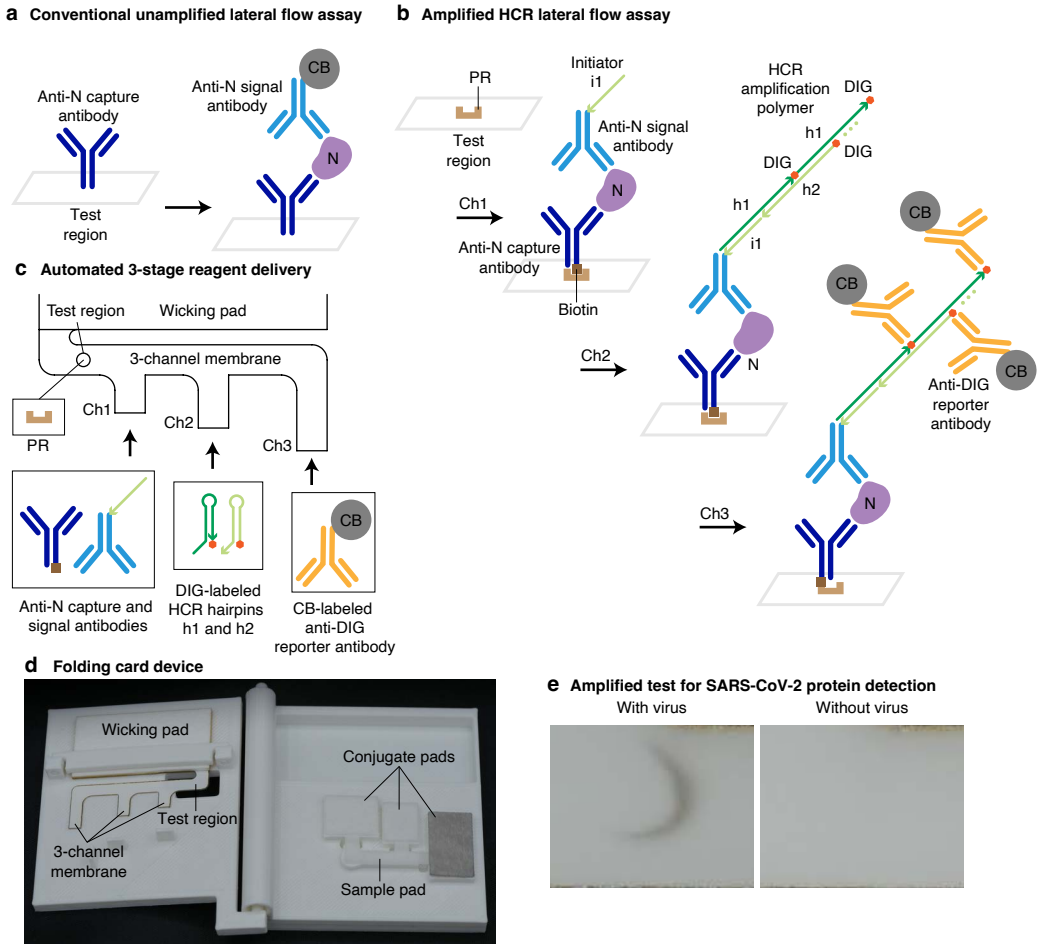

Figure 4.1: Amplified HCR lateral flow assay for SARS-CoV-2 via detection of nucleocapsid protein (N). (A) Conventional unamplified lateral flow assay. Each target protein N is immobilized in the test region in a sandwich between an anti-N capture antibody and a CB-labeled anti-N signal antibody, generating one unit of signal per target. N: nucleocapsid protein. CB: carbon black. (B) Amplified HCR lateral flow assay. Each target protein N is immobilized by PR in the test region in a sandwich between a biotinylated anti-N capture antibody and an anti-N signal antibody labeled with HCR initiator i1, triggering self-assembly of DIG-labeled HCR hairpins (h1 and h2) to form a tethered HCR amplification polymer decorated with DIG that is subsequently bound by multiple CB-labeled anti-DIG reporter antibodies, generating multiple units of signal per target. PR: polystreptavidin R. DIG: digoxigenin. (C) Automated delivery of reagents to the test region from Channels 1, 2, and 3 in succession using a 3-channel membrane. (D) Folding card device. The left page of the device contains the 3-channel membrane and wicking pad. The right page of the device contains three conjugate pads (containing dried reagents for Channels 1, 2, and 3) and a sample pad. To perform the test, the user adds the sample to the sample pad, closes the device, and reads the result after 60 min. (E) SARS-CoV-2 test with or without gamma-irradiated virus spiked into a mixture of saliva and extraction buffer at 1000 copies/μL.

delivered to the test region in three successive stages using a 3-channel membrane in which channels of different lengths lead into a unified channel before reaching the test region (Figure 4.1C). The anti-N signal and capture antibodies bind the target protein N and travel via the shortest membrane channel (Channel 1) to reach the test region first, where the antibody/target sandwich is immobilized via binding of biotinylated anti-N capture antibodies to pre-immobilized PR. DIG-labeled HCR hairpins travel via a channel of intermediate length (Channel 2) and reach the test region next, where initiators on the anti-N signal antibodies trigger growth of tethered DIG-labeled HCR amplification polymers. CB-labeled anti-DIG reporter antibodies travel via the longest channel (Channel 3) and arrive in the test region last, where they decorate the HCR amplification polymers to generate an amplified colored signal in the test region. Reagents for each channel are dried onto separate conjugate pads, which are rehydrated simultaneously when the user adds the sample to the sample pad. Upon rehydration, successive delivery of the reagents to the test region occurs automatically without user interaction, as draining of the first conjugate pad frees the unified channel for draining of the second conjugate pad, which in turn frees the unified channel for draining of the third conjugate pad (*104*). Our prototype device takes the form of a folding card (Figure 4.1D). The right page of the card contains the sample pad and three conjugate pads. The left page of the card contains the 3-channel membrane and the wicking pad, which absorbs liquid to induce continued capillary flow through the channels. The left page is functionalized with three prongs which disconnect the sample pad from the conjugate pads upon folding the card, limiting the volume that flows from each conjugate pad and preventing flow between conjugate pads.

To perform a test, the user adds saliva to a tube containing extraction buffer (disrupting the viral envelope to expose the protein targets N), adds the extracted sample to the sample pad, and closes the card to create contact between the membrane and the three conjugate pads, initiating the consecutive flow of liquid from Channels 1, 2, and 3 (Supplementary Movie 2). After 60 minutes, the user reads either a positive result (black signal) or a negative result (no signal) in the test region with the naked eye (Figure 4.1E). Due to automated multi-channel reagent delivery, this amplified HCR lateral flow assay retains the simplicity of conventional commercial unamplified lateral flow assays, requiring only sample addition and card closure before reading the result, with signal amplification occurring unbeknownst to the user.

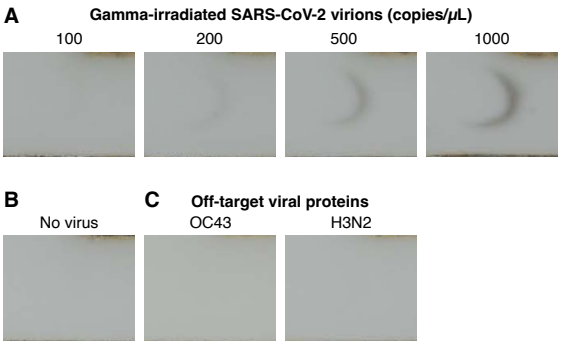

Figure 4.2: Amplified HCR lateral flow assay performance for SARS-CoV-2 via detection of nucleocapsid protein (N). (A) Sensitivity: gamma-irradiated SARS-CoV-2 spiked into a mixture of saliva and extraction buffer at different concentrations revealed a limit of detection of 200 copies/μL. (B) Background: no staining observed in the absence of virus. (C) Cross-reactivity: no staining observed for N protein from a different betacoronavirus (OC43; 83.74 ng/mL) or nucleoprotein from Influenza Type A (H3N2; 50.43 ng/mL) spiked into a mixture of saliva and extraction buffer. See Figures C.7 and C.8 for replicates.

To characterize sensitivity, we ran HCR lateral flow assays on gamma-irradiated SARS-CoV-2 virus spiked into a mixture of saliva and extraction buffer at a range of concentrations, revealing a limit of detection of 200 virus copies/μL (Figure 4.2A). No background staining was observed in the test region for experiments run without spiked-in virus (Figure 4.2B). To characterize cross-reactivity, experiments were run with spiked-in recombinant N protein from a different betacoronavirus (OC43) or with spiked-in nucleoprotein from Influenza Type A (H3N2); no staining was observed in the test region in either case even with off-target proteins at high concentration (equivalent to $\approx 10^6$ virions/μL (*110*, *115*); Figure 4.2C).

Assay performance was then benchmarked against five commercial SARS-CoV-2 lateral flow assays by spiking gamma-irradiated SARS-CoV-2 into the extraction buffer included with each test kit and loading the extracted sample according to the manufacturer's instructions. Each test was performed in triplicate at each concentration, and the limit of detection for a given kit was defined as the lowest tested concentration for which all three replicates had a visible signal. While the amplified HCR lateral flow assay detects gamma-irradiated SARS-CoV-2 at 200 copies/μL, none of the unamplified commercial tests were able to detect SARS-CoV-2 at this concentration. The limits of detection for the five kits were 500 copies/μL, 1000 copies/μL, 2000 copies/μL, 2000 copies/μL, and 20,000 copies/μL (see Table 4.1 for a summary and Figures C.7 and C.9–C.13 for replicate images). It is important

Test	Gamma-irradiated virus copies/μL 100	200	500	1,000	2,000	5,000	10,000	20,000	Duration (min)
Current work	✗✗✗	✓✓✓	✓✓✓	✓✓✓	n.t.	n.t.	n.t.	n.t.	60
BinaxNOW™	✗✗✗	✗✗✗	✗✗✗	✗✗✗	✓✓✓	n.t.	n.t.	n.t.	15
CareStart™	✗✗✗	✗✗✗	✗✗✗	✗✗✗	✓✓✓	n.t.	n.t.	n.t.	10
Flowflex®	✗✗✗	✗✗✗	✓✓✓	✓✓✓	n.t.	n.t.	n.t.	n.t.	15
GenBody	n.t.	n.t.	✗✗✗	✗✗✗	✗✗✗	✗✗✗	✗✗✗	✓✓✓	15
QuickVue®	✗✗✗	✗✗✗	✗✗✗	✓✓✓	✓✓✓	n.t.	n.t.	n.t.	10

Table 4.1: Test results for SARS-CoV-2 rapid tests detecting nucleocapsid protein (N): amplified HCR lateral flow assay vs five commercial unamplified lateral flow assays. Gamma-irradiated virus spiked into a mixture of saliva and extraction buffer (current work) or manufacturer-provided extraction buffer (commercial tests). All commercial tests use proprietary antibodies, while the current work uses commercially available antibodies. $N = 3$ replicates for each concentration. Each replicate was judged by eye for a positive (✓) or negative (✗) test result. Not tested (n.t.). See Figures C.7 and C.9–C.13 for images.

to note that these commercial tests use proprietary anti-N antibodies, the affinity of which play a critical role in assay sensitivity (*113*). Nevertheless, despite not having access to proprietary antibodies utilized by the test kit manufacturers, the HCR-amplified assay still achieves a lower limit of detection for SARS-CoV-2.

To quantify the amplification gain provided by HCR in a lateral flow context, we compared the signal using both HCR hairpins (h1 and h2) to the signal using only hairpin h1. In the h1-only condition, polymerization cannot proceed beyond the binding of h1 to the initiator, emulating the unamplified signal of a conventional lateral flow assay where each detected target generates one detectable signal. The amplification gain, calculated as the ratio of amplified to unamplified signal intensities, is 13.7 ± 0.8 (mean ± estimated standard error of the mean via uncertainty propagation for $N = 3$ replicate assays for each experiment type; Figure C.16 and Table C.2).

This amplified HCR lateral flow assay fulfills the five design requirements that we set in March 2020. Despite the incorporation of signal amplification into the assay, the test remains simple to use. Signal amplification occurs automatically using a 3-channel design, increasing sensitivity while remaining as simple as conventional unamplified lateral flow assays from the user's perspective. The inexpensive card device and reagents (PR, initiator-labeled anti-N signal antibody, biotinylated anti-N capture antibody, DIG-labeled HCR hairpins, and CB-labeled reporter antibody)

are disposable, comparable in cost to those for commercial lateral flow assays, and require no dedicated instrumentation beyond the human eye for readout. The reagents are robust and do not have cold-storage requirements. Despite the extra time required for successive automated delivery of reagents in three stages, the test remains rapid, delivering a result in 60 minutes. Finally, the assay is sensitive, enabling detection of 200 copies/μL of gamma-irradiated SARS-CoV-2 virus. This limit of detection is 2.5× to 100× lower than the limits of detection of 5 commercial SARS-CoV-2 lateral flow assays despite our lack of access to proprietary antibodies.

4.3 Discussion

Routine at-home testing with an amplified lateral flow assay could be transformative in preventing infectious disease transmission during a pandemic. For example, data and modeling suggest that more than half of SARS-CoV-2 infections are spread unknowingly by asymptomatic carriers (*116*, *117*). To enable routine at-home testing for SARS-CoV-2, we have developed an amplified HCR lateral flow assay for viral protein detection that is simple to use (comparable to a pregnancy test), inexpensive (using a disposable device with readout via the naked eye), robust (enzyme-free, using no reagents that require cold-storage), rapid (delivering a result in 60 minutes), and sensitive (detecting 200 copies/μL of gamma-irradiated SARS-CoV-2 in a mixture of saliva and extraction buffer). By comparison, five unamplified commercial lateral flow assays exhibited limits of detection that are 2.5×, 5×, 10×, 10×, and 100× higher than our amplified HCR lateral flow assay, despite the advantage of using proprietary antibodies. Lowering the limit of detection is of paramount importance because high false-negative rates using commercial unamplified SARS-CoV-2 lateral flow tests (e.g., 25%–50%) (*48*–*50*) indicate that their limits of detection fall toward the middle of the distribution of clinical viral loads, a regime in which further reduction of the limit of detection will be maximally impactful in reducing the false-negative rate.

This work demonstrates that it is possible to combine the enhanced sensitivity of HCR signal amplification with the simplicity of the lateral flow assay format, which was achieved using a 3-channel membrane to automatically deliver reagents to the test region in three successive stages without user interaction. In the future, it will be desirable to use best-in-class antibodies so that the enhanced sensitivity of HCR signal amplification pushes the limit of detection of the HCR lateral flow assay even closer to that of PCR tests. With further optimization of HCR in the context of automated lateral flow reagent delivery, there is also the potential to increase

the HCR signal gain from the current one order of magnitude to the two orders of magnitude achieved in HCR imaging applications. While we focused our assay development on saliva due to its convenience relative to nasopharyngeal swabbing (i.e., deep nasal swabbing), anterior nasal swabbing (i.e., shallow nasal swabbing) has emerged as a convenient alternative that is now used for numerous commercial SARS-CoV-2 tests and for which HCR lateral flow tests could also be developed.

While the 60-minute run time of our amplified test is higher than the 10-or-15-minute run time of unamplified commercial lateral flow assays, we anticipate that in many situations, users will prefer a test that offers superior sensitivity while still providing a result in 1 hour. In a next-generation device, it may be possible to decrease the assay duration by adjusting the material properties, configuration, and/or dimensions of the membrane channels. By switching out SARS-CoV-2 antibodies for antibodies targeting other pathogens, amplified HCR lateral flow assays offer a versatile platform for sensitive at-home testing, including for emerging pathogens.

4.4 Methods Summary

The disposable folding card device was printed with a 3D printer. The nitrocellulose membrane and wicking pad were overlapped on an adherent backing material and cut into a 3-channel geometry with a laser cutter. The sample pad was cut with a laser cutter, blocked, dried, and adhered to the right page of the card device. The conjugate pads were cut with a laser cutter, blocked, loaded with reagents (Channel 1: anti-N signal and capture antibodies; Channel 2: DIG-labeled HCR hairpins h1 and h2; Channel 3: CB-labeled anti-DIG reporter antibody), dried, and adhered to the right page of the device. The membrane was spotted with PR in the test region, dried, and adhered to the left page of the device. To run the assay, gamma-irradiated SARS-CoV-2 virus (or off-target viral protein) was spiked into a mixture of human saliva and extraction buffer to create a 300 μL test sample at the target concentration, and then the entire sample was added to the sample pad before closing the folding card device to start the test. After 60 min, the test region was photographed. For comparison tests of commercial SARS-CoV-2 lateral flow assays, gamma-irradiated SARS-CoV-2 virus was added directly to the extraction buffer provided by the manufacturer.

Chapter 5

CONCLUSIONS

HCR RNA-FISH v3.0 and HCR IF enable quantitative, sensitive, user-friendly imaging of RNA and protein targets in highly autofluorescent tissues, permitting multidimensional quantitative study of gene expression at high resolution within the anatomical context of biological samples (*36*, *39*). This thesis furthers the capabilities of HCR in three domains, enabling 10-plex quantitative imaging of RNA and protein targets in highly autofluorescent samples, multiplexed detection of protein:protein complexes, and amplified at-home detection of infectious disease.

In Chapter 2, we effectively double the number of targets researchers can simultaneously image by developing a 10-plex spectral imaging and linear unmixing method. With 10-plex HCR imaging, signal amplification is performed concurrently for RNA and protein targets. Targets detected by 10-plex HCR imaging are unrestricted in expression level and anatomical location, permitting detection of high- and low-expression targets with overlapping expression patterns. Robust linear unmixing generates quantitative voxel intensities across all 10 channels, allowing for relative quantitation of target expression. We show that spectral imaging with linear unmixing enables digital HCR imaging for absolute quantitation of RNA expression, detecting single-molecule punctae in a whole-mount zebrafish embryo. Because the signal generated from each target is amplified by an orthogonal HCR system, users can perform 10-plex imaging even in highly autofluorescent tissues, such as whole-mount vertebrate embryos and mouse brain sections.

In Chapter 3, we draw on the split-initiator principle of HCR RNA-FISH v3.0 and demonstrate HCR imaging of protein:protein complexes (*39*). Each protein of the complex is bound by an antibody carrying half of an HCR initiator, and a DNA ruler strand colocalizes the two initiator halves if the antibodies bind proximal to one another in the sample, forming a full HCR initiator to trigger signal amplification. If the two proteins are not proximal to one another, the ruler strand is incapable of binding to both fractional initiator probes, preventing colocalization of a full HCR initiator. As a built-in feature, quantitative HCR imaging of protein:protein complexes generates subcellular voxel intensities that scale with the number of protein:protein complexes present. We further demonstrate multiplexed detection

of protein:protein complexes by using the NUPACK software suite to design three sets of interaction probes and ruler strands. Lastly, we describe a unified protocol for the co-detection of RNA targets, protein targets, and protein:protein complexes.

In Chapter 4, we demonstrate that the room-temperature, enzyme-free signal amplification mechanism of HCR makes it well-suited for sensitive at-home detection of infectious disease. While laboratory-based PCR tests achieve the most sensitive detection of pathogenic nucleic acids, they require laboratory instrumentation and can take hours or days to return a result (*46*, *47*). In contrast, at-home lateral flow antigen tests allow users to test themselves for the presence of viral protein within 10–15 minutes, but the absence of signal amplification leads to an unacceptably high rate of false-negative results (*48–50*). We aimed to bridge the sensitivity gap between these two test types while preserving the simplicity of the lateral flow assay format, enabling users to perform one-step, amplified detection of pathogenic protein in one hour or less. Leveraging a 3-channel assay format for automated delivery of initiator-labeled antibody, HCR hairpins, and a colorimetric readout antibody, we demonstrate a limit of detection for the SARS-CoV-2 N protein that is between 2.5× and 100× lower than five commercial unamplified antigen tests. From the user's perspective, the test remains as simple to use as a conventional lateral flow assay, only requiring sample addition before closing the device, and the result is returned to the user within an hour.

5.1 Future Directions

HCR spectral imaging: 10-Plex quantitative RNA fluorescence in situ hybridization and immunofluorescence in highly autofluorescent samples

While we demonstrate robust imaging of 10 targets, higher levels of multiplexing may be achievable. Using fluorophores with narrower excitation and emission spectra would lessen crosstalk between channels, allowing for more fluorophores to be used while preserving robust unmixing performance. Another means of increasing the number of fluorophores without increasing crosstalk is to use fluorophores with similar excitation spectra but different emission spectra (i.e., fluorophores with different Stokes shifts). This would allow for the same wavelength of light to excite multiple fluorophores, while the emission spectra could be distinguished by using bandpass filters at different wavelengths. As an additional axis for fluorophore separation, the fluorescence lifetime of each fluorophore could be used to distinguish fluorophores with highly overlapping spectra. The fluorescence lifetime describes the amount of time it takes for a fluorophore to emit a photon after being excited

to a high-energy state. When using a pulsed laser, in which the light source is rapidly cycled on and off, microscopes can measure the fluorescence lifetime by characterizing the fluorescence decay during the time when the laser light is off (*118*); this functionality is present on modern day confocal fluorescence microscopes such as the Leica Stellaris 8. With fluorescence lifetime imaging, it may be possible to use fluorophores with overlapping excitation and emission spectra if their fluorescence lifetimes are sufficiently distinguishable from one another, and this information could be incorporated into an unmixing algorithm as an additional dimension for fluorophore separation. A new unmixing algorithm could also incorporate other unmixing paradigms, such as mutual information minimization, which may offer even better performance than linear unmixing (*119*). Lastly, in addition to one 10-plex imaging round, it may be possible to perform multiple 10-plex imaging rounds in which the signal is extinguished or removed between rounds, though this approach would be largely limited to samples affixed to a coverslip or slide due to the need for image alignment between imaging rounds. For each of these possible future directions, simplicity from the user's perspective and unmixing fidelity must be rigorously upheld.

Multiplexed quantitative imaging of protein:protein complexes using cooperative probes for logical control over HCR signal amplification

In addition to detecting protein:protein complexes, it may be possible to detect complexes of other types of biological macromolecules with automatic background suppression. These include RNA:RNA complexes, which would be of particular interest in the case of mRNA translation, as well as RNA:protein complexes. Another variation of the method could allow for users to examine the degree of proximity between two targets of interest by changing the length of the DNA ruler strand. For example, if the ruler strand is shortened, it may no longer be able to bind to both interaction probes labeling the secondary antibodies, preventing HCR signal amplification. Users could perform several experiments in parallel with different ruler strand lengths and observe the ruler strand length that is sufficient for HCR signal amplification, providing additional information regarding how proximal the targets are to one another.

To further improve the user-friendliness of the method, another future direction is to employ oligonucleotide-labeled primary antibodies instead of oligonucleotide-labeled secondary antibodies. This would remove the requirement of using primary antibodies from different species or isotypes, though this would also likely re-

sult in the formation of fewer P1-P2-ruler junctions (due to the ability of multiple secondary antibodies to bind each primary antibody), reducing the signal intensity. As a prerequisite to using labeled primary antibodies, novel approaches for oligonucleotide-antibody conjugation should be explored to reduce the likelihood that the conjugation disrupts the epitope-binding site of the antibody.

HCR lateral flow tests for sensitive, instrument-free, at-home pathogen detection

A next-generation device for HCR lateral flow assays could focus on achieving enhanced sensitivity. We estimated the polymer length of the current iteration of the test by determining the ratio of the signal intensities for two experiment types using fluorescent hairpins: in one experiment, both hairpins h1 and h2 are added, while in another experiment, only hairpin h1 is added, preventing polymerization beyond binding of the first HCR hairpin (Figure C.15 and Table C.1). We found an estimated polymer length of 41 ± 8 (mean ± estimated standard error of the mean via uncertainty propagation for $N = 3$ replicate assays for each experiment type), which is below the polymer length we have previously observed for in situ HCR experiments (*36*, *39*). While we may not expect to reach the same polymer length as in situ experiments due to the shortened amplification time, we nevertheless know it is possible for polymers to grow beyond the polymer length we observe. To achieve longer polymers, we could explore using other HCR systems, which may have faster polymerization times. We could also increase the concentration of HCR hairpins to speed polymerization, and we could explore using multiple layers of polymers to achieve quadratic HCR signal amplification, though this approach may increase the test duration. Lastly, in the future, it will be desirable to use high-performance, best-in-class antibodies so that the enhanced sensitivity of HCR signal amplification pushes the limit of detection of the HCR lateral flow assay even closer to that of PCR tests.

Another method to enhance sensitivity is to optimize the colorimetric label on the readout antibody of Channel 3. We estimated the amplification gain for the current iteration of the assay using a similar approach for determining the polymer length, instead using DIG-labeled HCR hairpins and an anti-DIG carbon black antibody in Channel 3, observing an estimated amplification gain of 13.7 ± 0.8 (mean ± estimated standard error of the mean via uncertainty propagation for $N = 3$ replicate assays for each experiment type; Figure C.16 and Table C.2). Taken together, the estimated polymer length of 41 ± 8 and the estimated amplification gain of 13.7

± 0.8 strikingly indicates that roughly two out of three hairpins are not bound by a readout antibody from Channel 3. To further increase sensitivity, it would be desirable for each HCR hairpin to bind to a colorimetric readout antibody. The low amplification gain we currently observe is likely a function of the size of the carbon black nanoparticle, which leads to a crowding effect preventing adjacent DIG haptens from binding to a readout antibody. Therefore, it may be that smaller colorimetric labels allow for more readout antibodies to bind to the amplification polymer, further increasing the signal intensity. However, smaller colorimetric labels may also generate less signal, so the effect of more colorimetric labels becoming captured at the test line may be counteracted by the lower signal intensity of each label.

While the current test provides results within one hour, conventional lateral flow tests provide a result within 10–15 minutes. To decrease the running time of an HCR lateral flow assay, it may be possible to consolidate all signal amplification reagents into a single channel via layered delivery of reagents (*120*) or via depositing all reagents onto the same conjugate pad. One possible hurdle to depositing all reagents on the same conjugate pad is that long polymers decorated with readout antibodies that form before reaching the test line may become too large to flow through the small pores of the nitrocellulose membrane. Alternatively, to shorten the assay duration, it may be possible to explore new 3-channel geometries with shorter channel lengths.

Lastly, to increase the versatility of the test, future iterations of the assay could perform multiplexed detection of pathogens by using antibodies specific to target proteins from each pathogen. Capture antibodies could be deposited in spatially separate test regions, and users would then determine which pathogen is present in the sample based on the location of the test region that generates a signal. The signal antibodies could use initiators from the same HCR system, though this may lead to a depletion of HCR hairpins if multiple pathogens are present. If depletion occurs, each signal antibody could instead use an orthogonal HCR initiator, and each HCR amplifier would then correspond to only one pathogen. Lastly, if the colorimetric readout antibody is depleted due to the presence of multiple pathogens, the HCR hairpins from different systems could be labeled with orthogonal haptens. In this case, each HCR amplifier and colorimetric readout antibody would only correspond to one pathogen.

BIBLIOGRAPHY

(*1*) Di Liegro, C. M., Schiera, G., and Di Liegro, I. (2014). Regulation of mRNA transport, localization and translation in the nervous system of mammals (Review). *International Journal of Molecular Medicine 33*, 747–762.

(*2*) Sahni, N. et al. (2015). Widespread macromolecular interaction perturbations in human genetic disorders. *Cell 161*, 647–660.

(*3*) Murakami, Y., Tripathi, L. P., Prathipati, P., and Mizuguchi, K. (2017). Network analysis and in silico prediction of protein–protein interactions with applications in drug discovery. *Current Opinion in Structural Biology 44*, 134–142.

(*4*) Coons, A. H., Creech, H. J., Jones, R. N., and Berliner, E. (1942). The demonstration of pneumococcal antigen in tissues by the use of fluorescent antibody. *The Journal of Immunology 45*, 159–170.

(*5*) Gall, J. G., and Pardue, M. L. (1969). Formation and detection of RNA-DNA hybrid molecules in cytological preparations. *Proceedings of the National Academy of Sciences of the United States of America 63*, 378–383.

(*6*) John, H. A., Birnstiel, M. L., and Jones, K. W. (1969). RNA-DNA hybrids at the cytological level. *Nature 223*, 582–587.

(*7*) Buongiorno-Nardelli, M., and Amaldi, F. (1970). Autoradiographic detection of molecular hybrids between rRNA and DNA in tissue sections. *Nature 225*, 946–948.

(*8*) Harrison, P. R., Conkie, D., and Paul, J. (1973). Localisation of cellular globin messenger RNA by in situ hybridisation to complementary DNA. *FEBS Letters 32*, 109–112.

(*9*) Femino, A., Fay, F. S., Fogarty, K., and Singer, R. H. (1998). Visualization of single RNA transcripts in situ. *Science 280*, 585–590.

(*10*) Barroso-Chinea, P., Aymerich, M. S., Castle, M. M., Perez-Manso, M., Tunon, T., Erro, E., and Lanciego, J. L. (2007). Detection of two different mRNAs in a single section by dual in situ hybridization: A comparison between colorimetric and fluorescent detection. *Journal of Neuroscience Methods 162*, 119–128.

(*11*) Levsky, J. M., Shenoy, S. M., Pezo, R. C., and Singer, R. H. (2002). Single-cell gene expression profiling. *Science 297*, 836–840.

(*12*) Kosman, D., Mizutani, C. M., Lemons, D., Cox, W. G., McGinnis, W., and Bier, E. (2004). Multiplex detection of RNA expression in *Drosophila* embryos. *Science 305*, 846.

(*13*) Raj, A., van den Bogaard, P., Rifkin, S. A., van Oudenaarden, A., and Tyagi, S. (2008). Imaging individual mRNA molecules using multiple singly labeled probes. *Nature Methods 5*, 877–879.

(*14*) Bobrow, M. N., Harris, T. D., Shaughnessy, K. J., and Litt, G. J. (1989). Catalyzed reporter deposition, a novel method of signal amplification application to immunoassays. *Journal of Immunological Methods 125*, 279–285.

(*15*) Hunyady, B., Krempels, K., Harta, G., and Mezey, E. (1996). Immunohistochemical signal amplification by catalyzed reporter deposition and its application in double immunostaining. *Journal of Histochemistry and Cytochemistry 44*, 1353–1362.

(*16*) Tautz, D., and Pfeifle, C. (1989). A non-radioactive in situ hybridization method for the localization of specific RNAs in *Drosophila* embryos reveals translational control of the segmentation gene hunchback. *Chromosoma 98*, 81–85.

(*17*) Kerstens, H. M. J., Poddighe, P. J., and Hanselaar, A. G. J. M. (1995). A novel in-situ hybridization signal amplification method based on the deposition of biotinylated tyramine. *Journal of Histochemistry and Cytochemistry 43*, 347–352.

(*18*) Piette, D., Hendrickx, M., Willems, E., Kemp, C. R., and Leyns, L. (2008). An optimized procedure for whole-mount in situ hybridization on mouse embryos and embryoid bodies. *Nature Protocols 3*, 1194–1201.

(*19*) Glass, G., Papin, J. A., and Mandell, J. W. (2009). SIMPLE: A sequential immunoperoxidase labeling and erasing method. *Journal of Histochemistry and Cytochemistry 57*, 899–905.

(*20*) Tsujikawa, T. et al. (2017). Quantitative multiplex immunohistochemistry reveals myeloid-inflamed tumor-immune complexity associated with poor prognosis. *Cell Reports 19*, 203–217.

(*21*) Collins, M. L., Irvine, B., Tyner, D., Fine, E., Zayati, C., Chang, C. A., Horn, T., Ahle, D., Detmer, J., Shen, L.-P., Kolberg, J., Bushnell, S., Urdea, M. S., and Ho, D. D. (1997). A branched DNA signal amplification assay for quantification of nucleic acid targets below 100 molecules/ml. *Nucleic Acids Research 25*, 2979–2984.

(*22*) Bushnell, S., Budde, J., Catino, T., Cole, J., Derti, A., Kelso, R., Collins, M. L., Molino, G., Sheridan, P., Monahan, J., and Urdea, M. (1999). ProbeDesigner: for the design of probesets for branched DNA (bDNA) signal amplification assays. *Bioinformatics 15*, 348–355.

(*23*) Player, A. N., Shen, L.-P., Kenny, D., Antao, V. P., and Kolberg, J. A. (2001). Single-copy gene detection using branched DNA (bDNA) in situ hybridization. *Journal of Histochemistry and Cytochemistry 49*, 603–611.

(*24*) Wang, F., Flanagan, J., Su, N., Wang, L.-C., Bui, S., Nielson, A., Wu, X. Y., Vo, H.-T., Ma, X.-J., and Luo, Y. L. (2012). RNAscope: a novel in situ RNA analysis platform for formalin-fixed, paraffin-embedded tissues. *Journal of Molecular Diagnostics 14*, 22–29.

(*25*) Kishi, J. Y., Lapan, S. W., Beliveau, B. J., West, E. R., Zhu, A., Sasaki, H. M., Saka, S. K., Wang, Y., Cepko, C. L., and Yin, P. (2019). SABER amplifies FISH: enhanced multiplexed imaging of RNA and DNA in cells and tissues. *Nature Methods 16*, 533–544.

(*26*) Saka, S. K. et al. (2019). Immuno-SABER enables highly multiplexed and amplified protein imaging in tissues. *Nature Biotechnology 37*, 1080–1090.

(*27*) Zhou, Y., Calciano, M., Hamann, S., Leamon, J. H., Strugnell, T., Christian, M. W., and Lizardi, P. M. (2001). In situ detection of messenger RNA using digoxigenin-labeled oligonucleotides and rolling circle amplification. *Experimental and Molecular Pathology 70*, 281–288.

(*28*) Larsson, C., Koch, J., Nygren, A., Janssen, G., Raap, A. K., Landegren, U., and Nilsson, M. (2004). In situ genotyping individual DNA molecules by target-primed rolling-circle amplification of padlock probes. *Nature Methods 1*, 227–232.

(*29*) Larsson, C., Grundberg, I., Söderberg, O., and Nilsson, M. (2010). In situ detection and genotyping of individual mRNA molecules. *Nature Methods 7*, 395–397.

(*30*) Aldridge, S., and Teichmann, S. A. (2020). Single cell transcriptomics comes of age. *Nature Communications 11*, 4307.

(*31*) Lubeck, E., Coskun, A. F., Zhiyentayev, T., Ahmad, M., and Cai, L. (2014). Single-cell in situ RNA profiling by sequential hybridization. *Nature Methods 11*, 360–1.

(*32*) Moffitt, J. R., and Zhuang, X. (2016). RNA imaging with Multiplexed Error-Robust Fluorescence In Situ Hybridization (MERFISH). *Methods in Enzymology 572*, 1–49.

(*33*) Lin, J.-R., Fallahi-Sichani, M., and Sorger, P. K. (2015). Highly multiplexed imaging of single cells using a high-throughput cyclic immunofluorescence method. *Nature Communications 6*, 8390.

(*34*) Xia, C., Fan, J., Emanuel, G., Hao, J., and Zhuang, X. (2019). Spatial transcriptome profiling by MERFISH reveals subcellular RNA compartmentalization and cell cycle-dependent gene expression. *Proceedings of the National Academy of Sciences of the United States of America 116*, 19490–19499.

(*35*) Dirks, R. M., and Pierce, N. A. (2004). Triggered amplification by hybridization chain reaction. *Proceedings of the National Academy of Sciences of the United States of America 101*, 15275–15278.

(*36*) Schwarzkopf, M., Liu, M. C., Schulte, S. J., Ives, R., Husain, N., Choi, H. M. T., and Pierce, N. A. (2021). Hybridization chain reaction enables a unified approach to multiplexed, quantitative, high-resolution immunohistochemistry and in situ hybridization. *Development 148*, dev199847.

(*37*) Choi, H. M. T., Chang, J. Y., Trinh, L. A., Padilla, J. E., Fraser, S. E., and Pierce, N. A. (2010). Programmable in situ amplification for multiplexed imaging of mRNA expression. *Nature Biotechnology 28*, 1208–12.

(*38*) Choi, H. M. T., Beck, V. A., and Pierce, N. A. (2014). Next-generation in situ hybridization chain reaction: Higher gain, lower cost, greater durability. *ACS Nano 8*, 4284–4294.

(*39*) Choi, H. M. T., Schwarzkopf, M., Fornace, M. E., Acharya, A., Artavanis, G., Stegmaier, J., Cunha, A., and Pierce, N. A. (2018). Third-generation in situ hybridization chain reaction: multiplexed, quantitative, sensitive, versatile, robust. *Development 145*, dev165753.

(*40*) Zadeh, J. N., Steenberg, C. D., Bois, J. S., Wolfe, B. R., Pierce, M. B., Khan, A. R., Dirks, R. M., and Pierce, N. A. (2011). NUPACK: Analysis and design of nucleic acid systems. *Journal of Computational Chemistry 32*, 170–173.

(*41*) Wolfe, B. R., Porubsky, N. J., Zadeh, J. N., Dirks, R. M., and Pierce, N. A. (2017). Constrained multistate sequence design for nucleic acid reaction pathway engineering. *Journal of the American Chemical Society 139*, 3134–3144.

(*42*) Fornace, M. E., Porubsky, N. J., and Pierce, N. A. (2020). A unified dynamic programming framework for the analysis of interacting nucleic acid strands: enhanced models, scalability, and speed. *ACS Synthetic Biology 9*, 2665–2678.

(*43*) Trivedi, V., Choi, H. M. T., Fraser, S. E., and Pierce, N. A. (2018). Multidimensional quantitative analysis of mRNA expression within intact vertebrate embryos. *Development 145*, dev156869.

(*44*) Shah, S., Lubeck, E., Schwarzkopf, M., He, T.-F., Greenbaum, A., Sohn, C. H., Lignell, A., Choi, H. M. T., Gradinaru, V., Pierce, N. A., and Cai, L. (2016). Single-molecule RNA detection at depth via hybridization chain reaction and tissue hydrogel embedding and clearing. *Development 143*, 2862–2867.

(*45*) Choi, H. M. T. et al. (2016). Mapping a multiplexed zoo of mRNA expression. *Development 143*, 3632–3637.

(*46*) Corman, V. M. et al. (2020). Detection of 2019 novel coronavirus (2019-nCoV) by real-time RT-PCR. *Eurosurveillance 25*, DOI: 10.2807/1560-7917.ES.2020.25.3.2000045.

(*47*) Chan, J. F.-W. et al. (2020). Improved molecular diagnosis of COVID-19 by the novel, highly sensitive and specific COVID-19-RdRp/Hel real-time reverse transcription-polymerase chain reaction assay validated *in vitro* and with clinical specimens. *Journal of Clinical Microbiology 58*, 1–10.

(*48*) Caruana, G., Croxatto, A., Kampouri, E., Kritikos, A., Opota, O., Foerster, M., Brouillet, R., Senn, L., Lienhard, R., Egli, A., Pantaleo, G., Carron, P.-N., and Greub, G. (2021). Implementing SARS-CoV-2 rapid antigen testing in the emergency ward of a Swiss university hospital: The INCREASE study. *Microorganisms 9*, 798.

(*49*) Wölfl-Duchek, M., Bergmann, F., Jorda, A., Weber, M., Müller, M., Seitz, T., Zoufaly, A., Strassl, R., Zeitlinger, M., Herkner, H., Schnidar, H., Anderle, K., and Derhaschnig, U. (2022). Sensitivity and specificity of SARS-CoV-2 rapid antigen detection tests using oral, anterior nasal, and nasopharyngeal swabs: A diagnostic accuracy study. *Microbiology Spectrum 10*, ed. by Mostafa, H. H., e02029–21.

(*50*) Dinnes, J. et al. (2022). Rapid, point-of-care antigen tests for diagnosis of SARS-CoV-2 infection. *Cochrane Database of Systematic Reviews 2022*, ed. by Cochrane Infectious Diseases Group, DOI: 10.1002/14651858.CD013705.pub3.

(*51*) Coons, A. H., Creech, H. J., and Jones, R. N. (1941). Immunological properties of an antibody containing a fluorescent group. *Proceedings of the Society of Experimental Biology and Medicine 47*, 200–202.

(*52*) Kim, S.-W., Roh, J., and Park, C.-S. (2016). Immunohistochemistry for pathologists: protocols, pitfalls, and tips. *Journal of Pathology and Translational Medicine 50*, 411–418.

(*53*) Qian, X., Jin, L., and Lloyd, R. V. (2004). In situ hybridization: Basic approaches and recent development. *The Journal of Histotechnology 27*, 53–67.

(*54*) Qian, X., and Lloyd, R. V. (2003). Recent developments in signal amplification methods for in situ hybridization. *Diagnostic Molecular Pathology 12*, 1–13.

(*55*) Ramos-Vara, J. A., and Miller, M. A. (2014). When tissue antigens and antibodies get along: revisiting the technical aspects of immunohistochemistry-the red, brown, and blue technique. *Veterinary Pathology 51*, 42–87.

(*56*) Chen, F., Tillberg, P. W., and Boyden, E. S. (2015). Expansion microscopy. *Science 347*, 543–548.

(*57*) Shah, S., Lubeck, E., Zhou, W., and Cai, L. (2016). In situ transcription profiling of single cells reveals spatial organization of cells in the mouse hippocampus. *Neuron 92*, 342–357.

(*58*) Garini, Y., Young, I. T., and McNamara, G. (2006). Spectral imaging: principles and applications. *Cytometry A 69*, 735–47.

(*59*) Valm, A. M., Oldenbourg, R., and Borisy, G. G. (2016). Multiplexed spectral imaging of 120 different fluorescent labels. *PLoS One 11*, e0158495.

(*60*) Cutrale, F., Trivedi, V., Trinh, L. A., Chiu, C. L., Choi, J. M., Artiga, M. S., and Fraser, S. E. (2017). Hyperspectral phasor analysis enables multiplexed 5D in vivo imaging. *Nature Methods 14*, 149–152.

(*61*) Mansfield, J. R., Hoyt, C., and Levenson, R. M. (2008). Visualization of microscopy-based spectral imaging data from multi-label tissue sections. *Current Protocols in Molecular Biology 84*, 14.19.1–14.19.15.

(*62*) Moreno-Ayala, R., Schnabel, D., Salas-Vidal, E., and Lomelí, H. (2015). PIAS-like protein Zimp7 is required for the restriction of the zebrafish organizer and mesoderm development. *Developmental Biology 403*, 89–100.

(*63*) Jurynec, M. J., Bai, X., Bisgrove, B. W., Jackson, H., Nechiporuk, A., Palu, R. A. S., Grunwald, H. A., Su, Y.-C., Hoshijima, K., Yost, H. J., Zon, L. I., and Grunwald, D. J. (2019). The Paf1 Complex and P-TEFb have reciprocal and antagonist roles in maintaining multipotent neural crest progenitors. *Development*, dev.180133.

(*64*) Chen, J., Poskanzer, K. E., Freeman, M. R., and Monk, K. R. (2020). Live-imaging of astrocyte morphogenesis and function in zebrafish neural circuits. *Nature Neuroscience 23*, 1297–1306.

(*65*) Kok, F. O., Taibi, A., Wanner, S. J., Xie, X., Moravec, C. E., Love, C. E., Prince, V. E., Mumm, J. S., and Sirotkin, H. I. (2012). Zebrafish *rest* regulates developmental gene expression but not neurogenesis. *Development 139*, 3838–3848.

(*66*) Ganassi, M., Badodi, S., Ortuste Quiroga, H. P., Zammit, P. S., Hinits, Y., and Hughes, S. M. (2018). Myogenin promotes myocyte fusion to balance fibre number and size. *Nature Communications 9*, 4232.

(*67*) Ruf-Zamojski, F., Trivedi, V., Fraser, S. E., and Trinh, L. A. (2015). Spatiotemporal differences in dystrophin dynamics at mRNA and protein levels revealed by a novel FlipTrap line. *PLoS One 10*, e0128944.

(*68*) Dobrzycki, T., Mahony, C. B., Krecsmarik, M., Koyunlar, C., Rispoli, R., Peulen-Zink, J., Gussinklo, K., Fedlaoui, B., De Pater, E., Patient, R., and Monteiro, R. (2020). Deletion of a conserved Gata2 enhancer impairs haemogenic endothelium programming and adult Zebrafish haematopoiesis. *Communications Biology 3*, 71.

(*69*) Gjini, E. et al. (2015). A zebrafish model of myelodysplastic syndrome produced through *tet2* genomic editing. *Molecular and Cellular Biology 35*, 789–804.

(*70*) Giasson, B. I., and Mushynski, W. E. (1996). Aberrant stress-induced phosphorylation of perikaryal neurofilaments. *Journal of Biological Chemistry 271*, 30404–30409.

(*71*) Zhang, Z. et al. (2021). Monomeric C-reactive protein via endothelial CD31 for neurovascular inflammation in an ApoE genotype-dependent pattern: A risk factor for Alzheimer's disease? *Aging Cell 20*, e13501.

(*72*) Lucas, C.-H., Calvez, M., Babu, R., and Brown, A. (2014). Altered subcellular localization of the NeuN/Rbfox3 RNA splicing factor in HIV-associated neurocognitive disorders (HAND). *Neuroscience Letters 558*, 97–102.

(*73*) Wang, Y., Kerrisk Campbell, M., Tom, I., Foreman, O., Hanson, J. E., and Sheng, M. (2020). PCDH7 interacts with GluN1 and regulates dendritic spine morphology and synaptic function. *Scientific Reports 10*, 10951.

(*74*) Tasic, B. et al. (2018). Shared and distinct transcriptomic cell types across neocortical areas. *Nature 563*, 72–78.

(*75*) Tiveron, M.-C., Beurrier, C., Céni, C., Andriambao, N., Combes, A., Koehl, M., Maurice, N., Gatti, E., Abrous, D. N., Kerkerian-Le Goff, L., Pierre, P., and Cremer, H. (2016). LAMP5 fine-tunes GABAergic synaptic transmission in defined circuits of the mouse brain. *PLoS One 11*, ed. by Pendyala, G., e0157052.

(*76*) Zeisel, A., Muñoz-Manchado, A. B., Codeluppi, S., Lönnerberg, P., La Manno, G., Juréus, A., Marques, S., Munguba, H., He, L., Betsholtz, C., Rolny, C., Castelo-Branco, G., Hjerling-Leffler, J., and Linnarsson, S. (2015). Cell types in the mouse cortex and hippocampus revealed by single-cell RNA-seq. *Science 347*, 1138–1142.

(*77*) Vogel, C., and Marcotte, E. M. (2012). Insights into the regulation of protein abundance from proteomic and transcriptomic analyses. *Nature Reviews Genetics 13*, 227–232.

(*78*) Koussounadis, A., Langdon, S. P., Um, I. H., Harrison, D. J., and Smith, V. A. (2015). Relationship between differentially expressed mRNA and mRNA-protein correlations in a xenograft model system. *Scientific Reports 5*, 10775.

(*79*) Söderberg, O., Gullberg, M., Jarvius, M., Ridderstrale, K., Leuchowius, K. J., Jarvius, J., Wester, K., Hydbring, P., Bahram, F., Larsson, L. G., and Landegren, U. (2006). Direct observation of individual endogenous protein complexes in situ by proximity ligation. *Nature Methods 3*, 995–1000.

(*80*) Leuchowius, K. J., Clausson, C. M., Grannas, K., Erbilgin, Y., Botling, J., Zieba, A., Landegren, U., and Söderberg, O. (2013). Parallel visualization of multiple protein complexes in individual cells in tumor tissue. *Molecular & Cellular Proteomics 12*, 1563–71.

(*81*) Koos, B., Andersson, L., Clausson, C. M., Grannas, K., Klaesson, A., Cane, G., and Söderberg, O. (2014). Analysis of protein interactions in situ by proximity ligation assays. *Current Topics in Microbiology and Immunology 377*, 111–26.

(*82*) Klaesson, A., Grannas, K., Ebai, T., Heldin, J., Koos, B., Leino, M., Raykova, D., Oelrich, J., Arngården, L., Söderberg, O., and Landegren, U. (2018). Improved efficiency of in situ protein analysis by proximity ligation using UnFold probes. *Scientific Reports 8*, 5400.

(*83*) Koos, B. et al. (2015). Proximity-dependent initiation of hybridization chain reaction. *Nature Communications 6*, 7294.

(*84*) Leino, M., Heldin, J., Sander, M. R., Kermpatsou, D., Raykova, D., Koos, B., and Söderberg, O. (2019). Optimization of proximity-dependent initiation of hybridization chain reaction for improved performance. *Molecular Systems Design & Engineering 4*, 1058–1065.

(*85*) Chitaev, N. A., and Troyanovsky, S. M. (1998). Adhesive but not lateral E-cadherin complexes require calcium and catenins for their formation. *Journal of Cell Biology 142*, 837–846.

(*86*) Wahl, J. K., Kim, Y. J., Cullen, J. M., Johnson, K. R., and Wheelock, M. J. (2003). N-cadherin-catenin complexes form prior to cleavage of the proregion and transport to the plasma membrane. *Journal of Biological Chemistry 278*, 17269–17276.

(*87*) Yano, H., Mazaki, Y., Kurokawa, K., Hanks, S. K., Matsuda, M., and Sabe, H. (2004). Roles played by a subset of integrin signaling molecules in cadherin-based cell–cell adhesion. *Journal of Cell Biology 166*, 283–295.

(*88*) Dionne, C. J., Tse, K. Y., Weiss, A. H., Franco, C. B., Wiest, D. L., Anderson, M. K., and Rothenberg, E. V. (2005). Subversion of T lineage commitment by PU.1 in a clonal cell line system. *Developmental Biology 280*, 448–466.

(*89*) Petrovick, M. S., Hiebert, S. W., Friedman, A. D., Hetherington, C. J., Tenen, D. G., and Zhang, D. (1998). Multiple functional domains of AML1: PU.1 and C/EBPα synergize with different regions of AML1. *Molecular and Cellular Biology 18*, 3915–3925.

(*90*) Rothenberg, E. V., Hosokawa, H., and Ungerbäck, J. (2019). Mechanisms of action of hematopoietic transcription factor PU.1 in initiation of T-cell development. *Frontiers in Immunology 10*, 228.

(*91*) Shin, B., Hosokawa, H., Romero-Wolf, M., Zhou, W., Masuhara, K., Tobin, V. R., Levanon, D., Groner, Y., and Rothenberg, E. V. (2021). Runx1 and Runx3 drive progenitor to T-lineage transcriptome conversion in mouse T cell commitment via dynamic genomic site switching. *Proceedings of the National Academy of Sciences of the United States of America 118*, e2019655118.

(*92*) Berx, G., and Roy, F. V. (2021). The E-cadherin/catenin complex: An important gatekeeper in breast cancer tumorigenesis and malignant progression. *Breast Cancer Research 3*, 289.

(*93*) Karayiannakis, A. J., Nakopoulou, L., Gakiopoulou, H., Keramopoulos, A., Davaris, P. S., and Pignatelli, M. (2001). Expression patterns of β-catenin in in situ and invasive breast cancer. *European Journal of Surgical Oncology (EJSO) 27*, 31–36.

(*94*) Hanewich-Hollatz, M. H., Chen, Z., Hochrein, L. M., Huang, J., and Pierce, N. A. (2019). Conditional guide RNAs: Programmable conditional regulation of CRISPR/Cas function in bacterial and mammalian cells via dynamic RNA nanotechnology. *ACS Central Science 5*, 1241–1249.

(*95*) Söderberg, O., Leuchowius, K.-J., Gullberg, M., Jarvius, M., Weibrecht, I., Larsson, L.-G., and Landegren, U. (2008). Characterizing proteins and their interactions in cells and tissues using the in situ proximity ligation assay. *Methods 45*, 227–232.

(*96*) Greenwood, C., Ruff, D., Kirvell, S., Johnson, G., Dhillon, H. S., and Bustin, S. A. (2015). Proximity assays for sensitive quantification of proteins. *Biomolecular Detection and Quantification 4*, 10–16.

(*97*) Tiplady, S. In *The Immunoassay Handbook*; Elsevier: 2013, pp 533–536.

(*98*) Larsen, J., Buchanan, P., Johnson, S., Godbert, S., and Zinaman, M. (2013). Human chorionic gonadotropin as a measure of pregnancy duration. *International Journal of Gynecology & Obstetrics 123*, 189–195.

(*99*) Gnoth, C., and Johnson, S. (2014). Strips of hope: accuracy of home pregnancy tests and new developments. *Geburtshilfe und Frauenheilkunde 74*, 661–669.

(*100*) Khelifa, L., Hu, Y., Jiang, N., and Yetisen, A. K. (2022). Lateral flow assays for hormone detection. *Lab on a Chip 22*, 2451–2475.

(*101*) To, K. K.-W. et al. (2020). Consistent detection of 2019 novel coronavirus in saliva. *Clinical Infectious Diseases 71*, 841–843.

(*102*) To, K. K.-W. et al. (2020). Temporal profiles of viral load in posterior oropharyngeal saliva samples and serum antibody responses during infection by SARS-CoV-2: an observational cohort study. *The Lancet Infectious Diseases 20*, 565–574.

(*103*) Labcorp's COVID-19 RT-PCR Test EUA Summary., Report, 2022.

(*104*) Fu, E., Liang, T., Spicar-Mihalic, P., Houghtaling, J., Ramachandran, S., and Yager, P. (2012). Two-dimensional paper network format that enables simple multistep assays for use in low-resource settings in the context of malaria antigen detection. *Analytical Chemistry 84*, 4574–4579.

(*105*) Ramachandran, S., Fu, E., Lutz, B., and Yager, P. (2014). Long-term dry storage of an enzyme-based reagent system for ELISA in point-of-care devices. *The Analyst 139*, 1456–1462.

(*106*) Zhang, C., Zheng, T., Wang, H., Chen, W., Huang, X., Liang, J., Qiu, L., Han, D., and Tan, W. (2021). Rapid one-pot detection of SARS-CoV-2 based on a lateral flow assay in clinical samples. *Analytical Chemistry 93*, 3325–3330.

(*107*) Chen, X., Zhou, Q., Li, S., Yan, H., Chang, B., Wang, Y., and Dong, S. (2021). Rapid and visual detection of SARS-CoV-2 using multiplex reverse transcription loop-mediated isothermal amplification linked with gold nanoparticle-based lateral flow biosensor. *Frontiers in Cellular and Infection Microbiology 11*, 581239.

(*108*) Xiong, D. et al. (2020). Rapid detection of SARS-CoV-2 with CRISPR-Cas12a. *PLoS Biology 18*, ed. by Sugden, B., e3000978.

(*109*) Broughton, J. P. et al. (2020). CRISPR–Cas12-based detection of SARS-CoV-2. *Nature Biotechnology 38*, 870–874.

(*110*) Bar-On, Y. M., Flamholz, A., Phillips, R., and Milo, R. (2020). SARS-CoV-2 (COVID-19) by the numbers. *eLife 9*, e57309.

(*111*) Long, Q.-X. et al. (2020). Antibody responses to SARS-CoV-2 in patients with COVID-19. *Nature Medicine 26*, 845–848.

(*112*) Smits, V. A. J., Hernández-Carralero, E., Paz-Cabrera, M. C., Cabrera, E., Hernández-Reyes, Y., Hernández-Fernaud, J. R., Gillespie, D. A., Salido, E., Hernández-Porto, M., and Freire, R. (2021). The nucleocapsid protein triggers the main humoral immune response in COVID-19 patients. *Biochemical and Biophysical Research Communications 543*, 45–49.

(*113*) Cate, D. M. et al. (2021). Antibody screening results for anti-nucleocapsid antibodies toward the development of a lateral flow assay to detect SARS-CoV-2 nucleocapsid protein. *ACS Omega 6*, 25116–25123.

(*114*) Grant, B. D., Anderson, C. E., Alonzo, L. F., Garing, S. H., Williford, J. R., Baughman, T. A., Rivera, R., Glukhova, V. A., Boyle, D. S., Dewan, P. K., Weigl, B. H., and Nichols, K. P. (2021). A SARS-CoV-2 coronavirus nucleocapsid protein antigen-detecting lateral flow assay. *PLoS One 16*, ed. by Ito, E., e0258819.

(*115*) Hutchinson, E. C., Charles, P. D., Hester, S. S., Thomas, B., Trudgian, D., Martínez-Alonso, M., and Fodor, E. (2014). Conserved and host-specific features of influenza virion architecture. *Nature Communications 5*, 4816.

(*116*) Tindale, L. C., Stockdale, J. E., Coombe, M., Garlock, E. S., Lau, W. Y. V., Saraswat, M., Zhang, L., Chen, D., Wallinga, J., and Colijn, C. (2020). Evidence for transmission of COVID-19 prior to symptom onset. *eLife 9*, e57149.

(*117*) Johansson, M. A., Quandelacy, T. M., Kada, S., Prasad, P. V., Steele, M., Brooks, J. T., Slayton, R. B., Biggerstaff, M., and Butler, J. C. (2021). SARS-CoV-2 transmission from people without COVID-19 symptoms. *JAMA Network Open 4*, e2035057.

(*118*) Datta, R., Heaster, T. M., Sharick, J. T., Gillette, A. A., and Skala, M. C. (2020). Fluorescence lifetime imaging microscopy: fundamentals and advances in instrumentation, analysis, and applications. *Journal of Biomedical Optics 25*, 1.

(*119*) Seo, J., Sim, Y., Kim, J., Kim, H., Cho, I., Nam, H., Yoon, Y.-G., and Chang, J.-B. (2022). PICASSO allows ultra-multiplexed fluorescence imaging of spatially overlapping proteins without reference spectra measurements. *Nature Communications 13*, 2475.

(*120*) Jahanshahi-Anbuhi, S., Kannan, B., Pennings, K., Ali, M. M., Leung, V., Giang, K., Wang, J., White, W., Li, Y., Pelton, R. H., Brennan, J. D., and Filipe, C. D. M. (2017). Automating multi-step paper-based assays using integrated layering of reagents. *Lab on a Chip 17*, 943–950.

(*121*) Hosokawa, H., Ungerbäck, J., Wang, X., Matsumoto, M., Nakayama, K. I., Cohen, S. M., Tanaka, T., and Rothenberg, E. V. (2018). Transcription factor PU.1 represses and activates gene expression in early T cells by redirecting partner transcription factor binding. *Immunity 48*, 1119–1134.e7.

(*122*) Ross, G., Bremer, M., Wichers, J., van Amerongen, A., and Nielen, M. (2018). Rapid antibody selection using surface plasmon resonance for high-speed and sensitive hazelnut lateral flow prototypes. *Biosensors 8*, 130.

Appendix A

SUPPLEMENTARY INFORMATION FOR CHAPTER 2

A.1 Materials and methods

A.1.1 Probe and amplifier details for RNA targets using HCR RNA-FISH

Species	Sample	RNA target	Split-initiator probe pairs	Supplier (catalog #)	HCR amplifier	Figures
D. rerio	whole-mount embryo	*hbae1*	3	MT (4503/E784)	B1-Alexa405	2.2, A.1–A.3
		mylpfa	13	MT (4644/E992)	B2-Atto425	2.2, A.1–A.3
		mylpfa	6	MT (4607/E924)	B2-Atto425	2.3, A.5, A.10, A.14
		mylpfa	6	MT (4607/E922)	B3-Alexa700	2.3, A.5, A.10, A.14
		gfap	17	MT (3974/E108)	B6-Alexa488	2.2, A.1–A.3
		kdrl	60	MT (4503/E786)	B9-Alexa514	2.2, A.1–A.3
		kdrl	30	MT (3665/D679)	B9-Alexa514	2.3, 2.4, A.7, A.12, A.14, A.15
		kdrl	30	MT (4644/E994)	B8-Atto633	2.3, 2.4, A.7, A.12, A.14, A.15
		shha	20	MT (3699/D741)	B7-Alexa546	2.2, A.1–A.3
		elavl3	20	MT (4362/E588)	B10-Alexa594	2.2, A.1–A.3
		elavl3	20	MT (4607/E908)	B6-Alexa488	2.3, A.6, A.11, A.14
		elavl3	20	MT (4607/E910)	B10-Alexa594	2.3, A.6, A.11, A.14
		sox10	34	MT (4644/E990)	B8-Atto633	2.2, A.1–A.3
		ntla	20	MT (2196/A430)	B3-Alexa700	2.2, A.1–A.3
		dmd	20	MT (4607/E930)	B5-Alexa750	2.2, 2.3, A.1–A.3, A.8, A.14
		dmd	20	MT (4607/E932)	B7-Alexa546	2.3, A.8, A.13, A.14
		col2a1a	15	MT (4560/E856)	B4-iFluor800	2.2, A.1–A.3
		col2a1a	10	MT (4607/E918)	B1-Alexa405	2.3, A.4, A.9, A.14
		col2a1a	10	MT (4607/E920)	B4-iFluor800	2.3, A.4, A.9, A.14
M. musculus	brain section	*Slc17a7*	20	MT (4671/F037-P)	B6-Alexa488	2.5, A.17–A.23
		Gad1	33	MT (4631/E968-P)	B9-Alexa514	2.5, A.17–A.23
		Sst	11	MT (4797/F111-P)	B7-Alexa546	2.5, A.17–A.23
		Actb	20	MT (2306/A758-P)	B5-Alexa594	2.5, A.17–A.23
		Lamp5	27	MT (4761/F033-P)	B8-Atto633	2.5, A.17–A.23
		Plp1	24	MT (4787/F081-P)	B3-Alexa700	2.5, A.17–A.23
		Vip	24	MT (4611/E972-P)	B10-Alexa750	2.5, A.17–A.23

Table A.1: Organism, sample type, target RNA, probe set details, HCR amplifier details, and figure numbers for HCR RNA-FISH. For HCR RNA-FISH, HCR probe sets, amplifiers, and buffers (probe hybridization buffer, probe wash buffer, amplification buffer) were obtained from Molecular Technologies (MT) within the Beckman Institute at Caltech.

A.1.2 Probe and amplifier details for protein targets using HCR IF

Species	Sample	Protein target	1°Ab probe (unlabeled) 2°Ab probe (initiator-labeled)	Dilution factor Working conc. (μg/mL)	Supplier (catalog #)	HCR amplifier	Figures
M. musculus	brain section	NFH	1°pAb chicken IgY anti-NFH	1:2,000	Inv (PA1-10002)		
			2°pAb donkey anti-chicken IgY-B1	1	MI	B1-Alexa405	2.5, A.17–A.23
		CD31	1°mAb rat IgG anti-CD31	1:10	BDB (550274)		
			2°pAb donkey anti-rat IgG-B2	1	MI	B2-Atto425	2.5, A.17–A.23
		RBFOX3	1°mAb rabbit IgG anti-RBFOX3	1:5,000	CST (24307)		
			2°pAb donkey anti-rabbit IgG-B4	1	MI	B4-iFluor800	2.5, A.17–A.23

Table A.2: Organism, sample type, target protein, 1°Ab probe details, 2°Ab probe details, HCR amplifier details, and figure numbers for HCR IF. For HCR IF, initiator-labeled secondary antibody probes and antibody buffer were obtained from Molecular Instruments (MI). Inv: Invitrogen. BDB: BD Biosciences. CST: Cell Signaling Technology.

A.1.3 Confocal microscope settings

Sample	Target	Objective	Fluorophore	Laser (nm)	Detector(s)	Detection wavelengths (nm)	Pixel size ($x \times y \times z$ μm)	Figures
Whole-mount embryo	*hbae1*	20×	Alexa405	405	HyD S 1	410–450	$0.568 \times 0.568 \times 4.0$	2.2, A.1–A.3
	mylpfa	20×	Atto425	440	HyD S 1, S 2, S 3	450–475, 475–495, 495–520	$0.568 \times 0.568 \times 4.0$	2.2, A.1–A.3
		63×	Atto425	440	HyD S 1, S 2, S 3	450–475, 475–495, 495–520	$0.180 \times 0.180 \times 1.2$	2.3, A.5, A.10, A.14
	gfap	20×	Alexa488	488	HyD S 1, S 2	493–513, 513–533	$0.568 \times 0.568 \times 4.0$	2.2, A.1–A.3
	kdrl	20×	Alexa514	518	HyD S 1, S 2, S 3	523–543, 543–563, 563–583	$0.568 \times 0.568 \times 4.0$	2.2, A.1–A.3
		63×	Alexa514	518	HyD S 1, S 2, S 3	523–543, 543–563, 563–583	$0.180 \times 0.180 \times 1.2$	2.3, 2.4, A.7, A.12, A.14, A.15
	shha	20×	Alexa546	557	HyD S 1, S 2, S 3	566–580, 580–600, 600–620	$0.568 \times 0.568 \times 4.0$	2.2, A.1–A.3
	elavl3	20×	Alexa594	590	HyD S 1, S 2, S 3	600–620, 620–640, 640–660	$0.568 \times 0.568 \times 4.0$	2.2, A.1–A.3
		63×	Alexa594	590	HyD S 1, S 2, S 3	600–620, 620–640, 640–660	$0.180 \times 0.180 \times 1.2$	2.3, A.6, A.11, A.14
	sox10	20×	Atto633	629	HyD S 2, S 3	640–660, 660–680	$0.568 \times 0.568 \times 4.0$	2.2, A.1–A.3
	ntla	20×	Alexa700	686	HyD S 2	696–723	$0.568 \times 0.568 \times 4.0$	2.2, A.1–A.3
	dmd	20×	Alexa750	755	HyD S 2, S 3	765–780, 780–795	$0.568 \times 0.568 \times 4.0$	2.2, A.1–A.3
		63×	Alexa750	755	HyD S 2, S 3	765–780, 780–795	$0.180 \times 0.180 \times 1.2$	2.3, A.8, A.13, A.14
	col2a1a	20×	iFluor800	790	HyD S 3, R 5	815–830, 835–850	$0.568 \times 0.568 \times 4.0$	2.2, A.1–A.3
		63×	iFluor800	790	HyD S 3 , R 5	815–830, 835–850	$0.180 \times 0.180 \times 1.2$	2.3, A.4, A.9, A.14
	Autofluorescence	20×	–	459	HyD S 1, S 2, S 3, X 4	465–500, 500–535, 535–570, 570–630	$0.568 \times 0.568 \times 4.0$	2.2, A.1–A.3
		63×	–	459	HyD S 1, S 2, S 3, X 4	465–500, 500–535, 535–570, 570–630	$0.180 \times 0.180 \times 1.2$	2.3, A.4–A.14

Table A.3: Microscope settings for whole-mount zebrafish embryo imaging. Confocal microscopy was performed with a Leica Stellaris 8 inverted confocal microscope. Objectives were as follows: HC PL APO 20×/0.75 IMM CORR CS2 (catalog # 11506343), HC PL APO 63×/1.40 OIL CS2 (catalog # 11506350); both utilized with oil immersion.

Sample	Target	Objective	Fluorophore	Laser (nm)	Detector(s)	Detection wavelengths (nm)	Pixel size ($x \times y \times z$ μm)	Figures
Brain section	NFH	20×	Alexa405	405	HyD S 1	410–450	$0.568 \times 0.568 \times 4.0$	2.5, A.17–A.23
	CD31	20×	Atto425	440	HyD S 1, S 2, S 3	450–475, 475–495, 495–520	$0.568 \times 0.568 \times 4.0$	2.5, A.17–A.23
	Slc17a7	20×	Alexa488	488	HyD S 1, S 2	493–513, 513–533	$0.568 \times 0.568 \times 4.0$	2.5, A.17–A.23
	Gad1	20×	Alexa514	518	HyD S 1, S 2, S 3	523–543, 543–563, 563–583	$0.568 \times 0.568 \times 4.0$	2.5, A.17–A.23
	Sst	20×	Alexa546	557	HyD S 1, S 2, S 3	566–580, 580–600, 600–620	$0.568 \times 0.568 \times 4.0$	2.5, A.17–A.23
	Actb	20×	Alexa594	590	HyD S 1, S 2, S 3	600–620, 620–640, 640–660	$0.568 \times 0.568 \times 4.0$	2.5, A.17–A.23
	Lamp5	20×	Atto633	629	HyD S 2, S 3	640–660, 660–680	$0.568 \times 0.568 \times 4.0$	2.5, A.17–A.23
	Plp1	20×	Alexa700	686	HyD S 2	696–723	$0.568 \times 0.568 \times 4.0$	2.5, A.17–A.23
	Vip	20×	Alexa750	755	HyD S 2, S 3	765–780, 780–795	$0.568 \times 0.568 \times 4.0$	2.5, A.17–A.23
	RBFOX3	20×	iFluor800	790	HyD S 3, R 5	815–830, 835–850	$0.568 \times 0.568 \times 4.0$	2.5, A.17–A.23
	Autofluorescence	20×	–	459	HyD S 1, S 2, S 3, X 4	465–500, 500–535, 535–570, 570–630	$0.568 \times 0.568 \times 4.0$	2.5, A.17–A.23

Table A.4: Microscope settings for mouse brain section imaging. Confocal microscopy was performed with a Leica Stellaris 8 inverted confocal microscope. Objective was as follows: HC PL APO 20×/0.75 IMM CORR CS2 (catalog # 11506343) utilized with oil immersion.

A.1.4 Image analysis

We build on an image analysis framework developed over a series of publications (*36–38*, *43*, *45*). For convenience, here we provide a self-contained description of the details relevant to the present work.

Raw pixel intensities

The total fluorescence within a pixel is a combination of signal and background. Fluorescent background (BACK) arises from three sources in each channel:

- autofluorescence (AF): fluorescence inherent to the sample.
- non-specific detection (NSD): probes that bind non-specifically in the sample and subsequently trigger HCR amplification. For HCR IF experiments using both primary antibody probes and secondary antibody probes, NSD_{1° arises from non-specific binding of primary antibody probes and NSD_{2° arises from non-specific binding of secondary antibody probes, with $\mathrm{NSD} = \mathrm{NSD}_{1^\circ} + \mathrm{NSD}_{2^\circ}$.
- non-specific amplification (NSA): HCR hairpins that bind non-specifically in the sample.

Fluorescent signal (SIG) in each channel corresponds to:

- signal (SIG): probes that bind specifically to the target and subsequently trigger HCR amplification.

For pixel i of replicate sample n, we denote the background

$$X_{n,i}^{\mathrm{BACK}} = X_{n,i}^{\mathrm{NSD}} + X_{n,i}^{\mathrm{NSA}} + X_{n,i}^{\mathrm{AF}}, \tag{A.1}$$

the signal:

$$X_{n,i}^{\mathrm{SIG}}, \tag{A.2}$$

and the total fluorescence (SIG+BACK):

$$X_{n,i}^{\mathrm{SIG+BACK}} = X_{n,i}^{\mathrm{SIG}} + X_{n,i}^{\mathrm{BACK}}. \tag{A.3}$$

Measurement of signal, background, and signal-to-background

For each target, background (BACK) is characterized for pixels in one or more representative rectangular regions of no- or low-expression and the combination

of signal plus background (SIG+BACK) is characterized for pixels in one or more representative rectangular regions of high expression (e.g., Figures A.3, A.14, A.23). For the pixels in these regions, we characterize the distribution by plotting an intensity histogram and characterize average performance by calculating the mean pixel intensities

$$\bar{X}_n^{\mathrm{BACK}}, \qquad \bar{X}_n^{\mathrm{SIG\ +\ BACK}} \tag{A.4}$$

for replicate n. Performance across replicates is characterized by calculating the sample means

$$\bar{X}^{\mathrm{BACK}}, \qquad \bar{X}^{\mathrm{SIG+BACK}} \tag{A.5}$$

and standard error of the mean

$$s_{\bar{X}^{\mathrm{BACK}}}, \qquad s_{\bar{X}^{\mathrm{SIG+BACK}}}. \tag{A.6}$$

The mean signal is then estimated as

$$\bar{X}^{\mathrm{SIG}} = \bar{X}^{\mathrm{SIG+BACK}} - \bar{X}^{\mathrm{BACK}} \tag{A.7}$$

with the standard error of the mean estimated via uncertainty propagation as

$$s_{\bar{X}^{\mathrm{SIG}}} \leq \sqrt{(s_{\bar{X}^{\mathrm{SIG+BACK}}})^2 + (s_{\bar{X}^{\mathrm{BACK}}})^2}. \tag{A.8}$$

The signal-to-background ratio is estimated as:

$$\bar{X}^{\mathrm{SIG/BACK}} = \bar{X}^{\mathrm{SIG}} / \bar{X}^{\mathrm{BACK}} \tag{A.9}$$

with standard error of the mean estimated via uncertainty propagation as

$$s^{\mathrm{SIG/BACK}} \leq \bar{X}^{\mathrm{SIG/BACK}} \sqrt{\left(\frac{s_{\bar{X}^{\mathrm{SIG}}}}{\bar{X}^{\mathrm{SIG}}}\right)^2 + \left(\frac{s_{\bar{X}^{\mathrm{BACK}}}}{\bar{X}^{\mathrm{BACK}}}\right)^2}. \tag{A.10}$$

These upper bounds on estimated standard errors hold under the assumption that the correlation between SIG and BACK is non-negative.

Normalized voxel intensities for qHCR imaging: analog RNA relative quantitation with subcellular resolution in an anatomical context

For quantitative imaging using HCR, precision increases with voxel size as long as the imaging voxels remain smaller than the features in the expression pattern (see

Section S2.2 of (*43*)). To increase precision, we calculate raw voxel intensities by averaging neighboring pixel intensities while still maintaining a subcellcular voxel size. To facilitate relative quantitation between voxels, we estimate the normalized HCR signal of voxel j in replicate n as:

$$x_{n,j} \equiv \frac{X_{n,j}^{\text{SIG+BACK}} - X^{\text{BOT}}}{X^{\text{TOP}} - X^{\text{BOT}}}, \tag{A.11}$$

which translates and rescales the data so that the voxel intensities in each channel fall in the interval [0,1]. Here,

$$X^{\text{BOT}} \equiv \bar{X}^{\text{BACK}} \tag{A.12}$$

is the mean background across replicates (see Section A.1.4) and

$$X^{\text{TOP}} \equiv \max_{n,j} X_{n,j}^{\text{SIG+BACK}} \tag{A.13}$$

is the maximum total fluorescence for a voxel across replicates.

Pairwise expression scatter plots that each display normalized voxel intensities for two channels (e.g., Figures 4 and 5 of (*43*)) provide a powerful quantitative framework for performing multidimensional read-out/read-in analyses (Figure 6 of (*43*)). Read-out from anatomical space to expression space enables discovery of expression clusters of voxels with quantitatively related expression levels and ratios (amplitudes and slopes in the expression scatter plots), while read-in from expression space to anatomical space enables discovery of the corresponding anatomical locations of these expression clusters within the embryo. The simple and practical normalization approach of (B.11)–(B.13) translates and rescales all voxels identically within a given channel (enabling comparison of amplitudes and slopes in scatter plots between replicates), and does not attempt to remove scatter in the normalized signal estimate that is caused by scatter in the background.

To validate qHCR spectral imaging with subcellular resolution (2.0×2.0×1.2 μm voxels) in whole-mount zebrafish embryos, Figures 2.3 and A.4–A.8 display highly correlated normalized voxel intensities for 2-channel redundant detection of five target RNAs. In this setting, accuracy corresponds to linearity with zero intercept, and precision corresponds to scatter around the line (*43*). To address chromatic aberration resulting from the wide range of wavelengths used, Huygens chromatic aberration correction was applied. As a point of reference, Figures A.9–A.13 display normalized voxel intensities for 2-channel redundant detection of five target RNAs without chromatic aberration correction.

Dot detection and colocalization for dHCR imaging: digital mRNA absolute quantitation in an anatomical context

To validate the performance of spectral imaging with linear unmixing for single-molecule imaging, we perform a 2-channel redundant detection experiment in which target RNA *kdrl* is detected using two independent probe sets and HCR amplifiers in Ch4 and Ch7 of a 10-plex experiment. Let N_4 denote the number of dots detected in Ch4, N_7 the number of dots detected in Ch7, and N_{47} the number of colocalized dots appearing in both channels. We define the colocalization fraction for each channel:

$$C_4 = N_{47}/N_4 \tag{A.14}$$

$$C_7 = N_{47}/N_7 \tag{A.15}$$

As the false-positive and false-negative rates for single-molecule detection go to zero, C_4 and C_7 will both approach 1 from below, providing a quantitative basis for evaluating performance. Single molecules were identified in each channel using a novel algorithm we developed for dot detection. The DotDetection 2.0 notebook with the novel dot detection algorithm is available for download from www.moleculartechnologies.org.

The following settings were used for dot detection in dHCR images:

- max_dots = 2000
- lo_pass = 0
- hi_pass = 40
- sigma = 0.3
- weight_sigma = 0.3
- hi_pass_factor = 1
- agglomerate = False
- min_ratio = 2
- optimize = center
- max_maxima = $int(1e5)$

- allow_edges = True

The following settings were used for dot colocalization thresholds (μm):

- xy threshold = 0.5
- z threshold = 1.0

The following settings were used for dot intensity thresholds (Ch4, Ch7):

- Replicate 1: $(250, 400)$
- Replicate 2: $(250, 300)$
- Replicate 3: $(290, 350)$

A.2 Protocols

A.2.1 Protocols for 10-plex HCR spectral imaging and linear unmixing

Spectral imaging and linear unmixing sample preparation

1. Perform 12 types of HCR experiments (HCR IF and/or HCR RNA-FISH for a total of 10 protein and/or RNA targets):

    a) 10-plex (1 sample, or multiple replicate samples as desired): Use all 10 HCR probe sets and amplifiers.

    b) 1-plex for each of 10 targets (1 sample per target): For each of the 10 targets, use the corresponding HCR probe set and amplifier.

    c) Autofluorescence (2 samples): Omit all HCR probe sets and amplifiers.

Spectral imaging and linear unmixing workflow overview

1. Use one autofluorescence sample to perform an excitation-emission scan to determine the optimal autofluorescence excitation wavelength and detection wavelengths for the sample type being imaged.

2. Image the 10-plex sample using 11 excitation wavelengths (1 optimized for each fluorophore and 1 optimized for autofluorescence).

3. Image each 1-plex reference sample using 11 excitation wavelengths to obtain a reference spectrum for each fluorophore.

4. Image the other autofluorescence sample using 11 excitation wavelengths to obtain a reference spectrum for autofluorescence.

5. Use the 11 reference spectra (one per fluorophore and one for autofluorescence) to linearly unmix the 10-plex image and produce 11 channels (one for each fluorophore and one for autofluoresence).

Protocol for performing an excitation-emission scan

1. Open the LAS X software.
2. At the top of the window, click "Configuration" > "Hardware" > change "Bit Depth" to 16.
3. Click "Acquire" at the top of the window to return to the image acquisition screen.
4. Place one of the autofluorescence samples on the microscope to conduct an excitation-emission scan (also known as a $\Lambda\lambda$ scan) to determine the optimal autofluorescence excitation wavelength.
5. In the left panel, under "Acquisition Mode", change "xyz" to "xy$\Lambda\lambda$".
6. In the left panel, in the "$\Lambda\lambda$: Excitation Emission Scan Settings" sub-panel, click the plus sign in the upper lefthand corner.
7. In the pop-up menu, click "Reset Values to Default".
8. In the pop-up menu, in the following order, use the mouse scroll wheel to set "Excitation Steps" to 18 (this will automatically also set "Excitation Stepsize" to 20 nm), "Detection Steps" to 14, "Detection Bandwidth" to 20 nm, and "Detection Stepsize" to 24 nm. Close the pop-up menu.
9. Under the eyepiece, navigate to the region of the autofluorescence sample with the most intense autofluorescence.
10. Enter "Live" imaging mode, and adjust the laser intensity and/or detector gain so that the highest pixel intensity is approximately 25% of the maximum possible pixel intensity. The laser line and HyD S 1 detector may need to be moved to different wavelengths to see the autofluorescence.
    NOTE: *Keeping the pixel intensities low ensures pixel saturation will not occur during the $\Lambda\lambda$ scan, as pixel saturation would obscure the spectral information.*
11. Click "Start" to begin the excitation-emission scan.
12. When the scan is finished, click on the "LambdaLambda 001" file under "Open projects" in the left panel.

13. Click “Process” at the top of the window.

14. Click “Excitation / Emission Contour Plot” in the left panel.

15. In the right panel, drag the “t” slider so that the sample is visible. The “Λ” slider and pixel intensity slider may also need to be adjusted to make the sample visible.

16. In the right panel, click the Rectangle, Oval, or Polygon button at the top of the screen, and draw a region in the image around the brightest autofluorescence.

17. In the middle panel, click “Apply” at the bottom of the screen. This will display a contour plot.

18. Reposition the crosshairs to the maximum of the contour plot, and make note of the Excitation wavelength displayed at the bottom right of the plot. This wavelength, henceforth denoted as λ_{AF}, will serve as the optimal autofluorescence excitation wavelength.
    NOTE: *Going forward, if the sample preparation protocol remains the same, the optimal autofluorescence excitation wavelength (λ_{AF}) determined here can be used for future batches of experiments with this sample type, and this excitation-emission scan does not need to be repeated for each batch.*

Protocol for spectral imaging

1. Open the LAS X software.

2. At the top of the window, click “Configuration” > “Hardware” > and make sure “Bit Depth” is set to 16.

3. Click “Acquire” at the top of the window to return to the image acquisition screen.

4. Click “Acquisition” in the left panel, and make sure “Acquisition Mode” is set to “xyz”.

5. In the middle panel of the software, create 11 Settings. Settings 1-10 are used to image the target fluorophores, while Setting 11 is used to image the autofluorescence.

Setting	Laser line (nm)	Detector(s)	Detector wavelengths (nm)	Fluorophore
1	405	HyD S 1	410–450	Alexa405
2	440	HyD S 1, S 2, S 3	450–475, 475–495, 495–520	Atto425
3	488	HyD S 1, S 2	493–513, 513–533	Alexa488
4	518	HyD S 1, S 2, S 3	523–543, 543–563, 563–583	Alexa514
5	557	HyD S 1, S 2, S 3	566–580, 580–600, 600–620	Alexa546
6	590	HyD S 1, S 2, S 3	600–620, 620–640, 640–660	Alexa594
7	629	HyD S 2, S 3	640–660, 660–680	Atto633
8	686	HyD S 2	696–723	Alexa700
9	755	HyD S 2, S 3	765–780, 780–795	Alexa750
10	790	HyD S 3, R 5	815–830, 835–850	iFluor800

Table A.5: Settings 1-10 configurations for spectral imaging.

6. Configure Settings 1-10 as follows:

7. For Setting 11 (autofluorescence), set the laser line to the optimal autofluorescence excitation wavelength (λ_{AF}) determined via the excitation-emission scan above.

8. For Setting 11, activate the HyD S 1, S 2, S 3, and X 4 detectors. The detector wavelengths will be determined by the optimal autofluorescence excitation wavelength (λ_{AF}) determined via the excitation-emission scan above. Configure the detectors for Setting 11 as follows:

Detector	Lower wavelength (nm)	Upper wavelength (nm)
HyD S 1	λ_{AF} + 6	λ_{AF} + 41
HyD S 2	λ_{AF} + 41	λ_{AF} + 76
HyD S 3	λ_{AF} + 76	λ_{AF} + 111
HyD X 4	λ_{AF} + 111	λ_{AF} + 171

Table A.6: Setting 11 configuration for spectral imaging. λ_{AF}: optimal autofluorescence excitation wavelength.

   For example, if the optimal autofluorescence excitation wavelength (λ_{AF}) were determined to be 459 nm, the Setting 11 detectors would be configured as follows:

   - HyD S 1: 465–500 nm
   - HyD S 2: 500–535 nm
   - HyD S 3: 535–570 nm
   - HyD X 4: 570–630 nm

9. Place the 10-plex sample on the microscope.

10. For each of the 11 Settings:

    a) Navigate to the position in the sample that has the maximum intensity for the fluorophore corresponding to that Setting.

    b) For the linear unmixing to perform properly, it is important that no pixels are saturated. Therefore, while using the "Live" mode, set the laser intensity and detector gain(s) for that Setting so that the maximum pixel intensity for each detector is no more than 50% of the maximum possible value. Do not change the laser wavelength or detector wavelengths; the Format, Speed, Zoom, Averaging, and Accumulation settings may be adjusted as needed.

    NOTE: *Each detector collects emissions spectra over a range of wavelengths. For some Settings, multiple detectors are utilized to collect a broader range of emissions spectra for a given fluorophore.*

    c) Click "Capture Image", and double-check that the captured image reaches no more than 50% of saturation for all pixels in all detectors. The captured image may then be deleted.

11. As a final check, to ensure that no pixels will become saturated, while in "Live" mode, traverse the entire sample and verify that no pixel intensities exceed 50% of saturation in any of the detectors. Because it is possible that the laser for one Setting can cross-excite a fluorophore corresponding to a neighboring Setting, be sure to check that the chosen laser intensities and detector gains do not result in pixel intensities above 50% of saturation in the detectors of neighboring Settings. Decrease the laser intensities and/or detector gains if any pixel intensities are too high.

12. Now that the laser intensity and detector gain settings are determined for all 11 Settings, do not change the laser intensity or detector gain settings again.

13. Collect a Z-stack for the 10-plex sample by setting the "Begin" and "End" locations for a Z-stack and clicking "Start".

14. One by one, place each of the 10 reference spectrum samples on the microscope. Find the area of the sample with the brightest fluorescence, and collect a single Z-section at that location. Rename each image file to indicate the target name and fluorophore number.

    NOTE: *All 11 Settings should still be active when collecting the reference spectrum sample images.*

15. Place the other autofluorescence sample on the microscope. Find the area of the sample with the brightest autofluorescence, and collect a single Z-section at that location. Rename the image file to "autofluorescence".
    NOTE: *All 11 Settings should still be active when collecting the autofluorescence sample image.*

Protocol for linear unmixing using the LAS X software

1. Click "Process" along the top of the window.
2. Within the "ProcessTools" menu in the left panel, click "Channel Dye Separation" (under "Dye Separation").
3. Click "Open Projects" at the top of the left panel.
4. One by one, for each reference spectrum file and the autofluorescence image file:
    a) Click on the image file in the left panel.
    b) In the right panel, look at the image(s) corresponding to the Setting for that sample, and reposition and resize the circular region selector so that it covers the brightest region of the target (or the brightest region of the autofluorescence for the autofluorescence sample). Avoid including pixels that are outside the brightest region to prevent corruption of the fluorophore spectrum.
    c) Click "Add" near the bottom of the middle panel. This records a reference spectrum for the fluorophore.
5. Click "Save Matrix" in the middle panel, give the matrix a descriptive name, and click "Save".
6. Click on the 10-plex image file in the left panel.
7. Click "ProcessTools" at the top of the left panel.
8. Click "Automatic Dye Separation" in the left panel.
9. Within the middle panel, under "Method", click the "Manual" circle, which allows the matrix to be loaded.

10. Enter “11” for “Fluorescent Dyes” in the middle panel.
    NOTE: *Rescale should be left as “All Channels”.*

11. Click on the dividing line between the right and middle panels of the software and drag it all the way to the right (thereby making the panel with the 26 channels of images as small as possible). This reveals a button at the bottom of the middle panel labeled “Load”. Click the “Load” button.

12. Navigate to the saved matrix file, click on the matrix file, and click “Open”.

13. Click the “Apply” button located to the right of the “Load” button.

14. Click the “Apply” button at the bottom of the screen to unmix the 10-plex image.

15. To view the unmixed image, click “Acquire” at the top of the window. In the left panel, the 11-channel unmixed image (one channel per target plus one channel for autofluorescence) will have appeared with “DyeSep” added near the end of the file name.

16. Save the project.

A.2.2 Protocols for RNA imaging in whole-mount zebrafish embryos

Protocols for HCR RNA-FISH in whole-mount zebrafish embryos are adapted from (*39*, *45*). Experiments were performed in AB wild-type whole-mount zebrafish embryos (fixed 27 hpf) from the Zebrafish Facility of the Beckman Institute at Caltech. Procedures for the care and use of zebrafish embryos were approved by the Caltech IACUC.

Preparation of fixed whole-mount zebrafish embryos

1. Collect zebrafish embryos and incubate at 28 °C in a Petri dish with egg H_2O.
   NOTE: *Collect no more than 100 embryos per Petri dish.*
2. Replace the egg H_2O with fresh egg H_2O 6 hours after collecting the embryos.
3. At 27 hours post-fertilization (hpf), dechorionate the embryos by replacing the egg H_2O with 1 mg/mL pronase solution. After 5 min, gently pipet up and down with a glass pipette to dechorionate the embryos.
4. Remove dechorionated embryos to a Petri dish with fresh egg H_2O.
5. Gently wash the dechorionated embryos twice with egg H_2O.
6. Transfer up to 80 embryos to a 2 mL Eppendorf tube and remove excess egg H_2O.
7. Fix embryos in 2 mL of 4% paraformaldehyde (PFA) for 24 h at 4 °C.
   CAUTION: *Use PFA with extreme care, as it is a hazardous material.*
   NOTE: *Cool PFA to 4 °C before use.*
8. Wash embryos 3 × 5 min with 1 mL of 1× phosphate-buffered saline (PBS) to stop the fixation.
   NOTE: *Avoid using calcium chloride and magnesium chloride in PBS, as this leads to increased autofluorescence in the samples.*
9. Dehydrate and permeabilize with a series of methanol (MeOH) washes (1 mL each):
   a) 100% MeOH for 4 × 10 min
   b) 100% MeOH for 1 × 50 min.
10. Remove the final 100% MeOH wash.

11. Add 1 mL 100% MeOH and store embryos overnight at −20 °C before use.
    NOTE: *Embryos can be stored for at least one year at −20 °C.*

12. Transfer the required number of embryos for an experiment to a 2 mL Eppendorf tube.

13. Rehydrate with a series of graded 1 mL MeOH/PBST washes for 5 min each at room temperature:

    a) 75% MeOH / 25% PBST

    b) 50% MeOH / 50% PBST

    c) 25% MeOH / 75% PBST

    d) 5 × 100% PBST.

Buffer recipes for sample preparation

10 mg/mL pronase stock solution: 10 mg/mL pronase in ultrapure H_2O

For 10 mL of solution:

- 100 mg of pronase powder
- Fill up to 10 mL with ultrapure H_2O

1 mg/mL pronase solution: 1 mg/mL pronase in egg H_2O

For 25 mL of solution:

- 2.5 mL of 10 mg/mL pronase stock solution
- Fill up to 25 mL with egg H_2O

4% paraformaldehyde (PFA): 4% PFA, 1× PBS

For 25 mL of solution:

- 1 g of PFA powder
- 25 mL of 1× PBS
- Heat solution at 50–60 °C to dissolve powder
- Aliquot and store at −20 °C

PBST: 1× PBS, 0.1% Tween-20

For 500 mL of solution:

- 50 mL of 10× PBS
- 5 mL of 10% Tween-20
- Fill up to 500 mL with ultrapure H_2O
- Filter with a 0.2 μm Nalgene Rapid-Flow filter

NOTE: *Avoid using calcium chloride and magnesium chloride in PBS, as this leads to increased autofluorescence in the samples.*

NOTE: *Handle pronase powder and PFA powder with extreme care, as they are hazardous materials.*

HCR RNA-FISH in whole-mount zebrafish embryos

Detection stage

1. For each sample, move 5–8 embryos to a 1.5 mL Eppendorf tube and remove excess liquid.

2. Add 350 μL of pre-heated 30% probe hybridization buffer and incubate for 30 min at 37 °C.
   CAUTION: *Probe hybridization buffer contains formamide, a hazardous material.*
   NOTE: *Probe hybridization buffer should be pre-heated to 37 °C before use.*

3. Prepare probe solution by adding 4 μL of each 2 μM odd and even probe set to probe hybridization buffer and mixing well. Use a volume of probe hybridization buffer such that the final volume is 500 μL.

4. Remove the probe hybridization buffer from the samples and add the probe solution.

5. Incubate embryos overnight (>12 h) at 37 °C.

6. Remove excess probes by washing embryos 4 × 15 min with 500 μL of 30% probe wash buffer at 37 °C.
   CAUTION: *Probe wash buffer contains formamide, a hazardous material.*
   NOTE: *Probe wash buffer should be pre-heated to 37 °C before use.*

7. Wash embryos 3 × 5 min with 500 μL of 5× SSCT at room temperature.

Amplification stage

1. Add 350 μL of amplification buffer and incubate for 30 min at room temperature.
   NOTE: *Bring amplification buffer to room temperature before use.*

2. Separately prepare 30 pmol of hairpin h1 and 30 pmol of hairpin h2 by snap cooling 10 μL of 3 μM hairpin stock solution (heat at 95 °C for 90 seconds and cool to room temperature in a dark drawer for 30 min).
   NOTE: *HCR hairpins h1 and h2 are provided in hairpin storage buffer and are ready for snap cooling.*
   HCR hairpins h1 and h2 should be snap cooled in separate tubes.

3. Prepare hairpin solution by adding 10 μL of each snap-cooled hairpin to amplification buffer and mixing well. Use a volume of amplification buffer such that the final volume is 500 μL.

4. Remove the amplification buffer from the samples and add the hairpin solution.

5. Incubate embryos overnight (>12 h) in the dark at room temperature.

6. Remove excess hairpins by washing with 500 μL of 5× SSCT at room temperature:

    a) 2×5 min

    b) 2×30 min

    c) 1×5 min

Sample mounting for microscopy

1. Transfer embryos on to a No. 1.5 coverslip and remove excess liquid.

2. Add 60 μL ProLong Glass Antifade Mountant on top of the embryos.

3. Use an eyelash tool to gently position the embryos in a lateral position for imaging.

4. Place the coverslip on a 37 °C surface (such as a slide moat) for 1 h to set the mountant.

Buffer recipes for HCR RNA-FISH in whole-mount zebrafish embryos

5× SSCT: 5× SSC, 0.1% Tween-20
For 500 mL of solution:
• 125 mL of 20× SSC
• 5 mL of 10% Tween-20
• Fill up to 500 mL with ultrapure H_2O
• Filter with a 0.2 μm Nalgene Rapid-Flow filter

Reagents and supplies

Pronase (Roche, 10165921001)
Paraformaldehyde (PFA) (Sigma-Aldrich, P6148)
10× Phosphate-buffered saline (PBS) (Invitrogen, AM9625)
Methanol (Mallinckrodt Chemicals, 3016-16)
20× Saline sodium citrate (SSC) (Life Technologies, 15557-044)
10% Tween-20 solution (Teknova, T0025)
ProLong Glass Antifade Mountant (Invitrogen, P36984)

A.2.3 Protocols for protein and RNA imaging in fresh-frozen mouse brain sections

Protocols for HCR RNA-FISH in whole-mount zebrafish embryos are adapted from (*36*). Experiments were performed in C57BL/6 fresh-frozen coronal mouse brain sections (thickness: 5 μm; region: interaural 0.88 mm ± 0.2 mm; age: 8 weeks old; sex: male) from Acepix Biosciences (Cat. # A2203-0561).

Preparation of fresh-frozen mouse brain tissue sections

1. Remove slide-mounted sections from the −80 °C freezer and place on dry ice.
2. One by one, remove a slide from the slide storage box, draw a hydrophobic barrier around the tissue section, and add 100 μL of ice-cold 4% formaldehyde.
   CAUTION: *Use formaldehyde with extreme care, as it is a hazardous material.*
   NOTE: *The formaldehyde solution should be pre-cooled on ice before use.*
3. Fix for 2 h at 4 °C in a humidified chamber.
   NOTE: *A humidified chamber should be used for all future steps other than autofluorescence bleaching to prevent evaporation.*
4. Remove the 4% formaldehyde solution and add 2 mL of 1× of phosphate-buffered saline (PBS) across the entire slide to remove the optimal cutting temperature (OCT) compound and excess fixative. Incubate for 5 min at room temperature.
5. Wash 2 × 5 min with 1 mL of 1× PBS.
6. Remove 1× PBS and dry around the tissue section with a Kimwipe, taking care to not allow the tissue section to dry.
7. Re-apply the hydrophobic barrier around the tissue section if needed.
8. Wash 1 × 5 min with 200 μL of 1× PBS.
9. Optional: Proceed to autofluorescence bleaching protocol to reduce autofluorescence. Otherwise, proceed to **Protein detection stage**.

Autofluorescence bleaching protocol

1. Prepare bleaching solution fresh before use.
   CAUTION: *Keep bleaching solution uncapped inside a fume hood, as it produces gas.*
2. Add 200 μL of bleaching solution on top of the tissue.
3. Place slides under a 180 W LED light at 4 °C. Keep slides 15 cm away from the light source.
   CAUTION: *The LED light is extremely bright. Use the LED light in a covered area to avoid eye exposure.*
4. Expose the tissue to the LED light for 3 h.
   NOTE: *Turn off the light and check the slide every hour, re-applying additional fresh bleaching solution if necessary. Do not allow the slide to dry.*
5. Wash slide 4 × 10 min with 100 μL of PBST.
6. Proceed to HCR assay.

Buffer recipes for autofluorescence bleaching protocol

Bleaching solution: 4.5% hydrogen peroxide (H_2O_2), 24 mM sodium hydroxide (NaOH), 1× PBS
For 3 mL of solution:
• 2178 μL of nanopure H_2O
• 300 μL of 10× PBS
• 72μL of 1 N NaOH
• 450 μL of 30% H_2O_2

PBST: 1× PBS, 0.1% Tween-20
For 500 mL of solution:
• 50 mL of 10× PBS
• 5 mL of 10% Tween-20
• Fill up to 500 mL with ultrapure H_2O
• Filter with a 0.2 μm Nalgene Rapid-Flow filter

Multiplexed HCR IF with HCR RNA-FISH using unlabeled primary antibody probes and initiator-labeled secondary antibody probes for protein targets, split-initiator DNA probes for RNA targets, and simultaneous HCR signal amplification for all targets

Protein detection stage

1. Block tissue by applying 100 μL of antibody buffer on top of the tissue. Incubate for 1 h at room temperature.

2. Prepare the primary antibody solution by adding all primary antibodies to antibody buffer and mixing well. Use a volume of antibody buffer such that the final volume is 100 μL per section.
   NOTE: *Follow manufacturer's guidelines for primary antibody working concentration.*

3. Remove the blocking solution. Add the primary antibody solution and incubate overnight (>12 h) at 4 °C.
   NOTE: *Incubation may be optimized (e.g., 1–2 h at room temperature) depending on the antibodies used.*

4. Remove excess antibodies by washing 3 × 5 min with 100 μL of PBST at room temperature.

5. Prepare the initiator-labeled secondary antibody solution by adding all secondary antibodies to antibody buffer and mixing well. Use a volume of antibody buffer such that the final volume is 100 μL per section.
   NOTE: *Use a working concentration of 1 µg/mL for all initiator-labeled secondary antibodies.*

6. Add the secondary antibody solution and incubate for 1 h at room temperature.

7. Remove excess antibodies by washing 3 × 5 min with 100 μL of PBST at room temperature.

RNA detection stage

1. Post-fix sample by adding 100 μL of 4% formaldehyde on the tissue section and incubating for 10 min at room temperature.
   CAUTION: *Use formaldehyde with extreme care, as it is a hazardous material.*

2. Wash 3 × 5 min with 100 μL of PBST.

3. Wash 1 × 5 min with 100 μL of 5× SSCT.

4. Add 100 μL of pre-heated 30% probe hybridization buffer and incubate for 30 min at 37 °C.
   CAUTION: *Probe hybridization buffer contains formamide, a hazardous material.*
   NOTE: *Probe hybridization buffer should be pre-heated to 37 °C before use.*

5. Prepare probe solution by adding 0.8 μL of each 2 μM odd and even probe set to probe hybridization buffer and mixing well. Use a volume of probe hybridization buffer such that the final volume is 100 μL.

6. Remove the probe hybridization buffer and add the probe solution on top of the samples.

7. Incubate overnight (>12 h) at 37 °C.

8. Remove excess probes by washing 4 × 15 min with 100 μL of 30% probe wash buffer at 37 °C.
   CAUTION: *Probe wash buffer contains formamide, a hazardous material.*
   NOTE: *Probe wash buffer should be pre-heated to 37 °C before use.*

9. Wash 3 × 5 min with 100 μL of 5× SSCT at room temperature.

Amplification stage

1. Add 100 μL of amplification buffer and incubate for 30 min at room temperature.
   NOTE: *Bring amplification buffer to room temperature before use.*

2. Separately prepare 6 pmol of hairpin h1 and 6 pmol of hairpin h2 by snap cooling 2 μL of each 3 μM hairpin stock solution (heat at 95 °C for 90 seconds and cool to room temperature in a dark drawer for 30 min).
   NOTE: *HCR hairpins h1 and h2 are provided in hairpin storage buffer and are ready for snap cooling.*
   HCR hairpins h1 and h2 should be snap cooled in separate tubes.

3. Prepare hairpin solution by adding 2 μL of each snap-cooled hairpin to amplification buffer and mixing well. Use a volume of amplification buffer such that the final volume is 100 μL.

4. Remove the amplification buffer and add the hairpin solution on top of the samples.

5. Incubate overnight (>12 h) in the dark at room temperature.

6. Remove excess hairpins by washing with 100 μL of 5× SSCT at room temperature:

   a) 2 × 5 min

   b) 2 × 15 min

   c) 1 × 5 min

Sample mounting for microscopy

1. Aspirate 5× SSCT and carefully dry around the tissue section with a Kimwipe.
   NOTE: *Do not let the tissue section dry.*

2. Apply 60 μL of Fluoromount-G mountant on top of the tissue.

3. Slowly lower a 22 × 30 mm No. 1.5 coverslip on top of the mountant.

4. Store at 4 °C protected from light prior to imaging.

Buffers for HCR IF with HCR RNA-FISH

PBST: 1× PBS, 0.1% Tween-20
For 500 mL of solution:
• 50 mL of 10× PBS
• 5 mL of 10% Tween-20
• Fill up to 500 mL with ultrapure H_2O
• Filter with a 0.2 μm Nalgene Rapid-Flow filter

5× SSCT: 5× SSC, 0.1% Tween-20
For 500 mL of solution:
• 125 mL of 20× SSC
• 5 mL of 10% Tween-20
• Fill up to 500 mL with ultrapure H_2O
• Filter with a 0.2 μm Nalgene Rapid-Flow filter

Reagents and supplies

Image-iT 4% formaldehyde fixative solution in phosphate-buffered saline (PBS) (Invitrogen, FB002)
10× Phosphate-buffered saline (PBS) (Invitrogen, AM9624)
30% hydrogen peroxide (H_2O_2) (Sigma-Aldrich, H1009)
1 N sodium hydroxide (NaOH) (Sigma-Aldrich, S2770)
7-band 2.1 180 Watt LED Grow Light (HTG Supply, LED-7BV2.1180)
10% Tween-20 solution (Teknova, T0025)
20× Saline sodium citrate (SSC) (Life Technologies, 15557-044)
Fluoromount-G (SouthernBiotech, 0100-01)

A.3 Replicates and additional studies

A.3.1 Replicates, signal, and background for 10-plex RNA imaging with high signal-to-background in whole-mount zebrafish embryos (cf. Figure 2.2)

For 10-plex RNA imaging using HCR RNA-FISH in whole-mount zebrafish embryos, the reagents are listed in Table A.1.1. Additional studies are presented as follows:

- Figure A.1 displays 10-plex images for $N = 3$ replicate embryos unmixed using the Leica Stellaris LAS X software (cf. Figure 2.2).
- Figure A.2 displays 10-plex images for $N = 3$ replicate embryos unmixed using the LinearUnmixing 1.0 notebook we developed for the present work.
- Figure A.3 displays representative regions of individual channels used for measurement of signal and background for each target.
- Table A.7 displays estimated values for signal, background, and signal-to-background for each target.

Protocol: 10-plex HCR RNA-FISH (Section A.2.2) using split-initiator probes with HCR signal amplification for all 10 targets simultaneously.
Sample: Whole-mount zebrafish embryos; fixed 27 hpf.
Microscopy: Spectral confocal.

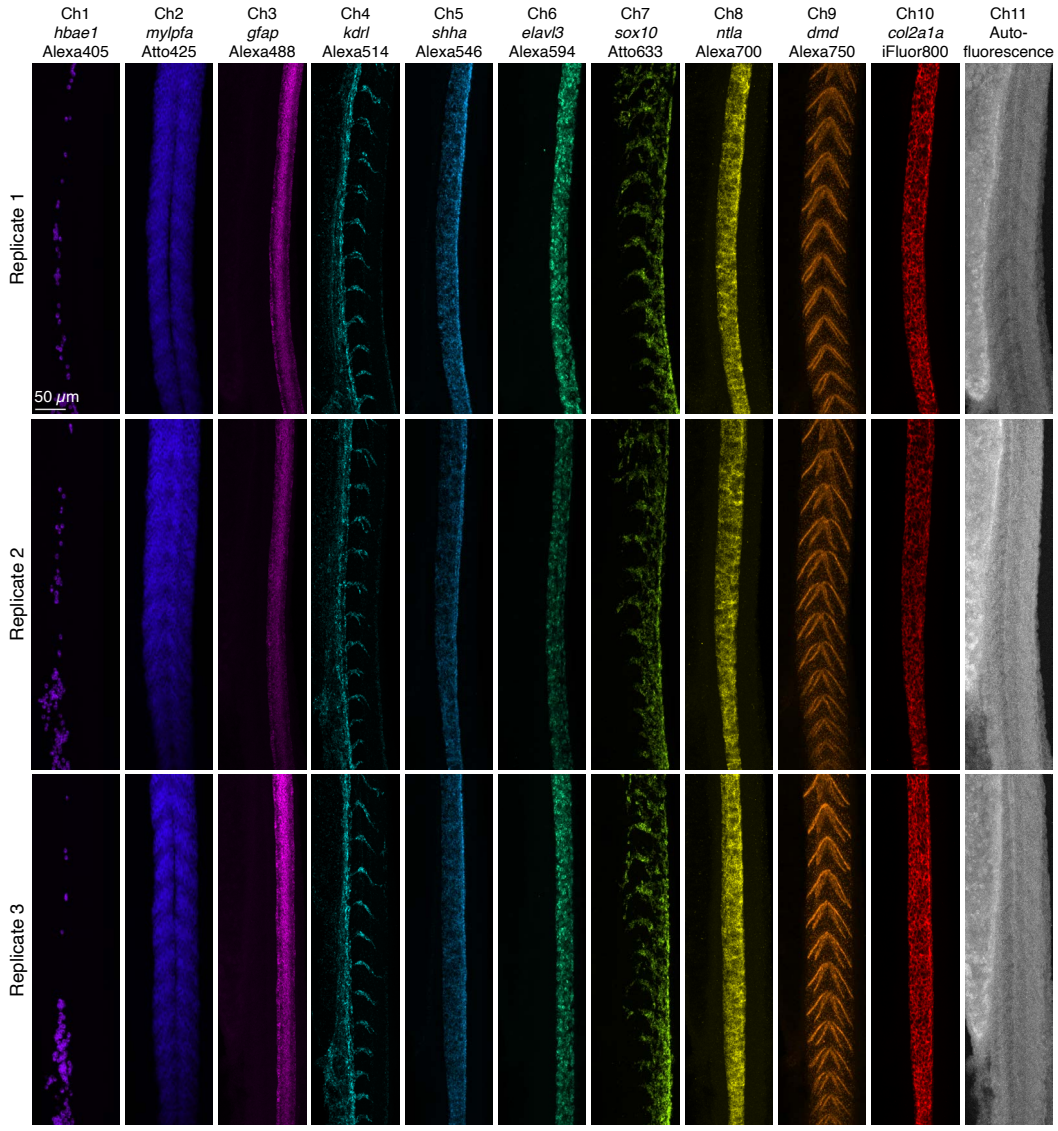

Figure A.1: Replicates for 10-plex RNA imaging using HCR RNA-FISH in whole-mount zebrafish embryos; unmixed with the Leica Stellaris LAS X software (cf. Figure 2.2). Ch1: *hbae1* (Alexa405). Ch2: *mylpfa* (Atto425). Ch3: *gfap* (Alexa488). Ch4: *kdrl* (Alexa514). Ch5: *shha* (Alexa546). Ch6: *elavl3* (Alexa594). Ch7: *sox10* (Atto633). Ch8: *ntla* (Alexa700). Ch9: *dmd* (Alexa750). Ch10: *col2a1a* (iFluor800). Replicate 1: maximum intensity z-projection of 64 z-dimension sections (85.6 μm total). Replicate 2: maximum intensity z-projection of 55 z-dimension sections (73.6 μm total). Replicate 3: maximum intensity z-projection of 77 z-dimension sections (103.0 μm total). Sample: Whole-mount zebrafish embryos; fixed 27 hpf.

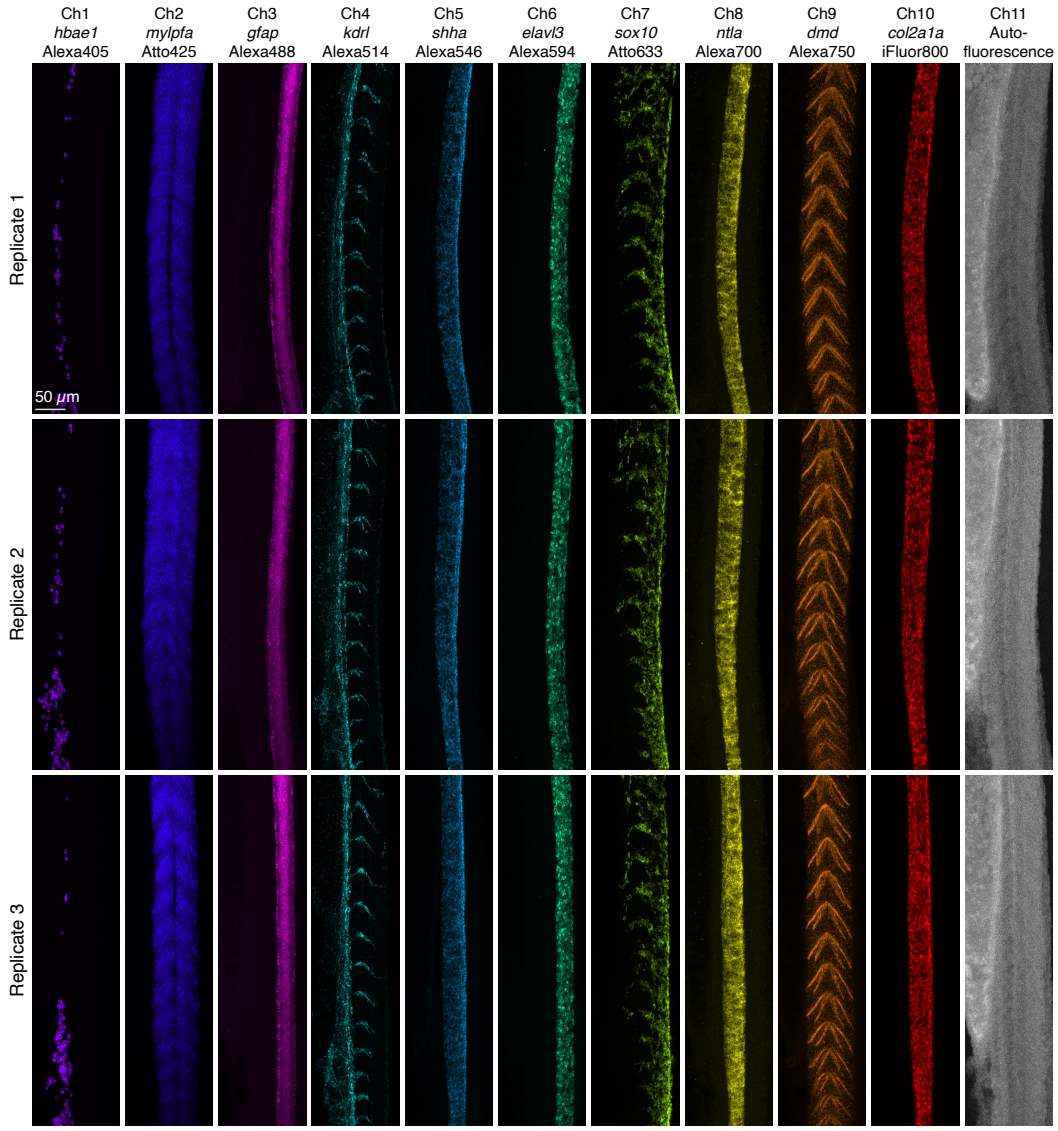

Figure A.2: Replicates for 10-plex RNA imaging using HCR RNA-FISH in whole-mount zebrafish embryos; unmixed with the LinearUnmixing 1.0 notebook. Ch1: *hbae1* (Alexa405). Ch2: *mylpfa* (Atto425). Ch3: *gfap* (Alexa488). Ch4: *kdrl* (Alexa514). Ch5: *shha* (Alexa546). Ch6: *elavl3* (Alexa594). Ch7: *sox10* (Atto633). Ch8: *ntla* (Alexa700). Ch9: *dmd* (Alexa750). Ch10: *col2a1a* (iFluor800). Replicate 1: maximum intensity z-projection of 64 z-dimension sections (85.6 μm total). Replicate 2: maximum intensity z-projection of 55 z-dimension sections (73.6 μm total). Replicate 3: maximum intensity z-projection of 77 z-dimension sections (103.0 μm total). Sample: Whole-mount zebrafish embryos; fixed 27 hpf.

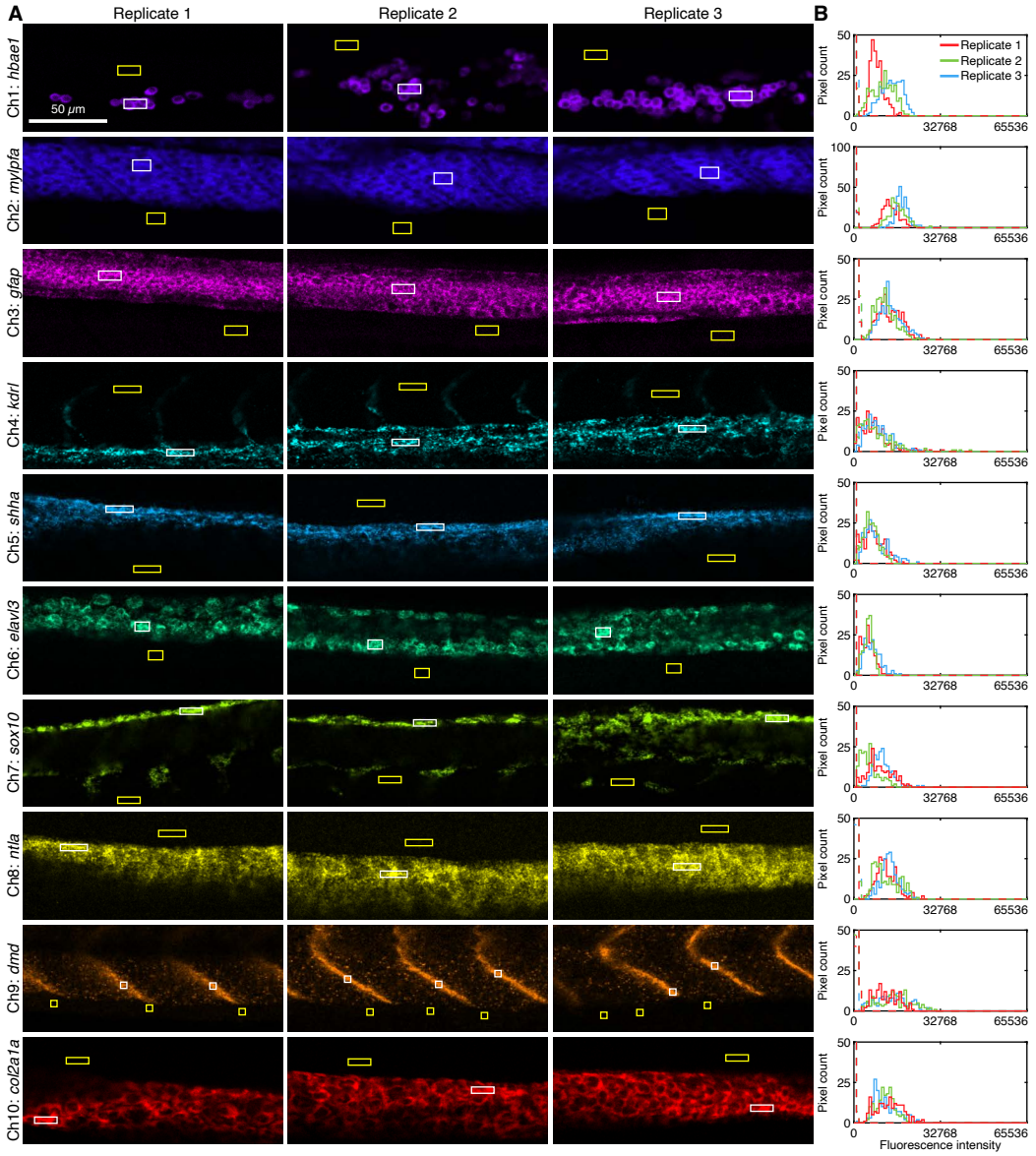

Figure A.3: Measurement of signal and background for 10-plex RNA imaging using HCR RNA-FISH in whole-mount zebrafish embryos (cf. Figure 2.2). (A) Individual channels of 10-plex confocal images. For each of three replicate embryos, a representative single optical section was selected for each channel based on the expression of the corresponding target RNA. (B) Pixel intensity histograms for Signal + Background (pixels within solid white boundary) and Background (pixels within solid yellow boundary). Confocal images collected with the microscope laser intensity and detector gain optimized to avoid saturating SIG+BACK pixels. Images were unmixed using the Leica Stellaris LAS X software. Ch1: *hbae1* (Alexa405). Ch2: *mylpfa* (Atto425). Ch3: *gfap* (Alexa488). Ch4: *kdrl* (Alexa514). Ch5: *shha* (Alexa546). Ch6: *elavl3* (Alexa594). Ch7: *sox10* (Atto633). Ch8: *ntla* (Alexa700). Ch9: *dmd* (Alexa750). Ch10: *col2a1a* (iFluor800). Sample: Whole-mount zebrafish embryos; fixed 27 hpf.

Target RNA	SIG+BACK	SIG	BACK	SIG/BACK
hbae1	11 000 ± 3000	11 000 ± 3000	197 ± 5	50 ± 10
mylpfa	16 000 ± 2000	16 000 ± 2000	249 ± 9	62 ± 9
gfap	13 000 ± 1000	12 000 ± 1000	650 ± 80	19 ± 3
kdrl	7800 ± 700	7600 ± 700	130 ± 20	60 ± 10
shha	6900 ± 900	6700 ± 900	170 ± 40	40 ± 10
elavl3	5500 ± 900	5300 ± 900	160 ± 30	33 ± 8
sox10	8000 ± 3000	8000 ± 3000	110 ± 20	70 ± 30
ntla	12 300 ± 700	11 600 ± 700	700 ± 200	17 ± 5
dmd	14 000 ± 1000	13 000 ± 1000	700 ± 90	18 ± 3
col2a1a	12 000 ± 800	11 800 ± 800	120 ± 30	100 ± 30

Table A.7: Estimated signal-to-background for 10-plex RNA imaging using HCR RNA-FISH in whole-mount zebrafish embryos (cf. Figure 2.2). Mean ± estimated standard error of the mean via uncertainty propagation for $N = 3$ replicate embryos. Analysis based on rectangular regions depicted in Figure A.3 using methods of Section A.1.4.

A.3.2 qHCR imaging: 10-plex RNA relative quantitation with subcellular resolution in an anatomical context (cf. Figure 2.3)

For redundant 2-channel imaging of 5 target RNAs (10 channels total) using HCR RNA-FISH whole-mount zebrafish embryos, the reagents are listed in Table A.1.1. Additional studies are presented as follows:

- Figures A.4–A.8 display 2-channel images and 2-channel voxel intensity scatter plots for each of 5 target RNAs in $N = 3$ replicate embryos.
- Table A.8 displays values used for signal normalization in Figures A.4–A.8.
- Figures A.9–A.13 display 2-channel images and 2-channel voxel intensity scatter plots for each of 5 target RNAs in $N = 3$ replicate embryos without chromatic aberration correction.
- Table A.9 displays values used for signal normalization in Figures A.9–A.13.
- Figure A.14 display representative regions used for measurement of signal and background for the 10 channels.
- Table A.10 displays estimated values for signal, background, and signal-to-background for 10 channels.

Protocol: HCR RNA-FISH (Section A.2.2) using split-initiator probes with HCR signal amplification for all 10 channels simultaneously.
Sample: Whole-mount zebrafish embryos; fixed 27 hpf.
Microscopy: Spectral confocal.

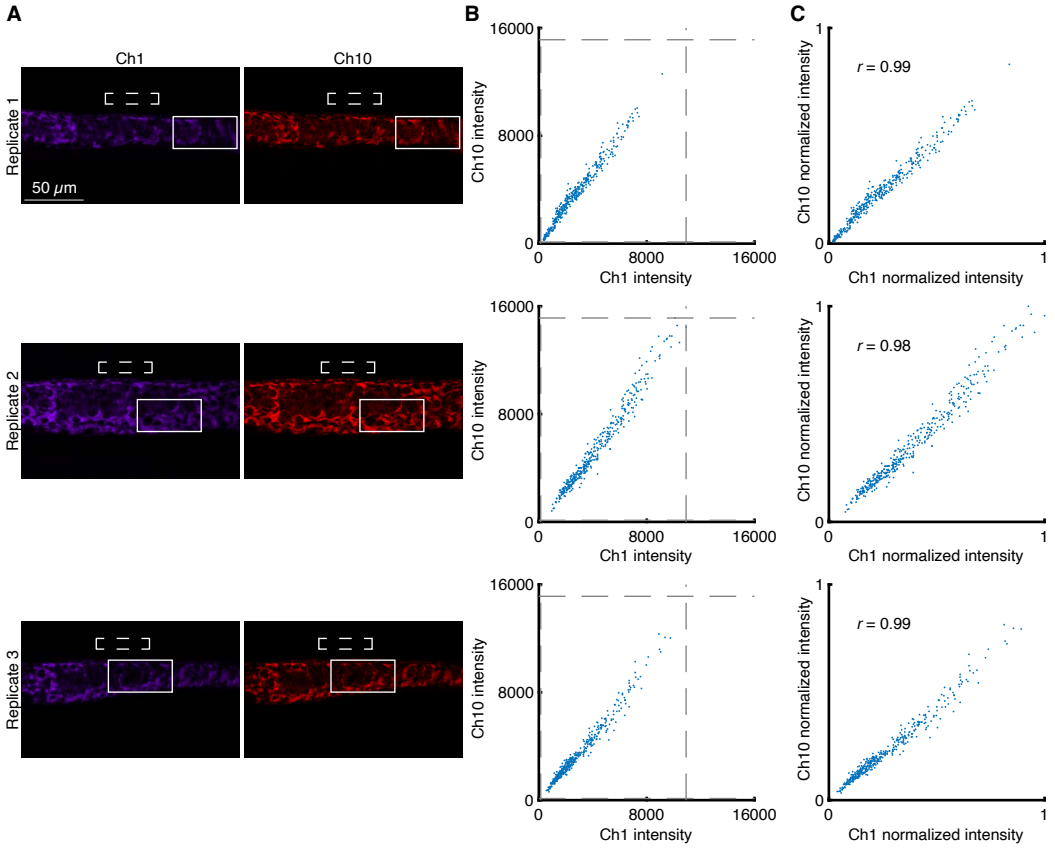

Figure A.4: Redundant 2-channel detection of target RNA *col2a1a* in whole-mount zebrafish embryos (cf. Figure 2.3). (A) Confocal images: individual channels and merge; single optical section. Images were corrected for chromatic aberration with Huygens chromatic aberration correction. Solid boundary denotes region of variable expression; dashed boundary denotes region of no/low expression. Pixel size: 0.180×0.180×1.2 μm. Sample: Whole-mount zebrafish embryos; fixed 27 hpf. (B) Raw voxel intensity scatter plots representing signal plus background for voxels within solid boundary of panel A. Voxel size: 2.0×2.0×1.2 μm. Dashed lines represent BOT and TOP values (Table A.8) used to normalize data for panel C using methods of Section A.1.4. (C) Normalized voxel intensity scatter plots representing estimated normalized signal (Pearson correlation coefficient, r). Ch1: *col2a1a* (Alexa405). Ch10: *col2a1a* (iFluor800). Sample: Whole-mount zebrafish embryos; fixed 27 hpf.

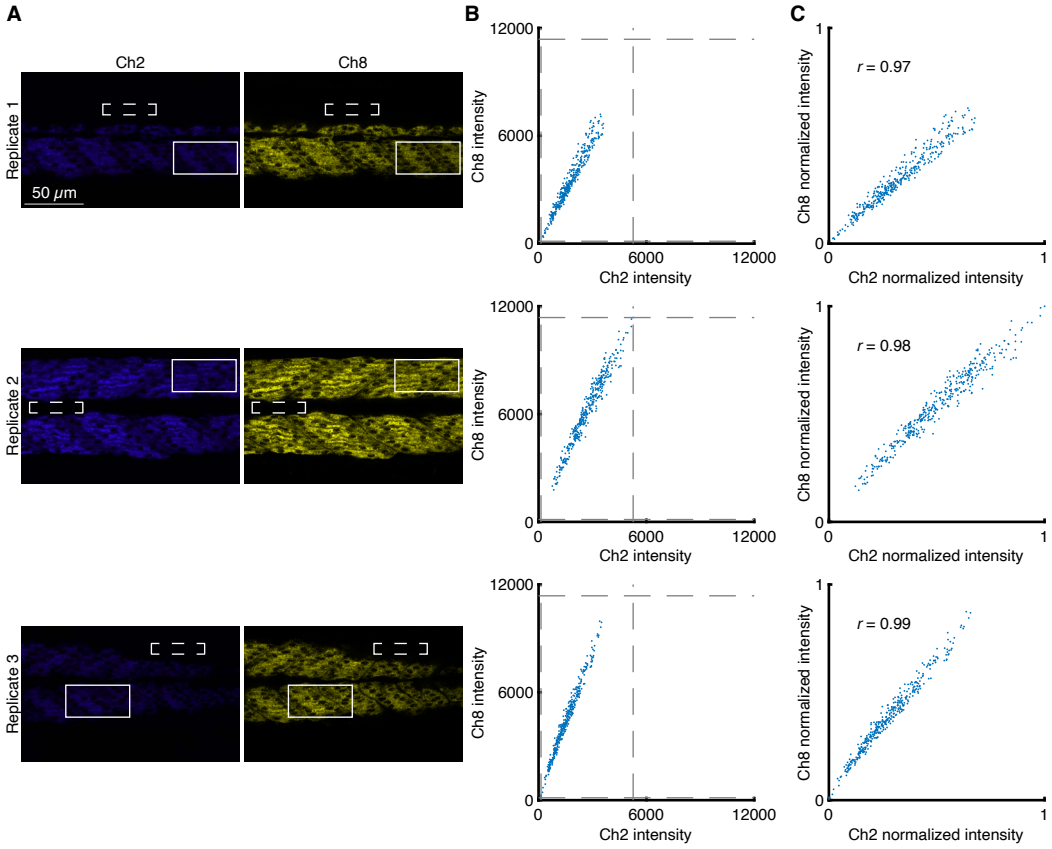

Figure A.5: Redundant 2-channel detection of target RNA *mylpfa* in whole-mount zebrafish embryos (cf. Figure 2.3). (A) Confocal images: individual channels and merge; single optical section. Images were corrected for chromatic aberration with Huygens chromatic aberration correction. Solid boundary denotes region of variable expression; dashed boundary denotes region of no/low expression. Pixel size: 0.180×0.180×1.2 μm. Sample: Whole-mount zebrafish embryos; fixed 27 hpf. (B) Raw voxel intensity scatter plots representing signal plus background for voxels within solid boundary of panel A. Voxel size: 2.0×2.0×1.2 μm. Dashed lines represent BOT and TOP values (Table A.8) used to normalize data for panel C using methods of Section A.1.4. (C) Normalized voxel intensity scatter plots representing estimated normalized signal (Pearson correlation coefficient, r). Ch2: *mylpfa* (Atto425). Ch8: *mylpfa* (Alexa700). Sample: Whole-mount zebrafish embryos; fixed 27 hpf.

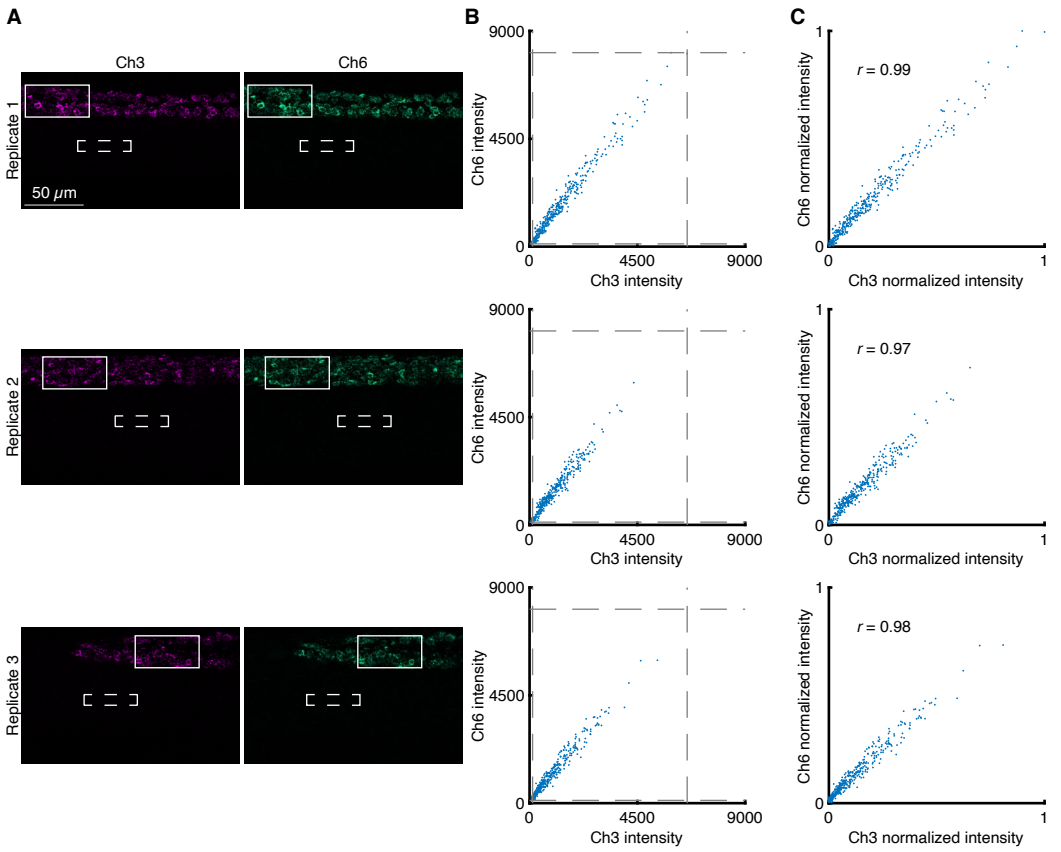

Figure A.6: Redundant 2-channel detection of target RNA *elavl3* in whole-mount zebrafish embryos (cf. Figure 2.3). (A) Confocal images: individual channels and merge; single optical section. Images were corrected for chromatic aberration with Huygens chromatic aberration correction. Solid boundary denotes region of variable expression; dashed boundary denotes region of no/low expression. Pixel size: 0.180×0.180×1.2 μm. Sample: Whole-mount zebrafish embryos; fixed 27 hpf. (B) Raw voxel intensity scatter plots representing signal plus background for voxels within solid boundary of panel A. Voxel size: 2.0×2.0×1.2 μm. Dashed lines represent BOT and TOP values (Table A.8) used to normalize data for panel C using methods of Section A.1.4. (C) Normalized voxel intensity scatter plots representing estimated normalized signal (Pearson correlation coefficient, r). Ch3: *elavl3* (Alexa488). Ch6: *elavl3* (Alexa594). Sample: Whole-mount zebrafish embryos; fixed 27 hpf.

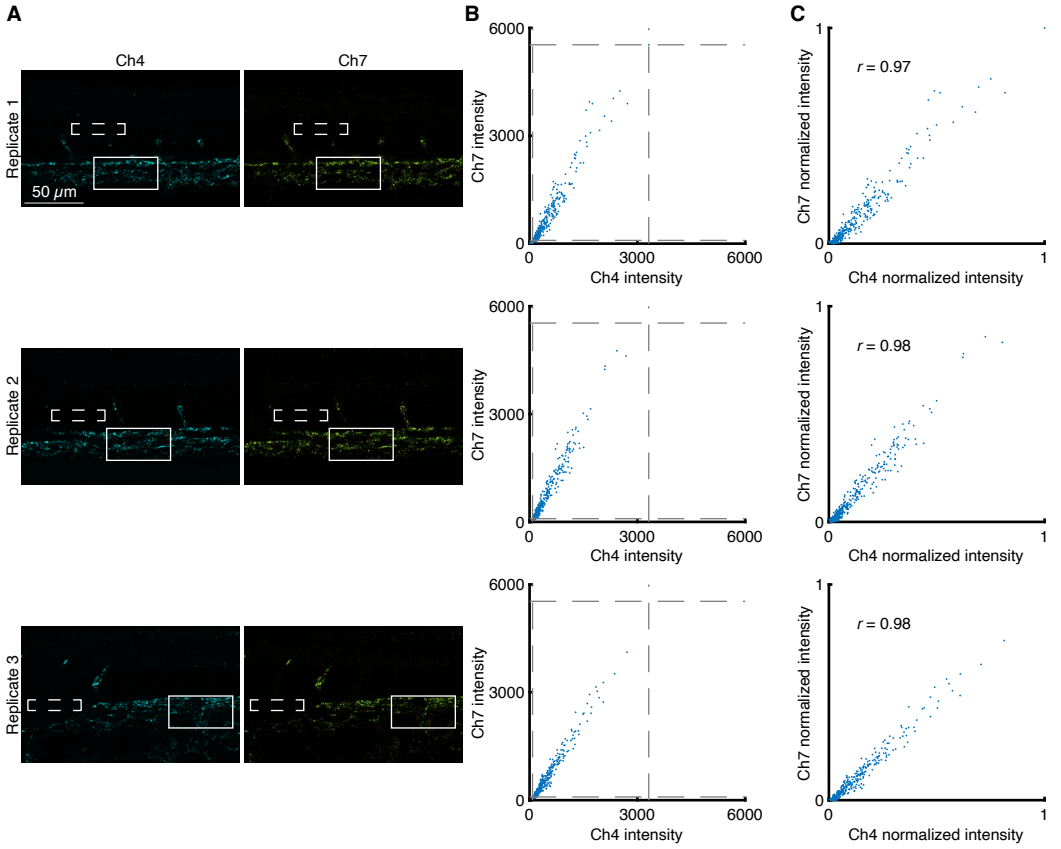

Figure A.7: Redundant 2-channel detection of target RNA *kdrl* in whole-mount zebrafish embryos (cf. Figure 2.3). (A) Confocal images: individual channels and merge; single optical section. Images were corrected for chromatic aberration with Huygens chromatic aberration correction. Solid boundary denotes region of variable expression; dashed boundary denotes region of no/low expression. Pixel size: 0.180×0.180×1.2 μm Sample: Whole-mount zebrafish embryos; fixed 27 hpf. (B) Raw voxel intensity scatter plots representing signal plus background for voxels within solid boundary of panel A. Voxel size: 2.0×2.0×1.2 μm. Dashed lines represent BOT and TOP values (Table A.8) used to normalize data for panel C using methods of Section A.1.4. (C) Normalized voxel intensity scatter plots representing estimated normalized signal (Pearson correlation coefficient, r). Ch4: *kdrl* (Alexa514). Ch7: *kdrl* (Atto633). Sample: Whole-mount zebrafish embryos; fixed 27 hpf.

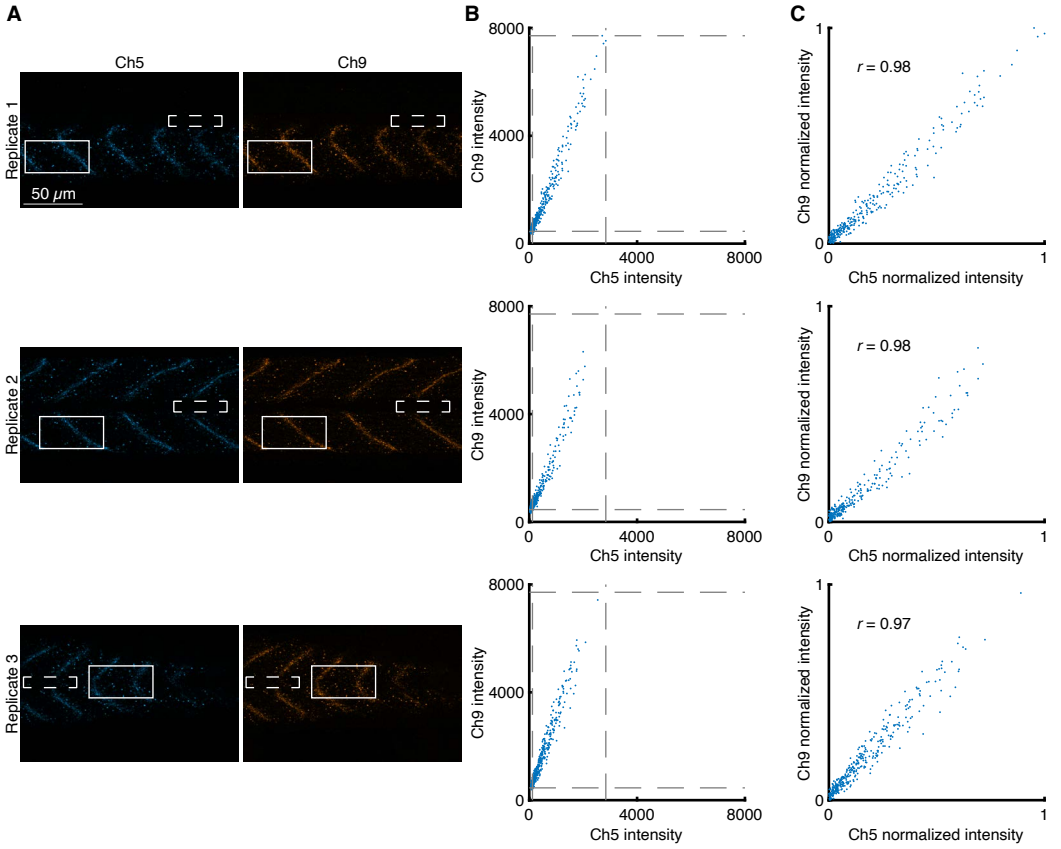

Figure A.8: Redundant 2-channel detection of target RNA *dmd* in whole-mount zebrafish embryos (cf. Figure 2.3). (A) Confocal images: individual channels and merge; single optical section. Images were corrected for chromatic aberration with Huygens chromatic aberration correction. Solid boundary denotes region of variable expression; dashed boundary denotes region of no/low expression. Pixel size: 0.180×0.180×1.2 μm. Sample: Whole-mount zebrafish embryos; fixed 27 hpf. (B) Raw voxel intensity scatter plots representing signal plus background for voxels within solid boundary of panel A. Voxel size: 2.0×2.0×1.2 μm. Dashed lines represent BOT and TOP values (Table A.8) used to normalize data for panel C using methods of Section A.1.4. (C) Normalized voxel intensity scatter plots representing estimated normalized signal (Pearson correlation coefficient, r). Ch5: *dmd* (Alexa546). Ch9: *dmd* (Alexa750). Sample: Whole-mount zebrafish embryos; fixed 27 hpf.

Channel	Target RNA	Fluorophore	BOT	TOP
Ch1	*col2a1a*	Alexa405	140	10923
Ch2	*mylpfa*	Atto425	136	5263
Ch3	*elavl3*	Alexa488	126	6577
Ch4	*kdrl*	Alexa514	83	3316
Ch5	*dmd*	Alexa546	70	2832
Ch6	*elavl3*	Alexa594	115	8094
Ch7	*kdrl*	Atto633	90	5532
Ch8	*mylpfa*	Alexa700	133	11371
Ch9	*dmd*	Alexa750	293	7750
Ch10	*col2a1a*	iFluor800	122	15125

Table A.8: BOT and TOP values used to calculate normalized voxel intensities for scatter plots of Figures 2.3C and A.4C–A.8C using methods of Section A.1.4. Analysis based on rectangular regions depicted in Figures A.4A–A.8A.

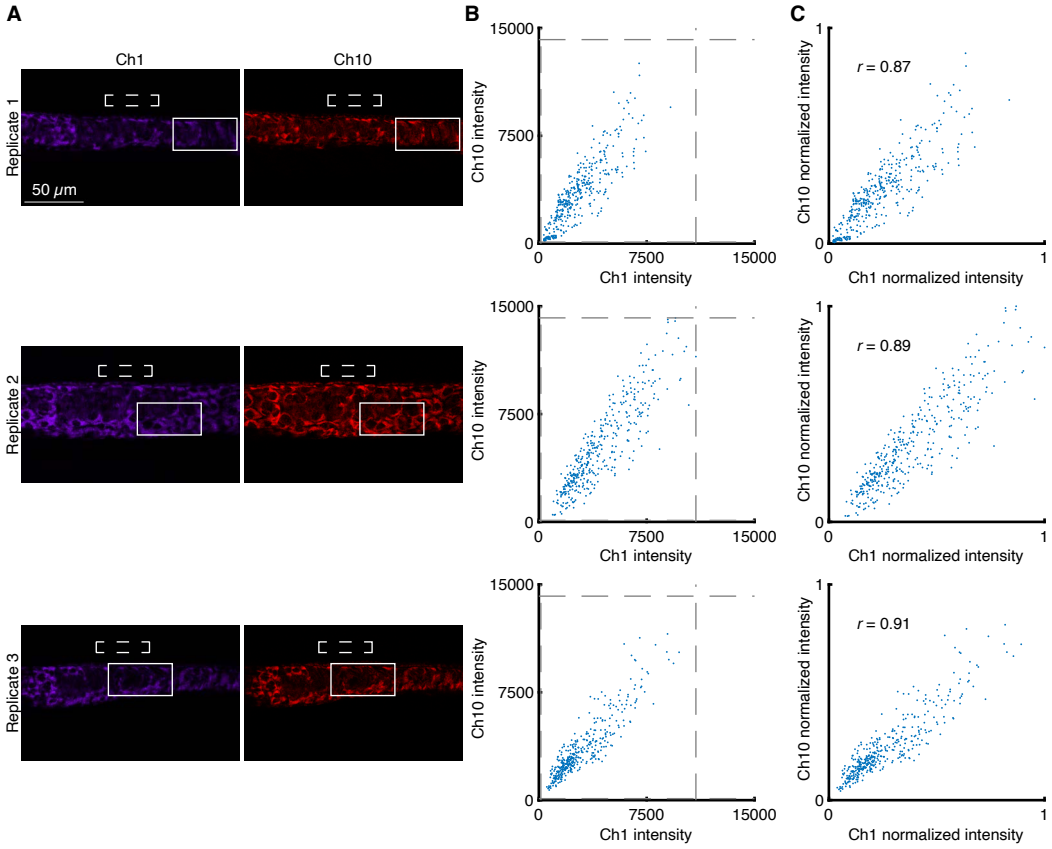

Figure A.9: Redundant 2-channel detection of target RNA *col2a1a* in whole-mount zebrafish embryos without chromatic aberration correction. (A) Confocal images: individual channels and merge; single optical section. Images were not corrected for chromatic aberration. Solid boundary denotes region of variable expression; dashed boundary denotes region of no/low expression. Pixel size: 0.180×0.180×1.2 μm. Sample: Whole-mount zebrafish embryos; fixed 27 hpf. (B) Raw voxel intensity scatter plots representing signal plus background for voxels within solid boundary of panel A. Voxel size: 2.0×2.0×1.2 μm. Dashed lines represent BOT and TOP values (Table A.9) used to normalize data for panel C using methods of Section A.1.4. (C) Normalized voxel intensity scatter plots representing estimated normalized signal (Pearson correlation coefficient, r). Ch1: *col2a1a* (Alexa405). Ch10: *col2a1a* (iFluor800). Sample: Whole-mount zebrafish embryos; fixed 27 hpf.

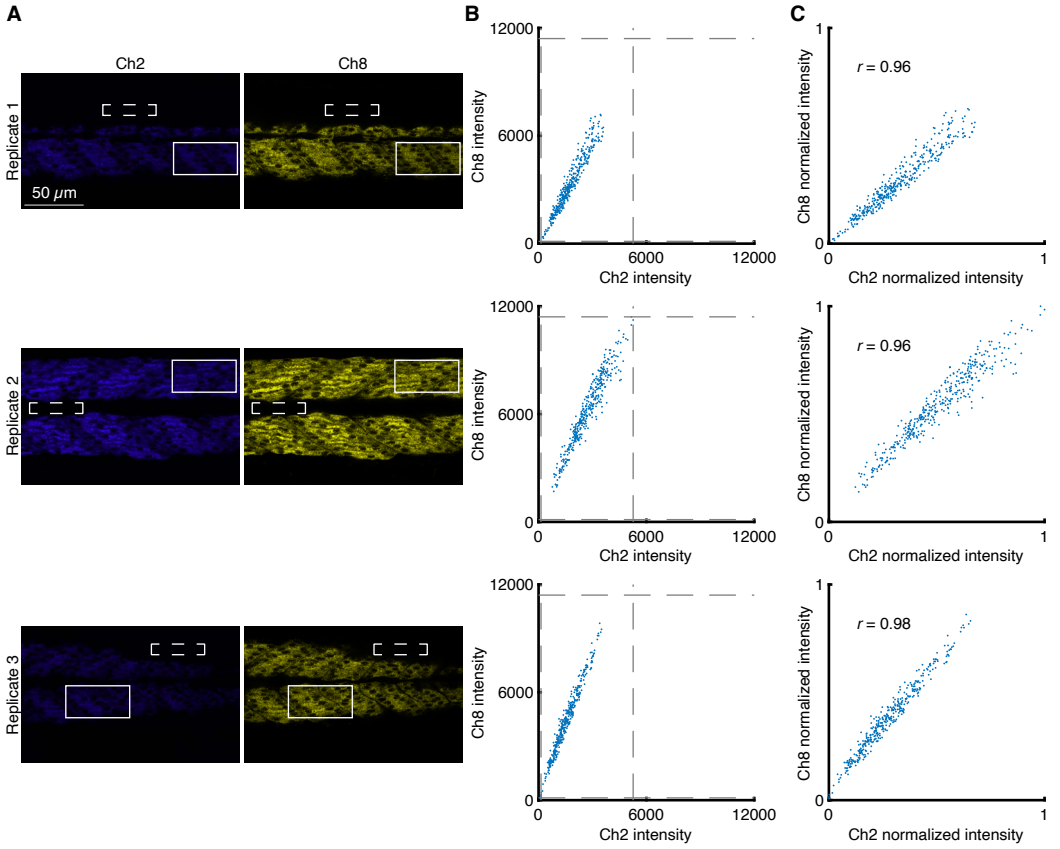

Figure A.10: Redundant 2-channel detection of target RNA *mylpfa* in whole-mount zebrafish embryos without chromatic aberration correction. (A) Confocal images: individual channels and merge; single optical section. Images were not corrected for chromatic aberration. Solid boundary denotes region of variable expression; dashed boundary denotes region of no/low expression. Pixel size: 0.180×0.180×1.2 μm. Sample: Whole-mount zebrafish embryos; fixed 27 hpf. (B) Raw voxel intensity scatter plots representing signal plus background for voxels within solid boundary of panel A. Voxel size: 2.0×2.0×1.2 μm. Dashed lines represent BOT and TOP values (Table A.9) used to normalize data for panel C using methods of Section A.1.4. (C) Normalized voxel intensity scatter plots representing estimated normalized signal (Pearson correlation coefficient, r). Ch2: *mylpfa* (Atto425). Ch8: *mylpfa* (Alexa700). Sample: Whole-mount zebrafish embryos; fixed 27 hpf.

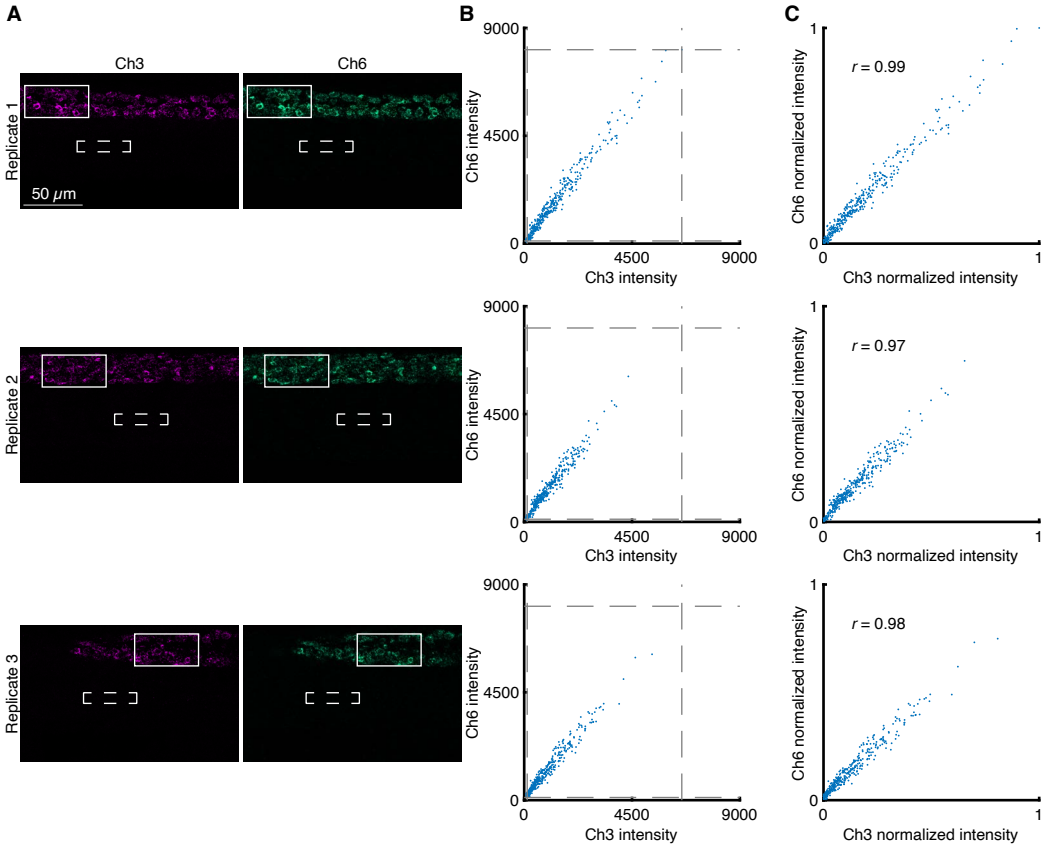

Figure A.11: Redundant 2-channel detection of target RNA *elavl3* in whole-mount zebrafish embryos without chromatic aberration correction. (A) Confocal images: individual channels and merge; single optical section. Images were not corrected for chromatic aberration. Solid boundary denotes region of variable expression; dashed boundary denotes region of no/low expression. Pixel size: 0.180×0.180×1.2 μm. Sample: Whole-mount zebrafish embryos; fixed 27 hpf. (B) Raw voxel intensity scatter plots representing signal plus background for voxels within solid boundary of panel A. Voxel size: 2.0×2.0×1.2 μm. Dashed lines represent BOT and TOP values (Table A.9) used to normalize data for panel C using methods of Section A.1.4. (C) Normalized voxel intensity scatter plots representing estimated normalized signal (Pearson correlation coefficient, r). Ch3: *elavl3* (Alexa488). Ch6: *elavl3* (Alexa594). Sample: Whole-mount zebrafish embryos; fixed 27 hpf.

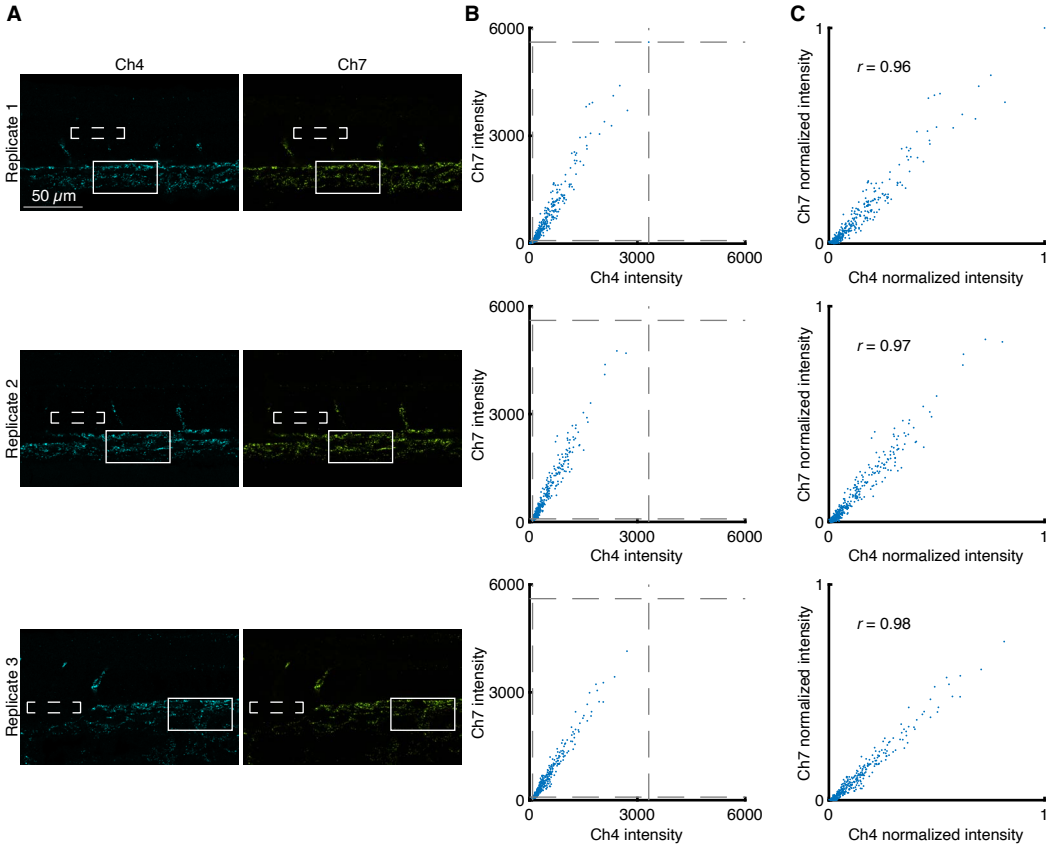

Figure A.12: Redundant 2-channel detection of target RNA *kdrl* in whole-mount zebrafish embryos without chromatic aberration correction. (A) Confocal images: individual channels and merge; single optical section. Images were not corrected for chromatic aberration. Solid boundary denotes region of variable expression; dashed boundary denotes region of no/low expression. Pixel size: 0.180×0.180×1.2 μm Sample: Whole-mount zebrafish embryos; fixed 27 hpf. (B) Raw voxel intensity scatter plots representing signal plus background for voxels within solid boundary of panel A. Voxel size: 2.0×2.0×1.2 μm. Dashed lines represent BOT and TOP values (Table A.9) used to normalize data for panel C using methods of Section A.1.4. (C) Normalized voxel intensity scatter plots representing estimated normalized signal (Pearson correlation coefficient, r). Ch4: *kdrl* (Alexa514). Ch7: *kdrl* (Atto633). Sample: Whole-mount zebrafish embryos; fixed 27 hpf.

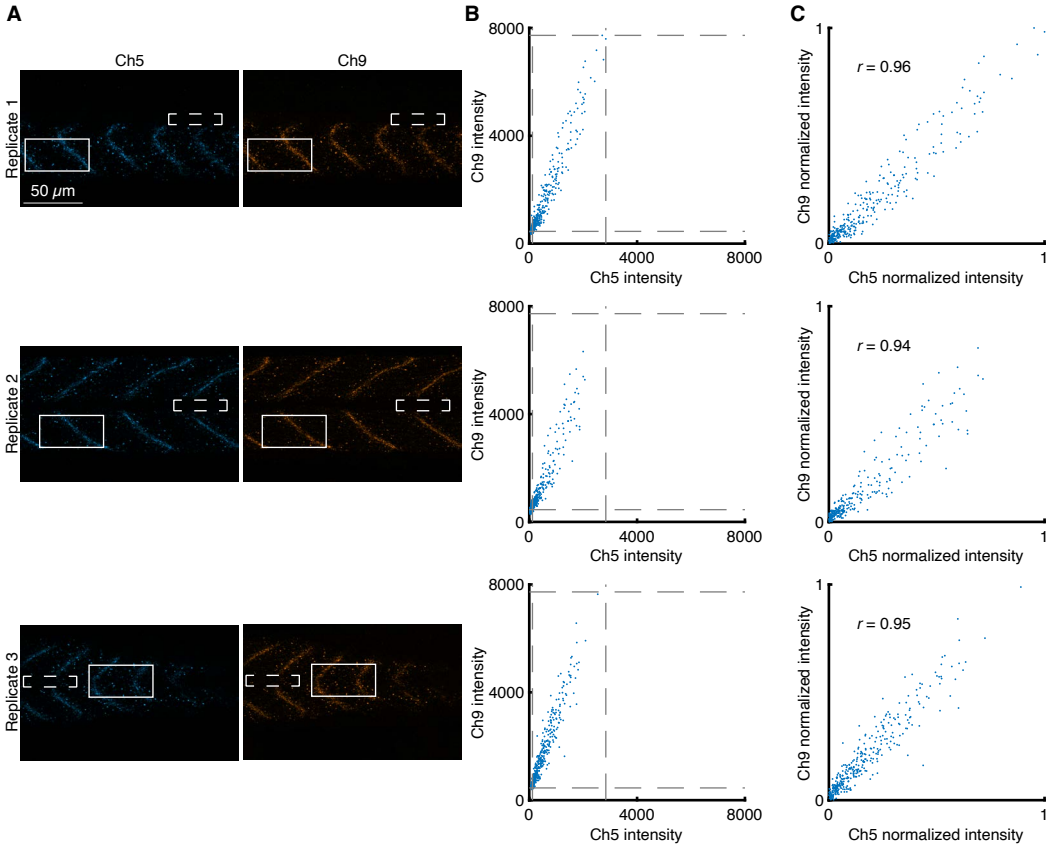

Figure A.13: Redundant 2-channel detection of target RNA *dmd* in whole-mount zebrafish embryos without chromatic aberration correction. (A) Confocal images: individual channels and merge; single optical section. Images were not corrected for chromatic aberration. Solid boundary denotes region of variable expression; dashed boundary denotes region of no/low expression. Pixel size: 0.180×0.180×1.2 μm. Sample: Whole-mount zebrafish embryos; fixed 27 hpf. (B) Raw voxel intensity scatter plots representing signal plus background for voxels within solid boundary of panel A. Voxel size: 2.0×2.0×1.2 μm. Dashed lines represent BOT and TOP values (Table A.9) used to normalize data for panel C using methods of Section A.1.4. (C) Normalized voxel intensity scatter plots representing estimated normalized signal (Pearson correlation coefficient, r). Ch5: *dmd* (Alexa546). Ch9: *dmd* (Alexa750). Sample: Whole-mount zebrafish embryos; fixed 27 hpf.

Channel	Target RNA	Fluorophore	BOT	TOP
Ch1	*col2a1a*	Alexa405	140	10923
Ch2	*mylpfa*	Atto425	136	5263
Ch3	*elavl3*	Alexa488	126	6577
Ch4	*kdrl*	Alexa514	83	3316
Ch5	*dmd*	Alexa546	70	2832
Ch6	*elavl3*	Alexa594	112	8092
Ch7	*kdrl*	Atto633	85	5606
Ch8	*mylpfa*	Alexa700	127	11410
Ch9	*dmd*	Alexa750	286	7506
Ch10	*col2a1a*	iFluor800	108	14190

Table A.9: BOT and TOP values used to calculate normalized voxel intensities for scatter plots of Figures A.9C–A.13C using methods of Section A.1.4 without chromatic aberration correction. Analysis based on rectangular regions depicted in Figures A.9A–A.13A.

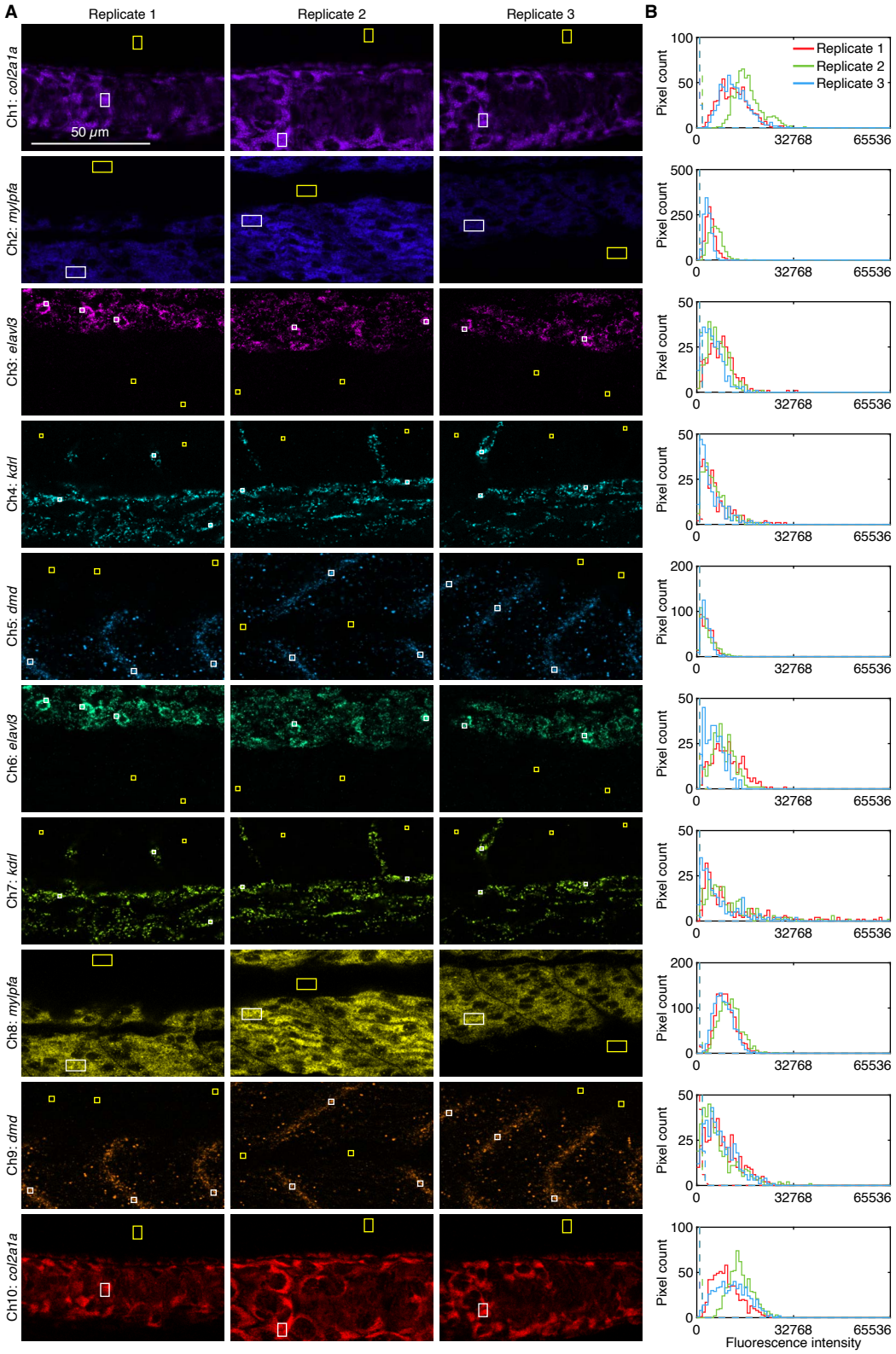

Figure A.14: Measurement of signal and background for redundant 2-channel detection of 5 target RNAs in whole-mount zebrafish embryos (cf. Figure 2.3).
Caption continues on next page.

Figure A.14 (continued). (A) Ch1: *col2a1a* (Alexa405). Ch2: *mylpfa* (Atto425). Ch3: *elavl3* (Alexa488). Ch4: *kdrl* (Alexa514). Ch5: *dmd* (Alexa546). Ch6: *elavl3* (Alexa594). Ch7: *kdrl* (Atto633). Ch8: *mylpfa* (Alexa700). Ch9: *dmd* (Alexa750). Ch10: *col2a1a* (iFluor800). Left: confocal images; single optical section. Images were not corrected for chromatic aberration. Solid white boundaries denote representative regions of high expression; solid yellow boundaries denote representative regions of no/low expression. Right: pixel intensity histograms for the depicted representative regions. Sample: Whole-mount zebrafish embryos; fixed 27 hpf.

Channel	Target RNA	Fluorophore	SIG+BACK	SIG	BACK	SIG/BACK
Ch1	*col2a1a*	Alexa405	14 000 ± 3000	14 000 ± 3000	160 ± 50	80 ± 30
Ch2	*mylpfa*	Atto425	4000 ± 1000	4000 ± 1000	123 ± 9	30 ± 10
Ch3	*elavl3*	Alexa488	6500 ± 900	6300 ± 900	130 ± 20	50 ± 10
Ch4	*kdrl*	Alexa514	5300 ± 900	5200 ± 900	100 ± 20	50 ± 10
Ch5	*dmd*	Alexa546	3000 ± 200	2900 ± 200	70 ± 10	40 ± 6
Ch6	*elavl3*	Alexa594	8000 ± 1000	8000 ± 1000	110 ± 40	70 ± 30
Ch7	*kdrl*	Atto633	10 000 ± 2000	10 000 ± 2000	90 ± 30	110 ± 40
Ch8	*mylpfa*	Alexa700	10 000 ± 1000	10 000 ± 1000	70 ± 20	130 ± 40
Ch9	*dmd*	Alexa750	7600 ± 600	7300 ± 600	270 ± 60	27 ± 7
Ch10	*col2a1a*	iFluor800	12 000 ± 2000	12 000 ± 2000	110 ± 30	100 ± 30

Table A.10: Estimated signal-to-background for redundant 2-channel detection of 5 target RNAs in whole-mount zebrafish embryos (cf. Figure 2.3). Mean ± standard error of the mean (SEM), $N = 3$ replicate embryos. Analysis based on rectangular regions depicted in Figure A.14 using methods of Section A.1.4.

A.3.3 dHCR imaging: RNA absolute quantitation in an anatomical context (cf. Figure 2.4)

For redundant single-molecule imaging of *kdrl* using HCR RNA-FISH in whole-mount zebrafish embryos, the reagents are listed in Table A.1.1. Section A.1.4 displays the dot detection settings used in the DotDetection 2.0 notebook. Additional studies are presented as follows:

- Figure A.15 displays images with single-molecule dots identified for target RNA *kdrl* in $N = 3$ replicate embryos.
- Table A.11 displays the number of dots detected per channel and the colocalization fraction for $N = 3$ replicate embryos.
- Figure A.16 displays all 10 unmixed channels in $N = 3$ replicate embryos.

Protocol: 10-plex HCR RNA-FISH (Section A.2.2) using split-initiator probes with HCR signal amplification for all 10 targets simultaneously.
Sample: Whole-mount zebrafish embryos; fixed 27 hpf.
Microscopy: Spectral confocal.

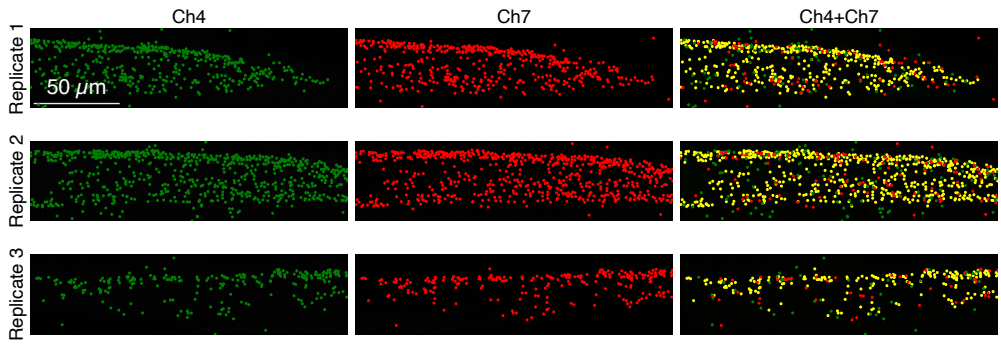

Figure A.15: Redundant 2-channel detection of target RNA *kdrl* in whole-mount zebrafish embryos in the context of 10-plex spectral imaging with linear unmixing (cf. Figure 2.4). Alongside four other redundantly detected targets, target RNA *kdrl* was redundantly detected using two split-initiator DNA probe sets labeled with orthogonal HCR initiators that bind interleaving locations along the target RNA. The 10-plex zebrafish embryo was spectrally imaged in the dorsal posterior tail, where *kdrl* is expressed as single molecule punctae, and linearly unmixed. Left: Ch4 (*kdrl*; Alexa514). Middle: Ch7 (*kdrl*; Atto633). Right: Ch4+Ch7 merge. Green circles denote dots detected in Ch4, red circles denote dots detected in Ch7, and yellow circles denote dots detected in both channels. See Table A.11 for colocalization rates. Dots were detected using the DotDetection 2.0 notebook (available for download from www.moleculartechnologies.org). For each replicate, a maximum intensity z-projection of 5 z-dimension sections (2.7 μm total) is shown. 0.180×0.180×1.2 μm pixels. Sample: 27 hpf whole-mount zebrafish embryo. Channels unmixed with the Leica LAS X software.

	Dots		Colocalized dots	Colocalization fractions	
	N_4	N_7	N_{47}	C_4	C_7
Replicate 1	453	445	364	0.80	0.82
Replicate 2	666	644	538	0.81	0.84
Replicate 3	235	232	187	0.80	0.81
Mean				0.80 ± 0.003	0.82 ± 0.009

Table A.11: Dot colocalization fractions for redundant 2-channel detection of *kdrl* RNA in whole-mount zebrafish embryos in the context of 10-plex spectral imaging with linear unmixing (cf. Figure 2.4). The *kdrl* target RNA was detected in Ch4 and Ch7 as part of a 10-plex experiment. Colocalization rate indicates the fraction of dots in each channel that are detected in both channels (mean ± estimated standard error of the mean via uncertainty propagation for $N = 3$ replicate embryos). Analysis based on the images in Figure A.15 using the methods of section A.1.4 and the DotDetection 2.0 notebook (available for download from www.moleculartechnologies.com).

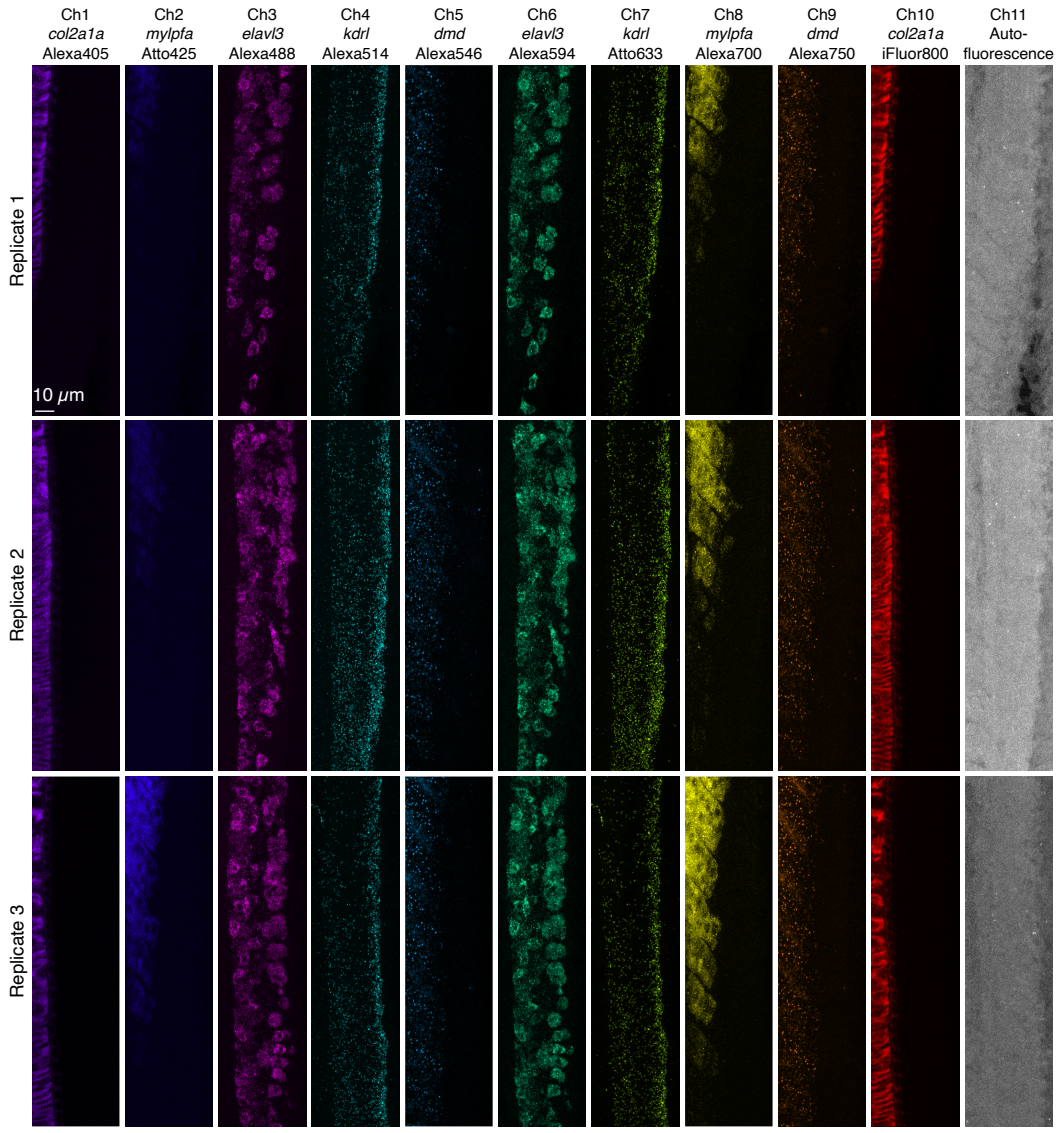

Figure A.16: All unmixed channels for 10-plex RNA imaging using HCR RNA-FISH in whole-mount zebrafish embryos; unmixed with the Leica Stellaris LAS X software (cf. Figure 2.4). Ch1: *col2a1a* (Alexa405). Ch2: *mylpfa* (Atto425). Ch3: *elavl3* (Alexa488). Ch4: *kdrl* (Alexa514). Ch5: *dmd* (Alexa546). Ch6: *elavl3* (Alexa594). Ch7: *kdrl* (Atto633). Ch8: *mylpfa* (Alexa700). Ch9: *dmd* (Alexa750). Ch10: *col2a1a* (iFluor800). Replicate 1: maximum intensity z-projection of 40 z-dimension sections (15.4 μm total). Replicate 2: maximum intensity z-projection of 45 z-dimension sections (17.3 μm total). Replicate 3: maximum intensity z-projection of 43 z-dimension sections (16.5 μm total). 0.180×0.180×1.2 μm pixels. Sample: 27 hpf whole-mount zebrafish embryo. Channels unmixed with the Leica LAS X software. Sample: Whole-mount zebrafish embryos; fixed 27 hpf.

A.3.4 Replicates, signal, and background for 10-plex protein and RNA imaging with high signal-to-background in fresh-frozen mouse brain sections (cf. Figure 2.5)

For 10-plex protein and RNA imaging using HCR IF + HCR RNA-FISH in fresh-frozen thick mouse brain sections, the reagents are listed in Table A.1.1. Additional studies are presented as follows:

- Figures A.17–A.19 displays 10-plex images unmixed using the Leica Stellaris LAS X software for $N = 3$ replicate fresh-frozen mouse brain sections (cf. Figure 2.5).
- Figures A.20–A.22 displays 10-plex images unmixed using the LinearUnmixing 1.0 notebook we developed for the present work for $N = 3$ replicate fresh-frozen mouse brain sections.
- Figure A.23 displays representative regions of individual channels used for measurement of signal and background for each target.
- Table A.12 displays estimated values for signal, background, and signal-to-background for each target.

Protocol: Simultaneous HCR IF + HCR RNA-FISH (Section A.2.3) using unlabeled primary antibody probes and initiator-labeled secondary antibody probes for protein targets, split-initiator DNA probes for RNA targets, and simultaneous HCR signal amplification for all 10 targets.
Sample: Fresh-frozen mouse brain section (coronal); thickness: 5 μm.
Microscopy: Spectral confocal.

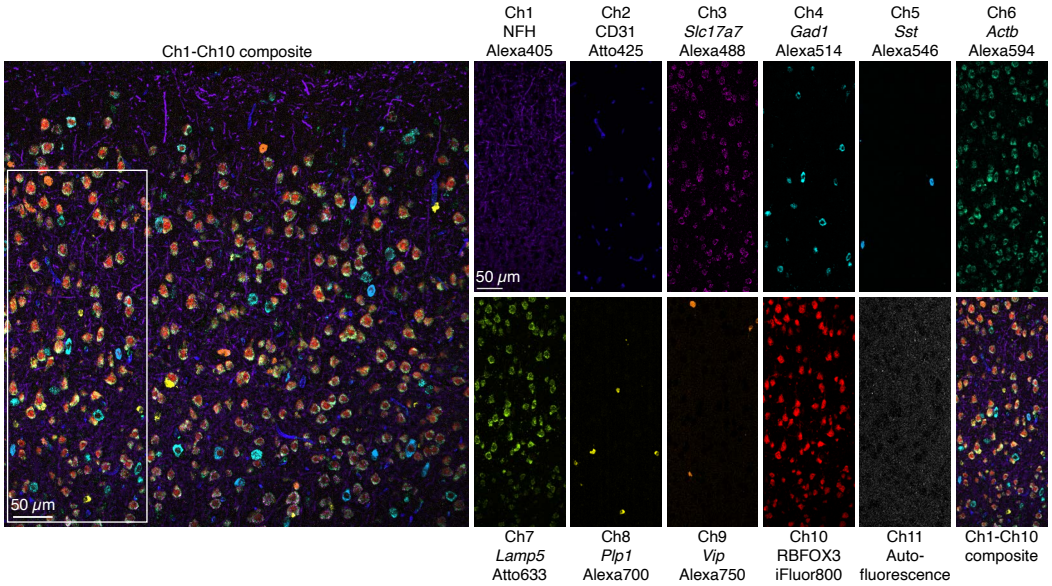

Figure A.17: Replicate 1 for 10-plex simultaneous protein and RNA imaging using HCR IF and HCR RNA-FISH in a fresh-frozen mouse brain section; unmixed with the Leica Stellaris LAS X software (cf. Figure 2.5). Left: Composite of Ch1-Ch10 confocal images for fresh-frozen mouse brain section replicate 1. Right: Single-channel images of the depicted region in the left panel. Ch1: target protein NFH (Alexa405). Ch2: target protein CD31 (Atto425). Ch3: target RNA *Slc17a7* (Alexa488). Ch4: target RNA *Gad1* (Alexa514). Ch5: target RNA *Sst* (Alexa546). Ch6: target RNA *Actb* (Alexa594). Ch7: target RNA *Lamp5* (Atto633). Ch8: target RNA *Plp1* (Alexa700). Ch9: target RNA *Vip* (Alexa750). Ch10: target protein RBFOX3 (iFluor800). Sample: Fresh-frozen mouse brain section (coronal); thickness: 5 μm. Single optical section shown.

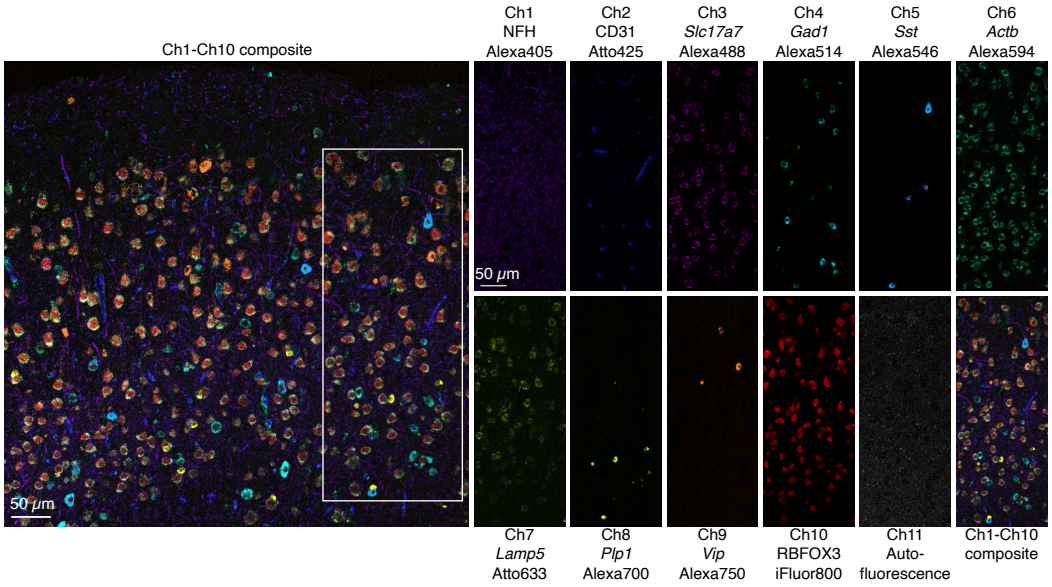

Figure A.18: Replicate 2 for 10-plex simultaneous protein and RNA imaging using HCR IF and HCR RNA-FISH in a fresh-frozen mouse brain section; unmixed with the Leica Stellaris LAS X software (cf. Figure 2.5). Left: Composite of Ch1-Ch10 confocal images for fresh-frozen mouse brain section replicate 2. Right: Single-channel images of the depicted region in the left panel. Ch1: target protein NFH (Alexa405). Ch2: target protein CD31 (Atto425). Ch3: target RNA *Slc17a7* (Alexa488). Ch4: target RNA *Gad1* (Alexa514). Ch5: target RNA *Sst* (Alexa546). Ch6: target RNA *Actb* (Alexa594). Ch7: target RNA *Lamp5* (Atto633). Ch8: target RNA *Plp1* (Alexa700). Ch9: target RNA *Vip* (Alexa750). Ch10: target protein RBFOX3 (iFluor800). Sample: Fresh-frozen mouse brain section (coronal); thickness: 5 μm. Single optical section shown.

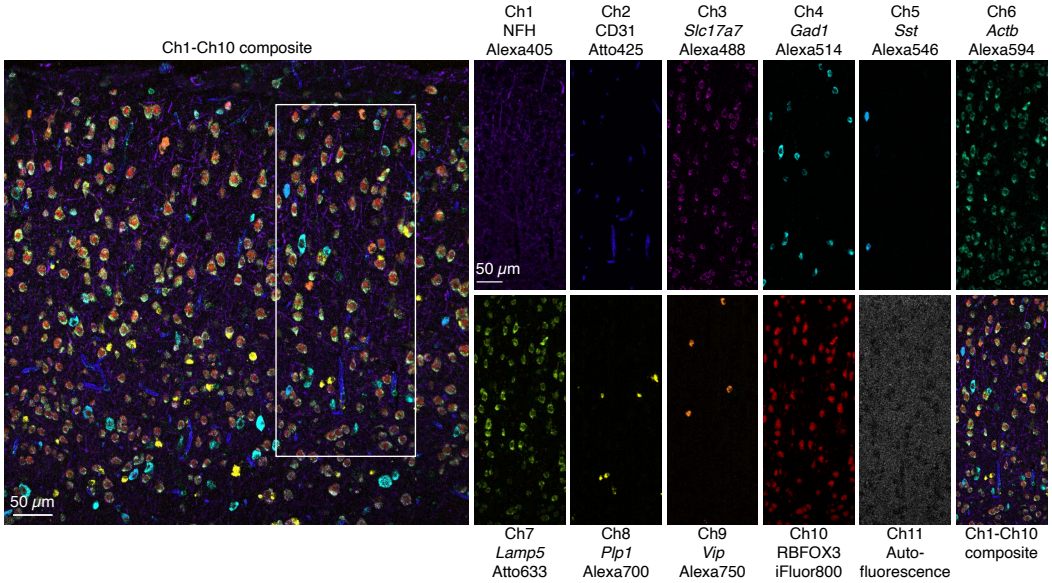

Figure A.19: Replicate 3 for 10-plex simultaneous protein and RNA imaging using HCR IF and HCR RNA-FISH in a fresh-frozen mouse brain section; unmixed with the Leica Stellaris LAS X software (cf. Figure 2.5). Left: Composite of Ch1-Ch10 confocal images for fresh-frozen mouse brain section replicate 3. Right: Single-channel images of the depicted region in the left panel. Ch1: target protein NFH (Alexa405). Ch2: target protein CD31 (Atto425). Ch3: target RNA *Slc17a7* (Alexa488). Ch4: target RNA *Gad1* (Alexa514). Ch5: target RNA *Sst* (Alexa546). Ch6: target RNA *Actb* (Alexa594). Ch7: target RNA *Lamp5* (Atto633). Ch8: target RNA *Plp1* (Alexa700). Ch9: target RNA *Vip* (Alexa750). Ch10: target protein RBFOX3 (iFluor800). Sample: Fresh-frozen mouse brain section (coronal); thickness: 5 μm. Single optical section shown.

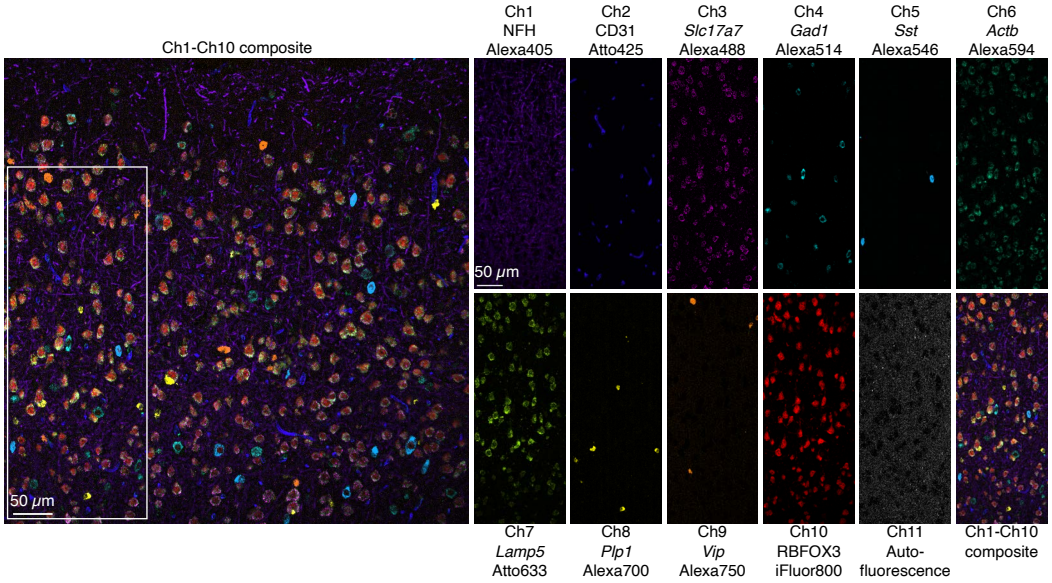

Figure A.20: Replicate 1 for 10-plex simultaneous protein and RNA imaging using HCR IF and HCR RNA-FISH in a fresh-frozen mouse brain section; unmixed with the LinearUnmixing 1.0 notebook. Left: Composite of Ch1-Ch10 confocal images for fresh-frozen mouse brain section replicate 1. Right: Single-channel images of the depicted region in the left panel. Ch1: target protein NFH (Alexa405). Ch2: target protein CD31 (Atto425). Ch3: target RNA *Slc17a7* (Alexa488). Ch4: target RNA *Gad1* (Alexa514). Ch5: target RNA *Sst* (Alexa546). Ch6: target RNA *Actb* (Alexa594). Ch7: target RNA *Lamp5* (Atto633). Ch8: target RNA *Plp1* (Alexa700). Ch9: target RNA *Vip* (Alexa750). Ch10: target protein RBFOX3 (iFluor800). Sample: Fresh-frozen mouse brain section (coronal); thickness: 5 μm. Single optical section shown.

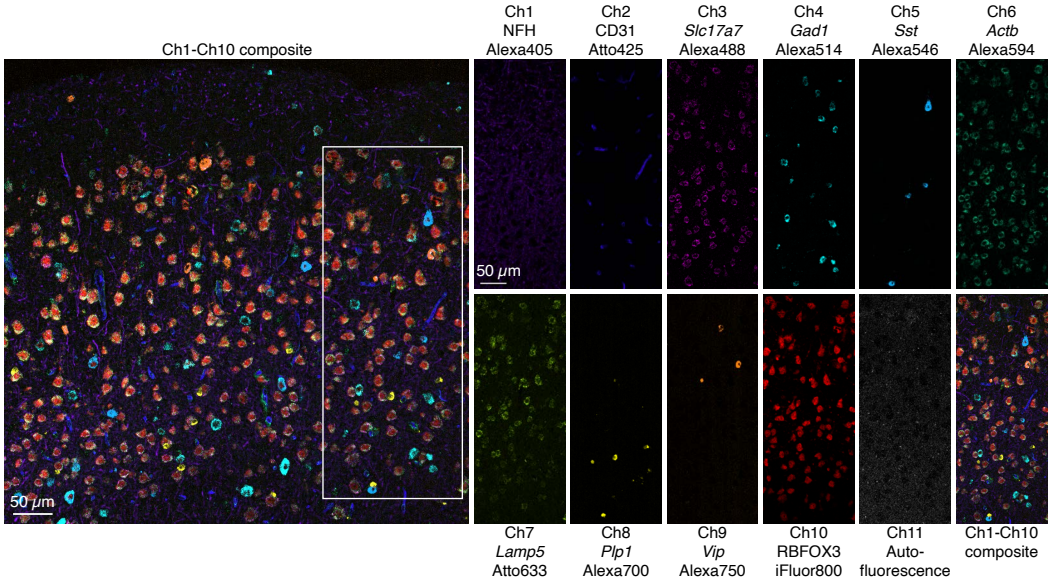

Figure A.21: Replicate 2 for 10-plex simultaneous protein and RNA imaging using HCR IF and HCR RNA-FISH in a fresh-frozen mouse brain section; unmixed with the LinearUnmixing 1.0 notebook. Left: Composite of Ch1-Ch10 confocal images for fresh-frozen mouse brain section replicate 2. Right: Single-channel images of the depicted region in the left panel. Ch1: target protein NFH (Alexa405). Ch2: target protein CD31 (Atto425). Ch3: target RNA *Slc17a7* (Alexa488). Ch4: target RNA *Gad1* (Alexa514). Ch5: target RNA *Sst* (Alexa546). Ch6: target RNA *Actb* (Alexa594). Ch7: target RNA *Lamp5* (Atto633). Ch8: target RNA *Plp1* (Alexa700). Ch9: target RNA *Vip* (Alexa750). Ch10: target protein RBFOX3 (iFluor800). Sample: Fresh-frozen mouse brain section (coronal); thickness: 5 μm. Single optical section shown.

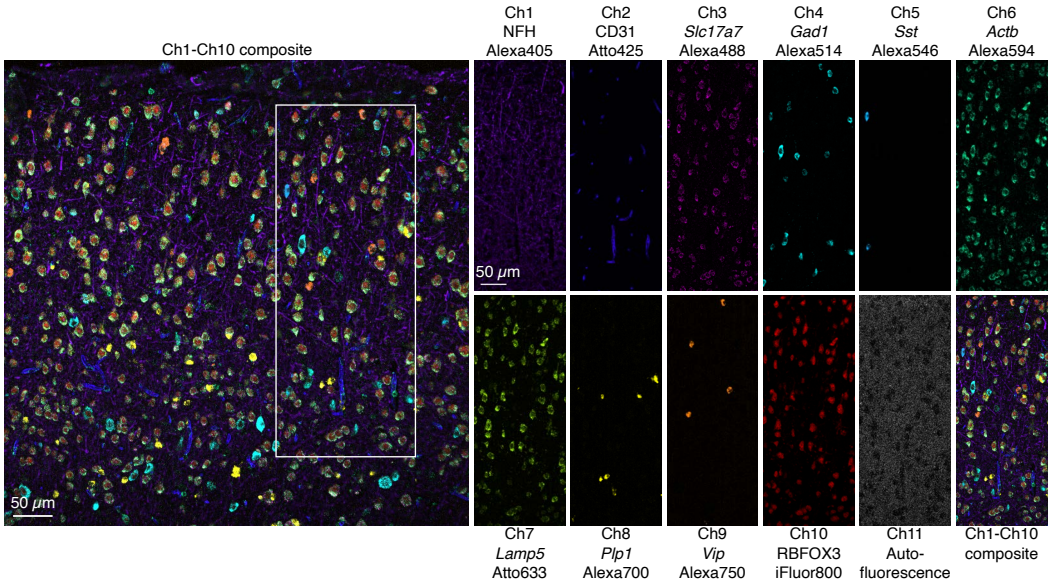

Figure A.22: Replicate 3 for 10-plex simultaneous protein and RNA imaging using HCR IF and HCR RNA-FISH in a fresh-frozen mouse brain section; unmixed with the LinearUnmixing 1.0 notebook. Left: Composite of Ch1-Ch10 confocal images for fresh-frozen mouse brain section replicate 3. Right: Single-channel images of the depicted region in the left panel. Ch1: target protein NFH (Alexa405). Ch2: target protein CD31 (Atto425). Ch3: target RNA *Slc17a7* (Alexa488). Ch4: target RNA *Gad1* (Alexa514). Ch5: target RNA *Sst* (Alexa546). Ch6: target RNA *Actb* (Alexa594). Ch7: target RNA *Lamp5* (Atto633). Ch8: target RNA *Plp1* (Alexa700). Ch9: target RNA *Vip* (Alexa750). Ch10: target protein RBFOX3 (iFluor800). Sample: Fresh-frozen mouse brain section (coronal); thickness: 5 μm. Single optical section shown.

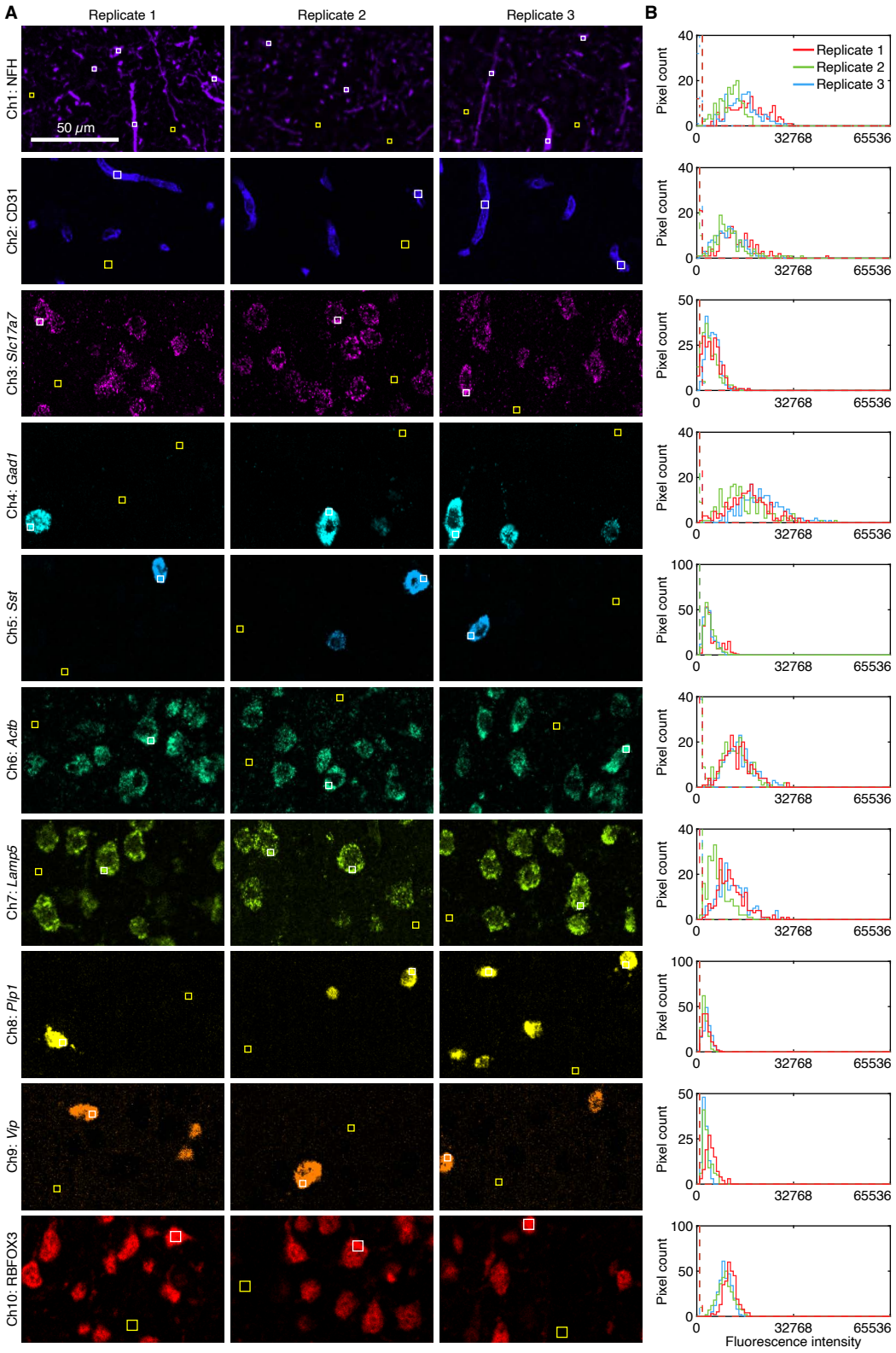

Figure A.23: Measurement of signal and background for 10-plex simultaneous protein and RNA imaging using HCR IF and HCR RNA-FISH in fresh-frozen mouse brain sections (cf. Figure 2.5). *Caption continues on next page.*

Figure A.23 (continued). (A) Individual channels of 10-channel confocal images. Single optical section shown. (B) Pixel intensity histograms for Signal + Background (pixels within solid white boundary) and Background (pixels within solid yellow boundary). Confocal images collected with the microscope laser intensity and detector gain optimized to avoid saturating SIG+BACK pixels. Images were unmixed using the Leica Stellaris LAS X software. Ch1: protein NFH (Alexa405). Ch2: protein CD31 (Atto425). Ch3: RNA *Slc17a7* (Alexa488). Ch4: RNA *Gad1* (Alexa514). Ch5: RNA *Sst* (Alexa546). Ch6: RNA *Actb* (Alexa594). Ch7: RNA *Lamp5* (Atto633). Ch8: RNA *Plp1* (Alexa700). Ch9: RNA *Vip* (Alexa750). Ch10: protein RBFOX3 (iFluor800). Sample: Fresh-frozen mouse brain section (coronal); thickness: 5 μm.

Channel	Target	Type	Fluorophore	SIG+BACK	SIG	BACK	SIG/BACK
Ch1	NFH	protein	Alexa405	14 000 ± 1000	14 000 ± 1000	520 ± 60	26 ± 4
Ch2	CD31	protein	Atto425	12 000 ± 1000	11 000 ± 1000	200 ± 40	60 ± 10
Ch3	*Slc17a7*	RNA	Alexa488	4500 ± 200	4300 ± 300	170 ± 20	25 ± 4
Ch4	*Gad1*	RNA	Alexa514	18 000 ± 2000	18 000 ± 2000	170 ± 20	110 ± 20
Ch5	*Sst*	RNA	Alexa546	4100 ± 800	4100 ± 800	28 ± 3	140 ± 30
Ch6	*Actb*	RNA	Alexa594	13 200 ± 600	13 000 ± 600	380 ± 60	34 ± 6
Ch7	*Lamp5*	RNA	Atto633	10 000 ± 1000	10 000 ± 1000	300 ± 50	30 ± 6
Ch8	*Plp1*	RNA	Alexa700	2700 ± 400	2700 ± 400	27 ± 5	100 ± 20
Ch9	*Vip*	RNA	Alexa750	3300 ± 700	3200 ± 700	39 ± 9	80 ± 30
Ch10	RBFOX3	protein	iFluor800	9800 ± 600	9700 ± 600	100 ± 10	100 ± 10

Table A.12: Estimated signal-to-background for 10-plex simultaneous protein and RNA imaging using HCR IF and HCR RNA-FISH in fresh-frozen mouse brain sections (cf. Figure 2.5). Mean ± estimated standard error of the mean via uncertainty propagation for $N = 3$ replicate brain sections. Analysis based on representative rectangular regions depicted in Figure A.23 using methods of Section A.1.4.

Appendix B

SUPPLEMENTARY INFORMATION FOR CHAPTER 3

B.1 Materials and methods

B.1.1 Cell culture and tissue sections

Experiments were performed in A-431 cells (ATCC, CRL-1555) cultured in Dulbecco's Modified Eagle Medium (DMEM) with high glucose and pyruvate (Gibco, 11995-073) supplemented with 10% fetal bovine serum (FBS) (Sigma-Aldrich, F4135), as well as in HeLa cells (ATCC, CRM-CCL-2) cultured in Eagle's Minimum Essential Medium (EMEM) (ATCC, 30-2003) supplemented with 10% FBS (Sigma-Aldrich, F4135). HCR imaging of protein:protein complexes was performed in Scid.adh.2C2 mouse pro-T cells (*88*) cultured in RPMI1640 media (Gibco, 31800022) supplemented with 10% FBS (Sigma-Aldrich, F2442), 1× Penicillin-Streptomycin-Glutamine (Gibco, 10378-016), 0.1 mM sodium pyruvate (Gibco, 11360-070), 1× MEM non-essential amino acids (Gibco, 11140-050), and 50 μM β-mercaptoethanol (Gibco, 21985-023) using the protocol detailed in Section B.2.3. HCR imaging of protein:protein complexes was performed in 5 μm normal FFPE human breast tissue sections (Acepix Biosciences, HuN-06-0027) and invasive lobular carcinoma FFPE human breast tissue sections (Acepix Biosciences, HuC-06-0101) from the same patient using the protocol details in Section B.2.2.

Species	Sample	Protein:protein complex	1°Ab probe Interaction probe	Dilution factor Working conc. (μg/mL)	Supplier (catalog #)	HCR amplifier	Figures
H. sapiens sapiens	Adherent cells	β-catenin:E-cadherin	1°mAb mouse IgG1 anti-β-catenin	1:100	Abc (ab237983)		
			2°pAb goat anti-mouse IgG1-P1-B1	1	MT (A9111-AB1)		
			1°mAb rabbit IgG anti-E-cadherin	1:200	CST (3195S)		
			2°pAb donkey anti-rabbit IgG-P2-B1	1	MT (A9230-ZB1)	B1-Alexa647	3.2, B.1, B.2
		β-tubulin:α-tubulin	1°mAb mouse IgG2a anti-β-tubulin	1:50	Inv (MA5-16308)		
			2°pAb goat anti-mouse IgG2a-P1-B6	1	MT (A9112-AB6)		
			1°pAb guinea pig IgG anti-α-tubulin	1:500	Sy (302 204)		
			2°pAb donkey anti-guinea pig IgG-P2-B6	1	MT (A9231-ZB6)	B6-Alexa488	3.6, B.7, B.8
		β-catenin:E-cadherin	1°pAb chicken IgY anti-β-catenin	1:100	Aves (BCAT-0020)		
			2°pAb donkey anti-chicken IgY-P1-B1	1	MT (A9232-AB1)		
			1°mAb mouse IgG2b anti-E-cadherin	1:100	Pr (60335-1-IG)		
			2°pAb goat anti-mouse IgG2b-P2-B1	1	MT (A9113-ZB1)	B1-Alexa546	3.6, B.7, B.9
		SC35:SON	1°mAb mouse IgG1 anti-SC35	1:200	Abc (ab11826)		
			2°pAb goat anti-mouse IgG1-P1-B9	1	MT (A9111-AB9)		
			1°pAb rabbit IgG anti-SON	1:100	Atlas (HPA023535)		
			2°pAb donkey anti-rabbit IgG-P2-B9	1	MT (A9230-ZB9)	B9-Alexa647	3.6, B.7, B.10
		β-catenin:E-cadherin	1°mAb mouse IgG1 anti-β-catenin	1:100	Abc (ab237983)		
			2°pAb goat anti-mouse IgG1-P1-B1	1	MT (A9111-AB1)		
			1°mAb rabbit IgG anti-E-cadherin	1:200	CST (3195S)		
			2°pAb donkey anti-rabbit IgG-P2-B1	1	MT (A9230-ZB1)	B1-Alexa546	3.7, B.11, B.12
		β-catenin:E-cadherin	1°mAb mouse IgG1 anti-β-catenin	1:100	Abc (ab237983)		
			2°pAb goat anti-mouse IgG1-P1-B6	1	MT (A9111-AB6)		
			1°mAb rabbit IgG anti-E-cadherin	1:200	CST (3195S)		
			2°pAb donkey anti-rabbit IgG-P2-B6	1	MT (A9230-ZB6)	B6-Alexa647	3.7, B.11, B.13
		β-tubulin:α-tubulin	1°mAb mouse IgG1 anti-β-tubulin	1:1000	Abc (ab231082)		
			2°pAb goat anti-mouse IgG1-P1-B1	1	MT (A9111-AB1)		
			1°mAb rabbit IgG anti-α-tubulin	1:350	Abc (ab176560)		
			2°pAb donkey anti-rabbit IgG-P2-B1	1	MT (A9230-ZB1)	B1-Alexa546	3.8, B.16, B.18

Table B.1: Organism, sample type, target protein, 1°Ab probe details, 2°Ab probe details, HCR amplifier details, and figure numbers for HCR imaging of protein:protein complexes in adherent cells. Interaction probes and antibody buffer were obtained from Molecular Technologies (MT) within the Beckman Institute at Caltech. Abc: Abcam. CST: Cell Signaling Technology. Inv: Invitrogen. Sy: Synaptic Systems. Aves: Aves Labs. Pr: Proteintech. Atlas: Atlas Antibodies.

Species	Sample	Protein:protein complex	1°Ab probe Interaction probe	Dilution factor Working conc. (μg/mL)	Supplier (catalog #)	HCR amplifier	Figures
	FFPE breast tissue	β-catenin:E-cadherin	1°mAb mouse IgG1 anti-β-catenin	1:100	Abc (ab237983)		
			2°pAb goat anti-mouse IgG1-P1-B1	1	MT (A9111-AB1)		
			1°mAb rabbit IgG anti-E-cadherin	1:200	CST (3195S)		
			2°pAb donkey anti-rabbit IgG-P2-B1	1	MT (A9230-ZB1)	B1-Alexa647	3.4, B.5, B.6
		β-catenin:E-cadherin	1°mAb mouse IgG1 anti-β-catenin	1:100	Abc (ab237983)		
			2°pAb goat anti-mouse IgG1-P1-B1	1	MT (A9111-AB1)		
			1°mAb rabbit IgG anti-E-cadherin	1:200	CST (3195S)		
			2°pAb donkey anti-rabbit IgG-P2-B1	1	MT (A9230-ZB1)	B1-Alexa546	3.7, B.14, B.15
		β-catenin:E-cadherin	1°mAb mouse IgG1 anti-β-catenin	1:100	Abc (ab237983)		
			2°pAb goat anti-mouse IgG1-P1-B9	1	MT (A9111-AB9)		
			1°mAb rabbit IgG anti-E-cadherin	1:200	CST (3195S)		
			2°pAb donkey anti-rabbit IgG-P2-B9	1	MT (A9230-ZB9)	B9-Alexa647	3.7, B.14, B.15

Table B.2: Organism, sample type, target protein, 1°Ab probe details, 2°Ab probe details, HCR amplifier details, and figure numbers for HCR imaging of protein:protein complexes in tissue sections. Interaction probes and antibody buffer were obtained from Molecular Technologies (MT) within the Beckman Institute at Caltech. Abc: Abcam. CST: Cell Signaling Technology.

Species	Sample	Protein:protein complex	1°Ab probe Interaction probe	Dilution factor Working conc. (μg/mL)	Supplier (catalog #)	HCR amplifier	Figures
M. musculus	Pro-T cells	RUNX1:PU.1	1°pAb sheep IgG anti-RUNX1	1:300	AO (ABIN350811)		
			2°pAb donkey anti-sheep IgG-P1-B1	1	MT (A9233-AB1)		
			1°mAb rabbit IgG anti-PU.1	1:500	Abc (ab227835)		
			2°pAb donkey anti-rabbit IgG-P2-B1	1	MT (A9230-ZB1)	B1-Alexa647	3.3, B.3, B.4

Table B.3: Organism, sample type, target protein, 1°Ab probe details, 2°Ab probe details, HCR amplifier details, and figure numbers for HCR imaging of protein:protein complexes in T cells. Interaction probes and antibody buffer were obtained from Molecular Technologies (MT) within the Beckman Institute at Caltech. AO: antibodies-online. Abc: Abcam.

B.1.2 Probe and amplifier details for RNA targets using HCR RNA-FISH

Species	Sample	RNA target	Split-initiator probe pairs	Supplier (catalog #)	HCR amplifier	Figures
H. sapiens sapiens	HeLa cells	*U6*	2	MT (3882/E032)	B3-Alexa647	3.8, B.16, B.19

Table B.4: Organism, sample type, target RNA, probe set details, HCR amplifier details, and figure numbers for HCR RNA-FISH. For HCR RNA-FISH, HCR probe sets, amplifiers, and buffers (probe hybridization buffer, probe wash buffer, amplification buffer) were obtained from Molecular Technologies (MT) within the Beckman Institute at Caltech.

B.1.3 Probe and amplifier details for protein targets using HCR IF

Species	Sample	Protein target	1°Ab probe (unlabeled) 2°Ab probe (initiator-labeled)	Dilution factor Working conc. (μg/mL)	Supplier (catalog #)	HCR amplifier	Figures
H. sapiens sapiens	HeLa cells	HSP60	1°mAb mouse IgG2a anti-HSP60 2°pAb goat anti-mouse IgG2a-B5	1:50 1	Inv (MA3-012) MT (A9112-B5)	B5-Alexa488	3.8, B.16, B.17

Table B.5: Organism, sample type, target protein, 1°Ab probe details, 2°Ab probe details, HCR amplifier details, and figure numbers for HCR IF. For HCR IF, initiator-labeled secondary antibody probes and antibody buffer were obtained from Molecular Technologies (MT) within the Beckman Institute at Caltech. Inv: Invitrogen.

B.1.4 Oligonucleotide sequences

HCR System	Oligo	Length (nt)	Sequence (5' to 3')
B1	P1	49	GAGGAGGGCAGCAAACGGTCGCCCATGTGTACCCGAAATTCAAGTCAGC
	P2	49	TTCCTGATTCTATTACTTGCCTGATCCCTATGAAGAGTCTTCCTTTACG
	Ruler	50	CTTGAATTTCGGGTACACATGGGCTAAGGGATCAGGCAAGTAATAGAATC
B6	P1	49	GCAAACTAAACATCCCACAAGGTGAAAGCTGGTACGAATAAGACTACGC
	P2	49	CTGCACCGGTATATGTTCTGAAGGTGATGCATCCAACTCTAACTAAATC
	Ruler	50	GTCTTATTCGTACCAGCTTTCACCACCATCACCTTCAGAACATATACCGG
B9	P1	49	CTAACAATCTAAACATACTCGAGGGTGCGGTCTATTCTATTTCCAACGT
	P2	49	TATTGCGTGTTAGGTGAGTTTGAGATTTGTACACGCCCAAGAACATAAA
	Ruler	50	GGAAATAGAATAGACCGCACCCTCACCAAATCTCAAACTCACCTAACACG

Table B.6: P1, P2, and ruler oligonucleotide sequences. Nucleotides comprising a fractional initiator are labeled in green (18 nt in length), while regions of complementarity between the ruler strand and the P1 or P2 oligonucleotides are labeled in red (24 nt in length).

B.1.5 Microscope settings

Sample	Complex or target	Objective	Fluorophore	Laser (nm)	Detector	Detection wavelength (nm)	Pixel size ($x \times y \times z$ μm)	Figures
Adherent human cells	β-catenin:E-cadherin	63×	Alexa647	638	HyD X 4	648–700	$0.180 \times 0.180 \times 0.8$	3.2, B.1, B.2
	—		DAPI	405	HyD S 1	415–440	$0.180 \times 0.180 \times 0.8$	3.2, B.1, B.2
	β-tubulin:α-tubulin	63×	Alexa488	488	HyD S 2	495–535	$0.180 \times 0.180 \times 0.8$	3.6, B.7, B.8
	β-catenin:E-cadherin		Alexa546	561	HyD S 3	570–605	$0.180 \times 0.180 \times 0.8$	3.6, B.7, B.9
	SC35:SON		Alexa647	638	HyD X 4	648–700	$0.180 \times 0.180 \times 0.8$	3.6, B.7, B.10
	—		DAPI	405	HyD S 1	415–440	$0.180 \times 0.180 \times 0.8$	3.6, B.7–B.10
	β-catenin:E-cadherin	63×	Alexa546	561	HyD S 3	570–605	$0.180 \times 0.180 \times 0.8$	3.7, B.11, B.12
	β-catenin:E-cadherin		Alexa647	638	HyD X 4	648–700	$0.180 \times 0.180 \times 0.8$	3.7, B.11, B.13
	—		DAPI	405	HyD S 1	415–440	$0.180 \times 0.180 \times 0.8$	3.7, B.11, B.12, B.13
	HSP60	63×	Alexa488	488	HyD S 2	495–535	$0.180 \times 0.180 \times 0.8$	3.8, B.16, B.17
	β-tubulin:α-tubulin		Alexa546	561	HyD S 3	570–605	$0.180 \times 0.180 \times 0.8$	3.8, B.16, B.18
	U6		Alexa647	638	HyD X 4	648–700	$0.180 \times 0.180 \times 0.8$	3.8, B.16, B.19
	—		DAPI	405	HyD S 1	415–440	$0.180 \times 0.180 \times 0.8$	3.8, B.16–B.19
Pro-T cells	RUNX1:PU.1	63×	Alexa647	638	HyD X 4	648–700	$0.180 \times 0.180 \times 0.8$	3.3, B.3, B.4
	—		DAPI	405	HyD S 1	415–440	$0.180 \times 0.180 \times 0.8$	3.3, B.3, B.4
FFPE human breast tissue	β-catenin:E-cadherin	20×	Alexa647	638	HyD X 4	648–700	$0.568 \times 0.568 \times 3.3$	3.4, B.5, B.6
	—		DAPI	405	HyD S 1	415–440	$0.568 \times 0.568 \times 3.3$	3.4, B.5, B.6
	β-catenin:E-cadherin	20×	Alexa546	561	HyD S 3	570–605	$0.568 \times 0.568 \times 3.3$	3.7, B.14, B.15
	β-catenin:E-cadherin		Alexa647	638	HyD X 4	648–700	$0.568 \times 0.568 \times 3.3$	3.7, B.14, B.15
	—		DAPI	405	HyD S 1	415–440	$0.568 \times 0.568 \times 3.3$	3.7, B.14, B.15

Table B.7: Microscope settings for RNA, protein, and protein:protein complex imaging. Confocal microscopy was performed with a Leica Stellaris 8 inverted confocal microscope. Objectives were as follows: HC PL APO 20×/0.75 IMM CORR CS2 (catalog # 11506343), HC PL APO 63×/1.40 OIL CS2 (catalog # 11506350), both utilized with oil immersion.

B.1.6 Image analysis

We build on an image analysis framework developed over a series of publications (*36–39*, *43*, *45*). For convenience, here we provide a self-contained description of the details relevant to the present work.

Raw pixel intensities

The total fluorescence within a pixel is a combination of signal and background. Fluorescent background (BACK) arises from up to four sources in each channel:

- autofluorescence (AF): fluorescence inherent to the sample.
- non-specific amplification (NSA): HCR hairpins that bind non-specifically in the sample.
- non-specific detection (NSD): probes that bind non-specifically in the sample and subsequently trigger HCR amplification.
- spurious amplification (SA): probes that bind specifically in the sample and subsequently trigger HCR amplification despite the absence of a full HCR initiator. $\mathrm{SA_{P1}}$ arises from the P1 interaction probe triggering HCR amplification in the absence of the P2 interaction probe, and $\mathrm{SA_{P2}}$ arises from the P2 interaction probe triggering HCR amplification in the absence of the P1 interaction probe, with $\mathrm{SA} = \mathrm{SA_{P1}} + \mathrm{SA_{P2}}$.

Fluorescent signal (SIG) in each channel corresponds to:

- signal (SIG): probes that bind specifically to the target and subsequently trigger HCR amplification.

For pixel i of replicate sample n, we denote the background

$$X_{n,i}^{\mathrm{BACK}} = X_{n,i}^{\mathrm{SA}} + X_{n,i}^{\mathrm{NSD}} + X_{n,i}^{\mathrm{NSA}} + X_{n,i}^{\mathrm{AF}}, \tag{B.1}$$

the signal:

$$X_{n,i}^{\mathrm{SIG}}, \tag{B.2}$$

and the total fluorescence (SIG+BACK):

$$X_{n,i}^{\mathrm{SIG+BACK}} = X_{n,i}^{\mathrm{SIG}} + X_{n,i}^{\mathrm{BACK}}. \tag{B.3}$$

Measurement of signal, background, and signal-to-background for HCR imaging of protein:protein complexes, HCR IF, and HCR RNA-FISH

Background and signal are characterized differently depending on the sample type and protein:protein complex detected:

- For cells on a coverslip, signal plus background (SIG+BACK) is characterized for pixels in a representative rectangular region of high protein:protein complex expression using an experiment of Type 1a (Table B.8) employing the full protocol. For cells for which a suitable control is available in which the protein:protein complex is present at low levels or is absent, background (BACK) can be characterized for pixels in a representative rectangular region of maximum intensity using an experiment of Type 1b (Table B.8) employing the full protocol. Alternatively, BACK is characterized for pixels in a representative rectangular region of maximum intensity using experiments of Type 2a and Type 2b (Table B.8) in which the interaction probe and 1° Ab against one protein of the protein:protein interaction are omitted, and BACK is estimated as the maximum value yielded from the two background experiments.
- For FFPE human breast tissue sections, signal plus background (SIG+BACK) is characterized for pixels in a representative rectangular region of high protein:protein complex expression using an experiment of Type 1a (Table B.8) employing the full protocol, and background (BACK) is characterized for pixels in a representative rectangular region of a different sample with no or low protein:protein complex expression using an experiment of Type 1b (Table B.8). Alternatively, SIG+BACK is characterized for pixels in a representative rectangular region of high protein:protein complex expression using an experiment of Type 3 (Table B.8) employing the full protocol, and background (BACK) is characterized for pixels in a representative rectangular region in the same sample with no or low protein:protein complex expression (Table B.8).

For HCR IF experiments, signal plus background (SIG+BACK) is characterized for pixels in a representative rectangular region of high protein expression employing the full protocol. Background (BACK) is characterized for pixels in a representative rectangular region of maximum intensity for an experiment in which the 1°Ab probe is omitted, yielding the partial background estimate BACK $\approx$ AF+NSA+NSD_{2°.

For HCR RNA-FISH experiments, signal plus background (SIG+BACK) is characterized for pixels in a representative rectangular region of high RNA expression

employing the full protocol. Background (BACK) is characterized for pixels in a representative rectangular region of maximum intensity for an experiment in which the split-initiator probes are omitted, yielding the partial background estimate BACK $\approx$ AF+NSA.

For the pixels in these regions, we characterize the distribution by plotting an intensity histogram and characterize average performance by calculating the mean pixel intensities

$$\bar{X}_n^{\text{BACK}}, \qquad \bar{X}_n^{\text{SIG + BACK}} \tag{B.4}$$

for replicate n. Performance across replicates is characterized by calculating the sample means

$$\bar{X}^{\text{BACK}}, \qquad \bar{X}^{\text{SIG+BACK}} \tag{B.5}$$

and standard error of the mean

$$s_{\bar{X}^{\text{BACK}}}, \qquad s_{\bar{X}^{\text{SIG+BACK}}}. \tag{B.6}$$

The mean signal is then estimated as

$$\bar{X}^{\text{SIG}} = \bar{X}^{\text{SIG+BACK}} - \bar{X}^{\text{BACK}} \tag{B.7}$$

with the standard error of the mean estimated via uncertainty propagation as

$$s_{\bar{X}^{\text{SIG}}} \leq \sqrt{(s_{\bar{X}^{\text{SIG+BACK}}})^2 + (s_{\bar{X}^{\text{BACK}}})^2}. \tag{B.8}$$

The signal-to-background ratio is estimated as:

$$\bar{X}^{\text{SIG/BACK}} = \bar{X}^{\text{SIG}} / \bar{X}^{\text{BACK}} \tag{B.9}$$

with standard error of the mean estimated via uncertainty propagation as

$$s^{\text{SIG/BACK}} \leq \bar{X}^{\text{SIG/BACK}} \sqrt{\left(\frac{s_{\bar{X}^{\text{SIG}}}}{\bar{X}^{\text{SIG}}}\right)^2 + \left(\frac{s_{\bar{X}^{\text{BACK}}}}{\bar{X}^{\text{BACK}}}\right)^2}. \tag{B.10}$$

These upper bounds on estimated standard errors hold under the assumption that the correlation between SIG and BACK is non-negative.

Experiment type	Quantity	Reagents						Complex expression region in sample
		Protein 1 1° Ab	Protein 2 1° Ab	P1 interaction probe	P2 interaction probe	Ruler	Hairpins	
1a	SIG+SA+NSD+NSA+AF = SIG+BACK	✓	✓	✓	✓	✓	✓	high
1b	SA+NSD+NSA+AF = BACK	✓	✓	✓	✓	✓	✓	no/low
2a	SA_{P1}+NSD+NSA+AF	✓		✓		✓	✓	high
2b	SA_{P2}+NSD+NSA+AF		✓		✓	✓	✓	high
3	SIG+SA+NSD+NSA+AF = SIG+BACK	✓	✓	✓	✓	✓	✓	high
3	SA+NSD+NSA+AF = BACK	✓	✓	✓	✓	✓	✓	no/low

Table B.8: Experiment types for protein:protein complex imaging with HCR. Characterize signal, background, and signal-to-background.

Experiment type	Quantity	Reagents			Expression region in sample
		1° Ab	2° Ab-initiator	Hairpins	
1	SIG+NSD+NSA+AF = SIG+BACK	✓	✓	✓	high
2	NSD_{2°+NSA+AF = BACK		✓	✓	high

Table B.9: Experiment types for HCR IF using unlabeled primary antibody probes and initiator-labeled secondary antibody probes. Characterize signal, background, and signal-to-background.

Experiment type	Quantity	Reagents		Expression region in sample
		Split-initiator probes	Hairpins	
1	SIG+NSD+NSA+AF = SIG+BACK	✓	✓	high
2	NSA+AF = BACK		✓	high

Table B.10: Experiment types for HCR RNA-FISH using split-initiator probes. Characterize signal, background, and signal-to-background.

Normalized voxel intensities for qHCR imaging: protein:protein complex relative quantitation with subcellular resolution in an anatomical context

For quantitative imaging using HCR, precision increases with voxel size as long as the imaging voxels remain smaller than the features in the expression pattern (see Section S2.2 of (*43*)). To increase precision, we calculate raw voxel intensities by averaging neighboring pixel intensities while still maintaining a subcellcular voxel size. To facilitate relative quantitation between voxels, we estimate the normalized HCR signal of voxel j in replicate n as:

$$x_{n,j} \equiv \frac{X_{n,j}^{SIG+BACK} - X^{BOT}}{X^{TOP} - X^{BOT}}, \tag{B.11}$$

which translates and rescales the data so that the voxel intensities in each channel fall in the interval [0,1]. Here,

$$X^{BOT} \equiv \bar{X}^{BACK} \tag{B.12}$$

is the mean background across replicates (see Section B.1.6) and

$$X^{TOP} \equiv \max_{n,j} X_{n,j}^{SIG+BACK} \tag{B.13}$$

is the maximum total fluorescence for a voxel across replicates.

Pairwise expression scatter plots that each display normalized voxel intensities for two channels (e.g., Figures 4 and 5 of (*43*)) provide a powerful quantitative framework for performing multidimensional read-out/read-in analyses (Figure 6 of (*43*)). Read-out from anatomical space to expression space enables discovery of expression clusters of voxels with quantitatively related expression levels and ratios (amplitudes and slopes in the expression scatter plots), while read-in from expression space to anatomical space enables discovery of the corresponding anatomical locations of these expression clusters within the embryo. The simple and practical normalization approach of (B.11)–(B.13) translates and rescales all voxels identically within a given channel (enabling comparison of amplitudes and slopes in scatter plots between replicates), and does not attempt to remove scatter in the normalized signal estimate that is caused by scatter in background.

To validate qHCR protein:protein complex imaging with subcellular resolution (2×2 μm voxels) in fixed adherent human cells and FFPE human breast tissue sections, Figures 3.7C, B.11C, and B.14C display highly correlated normalized voxel intensities for 2-channel redundant detection of a protein:protein complex. In this setting, accuracy corresponds to linearity with zero intercept, and precision corresponds to scatter around the line (*43*).

B.2 Protocols

B.2.1 Protocols for protein:protein complex imaging in fixed adherent mammalian cells

Preparation of fixed adherent mammalian cells on a chambered coverslip

1. Coat the bottom of each chamber by applying 100 μL of 0.01% poly-D-lysine prepared in molecular biology grade H_2O.
   NOTE: *For each step, a volume of 100 µL is sufficient per chamber on an 18-chamber coverslip. Scale volumes accordingly if using a different chambered format.*
2. Incubate for at least 30 min at room temperature.
3. Aspirate the coating solution and wash each chamber 2× with molecular biology grade H_2O.
4. Add the desired number of cells to each chamber.
5. Grow the cells to the desired confluency for 24–48 h.
6. Aspirate the growth media and wash each chamber with DPBS.
   NOTE: *Avoid using DPBS with calcium chloride and magnesium chloride, as this leads to increased autofluorescence.*
7. Add 4% formaldehyde in PBS to each chamber.
   CAUTION: *Use formaldehyde with extreme care, as it is a hazardous material.*
8. Incubate for 10 min at room temperature.
9. Remove fixative and wash each chamber 2× with DPBS.
10. Aspirate DPBS and add ice-cold 70% ethanol (EtOH) to permeabilize the cells.
11. Permeabilize cells for 3 h at 4 °C.
    NOTE: *Alternatively, the cells may be permeabilized overnight (or longer) at -20 °C.*

HCR protein:protein complex imaging with/without HCR IF and HCR RNA-FISH using simultaneous HCR signal amplification for all targets

Protein detection stage

1. Aspirate EtOH from sample and wash 2 × 5 min with 1× PBS.
2. Add antibody buffer to the sample. Incubate for 1 h at room temperature with gentle agitation.
3. Prepare working concentration of primary antibodies in antibody buffer.
   NOTE: *Follow the manufacturer's guidelines for the primary antibody working concentration.*
4. Replace antibody buffer with primary antibody solution and incubate overnight (>12 h) at 4 °C with gentle agitation.
   NOTE: *Incubation may be optimized (e.g., 1–2 h at room temperature) depending on the antibody used.*
5. Remove excess antibodies by washing 3 × 5 min with 1× PBST at room temperature with gentle agitation.
6. Prepare P1 and P2 interaction probes, and optionally initiator-labeled secondary antibodies for protein detection, at 1 μg/mL in antibody buffer.
7. Add P1 and P2 interaction probe solution (optionally with initiator-labeled secondary antibodies) to the sample. Incubate for 1 h at room temperature with gentle agitation.
8. Remove excess interaction probes and secondary antibodies by washing 3 × 5 min with 1× PBST at room temperature with gentle agitation.
9. Wash with 5× SSCT for 5 min at room temperature.
10. Add amplification buffer. Incubate for 30 min at room temperature.
    NOTE: *Equilibrate amplification buffer to room temperature before use.*
11. Prepare a 1.6 nM ruler strand solution in amplification buffer at room temperature.
12. Remove amplification buffer and add ruler strand solution. Incubate for 1 h at room temperature.

13. Wash 3 × 5 min with 5× SSCT at room temperature.
14. Proceed to **RNA detection stage** for co-detection of RNA. Otherwise, proceed to **Amplification stage**.

RNA detection stage

1. Post-fix sample with 4% formaldehyde in PBS. Incubate for 10 min at room temperature.
   CAUTION: *Use formaldehyde with extreme care, as it is a hazardous material.*
2. Wash 3 × 5 min with 1× PBST at room temperature.
3. Wash with 5× SSCT for 5 min at room temperature.
4. Add probe hybridization buffer. Incubate for 30 min at 37 °C.
   CAUTION: *Probe hybridization buffer contains formamide, a hazardous material.*
   NOTE: *Pre-heat probe hybridization buffer to 37 °C before use.*
5. Prepare a 16 nM probe solution in probe hybridization buffer at 37 °C.
6. Remove the probe hybridization buffer and add the probe solution.
7. Incubate overnight (>12 h) at 37 °C.
8. Remove excess probes by washing 4 × 5 min with probe wash buffer at 37 °C.
   CAUTION: *Probe wash buffer contains formamide, a hazardous material.*
   NOTE: *Pre-heat probe wash buffer to 37 °C before use.*
9. Wash 3 × 5 min with 5× SSCT at room temperature.
10. Proceed to **Amplification stage**.

Amplification stage

1. Add amplification buffer. Incubate for 30 min at room temperature.
   NOTE: *Equilibrate amplification buffer to room temperature before use.*
2. Separately prepare hairpin h1 and hairpin h2 by snap cooling (heat at 95 °C for 90 seconds and cool to room temperature in a dark drawer for 30 min).
   NOTE: *HCR hairpins h1 and h2 are provided in hairpin storage buffer ready for snap cooling. h1 and h2 should be snap cooled in separate tubes.*

3. Prepare a 60 nM hairpin solution by adding snap-cooled h1 hairpins and snap-cooled h2 hairpins to amplification buffer at room temperature.
4. Remove the amplification buffer and add the hairpin solution.
5. Incubate overnight (>12 h) protected from light at room temperature.
6. Remove excess hairpins by washing 5 × 5 min with 5× SSCT at room temperature.

Sample mounting for microscopy

1. Add DAPI Fluoromount-G mounting medium.
2. The coverslip can be stored at 4 °C protected from light prior to imaging.
   NOTE: *see Section B.1.5 for details of confocal microscopes used to image fixed adherent mammalian cells on a chambered coverslip.*

Buffers for HCR protein:protein complex imaging with/without HCR IF and HCR RNA-FISH

Initiator-labeled antibody probes, split-initiator DNA probes, amplifiers, and buffers (antibody buffer, probe hybridization buffer, probe wash buffer, amplification buffer) are available from Molecular Technologies. Probe hybridization buffer and probe wash buffer should be stored at -20 °C. Antibody buffer and amplification buffer should be stored at 4 °C. Make sure all solutions are well mixed before use.

PBST: 1× PBS, 0.1% Tween-20
For 500 mL of solution:
• 50 mL of 10× PBS
• 5 mL of 10% Tween-20
• Fill up to 500 mL with ultrapure H_2O
• Filter with a 0.2 μm Nalgene Rapid-Flow filter

5× SSCT: 5× SSC, 0.1% Tween-20
For 500 mL of solution:
• 125 mL of 20× SSC
• 5 mL of 10% Tween-20
• Fill up to 500 mL with ultrapure H_2O
• Filter with a 0.2 μm Nalgene Rapid-Flow filter

Reagents and supplies

ibidi μ-slide 18 well ibiTreat (ibidi, 81816)
Poly-D-lysine hydrobromide (Sigma-Aldrich, P7280)
Molecular biology grade H_2O (Corning, 46-000-CV)
DPBS, no calcium, no magnesium (Gibco, 14190144)
Image-iT 4% formaldehyde fixative solution in PBS (methanol-free) (Invitrogen, FB002)
100% EtOH (Koptec, V1001)
10× PBS (Invitrogen, AM9624)
20× Saline sodium citrate (SSC) (Invitrogen, 15557-044)
10% Tween-20 (Teknova, T0710)
DAPI Fluoromount-G (SouthernBiotech, 0100-20)

B.2.2 Protocols for protein:protein complex imaging in FFPE human breast tissue sections

Preparation of formalin-fixed paraffin-embedded (FFPE) human breast tissue sections

1. Bake slides in a dry oven for 1 h at 60 °C to improve sample adhesion to the slide.
2. In a fume hood, deparaffinize FFPE tissue by immersing the slide in Pro-Par Clearant for 2 × 5 min. Gently move the slide up and down every minute.
   NOTE: *If desired, a larger number of slides can be processed together using a Coplin jar.*
3. Immerse the slide in 100% ethanol (EtOH) for 2 × 3 min at room temperature. Gently move the slide up and down every minute.
4. Immerse the slide in 95% EtOH for 3 min at room temperature.
5. Immerse the slide in 70% EtOH for 3 min at room temperature.
6. Immerse the slide in nanopure H_2O for 3 min at room temperature.
7. Heat antigen retrieval buffer in a heatproof container with a digital steamer until >98 °C.
8. Immerse the slide in the heated antigen retrieval buffer in the digital steamer for 15 min.
9. Remove the slide from the antigen retrieval buffer and immediately immerse in nanopure H_2O for 10 min at room temperature.
10. Remove the slide and gently tap off excess nanopure H_2O.
11. Carefully dry around the tissue with a Kimwipe.
12. Draw a hydrophobic barrier around the tissue with a hydrophobic pen.
13. Place the slide in a humidified chamber.
    NOTE: *Keep the slide in a humidified chamber for all future steps to prevent evaporation.*

HCR protein:protein complex imaging in FFPE human breast tissue sections

Protein detection stage

1. Apply antibody buffer to the tissue section. Incubate for 1 h at room temperature.
   NOTE: *Scale volumes according to the size of the tissue. A volume of 100 µL was utilized here for each step.*

2. Prepare working concentration of primary antibodies in antibody buffer.
   NOTE: *Follow the manufacturer's guidelines for the primary antibody working concentration.*

3. Replace antibody buffer with primary antibody solution and incubate overnight (>12 h) at 4 °C.
   NOTE: *Incubation may be optimized (e.g., 1–2 h at room temperature) depending on the antibody used.*

4. Remove excess antibodies by washing 3 × 5 min with 1× PBST at room temperature.

5. Prepare P1 and P2 interaction probes at 1 µg/mL in antibody buffer.

6. Add P1 and P2 interaction probe solution to the sample. Incubate for 1 h at room temperature.

7. Remove excess interaction probes and secondary antibodies by washing 3 × 5 min with 1× PBST at room temperature.

8. Wash with 5× SSCT for 5 min at room temperature.

9. Add amplification buffer. Incubate for 30 min at room temperature.
   NOTE: *Equilibrate amplification buffer to room temperature before use.*

10. Prepare a 1.6 nM ruler strand solution in amplification buffer at room temperature.

11. Remove amplification buffer and add ruler strand solution. Incubate for 1 h at room temperature.

12. Wash 3 × 5 min with 5× SSCT at room temperature.

Amplification stage

1. Add amplification buffer. Incubate for 30 min at room temperature.
   NOTE: *Equilibrate amplification buffer to room temperature before use.*
2. Separately prepare hairpin h1 and hairpin h2 by snap cooling (heat at 95 °C for 90 seconds and cool to room temperature in a dark drawer for 30 min).
   NOTE: *HCR hairpins h1 and h2 are provided in hairpin storage buffer ready for snap cooling. h1 and h2 should be snap cooled in separate tubes.*
3. Prepare a 60 nM hairpin solution by adding snap-cooled h1 hairpins and snap-cooled h2 hairpins to amplification buffer at room temperature.
4. Remove the amplification buffer and add the hairpin solution.
5. Incubate overnight (>12 h) protected from light at room temperature.
6. Remove excess hairpins by washing with 5× SSCT at room temperature:
   a) 2 × 5 min
   b) 2 × 15 min
   c) 1 × 5 min

Sample mounting for microscopy

1. Carefully dry around the section with a Kimwipe.
2. Apply 60 μL of DAPI Fluoromount-G to the section.
3. Carefully lower a 22 mm × 30 mm No. 1.5 coverslip on top of the section.
4. Slides can be stored at 4 °C protected from light prior to imaging.
   NOTE: *see Section B.1.5 for details of confocal microscopes used to image FFPE human breast tissue sections.*

Buffers for HCR protein:protein complex imaging in FFPE human breast tissue sections

Amplifiers and buffers (antibody buffer and amplification buffer) are available from Molecular Technologies. Antibody buffer and amplification buffer should be stored at 4 °C. Make sure all solutions are well mixed before use.

PBST: 1× PBS, 0.1% Tween-20
For 500 mL of solution:
• 50 mL of 10× PBS
• 5 mL of 10% Tween-20
• Fill up to 500 mL with ultrapure H_2O
• Filter with a 0.2 μm Nalgene Rapid-Flow filter

5× SSCT: 5× SSC, 0.1% Tween-20
For 500 mL of solution:
• 125 mL of 20× SSC
• 5 mL of 10% Tween-20
• Fill up to 500 mL with ultrapure H_2O
• Filter with a 0.2 μm Nalgene Rapid-Flow filter

Reagents and supplies

Pro-Par Clearant (ANATECH LTD, 510)
100% EtOH (Koptec, V1001)
Antigen retrieval buffer (100X Citrate Buffer) (Abcam, ab93678)
10× PBS (Invitrogen, AM9624)
20× Saline sodium citrate (SSC) (Invitrogen, 15557-044)
10% Tween-20 (Teknova, T0710)
DAPI Fluoromount-G (SouthernBiotech, 0100-20)

B.2.3 Protocols for protein:protein complex imaging in pro-T cells

To revert Scid.adh.2C2 (*88*) cells to an earlier pre-commitment T cell stage, the PU.1 protein is exogenously provided by retroviral transduction as previously described (*121*). As a control, Scid.adh.2C2 cells are also retrovirally transduced with a control vector that does not encode for the PU.1 protein.

Retroviral packaging of vector DNA

1. Culture Phoenix-ECO cells in Dulbecco's Modified Eagle Medium (DMEM) supplemented with 10% fetal bovine serum (FBS) and 1× Penicillin-Streptomycin-Glutamine.

2. To perform retroviral vector DNA packaging, transfect Phoenix-ECO cells with retroviral vector DNA encoding for the PU.1 protein (or, as a control, with retroviral vector DNA not encoding for the PU.1 protein) via the FuGENE 6 transfection reagent according to the manufacturer's instructions.

3. After 48–72 h, collect the cell supernatant, which contains the packaged retrovirus, and filter through a 0.45 μm syringe filter.

4. Store the filtered retrovirus supernatant in 1 mL aliquots at -80 °C.

Retroviral infection, antibody labeling, and coverslip preparation of pro-T cells

1. Coat a non-treated 24-well plate with 300–500 μL of 50 μg/mL RetroNectin overnight at 4 °C.

2. Remove excess RetroNectin from the 24-well plate.

3. Wash each well with 500 μL 1× phosphate-buffered saline (PBS) (Gibco).

4. Thaw retrovirus supernatant in a 37 °C water bath.

5. Remove 1× PBS from the 24-well plate and add 1 mL retrovirus supernatant to each well.

6. Centrifuge the plate at 2000 rcf for 2 h in a pre-heated 32 °C centrifuge.

7. Aspirate the liquid from each well.

8. Add 1×10^5 Scid.adh.2C2 cells in 1 mL culture media to each well.
9. Centrifuge the plate at 2000 rcf for 5 min in a pre-heated 32 °C centrifuge.
10. Incubate overnight at 37 °C in a 5% CO_2 incubator.
11. The next day, scrape Scid.adh.2C2 cells from the surface of the 24-well plate.
12. Add Scid.adh.2C2 cells at a concentration of 1×10^5/mL to a new tissue culture-treated 24-well plate.
13. Incubate overnight at 37 °C in a 5% CO_2 incubator.
14. Remove Scid.adh.2C2 cells from the surface of the 24-well plate by pipetting.
15. Centrifuge Scid.adh.2C2 cells at 250 rcf for 7 min in a pre-cooled 4°C centrifuge.
16. Remove supernatant from the Scid.adh.2C2 cells and resuspend the cells in FACS buffer to a concentration of 1×10^4 cells/μL.
17. Add biotinylated anti-hNGFR (human NGFR) antibody to the cell solution to reach a final antibody dilution factor of 1:300. Mix gently.
18. Incubate the cell solution for 30 min on ice.
19. Centrifuge Scid.adh.2C2 cells at 250 rcf for 7 min in a pre-cooled 4°C centrifuge. Remove the supernatant.
20. Wash the cells twice by adding 300 μL FACS buffer, centrifuging at 250 rcf for 7 min in a pre-cooled 4°C centrifuge, and removing the supernatant.
21. Label hNGFR+ cells with streptavidin microbeads according to the manufacturer's instructions.
22. Enrich for hNGFR-positive cells by using MACS LS magnetic columns according to the manufacturer's instructions.
23. Centrifuge Scid.adh.2C2 cells at 250 rcf for 7 min in a pre-cooled 4°C centrifuge.
24. Remove supernatant from the Scid.adh.2C2 cells and resuspend the cells in FACS buffer to a concentration of 1×10^4 cells/μL.

25. Add Alexa488-labeled anti-CD45 antibody to the cell solution to reach a final antibody dilution factor of 1:600. Mix gently.

26. Incubate the cell solution for 30 min on ice.

27. Centrifuge Scid.adh.2C2 cells at 250 rcf for 7 min in a pre-cooled 4°C centrifuge. Remove the supernatant.

28. Wash the cells twice by adding 300 μL FACS buffer, centrifuging at 250 rcf for 7 min in a pre-cooled 4°C centrifuge, and removing the supernatant.

29. Resuspend the cells in 1× PBS (Gibco) and bring to a concentration of ~2,777 cells/μL.

Prepare pro-T cells on a chambered coverslip

1. Prepare a No. 1.5 coverslip by washing with 100% ethanol (EtOH) and drying.

2. Coat the coverslip by applying 1.5 mL of 0.01% poly-D-lysine for 1 h.

3. Aspirate the coating solution and wash the coverslip 3× with 1× PBS (Gibco). Air dry the coverslip after the final wash.

4. Affix a microchamber flow cell to the coverslip.

5. Add 18 μL of the ~2,777 cells/μL solution to each microchamber port (~50,000 cells/port).
   NOTE: *For each step, a volume of 18 μL is sufficient for each microchamber of the flow cell. Scale volumes accordingly if using a different chambered format.*

6. Centrifuge the coverslip at 250 rcf for 5 min in a pre-cooled 4°C centrifuge to adhere the cells to the coverslip.

7. Aspirate the 1× PBS.

8. Add 4% formaldehyde in PBS to each chamber.
   CAUTION: *Use formaldehyde with extreme care, as it is a hazardous material.*

9. Incubate for 10 min at room temperature.

10. Remove fixative and wash each chamber 2× with DPBS.

11. Aspirate DPBS and add ice-cold 70% ethanol (EtOH) to permeabilize the cells.

12. Permeabilize cells for 3 h at -20 °C in a humidified chamber.
    NOTE: *Keep the coverslip in a humidified chamber for all future steps to prevent evaporation.*

13. Transfer cells to 4 °C and further permeabilize for 20 min.

HCR protein:protein complex imaging in pro-T cells

Protein detection stage

1. Aspirate EtOH from sample and wash 2 × 5 min with 1× PBS.
2. Add antibody buffer to the sample. Incubate for 1 h at room temperature with gentle agitation.
3. Prepare working concentration of primary antibodies in antibody buffer.
   NOTE: *Follow the manufacturer's guidelines for the primary antibody working concentration.*
4. Replace antibody buffer with primary antibody solution and incubate overnight (>12 h) at 4 °C with gentle agitation.
   NOTE: *Incubation may be optimized (e.g., 1–2 h at room temperature) depending on the antibody used.*
5. Remove excess antibodies by washing 3 × 5 min with 1× PBST at room temperature with gentle agitation.
6. Prepare P1 and P2 interaction probes at 1 μg/mL in antibody buffer.
7. Add P1 and P2 interaction probe solution to the sample. Incubate for 1 h at room temperature with gentle agitation.
8. Remove excess interaction probes by washing 3 × 5 min with 1× PBST at room temperature with gentle agitation.
9. Wash with 5× SSCT for 5 min at room temperature.
10. Add amplification buffer. Incubate for 30 min at room temperature.
    NOTE: *Equilibrate amplification buffer to room temperature before use.*
11. Prepare a 1.6 nM ruler strand solution in amplification buffer at room temperature.
12. Remove amplification buffer and add ruler strand solution. Incubate for 1 h at room temperature.
13. Wash 3 × 5 min with 5× SSCT at room temperature.

Amplification stage

1. Add amplification buffer. Incubate for 30 min at room temperature.
   NOTE: *Equilibrate amplification buffer to room temperature before use.*

2. Separately prepare hairpin h1 and hairpin h2 by snap cooling (heat at 95 °C for 90 seconds and cool to room temperature in a dark drawer for 30 min).
   NOTE: *HCR hairpins h1 and h2 are provided in hairpin storage buffer ready for snap cooling. h1 and h2 should be snap cooled in separate tubes.*

3. Prepare a 60 nM hairpin solution by adding snap-cooled h1 hairpins and snap-cooled h2 hairpins to amplification buffer at room temperature.

4. Remove the amplification buffer and add the hairpin solution.

5. Incubate overnight (>12 h) protected from light at room temperature.

6. Remove excess hairpins by washing 5 × 5 min with 5× SSCT at room temperature.

Sample mounting for microscopy

1. Add DAPI Fluoromount-G mounting medium.

2. The coverslip can be stored at 4 °C protected from light prior to imaging.
   NOTE: *see Section B.1.5 for details of confocal microscopes used to image pro-T cells on a chambered coverslip.*

Buffers for HCR protein:protein complex imaging in pro-T cells

Amplifiers and buffers (antibody buffer and amplification buffer) are available from Molecular Technologies. Antibody buffer and amplification buffer should be stored at 4 °C. Make sure all solutions are well mixed before use.

FACS buffer: 1× HBSS, 10 mM HEPES, 0.5% BSA
For 50 mL of solution:
• 49.5 mL of 1× HBSS
• 0.5 mL of 1 M HEPES
• 250 mg of BSA

PBST: 1× PBS, 0.1% Tween-20
For 500 mL of solution:
• 50 mL of 10× PBS
• 5 mL of 10% Tween-20
• Fill up to 500 mL with ultrapure H_2O
• Filter with a 0.2 μm Nalgene Rapid-Flow filter

5× SSCT: 5× SSC, 0.1% Tween-20
For 500 mL of solution:
• 125 mL of 20× SSC
• 5 mL of 10% Tween-20
• Fill up to 500 mL with ultrapure H_2O
• Filter with a 0.2 μm Nalgene Rapid-Flow filter

Reagents and supplies

Phoenix-ECO cells (ATCC, CRL-3214)
DMEM (Gibco, 12430-054)
Fetal bovine serum (FBS) (Sigma-Aldrich, F2442)
Penicillin-Streptomycin-Glutamine (100X) (Gibco, 10378-016)
FuGENE 6 Transfection Reagent (Promega, E2691)
0.45 μm syringe filter (Pall, 4614)
Non-treated 24-well plate (Corning, 351147)

RetroNectin (Takara Bio, T100B)
1× PBS (Gibco, 10010-023)
Tissue culture-treated 24-well plate (Corning, 3524)
100% EtOH (Koptec, V1001)
RPMI1640 medium (Gibco, 31800022)
1× Hanks' Balanced Salt Solution (HBSS), no calcium, no magnesium, no phenol red (Gibco, 14175-095)
Bovine serum albumin (BSA) (Roche, 03117332001)
HEPES (1 M) (Gibco, 15630-080)
Biotinylated anti-hNGFR antibody (mouse IgG1 mAb) (BioLegend, 345122)
Streptavidin MicroBeads (Miltenyi Biotec, 130-048-101)
MACS LS magnetic columns (Miltenyi Biotec, 130-042-401)
Alexa488-labeled anti-CD45 antibody (rat IgG2b mAb) (BioLegend, 103122)
Poly-D-lysine (Gibco, A38904-01)
Microchambers (Grace Bio-Labs, custom SecureSeal Flowcell, 15 mm x 75 mm OD, 14 x (3 mm x 11 mm) ID, 0.5 mm thick, A2, 0.020" cover with ports)
DPBS, no calcium, no magnesium (Gibco, 14190144)
Image-iT 4% formaldehyde fixative solution in PBS (methanol-free) (Invitrogen, FB002)
10× PBS (Invitrogen, AM9624)
20× Saline sodium citrate (SSC) (Invitrogen, 15557-044)
10% Tween-20 (Teknova, T0710)
DAPI Fluoromount-G (SouthernBiotech, 0100-20)

B.3 Replicates and additional studies

B.3.1 Replicates, signal, and background for protein:protein complex imaging with high signal-to-background in fixed adherent cells (cf. Figure 3.2)

Whereas the A-431 adherent cell line expresses the β-catenin:E-cadherin protein:protein complex, the HeLa adherent cell line expresses β-catenin but not E-cadherin and therefore lacks expression of the β-catenin:E-cadherin complex (*85–87*). To assess the signal-to-background ratio for protein:protein complex imaging in fixed adherent cells, the full protocol for detection of the β-catenin:E-cadherin protein:protein complex was performed in both cell lines, and each cell line was imaged under identical conditions. The A-431 cell line provides an estimate of the signal + background (SIG+BACK), while the HeLa cell line provides an estimate of the background (BACK). Reagents are listed in Table B.1. Additional studies are presented as follows:

- Figure B.1 displays images for $N = 3$ replicate wells on a multi-well coverslip for fixed A-431 cells and $N = 3$ replicate wells on a multi-well coverslip for fixed HeLa cells (cf. Figure 3.2).
- Figure B.2 displays representative regions used for measurement of signal and background.
- Table B.11 displays estimated values for signal, background, and signal-to-background.

Protocol: Protein:protein complex imaging in fixed adherent cells (Section B.2.1).
Sample: Fixed A-431 and HeLa cells.

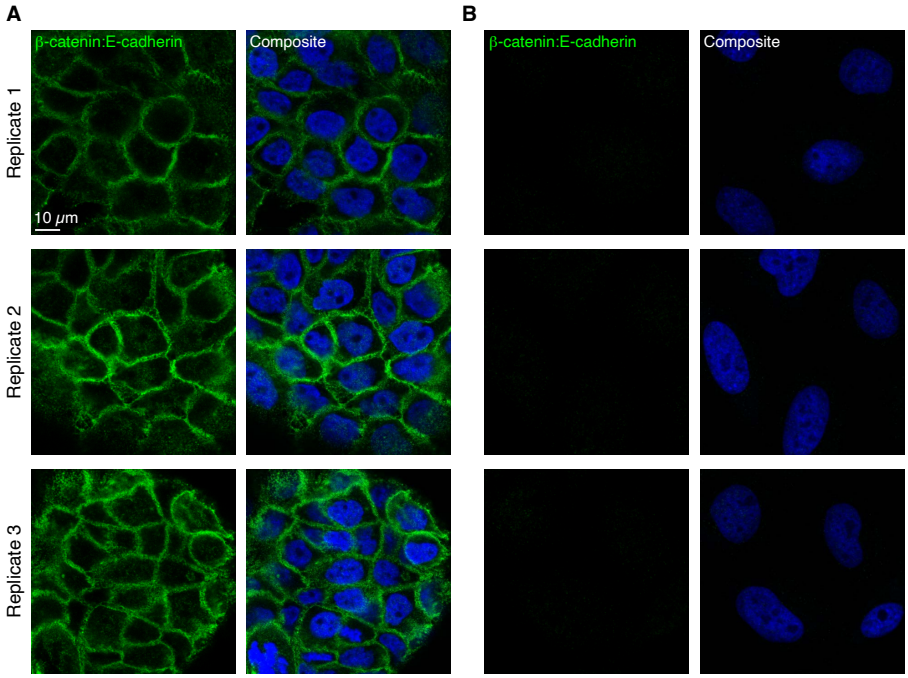

Figure B.1: Replicates for HCR imaging of a protein:protein complex in fixed adherent cells (cf. Figure 3.2). (A) Fixed A-431 cells. (B) Fixed HeLa cells. (A,B) 2-channel confocal images for 3 replicate wells on a multi-well coverslip; single optical section shown. Protein:protein complex β-catenin:E-cadherin (Alexa647). Composite: with DAPI.

Protein:protein complex	SIG+BACK	SIG	BACK	SIG/BACK
β-catenin:E-cadherin	19 000 ± 2000	18 000 ± 2000	700 ± 100	26 ± 5

Table B.11: Estimated signal-to-background for protein:protein complex imaging in fixed adherent cells (cf. Figure 3.2). The signal estimate SIG is calculated via an experiment of Type 1b in Table B.8 to measure BACK in a region of maximum background (pixels within rectangles) in fixed HeLa cells. Mean ± estimated standard error of the mean via uncertainty propagation for $N = 12$ rectangular regions (one rectangle in each of 4 individual cells in each of 3 replicate wells on a multi-well coverslip). Analysis based on rectangular regions depicted in Figure B.2 using methods of Section B.1.6.

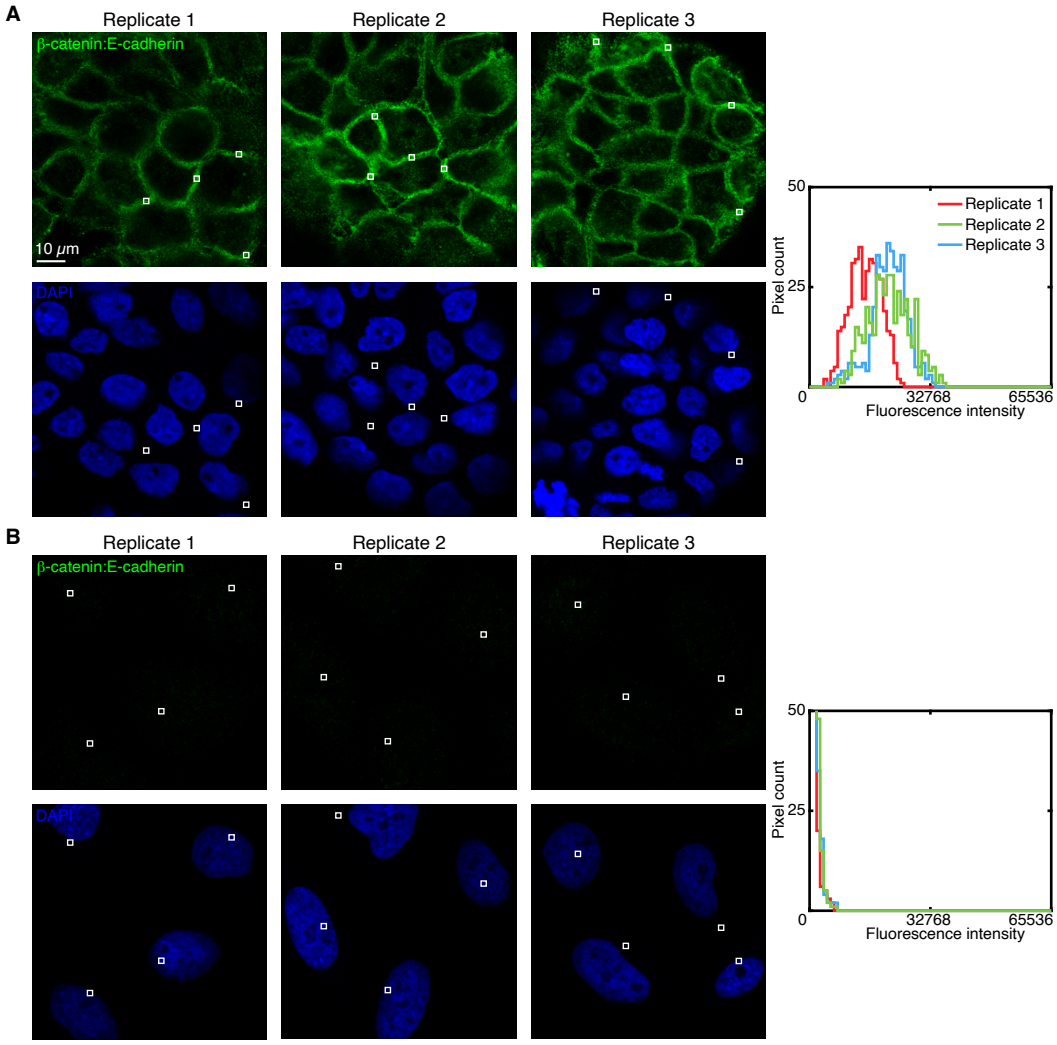

Figure B.2: Measurement of signal and background for protein:protein complex imaging in fixed adherent cells (cf. Figure 3.2). (A) Use experiment of Type 1a in Table B.8 to measure SIG+BACK in a region of high protein:protein complex expression (pixels within rectangles) in 3 replicates of fixed A-431 cells. (B) Use experiment of Type 1b in Table B.8 to measure BACK in a region of maximum background (pixels within rectangles) in 3 replicates of fixed HeLa cells. (A,B) Left: individual channels of confocal images collected with the microscope settings optimized to avoid saturating SIG+BACK pixels; DAPI channel contextualizes placement of the rectangles; single optical section. Ch1: protein:protein complex β-catenin:E-cadherin (Alexa647). Ch2: DAPI. Right: pixel intensity histograms for rectangular regions of Ch1 (one rectangle in each of 4 individual cells in each of 3 replicate wells on a multi-well coverslip).

B.3.2 Replicates, signal, and background for protein:protein complex imaging with high signal-to-background in pro-T cells (cf. Figure 3.3)

The DN3-like pro-T cell line Scid.adh.2C2 does not express the PU.1 protein and therefore does not form complexes between PU.1 and its protein binding partner RUNX1. However, upon expression of PU.1 in the Scid.adh.2C2 cell line via retroviral transduction of a PU.1 vector, the PU.1:RUNX1 protein:protein complex forms, reverting the Scid.adh.2C2 cell line to an earlier, pre-commitment T cell development time point (*89–91*). To assess the signal-to-background ratio for protein:protein complex imaging in fixed pro-T cells, the full protocol for detection of the RUNX1:PU.1 protein:protein complex was performed in Scid.adh.2C2 cells retrovirally transduced with a PU.1-expressing vector and in Scid.adh.2C2 cells retrovirally transduced with an empty vector, and each experiment type was imaged under identical conditions. Scid.adh.2C2 cells with PU.1 introduced provide an estimate of the signal + background (SIG+BACK), while Scid.adh.2C2 cells without PU.1 introduced provide an estimate of the background (BACK). Reagents are listed in Table B.3. Additional studies are presented as follows:

- Figure B.3 displays images for $N = 3$ replicate wells on a multi-well coverslip for pro-T cells retrovirally transduced with a PU.1 vector and $N = 3$ replicate wells on a multi-well coverslip for pro-T cells retrovirally transduced with an empty vector (cf. Figure 3.3).
- Figure B.4 displays representative regions used for measurement of signal and background.
- Table B.12 displays estimated values for signal, background, and signal-to-background.

Protocol: Protein:protein complex imaging in fixed pro-T cells (Section B.2.3).
Sample: Fixed Scid.adh.2C2 pro-T cells.

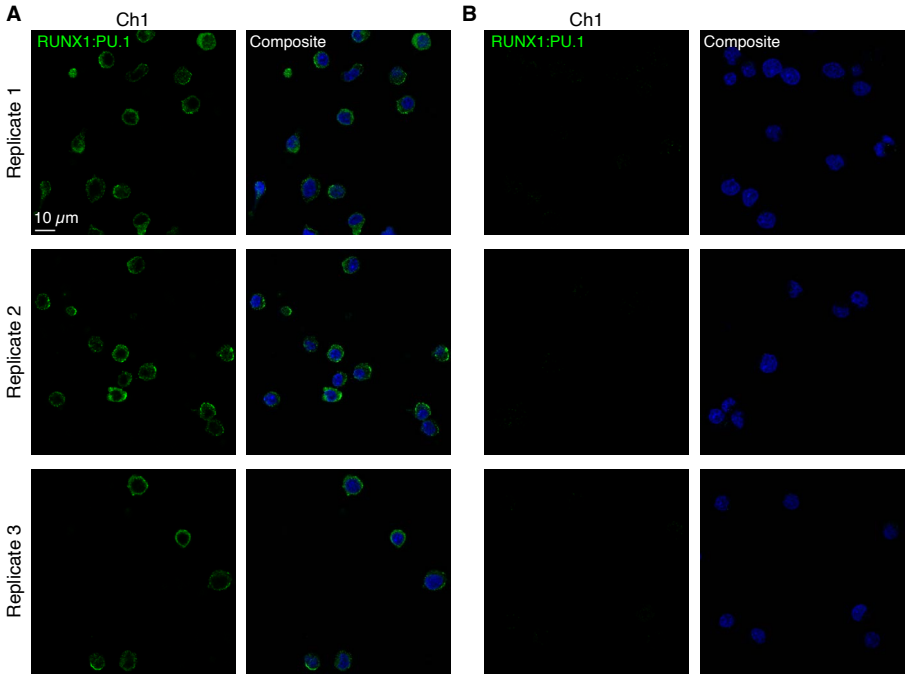

Figure B.3: Replicates for HCR imaging of a protein:protein complex in fixed pro-T cells (cf. Figure 3.3). (A) Scid.adh.2C2 cells retrovirally transduced with a PU.1-expressing vector. (B) Scid.adh.2C2 cells retrovirally transduced with an empty vector. (A,B) 2-channel confocal images for 3 replicate wells on a multi-well coverslip; single optical section shown. Protein:protein complex RUNX1:PU.1 (Alexa647). Composite: with DAPI.

Protein:protein complex	SIG+BACK	SIG	BACK	SIG/BACK
RUNX1:PU.1	11 000 ± 2000	11 000 ± 2000	700 ± 200	15 ± 4

Table B.12: Estimated signal-to-background for protein:protein complex imaging in fixed pro-T cells (cf. Figure 3.3). The signal estimate SIG is calculated via an experiment of Type 1b in Table B.8 to measure BACK in a region of maximum background (pixels within rectangles) in fixed Scid.adh.2C2 retrovirally transduced with an empty vector. Mean ± estimated standard error of the mean via uncertainty propagation for $N = 9$ rectangular regions (one rectangle in each of 3 individual cells in each of 3 replicate wells on a multi-well coverslip). Analysis based on rectangular regions depicted in Figure B.4 using methods of Section B.1.6.

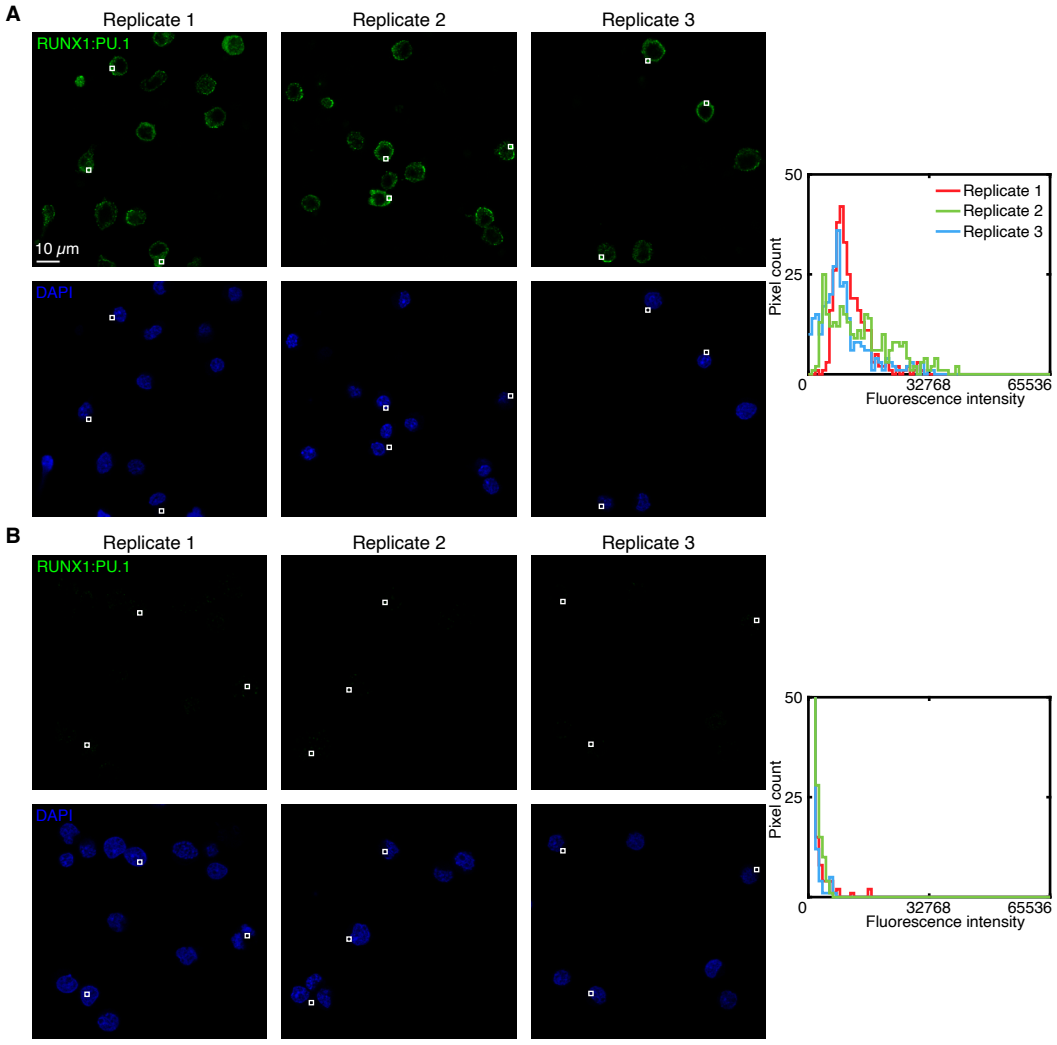

Figure B.4: Measurement of signal and background for protein:protein complex imaging in fixed pro-T cells (cf. Figure 3.3). (A) Use experiment of Type 1a in Table B.8 to measure SIG+BACK in a region of high protein:protein complex expression (pixels within rectangles) in 3 replicates of fixed Scid.adh.2C2 retrovirally transduced with a PU.1-expressing vector. (B) Use experiment of Type 1b in Table B.8 to measure BACK in a region of maximum background (pixels within rectangles) in 3 replicates of fixed Scid.adh.2C2 retrovirally transduced with an empty vector. (A,B) Left: individual channels of confocal images collected with the microscope settings optimized to avoid saturating SIG+BACK pixels; DAPI channel contextualizes placement of the rectangles; single optical section. Ch1: protein:protein complex RUNX1:PU.1 (Alexa647). Ch2: DAPI. Right: pixel intensity histograms for rectangular regions of Ch1 (one rectangle in each of 3 individual cells in each of 3 replicate wells on a multi-well coverslip).

B.3.3 Replicates, signal, and background for protein:protein complex imaging with high signal-to-background in FFPE human breast tissue sections (cf. Figure 3.4)

Whereas normal human breast tissue expresses the β-catenin:E-cadherin protein:protein complex, the invasive lobular carcinoma (ILC) disease process reduces β-catenin and E-cadherin expression, resulting in fewer β-catenin:E-cadherin protein:protein complexes (*92*, *93*). To assess the signal-to-background ratio for protein:protein complex imaging in FFPE human breast tissue sections, the full protocol for detection of the β-catenin:E-cadherin protein:protein complex was performed in both normal and ILC FFPE human breast tissue sections from the same patient, and each tissue type was imaged under identical conditions. The normal FFPE human breast tissue sections provide an estimate of the signal + background (SIG+BACK), while the ILC FFPE human breast tissue sections provide an estimate of the background (BACK). Reagents are listed in Table B.2. Additional studies are presented as follows:

- Figure B.5 displays images for $N = 3$ replicate FFPE normal human breast tissue sections and $N = 3$ paired replicate FFPE ILC human breast tissue sections (cf. Figure 3.4).
- Figure B.6 displays representative regions used for measurement of signal and background.
- Table B.13 displays estimated values for signal, background, and signal-to-background.

Protocol: Protein:protein complex imaging in FFPE human breast tissue sections (Section B.2.2).
Sample: FFPE normal and ILC human breast tissue sections; thickness: 5 μm.

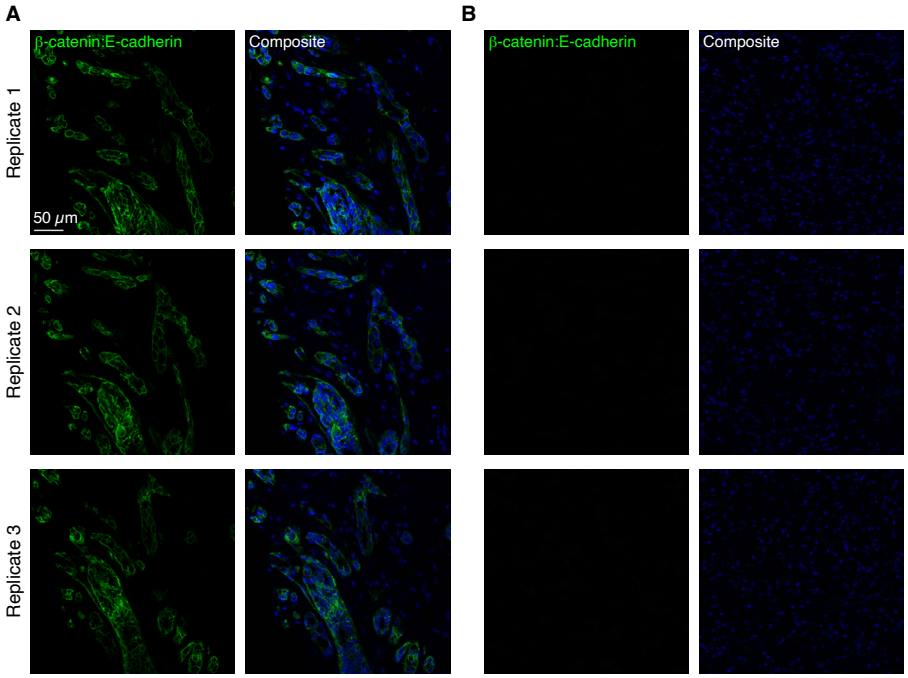

Figure B.5: Replicates for HCR imaging of a protein:protein complex in FFPE human breast tissue sections (cf. Figure 3.4). (A) FFPE normal human breast tissue sections. (B) FFPE invasive lobular carcinoma (ILC) human breast tissue sections. (A,B) 2-channel confocal images for 3 replicate FFPE human breast tissue sections; single optical section shown. Protein:protein complex β-catenin:E-cadherin (Alexa647). Composite: with DAPI.

Protein:protein complex	SIG+BACK	SIG	BACK	SIG/BACK
β-catenin:E-cadherin	14 000 ± 1000	14 000 ± 1000	460 ± 60	30 ± 5

Table B.13: Estimated signal-to-background for protein:protein complex imaging in FFPE human breast tissue sections (cf. Figure 3.4). The signal estimate SIG is calculated via an experiment of Type 1b in Table B.8 to measure BACK in a region of maximum background (pixels within rectangles) in FFPE invasive lobular carcinoma (ILC) human breast tissue sections. Mean ± estimated standard error of the mean via uncertainty propagation for $N = 12$ rectangular regions (4 rectangles in each of 3 replicate FFPE human breast tissue sections). Analysis based on rectangular regions depicted in Figure B.6 using methods of Section B.1.6.

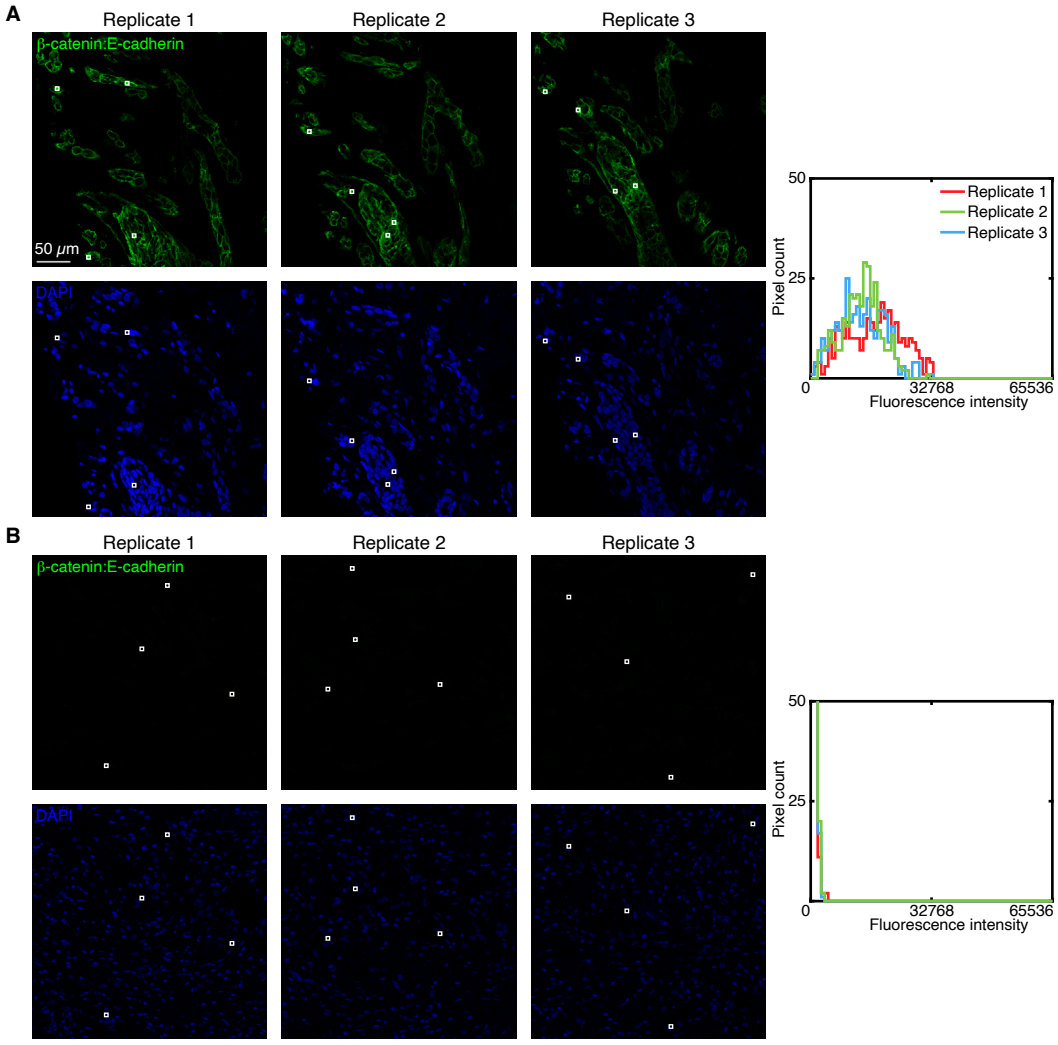

Figure B.6: Measurement of signal and background for protein:protein complex imaging in FFPE human breast tissue sections (cf. Figure 3.4). (A) Use experiment of Type 1a in Table B.8 to measure SIG+BACK in a region of high protein:protein complex expression (pixels within rectangles) in 3 replicate FFPE normal human breast tissue sections. (B) Use experiment of Type 1b in Table B.8 to measure BACK in a region of maximum background (pixels within rectangles) in 3 replicate paired FFPE invasive lobular carcinoma (ILC) human breast tissue sections. (A,B) Left: individual channels of confocal images collected with the microscope settings optimized to avoid saturating SIG+BACK pixels; DAPI channel contextualizes placement of the rectangles; single optical section. Ch1: protein:protein complex β-catenin:E-cadherin (Alexa647). Ch2: DAPI. Right: pixel intensity histograms for rectangular regions of Ch1 (4 rectangles in each of 3 replicate FFPE human breast tissue sections).

B.3.4 Replicates, signal, and background for 3-plex protein:protein complex imaging with high signal-to-background in fixed adherent cells (cf. Figure 3.6)

For 3-plex protein:protein complex imaging using HCR in mammalian cells on a coverslip, the 4 channels are (3 protein:protein complexes + DAPI):

- **Ch1:** Protein:protein complex β-tubulin:α-tubulin, amplifier B6-Alexa488.
- **Ch2:** Protein:protein complex β-catenin:E-cadherin, amplifier B1-Alexa546.
- **Ch3:** Protein:protein complex SC35:SON, amplifier B9-Alexa647.
- **Ch4:** DAPI.

Additional studies are presented as follows:

- Figure B.7 displays 3-plex images for $N = 3$ replicate wells on a multi-well coverslip (cf. Figure 3.6).
- Figures B.8–B.10 display representative regions of individual channels used for measurement of signal and background for each target.
- Table B.14 displays estimated values for signal, background, and signal-to-background for each channel.

Protocol: Multiplexed protein:protein complex imaging in fixed adherent cells (Section B.2.1).
Sample: A-431 cells.

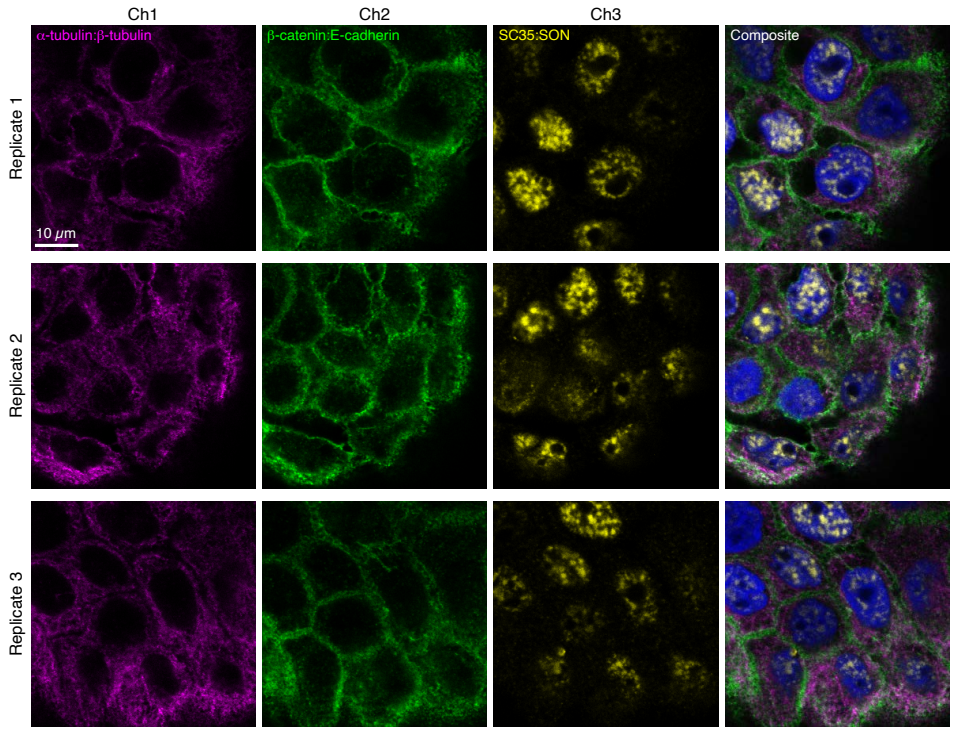

Figure B.7: Replicates for 3-plex protein:protein complex imaging using HCR in fixed adherent cells (cf. Figure 3.6). 4-channel images for 3 replicate wells on a multi-well coverslip; single optical section. Ch1: protein:protein complex β-tubulin:α-tubulin (Alexa488). Ch2: protein:protein complex β-catenin:E-cadherin (Alexa546). Ch3: protein:protein complex SC35:SON (Alexa647). Composite: with DAPI. Sample: A-431 cells.

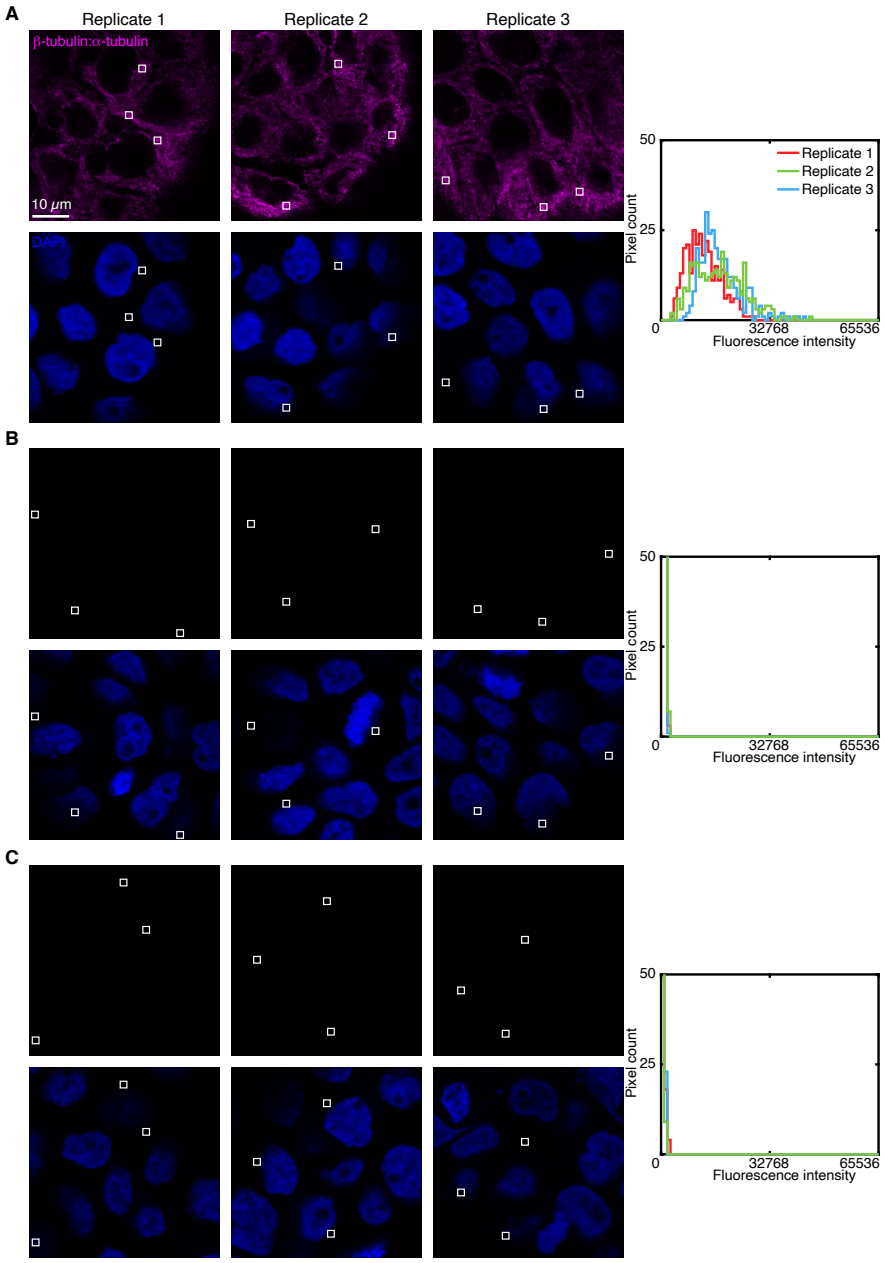

Figure B.8: Measurement of signal and background for protein:protein complex β-tubulin:α-tubulin in fixed adherent cells (cf. Figure 3.6). (A) Use experiment of Type 1a in Table B.8 to measure SIG+BACK in a region of high protein:protein complex expression (pixels within rectangles) in 3 replicates. (B) Use experiment of Type 2a in Table B.8 to measure SA_{P1}+NSD+NSA+AF in a region of maximum background (pixels within rectangles) in 3 replicates. (C) Use experiment of Type 2b in Table B.8 to measure SA_{P2}+NSD+NSA+AF in a region of maximum background (pixels within rectangles) in 3 replicates. (A,B,C) Left: individual channels of confocal images; DAPI channel contextualizes placement of the rectangles; single optical section. Ch1: protein:protein complex β-tubulin:α-tubulin (Alexa488). Right: pixel intensity histograms for rectangular regions of Ch1 (one rectangle in each of 3 individual cells in each of 3 replicate wells on a multi-well coverslip).

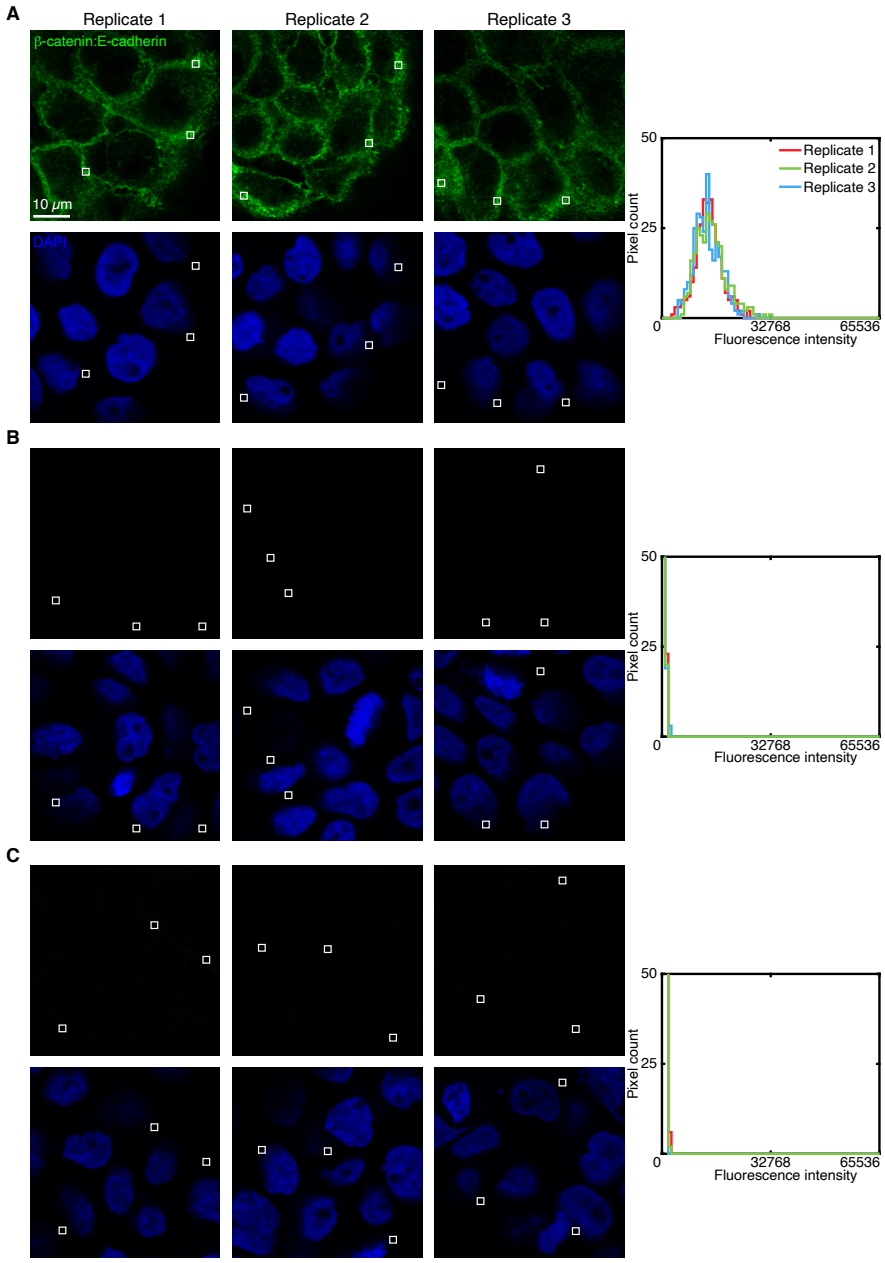

Figure B.9: Measurement of signal and background for protein:protein complex β-catenin:E-cadherin in fixed adherent cells (cf. Figure 3.6). (A) Use experiment of Type 1a in Table B.8 to measure SIG+BACK in a region of high protein:protein complex expression (pixels within rectangles) in 3 replicates. (B) Use experiment of Type 2a in Table B.8 to measure SA_{P1}+NSD+NSA+AF in a region of maximum background (pixels within rectangles) in 3 replicates. (C) Use experiment of Type 2b in Table B.8 to measure SA_{P2}+NSD+NSA+AF in a region of maximum background (pixels within rectangles) in 3 replicates. (A,B,C) Left: individual channels of confocal images; DAPI channel contextualizes placement of the rectangles; single optical section. Ch2: protein:protein complex β-catenin:E-cadherin (Alexa546). Right: pixel intensity histograms for rectangular regions of Ch2 (one rectangle in each of 3 individual cells in each of 3 replicate wells on a multi-well coverslip).

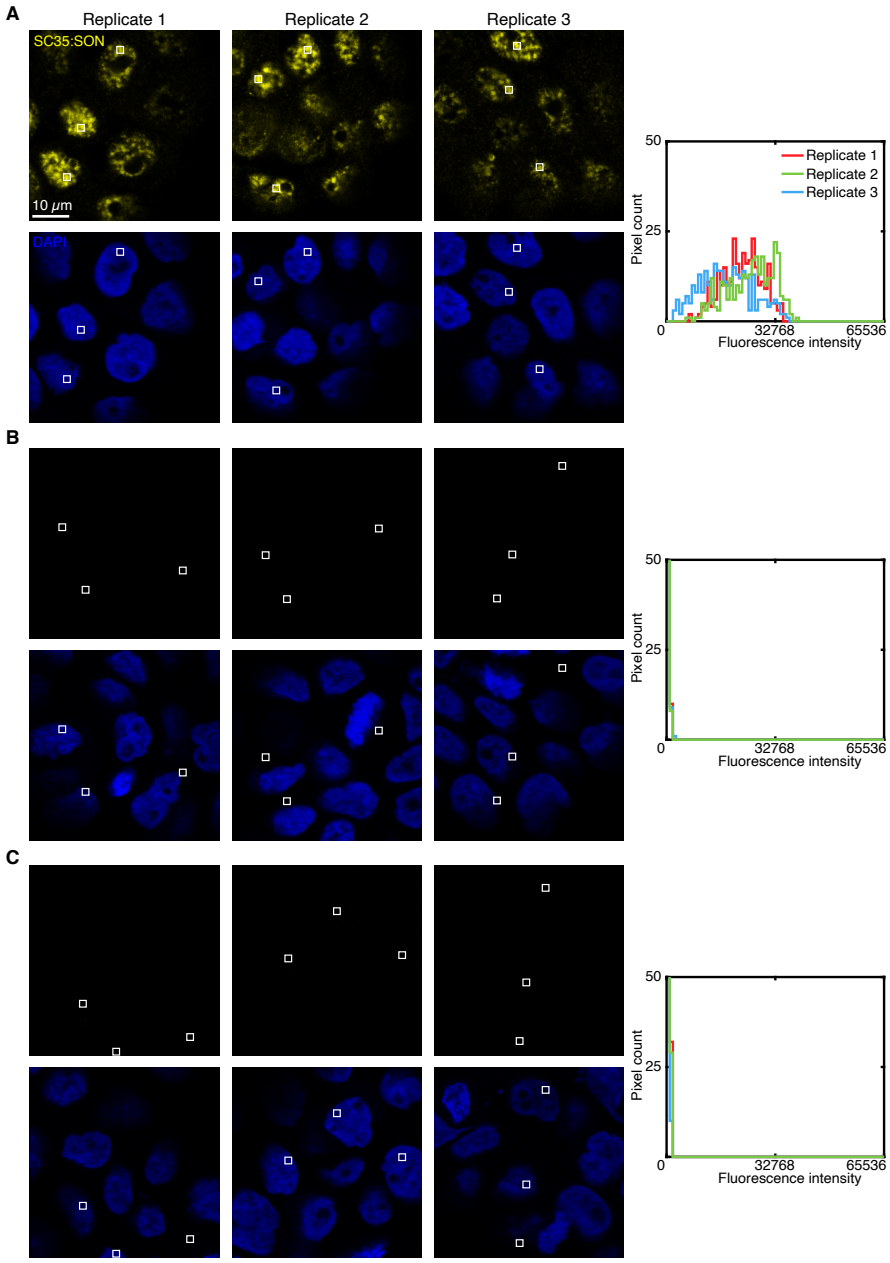

Figure B.10: Measurement of signal and background for protein:protein complex SC35:SON in fixed adherent cells (cf. Figure 3.6). (A) Use experiment of Type 1a in Table B.8 to measure SIG+BACK in a region of high protein:protein complex expression (pixels within rectangles) in 3 replicates. (B) Use experiment of Type 2a in Table B.8 to measure SA_{P1}+NSD+NSA+AF in a region of maximum background (pixels within rectangles) in 3 replicates. (C) Use experiment of Type 2b in Table B.8 to measure SA_{P2}+NSD+NSA+AF in a region of maximum background (pixels within rectangles) in 3 replicates. (A,B,C) Left: individual channels of confocal images; DAPI channel contextualizes placement of the rectangles; single optical section. Ch3: protein:protein complex SC35:SON (Alexa647). Right: pixel intensity histograms for rectangular regions of Ch3 (one rectangle in each of 3 individual cells in each of 3 replicate wells on a multi-well coverslip).

Protein:protein complex	SIG+BACK	SA_{P1}+NSD+NSA+AF	SA_{P2}+NSD+NSA+AF	BACK	SIG	SIG/BACK
β-tubulin:α-tubulin	16 000 ± 2000	350 ± 70	130 ± 40	350 ± 70	15 000 ± 2000	40 ± 10
β-catenin:E-cadherin	13 700 ± 600	170 ± 30	430 ± 90	430 ± 90	13 300 ± 600	31 ± 7
SC35:SON	22 000 ± 3000	90 ± 10	140 ± 40	140 ± 40	22 000 ± 3000	150 ± 50

Table B.14: Estimated signal-to-background for 3-plex protein:protein complex imaging in fixed adherent cells (cf. Figure 3.6). The signal estimate SIG is calculated via experiments of Type 2a and Type 2b in Table B.8 to measure BACK in a region of maximum background (pixels within rectangles). BACK is calculated as the maximum of SA_{P1}+NSD+NSA+AF and SA_{P2}+NSD+NSA+AF. Mean ± estimated standard error of the mean via uncertainty propagation for $N = 9$ rectangular regions (one rectangle in each of 3 individual cells in each of 3 replicate wells on a multi-well coverslip). Analysis based on rectangular regions depicted in Figures B.8–B.10 using methods of Section B.1.6.

B.3.5 qHCR imaging: protein:protein complex relative quantitation with subcellular resolution in an anatomical context (cf. Figure 3.7)

Redundant 2-channel imaging of the β-catenin:E-cadherin protein:protein complex using HCR in fixed adherent cells

To demonstrate qHCR imaging, the β-catenin:E-cadherin protein:protein complex is redundantly detected via 2-channel imaging in fixed adherent A-431 cells. Each protein is detected by a 1°Ab probe, which is then redundantly detected by two batches of interaction probes labeled with different HCR initiators that trigger orthogonal spectrally distinct HCR amplifiers.

Additional studies are presented as follows:

- Figure B.11 displays 2-plex images and 2-channel voxel intensity scatter plots for protein:protein complex β-catenin:E-cadherin in fixed A-431 cells for $N = 3$ replicate wells on a multi-well coverslip.
- Table B.15 displays values used for signal normalization in Figures B.11.
- Figures B.12 and B.13 display representative regions used for measurement of signal and background for protein:protein complex β-catenin:E-cadherin, as well as for determining the BOT value used to normalize data for Figure B.11C using methods of Section B.1.6.
- Table B.16 displays estimated values for signal, background, and signal-to-background for each channel.

Protocol: Protein:protein complex imaging in fixed adherent cells (Section B.2.2).
Sample: Fixed A-431 cells.

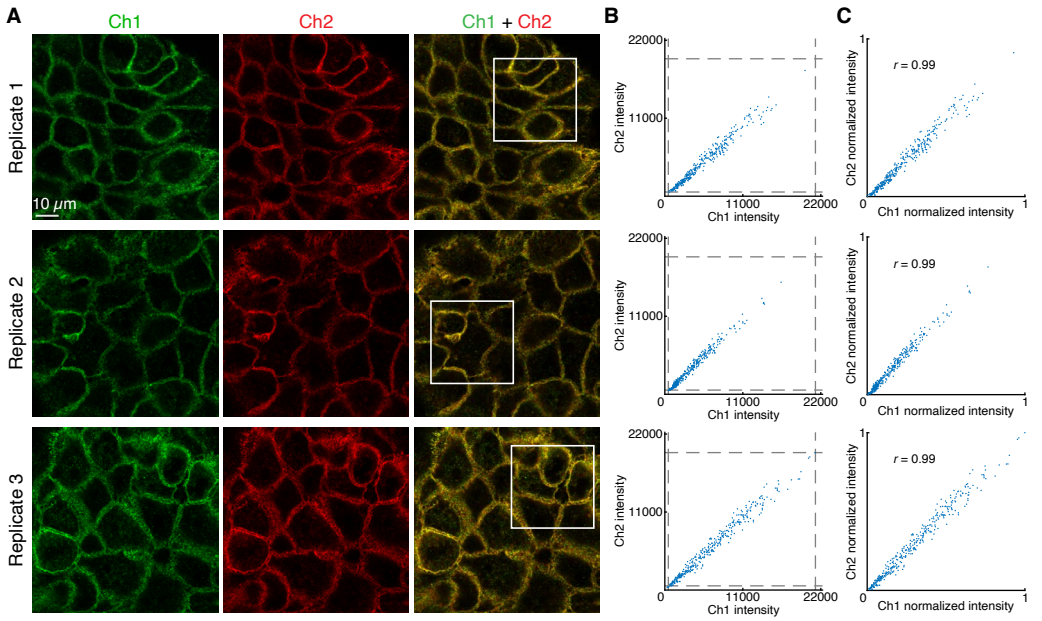

Figure B.11: Redundant 2-channel detection of protein:protein complex β-catenin:E-cadherin in fixed A-431 cells (cf. Figure 3.7). (A) Confocal images: individual channels and merge; single optical section. Ch1: β-catenin:E-cadherin (Alexa546). Ch2: β-catenin:E-cadherin (Alexa647). Solid boundaries denote regions of variable expression. Pixel size: 0.180×0.180×0.8 μm. Sample: Fixed A-431 cells. (B) Raw voxel intensity scatter plots representing signal plus background for voxels within solid boundaries of panel A. Voxel size: 2.0×2.0×0.8 μm. Dashed lines represent BOT and TOP values (Table B.15) used to normalize data for panel C using methods of Section B.1.6. The BOT value was determined from the solid boundaries (regions of no/low protein:protein complex expression) in Figures B.12BC and B.13BC. (C) Normalized voxel intensity scatter plots representing normalized signal (Pearson correlation coefficient, r).

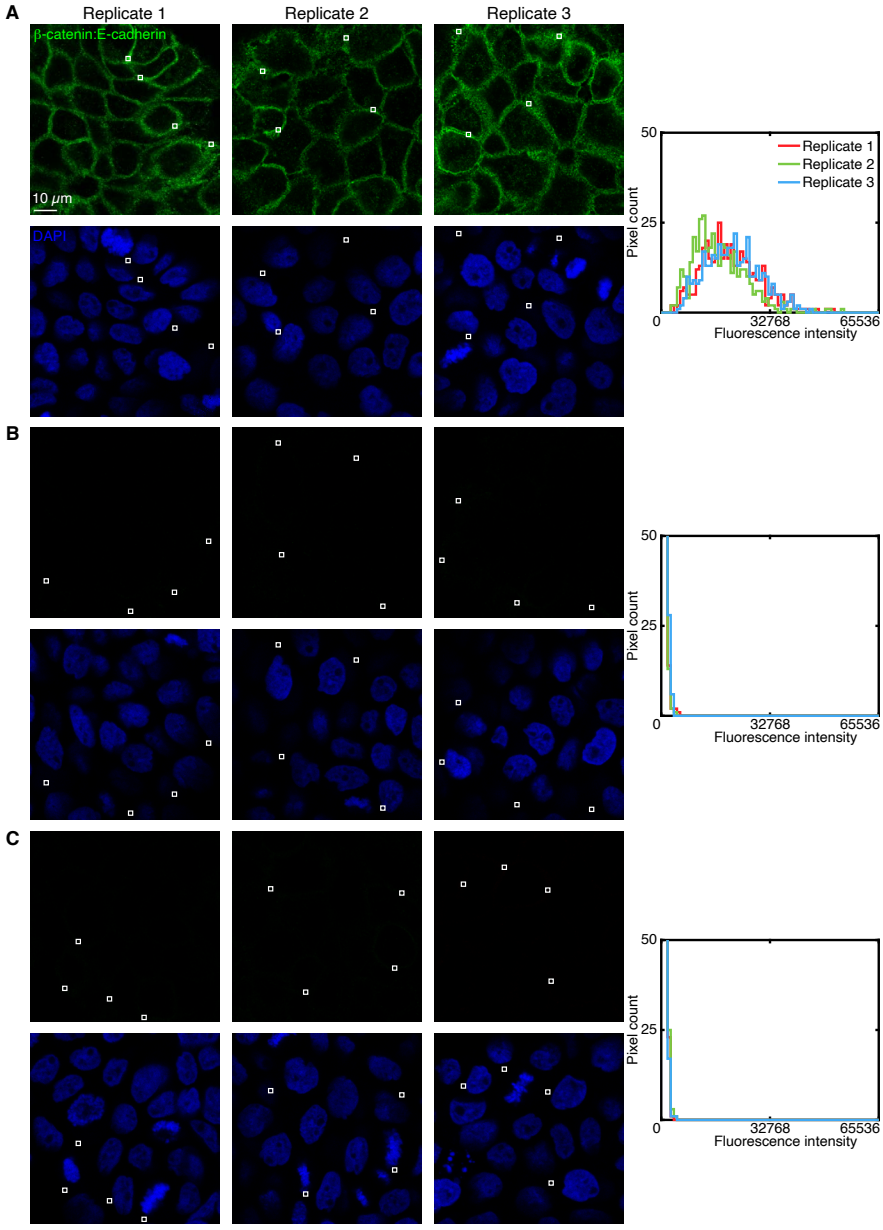

Figure B.12: Measurement of Ch1 signal, background, and BOT for redundant 2-channel detection of protein:protein complex β-catenin:E-cadherin in fixed A-431 cells (cf. Figure 3.7). (A) Ch1 (Alexa546) for redundant 2-channel imaging of protein:protein complex β-catenin:E-cadherin. Solid boundaries denote regions of high expression. (B) Experiment of Type 2a in Table B.8 to measure SA_{P1}+NSD+NSA+AF in a region of maximum background and determine the BOT value of Ch1 (Alexa546) for Figures 3.7C and B.11C using methods of Section B.1.6. Solid boundaries denote regions of maximum background. (C) Experiment of Type 2b in Table B.8 to measure SA_{P2}+NSD+NSA+AF in a region of maximum background and determine the BOT value of Ch1 (Alexa546) for Figures 3.7C and B.11C using methods of Section B.1.6. Solid boundaries denote regions of maximum background. (A,B,C) Left: confocal images; single optical section. Right: pixel intensity histograms for the depicted regions. Sample: Fixed A-431 cells.

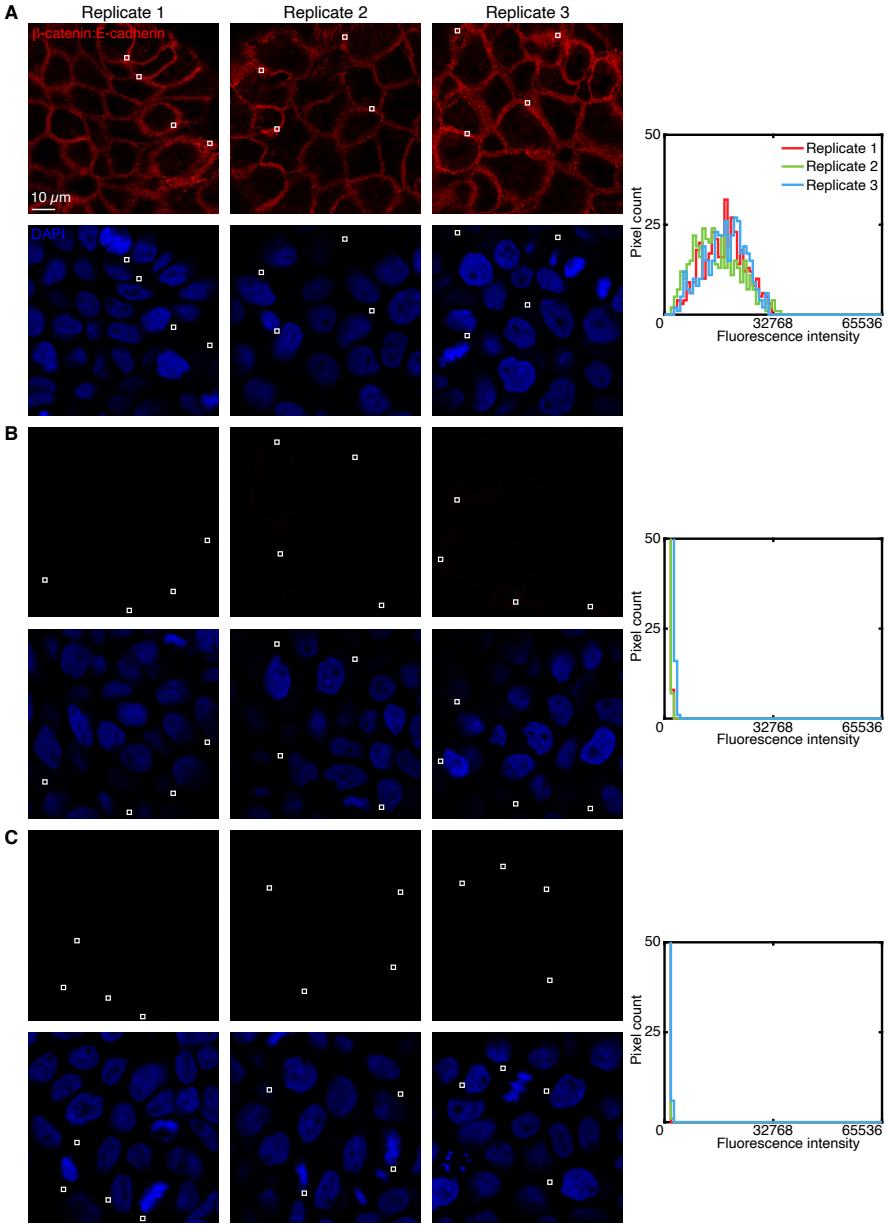

Figure B.13: Measurement of Ch2 signal, background, and BOT for redundant 2-channel detection of protein:protein complex β-catenin:E-cadherin in fixed A-431 cells (cf. Figure 3.7). (A) Ch2 (Alexa647) for redundant 2-channel imaging of target protein:protein complex β-catenin:E-cadherin. Solid boundaries denote regions of high expression. (B) Experiment of Type 2a in Table B.8 to measure SA_{P1}+NSD+NSA+AF in a region of maximum background and determine the BOT value of Ch2 (Alexa647) for Figures 3.7C and B.11C using methods of Section B.1.6. Solid boundaries denote regions of maximum background. (C) Experiment of Type 2b in Table B.8 to measure SA_{P2}+NSD+NSA+AF in a region of maximum background and determine the BOT value of Ch2 (Alexa647) for Figures 3.7C and B.11C using methods of Section B.1.6. Solid boundaries denote regions of maximum background. (A,B,C) Left: confocal images; single optical section. Right: pixel intensity histograms for the depicted regions. Sample: Fixed A-431 cells.

Channel	Protein:protein complex	Fluorophore	BOT	TOP
Ch1	β-catenin:E-cadherin	Alexa546	492	21241
Ch2	β-catenin:E-cadherin	Alexa647	591	19384

Table B.15: BOT and TOP values used to calculate normalized voxel intensities for scatter plots of Figures 3.7C (top panel) and B.11C using methods of Section B.1.6. Analysis based on rectangular regions depicted in Figures B.11A, B.12BC, and B.13BC.

Channel	Protein:protein complex	Fluorophore	SA_{P1}+NSD+NSA+AF	SA_{P2}+NSD+NSA+AF	BACK	SIG+BACK	SIG	SIG/BACK
Ch1	β-catenin:E-cadherin	Alexa546	490 ± 80	640 ± 70	640 ± 70	20 000 ± 2000	19 000 ± 2000	30 ± 4
Ch2	β-catenin:E-cadherin	Alexa647	700 ± 200	380 ± 50	700 ± 200	17 000 ± 2000	16 000 ± 2000	24 ± 6

Table B.16: Estimated signal-to-background for redundant 2-channel detection of protein:protein complex β-catenin:E-cadherin in fixed A-431 cells (cf. Figure 3.7). The signal estimate SIG is calculated via experiments of Type 2a and Type 2b in Table B.8 to measure BACK in a region of maximum background (pixels within rectangles). BACK is calculated as the maximum of SA_{P1}+NSD+NSA+AF and SA_{P2}+NSD+NSA+AF. Mean ± estimated standard error of the mean via uncertainty propagation for $N = 3$ replicate wells on a multi-well coverslip. Analysis based on rectangular regions depicted in Figures B.12 and B.13 using methods of Section B.1.6.

Redundant 2-channel imaging of the β-catenin:E-cadherin protein:protein complex using HCR in FFPE human breast tissue sections

To demonstrate qHCR imaging, the β-catenin:E-cadherin protein:protein complex is redundantly detected via 2-channel imaging in FFPE human breast tissue sections. Each protein is detected by a 1°Ab probe, which is then redundantly detected by two batches of interaction probes labeled with different HCR initiators that trigger orthogonal spectrally distinct HCR amplifiers.

Additional studies are presented as follows:

- Figure B.14 displays 2-plex images and 2-channel voxel intensity scatter plots for protein:protein complex β-catenin:E-cadherin in $N = 3$ replicate FFPE human breast tissue sections.
- Table B.17 displays values used for signal normalization in Figures B.14.
- Figure B.15 displays representative regions used for measurement of signal and background for protein:protein complex β-catenin:E-cadherin.
- Table B.18 displays estimated values for signal, background, and signal-to-background for each channel.

Protocol: Protein:protein complex imaging in FFPE human breast tissue sections (Section B.2.2).
Sample: FFPE normal human breast tissue sections; thickness: 5 μm.

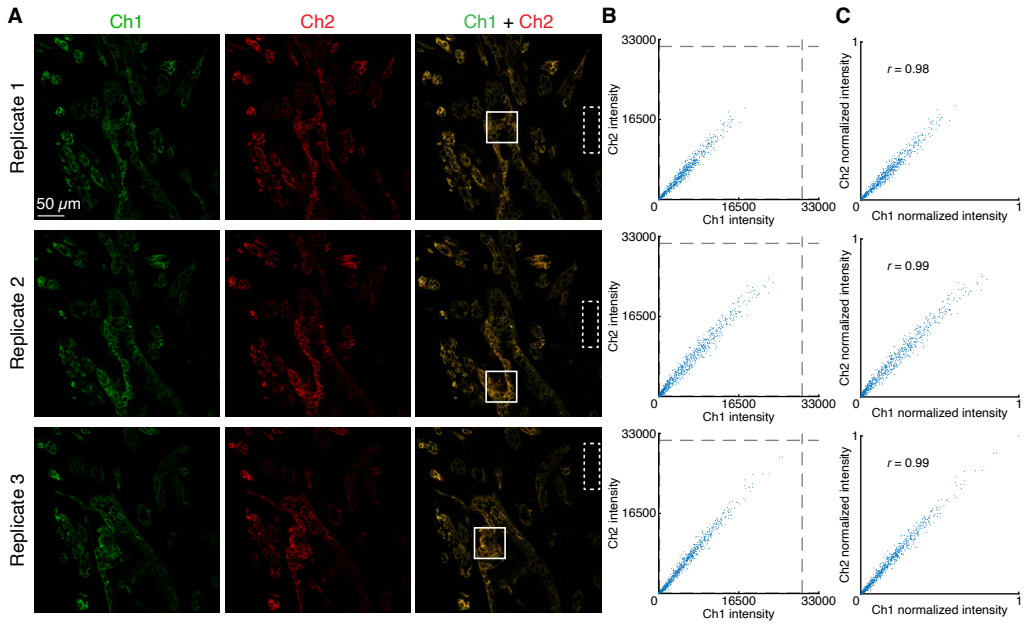

Figure B.14: Redundant 2-channel detection of protein:protein complex β-catenin:E-cadherin in FFPE human breast tissue sections (cf. Figure 3.7). (A) Confocal images: individual channels and merge; single optical section. Ch1: β-catenin:E-cadherin (Alexa546). Ch2: β-catenin:E-cadherin (Alexa647). Solid boundaries denote regions of variable expression. Dashed boundaries denote regions of no/low expression. Pixel size: 0.568×0.568×3.3 μm. Sample: FFPE human breast tissue sections. (B) Raw voxel intensity scatter plots representing signal plus background for voxels within solid boundaries of panel A. Voxel size: 2.0×2.0×3.3 μm. Dashed lines represent BOT and TOP values (Table B.17) used to normalize data for panel C using methods of Section B.1.6. (C) Normalized voxel intensity scatter plots representing normalized signal (Pearson correlation coefficient, r).

Channel	Protein:protein complex	Fluorophore	BOT	TOP
Ch1	β-catenin:E-cadherin	Alexa546	143	29571
Ch2	β-catenin:E-cadherin	Alexa647	75	31564

Table B.17: BOT and TOP values used to calculate normalized voxel intensities for scatter plots of Figures 3.7C (bottom panel) and B.14C using methods of Section B.1.6. Analysis based on rectangular regions depicted in Figure B.14A.

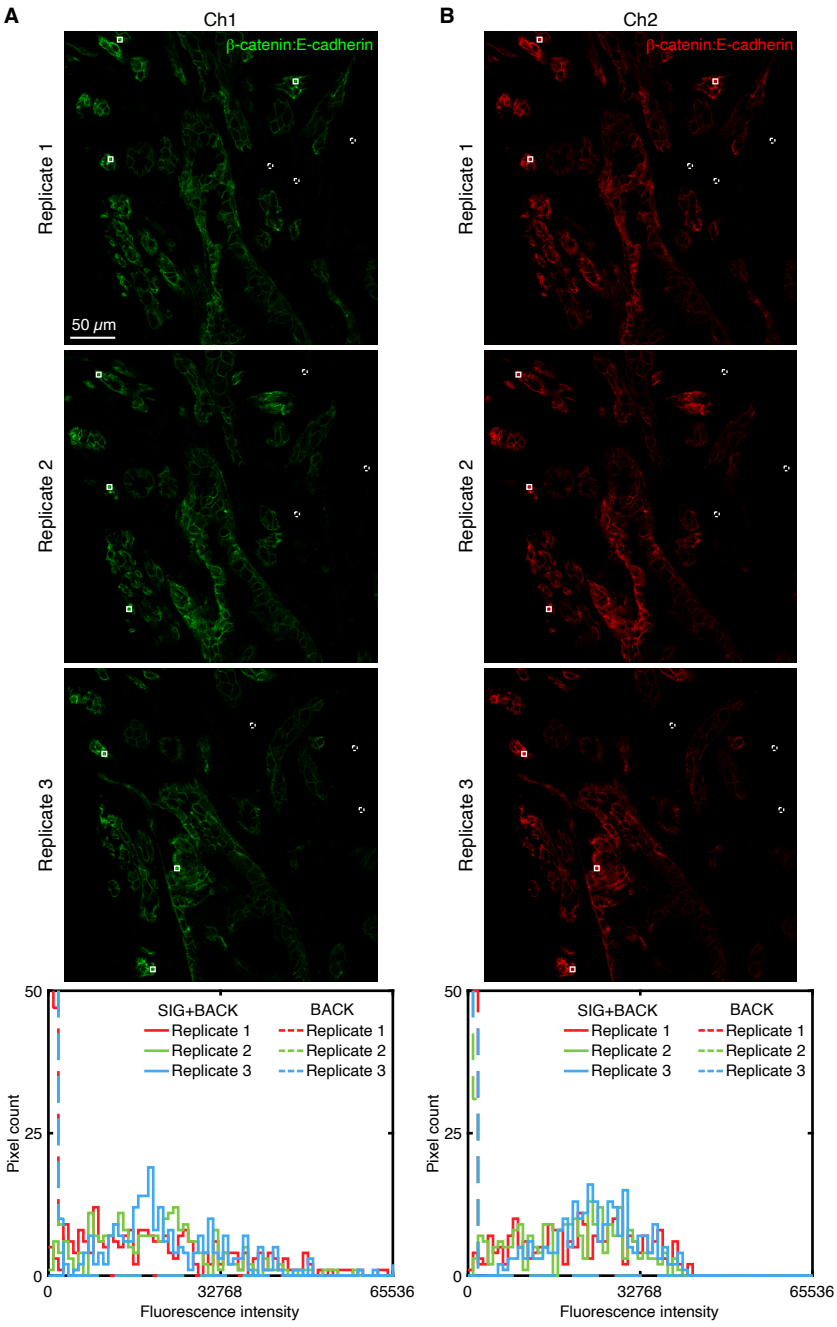

Figure B.15: Measurement of signal and background for redundant 2-channel detection of protein:protein complex β-catenin:E-cadherin in FFPE human breast tissue sections (cf. Figure 3.7). (A) Ch1 (Alexa546) of redundant 2-channel imaging of protein:protein complex β-catenin:E-cadherin. (B) Ch2 (Alexa647) of redundant 2-channel imaging of protein:protein complex β-catenin:E-cadherin. (A,B) Top: confocal images; single optical section. Solid boundaries denote representative regions of high expression; dashed boundaries denote representative regions of no/low expression. Bottom: pixel intensity histograms for the depicted representative regions. Sample: FFPE human breast tissue sections; thickness: 5 μm.

Channel	Protein:protein complex	Fluorophore	BACK	SIG+BACK	SIG	SIG/BACK
Ch1	β-catenin:E-cadherin	Alexa546	410 ± 70	21 300 ± 900	20 900 ± 900	52 ± 9
Ch2	β-catenin:E-cadherin	Alexa647	230 ± 50	21 000 ± 1000	21 000 ± 1000	90 ± 20

Table B.18: Estimated signal-to-background for redundant 2-channel detection of protein:protein complex β-catenin:E-cadherin in FFPE human breast tissue sections (cf. Figure 3.7). Mean ± estimated standard error of the mean via uncertainty propagation for $N = 3$ replicate FFPE human breast tissue sections. Analysis based on rectangular regions depicted in Figure B.15 using methods of Section B.1.6.

B.3.6 Replicates, signal, and background for simultaneous protein, protein:protein complex, and RNA imaging with high signal-to-background in fixed adherent cells (cf. Figure 3.8)

For simultaneous protein, protein:protein complex, and RNA imaging using HCR in mammalian cells on a coverslip, the 4 channels are (1 target protein + 1 protein:protein complex + 1 target RNA + DAPI):

- **Ch1:** Target protein HSP60, amplifier B5-Alexa488.
- **Ch2:** Protein:protein complex β-tubulin:α-tubulin, amplifier B1-Alexa546.
- **Ch3:** Target RNA *U6*, amplifier B3-Alexa647.
- **Ch4:** DAPI.

Additional studies are presented as follows:

- Figure B.16 displays images for $N = 3$ replicate wells on a multi-well coverslip (cf. Figure 3.8).
- Figures B.17–B.19 displays representative regions of individual channels used for measurement of signal and background for each target.
- Table B.19 displays estimated values for signal, background, and signal-to-background for each channel.

Protocol: Simultaneous protein, protein:protein complex, and RNA imaging in fixed adherent cells (Section B.2.1).
Sample: HeLa cells.

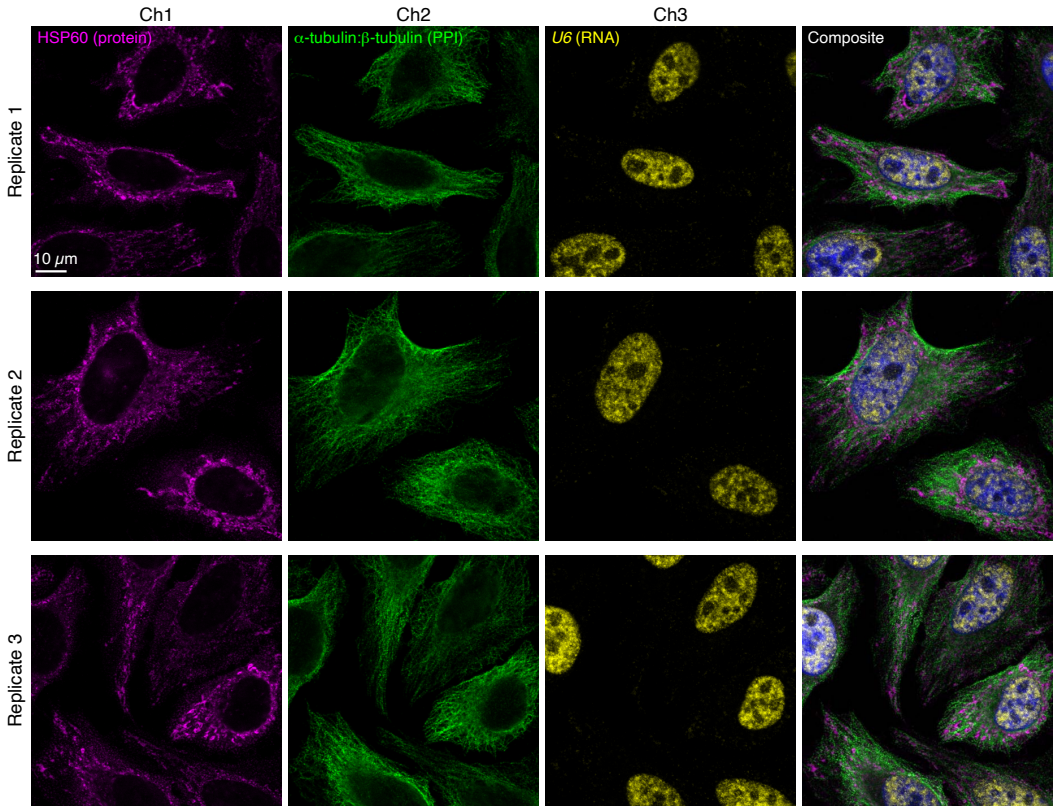

Figure B.16: Replicates for simultaneous target protein, protein:protein complex, and target RNA imaging using HCR in fixed adherent cells (cf. Figure 3.8). 4-channel images for 3 replicate wells on a multi-well coverslip; single optical section. Ch1: target protein HSP60 (Alexa488). Ch2: protein:protein complex β-tubulin:α-tubulin (Alexa546). Ch3: target RNA *U6* (Alexa647). Ch4: DAPI. Sample: HeLa cells.

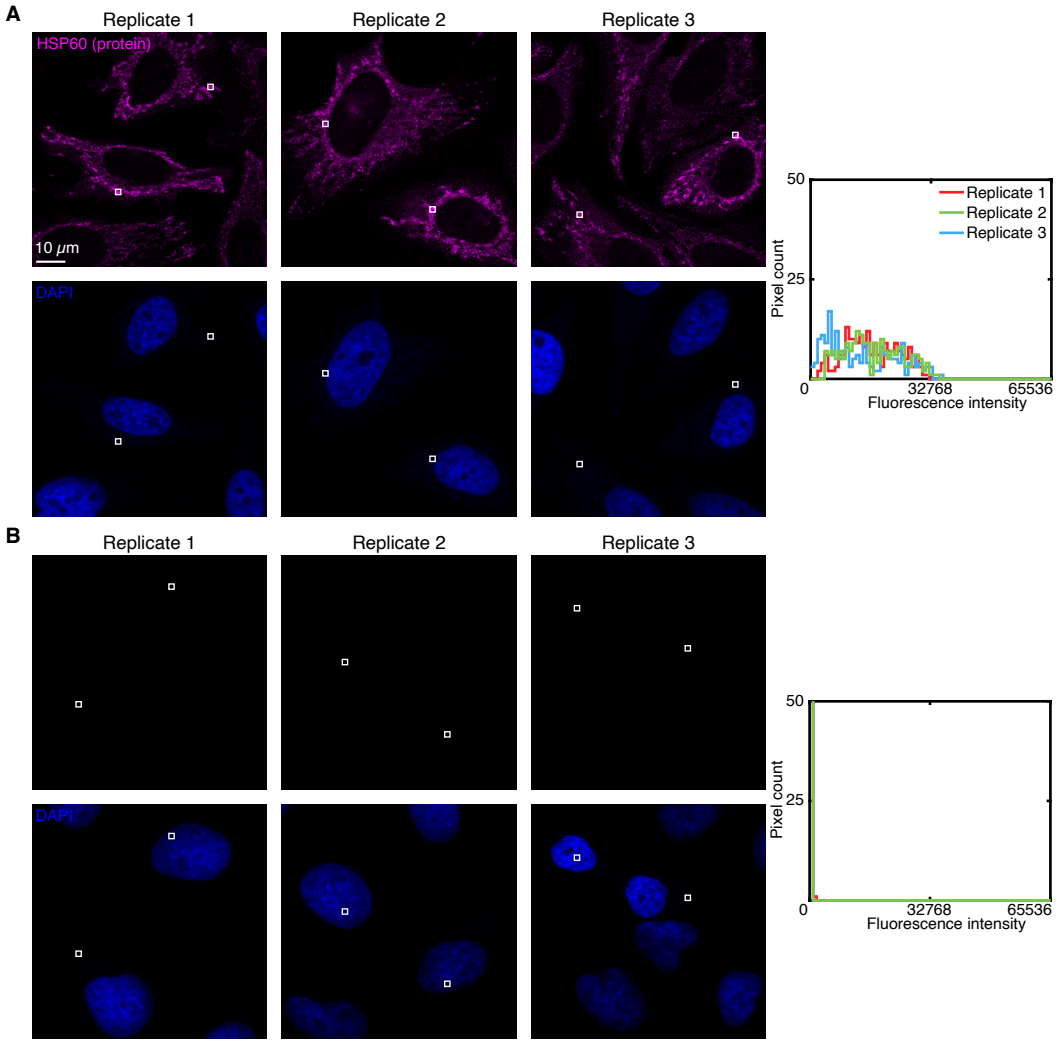

Figure B.17: Measurement of signal and background for target protein HSP60 using HCR IF in fixed adherent cells (cf. Figure 3.8). (A) Use experiment of Type 1 in Table B.9 to measure SIG+BACK in a region of high target protein expression (pixels within rectangles) in 3 replicates. (B) Use experiment of Type 2 in Table B.9 to measure BACK $\approx$ NSD_{2°+NSA+AF in a region of maximum background (pixels within rectangles) in 3 replicates. (A,B) Left: individual channels of confocal images collected with the microscope settings optimized to avoid saturating SIG+BACK pixels; DAPI channel contextualizes placement of the rectangles; single optical section. Ch1: target protein HSP60 (Alexa488). Ch4: DAPI. Right: pixel intensity histograms for rectangular regions of Ch1 (one rectangle in each of 2 individual cells in each of 3 replicate wells on a multi-well coverslip).

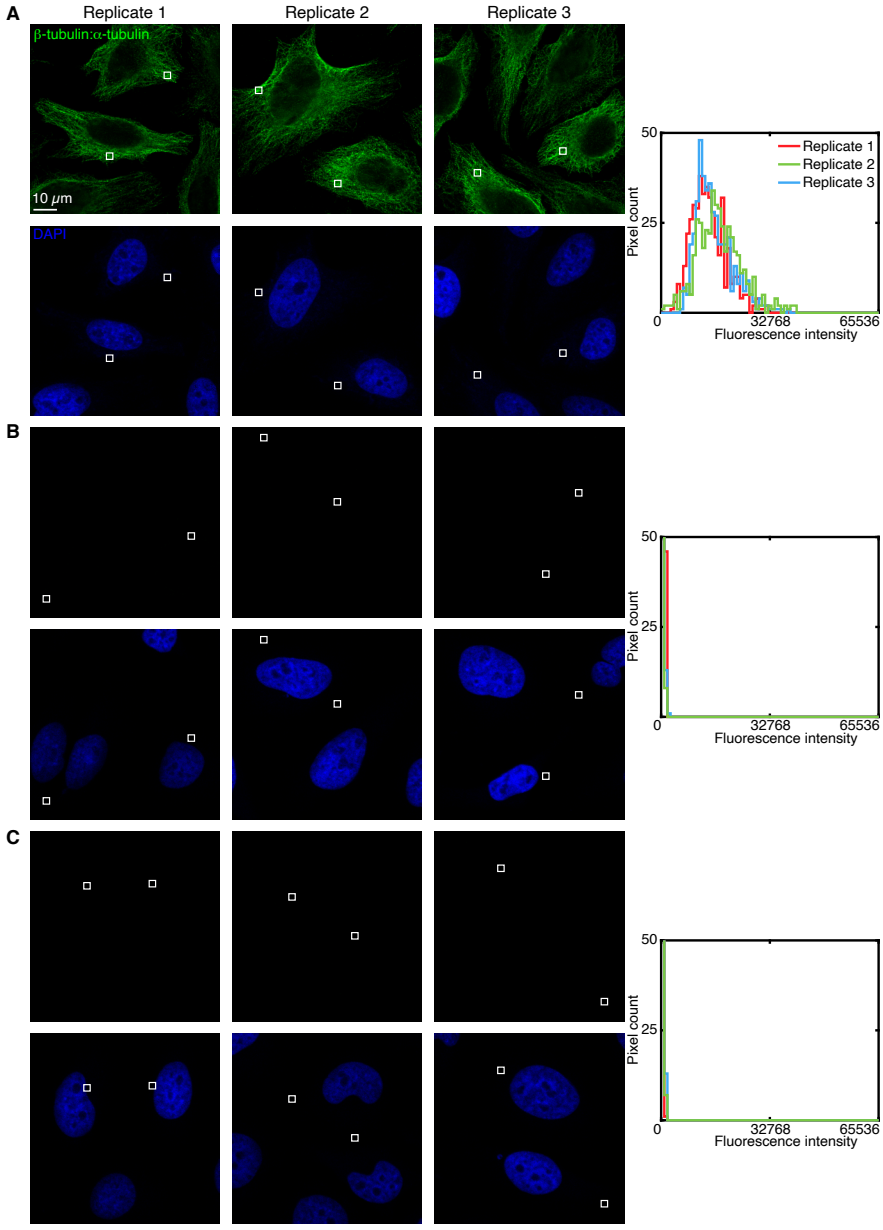

Figure B.18: Measurement of signal and background for protein:protein complex β-tubulin:α-tubulin using HCR in fixed adherent cells (cf. Figure 3.8). (A) Use experiment of Type 1a in Table B.8 to measure SIG+BACK in a region of high protein:protein complex expression (pixels within rectangles) in 3 replicates. (B) Use experiment of Type 2a in Table B.8 to measure SA_{P1}+NSD+NSA+AF in a region of maximum background (pixels within rectangles) in 3 replicates. (C) Use experiment of Type 2b in Table B.8 to measure SA_{P2}+NSD+NSA+AF in a region of maximum background (pixels within rectangles) in 3 replicates. (A,B,C) Left: individual channels of confocal images; DAPI channel contextualizes placement of the rectangles; single optical section. Ch2: protein:protein complex β-tubulin:α-tubulin (Alexa546). Right: pixel intensity histograms for rectangular regions of Ch2 (one rectangle in each of 2 individual cells in each of 3 replicate wells on a multi-well coverslip).

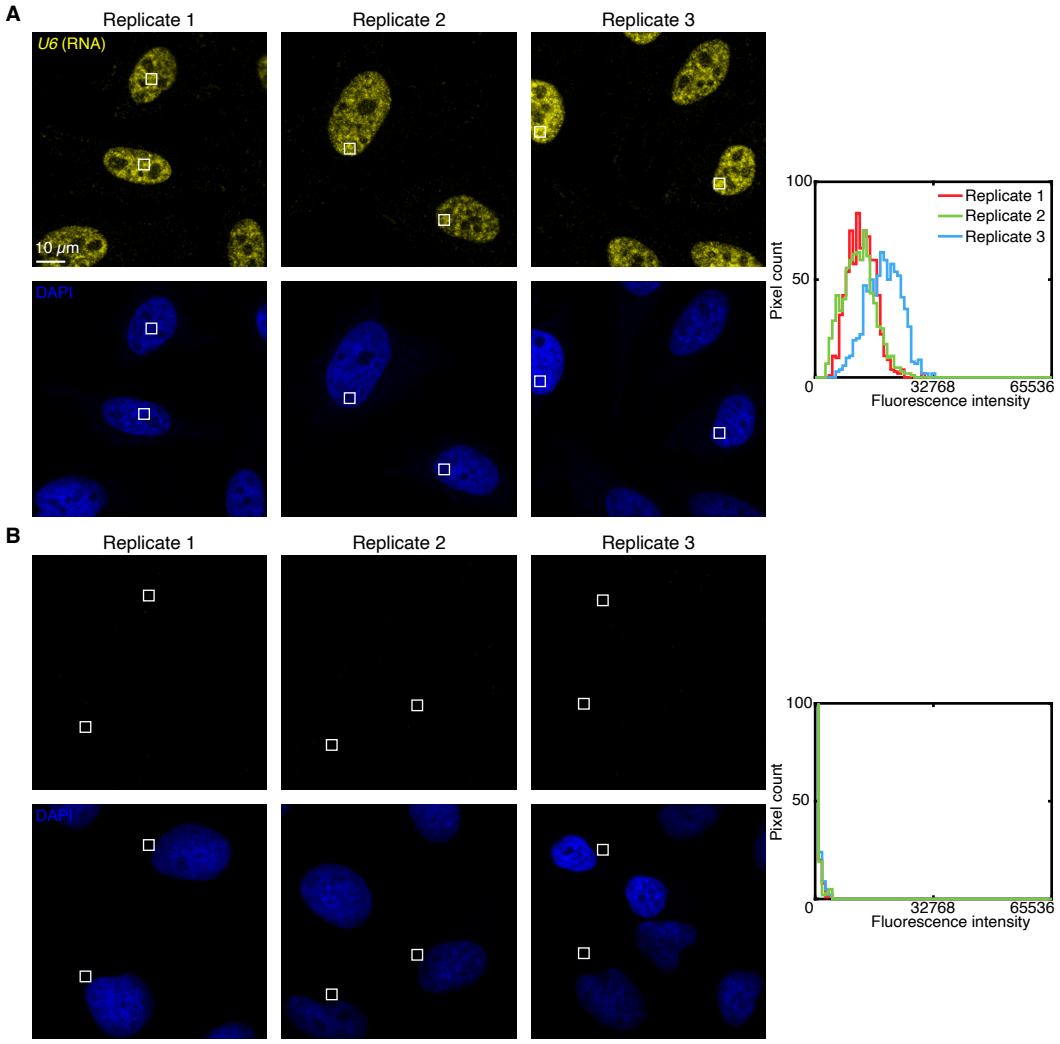

Figure B.19: Measurement of signal and background for target RNA *U6* using HCR RNA-FISH in fixed adherent cells (cf. Figure 3.8). (A) Use experiment of Type 1 in Table B.10 to measure SIG+BACK in a region of high target RNA expression (pixels within rectangles) in 3 replicates. (B) Use experiment of Type 2 in Table B.10 to measure BACK≈ NSA+AF in a region of maximum background (pixels within rectangles) in 3 replicates. (A,B) Left: individual channels of confocal images collected with the microscope settings optimized to avoid saturating SIG+BACK pixels; DAPI channel contextualizes placement of the rectangles; single optical section. Ch3: target RNA *U6* (Alexa647). Ch4: DAPI. Right: pixel intensity histograms for rectangular regions of Ch3 (one rectangle in each of 2 individual cells in each of 3 replicate wells on a multi-well coverslip).

Target or complex	SIG+BACK	SA_{P1}+NSD+NSA+AF	SA_{P2}+NSD+NSA+AF	BACK	SIG	SIG/BACK
HSP60	15 000 ± 2000	—	—	21 ± 4	15 000 ± 2000	800 ± 200
β-tubulin:α-tubulin	15 000 ± 1000	90 ± 50	54 ± 7	90 ± 50	15 000 ± 1000	200 ± 100
U6	14 000 ± 3000	—	—	90 ± 20	14 000 ± 3000	160 ± 40

Table B.19: Estimated signal-to-background for simultaneous protein, protein:protein complex, and RNA imaging using HCR in fixed adherent cells (cf. Figure 3.8). The target protein signal estimate SIG is calculated via an experiment of Type 2 in Table B.9 to measure BACK in a region of maximum background. The protein:protein complex signal estimate SIG is calculated via experiments of Type 2a and Type 2b in Table B.8 to measure BACK in a region of maximum background; BACK is calculated as the maximum of SA_{P1}+NSD+NSA+AF and SA_{P2}+NSD+NSA+AF. The target RNA signal estimate SIG is calculated via an experiment of Type 2 in Table B.10 to measure BACK in a region of maximum background. Mean ± estimated standard error of the mean via uncertainty propagation for $N = 6$ rectangular regions (one rectangle in each of 2 individual cells in each of 3 replicate wells on a multi-well coverslip). Analysis based on rectangular regions depicted in Figures B.17–B.19 using methods of Section B.1.6.

Appendix C

SUPPLEMENTARY INFORMATION FOR CHAPTER 4

C.1 Materials and methods

C.1.1 Conjugation of CB-labeled anti-DIG reporter antibodies

An anti-digoxigenin (DIG) antibody (Jackson ImmunoResearch Laboratories, 200-002-156) was passively conjugated to Special Black 4 carbon black (CB; The Cary Company, 24W208) (*122*). A 30K Amicon Ultra-0.5 mL Centrifugal Filter (Millipore Sigma, UFC503096) was prepared by centrifuging 450 μL 5 mM borate buffer (Thermo Scientific, 28341, diluted 1:200 in nanopure water) at room temperature for 5 min at 13.8k rcf. To the prepared centrifugal filter, 200 μL anti-DIG antibody (1.3 mg/mL) was added and centrifuged at room temperature for 5 min at 13.8k rcf to buffer exchange the antibody. Then, 350 μL 5 mM borate buffer was added and centrifuged at room temperature for 5 min at 13.8k rcf. The 5 mM borate buffer wash was repeated four additional times. The column was then turned upside down in a new tube, and the buffer-exchanged antibody was recovered by centrifuging at room temperature for 5 min at 1k rcf. The concentration of the buffer-exchanged antibody was determined by absorbance at 280 nm on a NanoDrop spectrophotometer, and the concentration was normalized to 1 mg/mL by the addition of 5 mM borate buffer.

A 1% (w/v) carbon black solution was prepared fresh in nanopure water, and the entire volume (2 mL) was continuously sonicated (cycle 1.0) for 15 min at room temperature at 100% amplitude with an ultrasonic processor (Hielscher Ultrasound Technology, UP50H). To 200 μL of 1 mg/mL buffer-exchanged anti-DIG antibody, 570 μL 0.2% (w/v) carbon black (diluted 1:5 in 5 mM borate buffer) was added in a SuperSpin polypropylene tube (Thomas Scientific, 20A00L069). The solution was pipetted up and down before mixing end-over-end on a rotary wheel for 3 h at room temperature. A 1% bovine serum albumin (BSA; Sigma-Aldrich, A2153) in 5 mM borate buffer solution was prepared, and the pH was adjusted to 8.5 by adding 1 M sodium hydroxide (NaOH) (Sigma-Aldrich, S2770). After 3 h of end-over-end rotation, 700 μL 1% BSA in 5 mM borate buffer (pH 8.5) was added to the carbon black mixture, and the mixture was vortexed briefly before end-over-end mixing on a rotary wheel for 15 min at room temperature to quench any unmodified carbon black. The mixture was centrifuged at room temperature for 15 min at 13.8k rcf, and the supernatant was discarded. A total of four times: the carbon black antibody conjugate was resuspended in 1 mL 1% BSA in 5 mM borate buffer (pH 8.5) by pipetting up and down and vortexing, the mixture was centrifuged at room temperature for 15 min at 13.8k rcf, and the supernatant was discarded. The CB-labeled anti-DIG antibodies were lastly resuspended in 1 mL 1% BSA in 5

mM borate buffer (pH 8.5) with 0.02% sodium azide (Sigma-Aldrich, S2002). The CB-labeled anti-DIG antibodies were stored at 4 °C.

C.1.2 Gel study of rapid HCR signal amplification

DNA HCR hairpins h1 and h2 at 3 μM (Molecular Technologies, B3-Alexa647) were separately snap-cooled (with h1 and h2 in separate tubes) by heating to 95 °C for 90 sec and cooling at room temperature in a dark drawer for at least 30 min. HPLC-purified HCR initiator i1 (Molecular Technologies, B3) was diluted in IDTE (pH 8.0) (Integrated DNA Technologies, 11-05-01-09) to 0.03 μM (0.01× initiator:hairpin ratio reaction). To a new tube was added: 1.2 μL 5× saline sodium citrate (SSC) (Life Technologies, 15557-044) with 1% Tween-20 (Teknova, T0025), 4.8 μL 5× SSC, 2 μL snap-cooled hairpin h1, and 2 μL snap-cooled hairpin h2. To trigger hairpin polymerization, 2 μL of diluted i1 was added and allowed to react for 10 min. For the leakage lane, initiator i1 was omitted, and an additional 2 μL IDTE (pH 8.0) was added and allowed to incubate for 10 min. To analyze HCR polymer formation, 2.4 μL 6× DNA Gel Loading Dye (Thermo Scientific, R0611) was added, and 12 μL of the reaction mixture was loaded into a 4.8 mm-wide well of a 1% (w/v) agarose (Invitrogen, 16500500) gel cast and run in 1× lithium borate (LB) buffer (Faster Better Media, LB20-10). A dsDNA ladder pre-stained with SYBR Gold was also loaded into the gel. To stain the ladder, a loading dye solution with SYBR Gold (Invitrogen, S11494) was first created by adding 1 μL 10,000× SYBR Gold solution to 400 μL 6× DNA Gel Loading Dye (Thermo Scientific, R0611). Then, to 11.04 μL nanopure water, 0.96 μL of GeneRuler 1 kb Plus DNA Ladder (Thermo Scientific, SM1331) and 2.40 μL loading dye solution with SYBR Gold were added, and 12 μL of this solution was loaded into the gel. The gel was run for 40 min at 150 V before imaging with an Amersham ImageQuant 800 Fluor imaging system (GE Life Sciences, 29399484) with the Cy2 (to image SYBR Gold) and Cy5 (to image Alexa647) filters.

C.1.3 Modification of anti-N capture and signal antibodies

The anti-N capture antibody (Sino Biological, 40143-MM08) was conjugated to NHS-dPEG$_{12}$-biotin (Quanta Biodesign Limited, 10198) (*114*). A 30k Amicon Ultra-0.5 mL Centrifugal Filter (Millipore Sigma, UFC503096) was prepared by centrifuging 500 μL 1× phosphate-buffered saline (PBS) (Ambion, AM9624) at room temperature for 5 min at 13.8k rcf. In a separate tube, 50 μL anti-N antibody (1 mg/mL) was combined with 400 μL 1× PBS, and the entire solution was loaded

into the centrifugal filter and centrifuged at room temperature for 5 min at 13.8k rcf to buffer exchange the antibody. Two times, 350 μL 1× PBS was added and centrifuged at room temperature for 5 min at 13.8k rcf. The column was then turned upside down in a new tube, and the buffer-exchanged antibody was recovered by centrifuging at room temperature for 5 min at 1k rcf. The concentration of the buffer-exchanged antibody was determined by absorbance at 280 nm on a NanoDrop spectrophotometer. To 10 mg NHS-dPEG$_{12}$-biotin, 800 μL 1× PBS was added, and this solution was added to the buffer-exchanged antibody at a 50:1 molar ratio (NHS-dPEG$_{12}$-biotin:buffer-exchanged antibody). After incubating the antibody biotinylation reaction at room temperature for 1 h, 500 μL 1× PBS was centrifuged at room temperature for 5 min at 13.8k rcf in a new centrifugal filter. To the biotinylated antibody solution, 400 μL 1× PBS was added, and the entire volume was loaded into the centrifugal filter and centrifuged at room temperature for 5 min at 13.8k rcf. A total of four times: 350 μL 1× PBS was added and centrifuged at room temperature for 5 min at 13.8k rcf. The column was turned upside down in a new tube, and the biotinylated antibody was recovered by centrifuging at room temperature for 5 min at 1k rcf. The concentration of the biotinylated antibody was determined by absorbance at 280 nm on a NanoDrop spectrophotometer, and the biotinylated antibody was diluted to 1 mg/mL with 1× PBS, aliquoted, and stored at -20 °C.

The anti-N signal antibody (Sino Biological, 40143-MM05) was conjugated to HCR initiator i1 (Molecular Technologies, B3) with an Antibody-Oligonucleotide All-in-One Conjugation Kit (Vector Laboratories, A-9202-001) according to the manufacturer's instructions. The concentration of the initiator-labeled antibody was determined with a Pierce BCA Protein Assay Kit (Thermo Scientific, 23225).

C.1.4 Lateral flow device assembly for viral protein detection

A 25 mm backed nitrocellulose membrane (Cytiva, FF80HP PLUS grade, 10547042) was adhered onto ultra optically clear double-sided tape (McMaster-Carr, 90727A110). A 30 mm wicking pad (Cytiva, CF7 grade, 8117-6621) was also adhered onto the double-sided tape with a 5 mm overlap on top of the nitrocellulose membrane. The wicking pad and nitrocellulose were then cut to size with a laser cutter (Full Spectrum Laser, Muse Core Desktop CO_2 Laser Cutter; see Figure C.1 for dimensions).

The sample pad (Ahlstrom-Munksjö, Chopped Glass w/Binder, Grade 8951) and conjugate pads (Ahlstrom-Munksjö, Chopped Glass w/Binder, Grade 8964) were

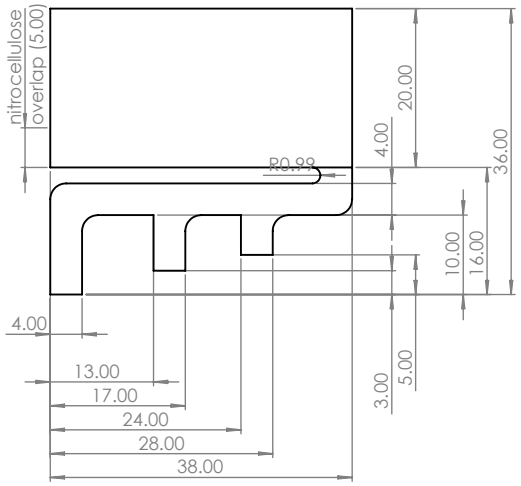

Figure C.1: Nitrocellulose membrane and wicking pad dimensions for viral protein detection. The nitrocellulose membrane and wicking pad were overlapped 5 mm on ultra optically clear double-sided tape and cut to size with a laser cutter. All dimensions are shown in millimeters (R: radius). All curved lines have a radius of 2.00 mm unless otherwise indicated.

cut to size with a laser cutter (see Figure C.2 for dimensions), submerged in blocking solution for 15 min with end-over-end rotation on a rotary wheel, and dried flat for 1 h in a fan-equipped oven (SciGene Model 2000 Micro Hybridization Incubator, 1040-50-1) set to 37 °C. The sample pad blocking solution consisted of 0.2% Blocker bovine serum albumin (BSA) (Thermo Fisher Scientific, 37525) and 0.2% Tween-20 (Teknova, T0025). The Channel 1 conjugate pad blocking solution consisted of 1% Blocker BSA, 1% sucrose (Sigma-Aldrich, S7903), 1% trehalose (Sigma-Aldrich, T9531), 0.02% Tween-20, and 0.2× PBS. The Channel 2 conjugate pad blocking solution consisted of 0.5% BSA (Sigma-Aldrich, A2153), 0.2% sucrose, 0.2% trehalose, 0.1% Tween-20, 1× SSC, and 0.1% dextran sulfate sodium salt (Sigma-Aldrich, D6001). The Channel 3 conjugate pad blocking solution consisted of 0.5% BSA, 0.2% sucrose, 0.5% Tween-20, and 0.2× PBS.

For each Channel 1 conjugate pad: to 75 μL Channel 1 conjugate pad blocking solution, biotinylated anti-N capture antibody was added to 2 μg/mL, and initiator-labeled anti-N signal antibody was added to 0.125 μg/mL. This solution was mixed by pipetting up and down, and 75 μL of this solution was pipetted onto the blocked Channel 1 conjugate pad. For each Channel 2 conjugate pad: 4 μL each of DIG-labeled HCR hairpins h1 and h2 (Molecular Instruments, B3-DIG) were separately snap-cooled (with h1 and h2 in separate tubes) by heating to 95 °C for 90 sec

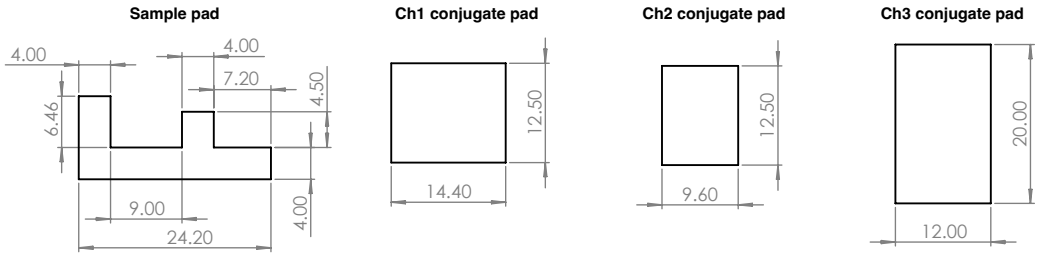

Figure C.2: Sample pad and conjugate pad dimensions for viral protein detection. Pads were cut to size with a laser cutter. All dimensions are shown in millimeters.

followed by cooling at room temperature for 30 min. To 50 μL Channel 2 conjugate pad blocking solution, 4 μL of each snap-cooled DIG-labeled HCR hairpin (h1 and h2) was added. For h1-only assays run without HCR hairpin h2, 4 μL HCR hairpin buffer was instead added (Molecular Technologies). This solution was mixed by pipetting up and down, and 50 μL of this solution was pipetted onto the blocked Channel 2 conjugate pad. For each Channel 3 conjugate pad: 4 μL CB-labeled anti-DIG reporter antibody was added to a microcentrifuge tube on ice and continuously sonicated (cycle 1.0) for 60 sec at 40% amplitude with an ultrasonic processor (Hielscher Ultrasound Technology, UP50H). To 115 μL Channel 3 conjugate pad blocking solution, 4 μL freshly sonicated CB-labeled anti-DIG reporter antibody was added. This solution was mixed by pipetting up and down, and 115 μL of this solution was pipetted onto the blocked Channel 3 conjugate pad. All conjugate pads were then dried flat for 1 h in a fan-equipped oven (SciGene Model 2000 Micro Hybridization Incubator, 1040-50-1) set to 25 °C.

A folding card device was created from 1.75 mm white polylactic acid (PLA) filament (HATCHBOX) with a 3D printer (Creality, Ender-5 Plus 3D Printer) with a 200 °C nozzle temperature and 60 °C bed temperature (see Figures C.3–C.5 for dimensions of the left page, right page, and pressure bar). Magnets (McMaster-Carr, 5862K102) were affixed into the device with hot glue to aid in holding the left and right pages together once the card is closed. Double-sided tape (McMaster-Carr, 7602A58) was cut with a laser cutter to the dimensions of the sample pad pedestal and applied to the sample pad pedestal. Double-sided tape was cut to shape with a laser cutter and applied to the conjugate pad pedestals, in each case leaving an exposed 2 mm region of the conjugate pad pedestal where the sample pad extends onto the conjugate pad pedestals. The adhesive backing was removed from the double-sided tape on the sample pad pedestal and conjugate pad pedestals, and the

blocked sample pad was adhered to the sample pad pedestal, with the ends of each sample pad channel extending onto the conjugate pad pedestals. The conjugate pads were adhered to the double-sided tape on the conjugate pad pedestals, with the leading edge of the conjugate pads overlapping on top of the three sample pad channels.

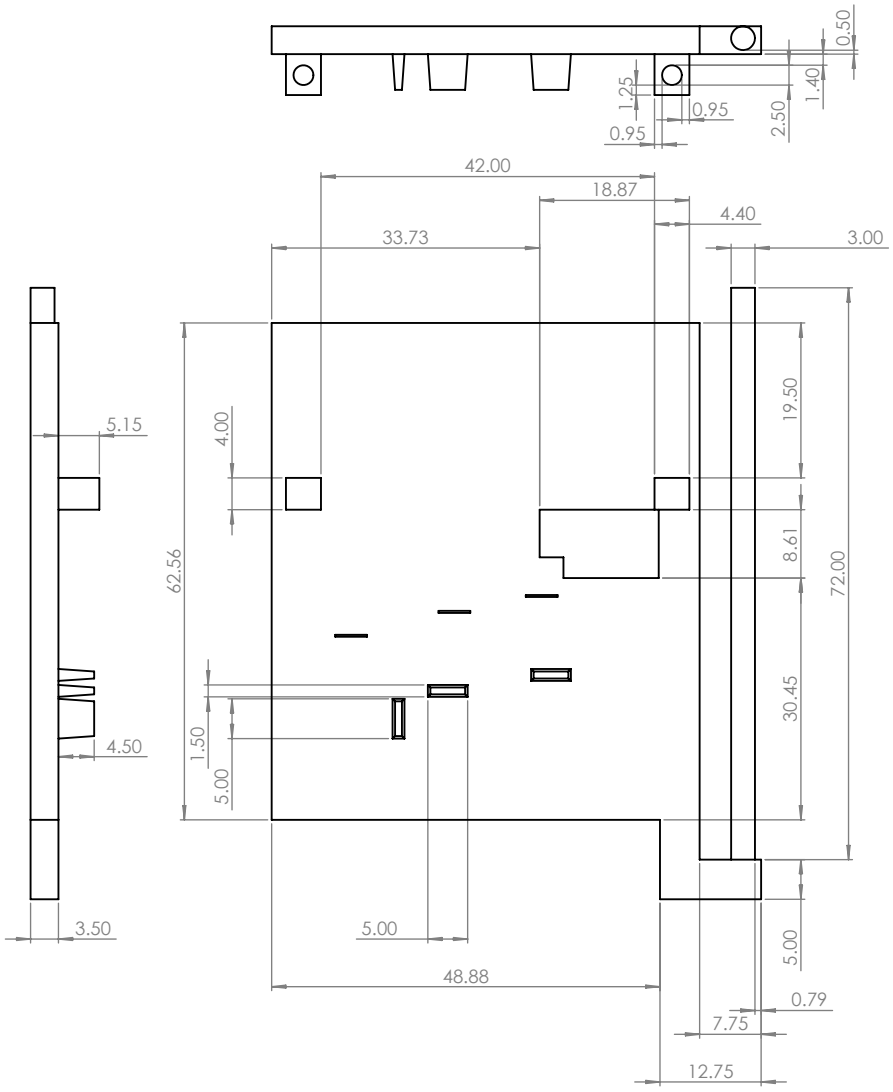

Figure C.3: Dimensions of the left page of the folding card device for viral protein detection. The left page of the folding card device was 3D-printed. All dimensions are shown in millimeters.

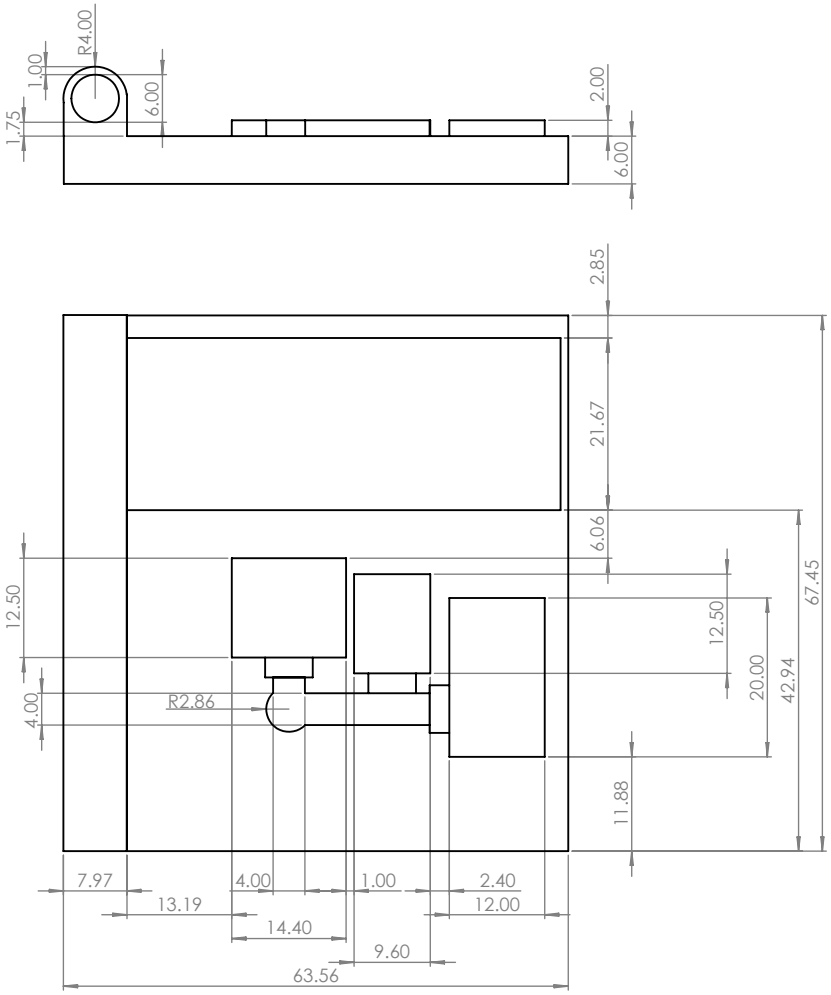

Figure C.4: Dimensions of the right page of the folding card device for viral protein detection. The right page of the folding card device was 3D-printed. All dimensions are shown in millimeters (R: radius).

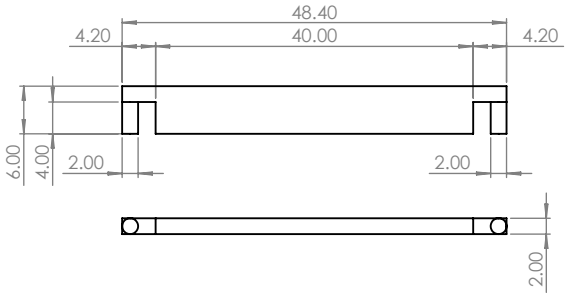

Figure C.5: Dimensions of the pressure bar of the folding card device for viral protein detection. The pressure bar was 3D-printed and attached to the left page of the folding card device to create pressure between the wicking pad and nitrocellulose membrane. All dimensions are shown in millimeters.

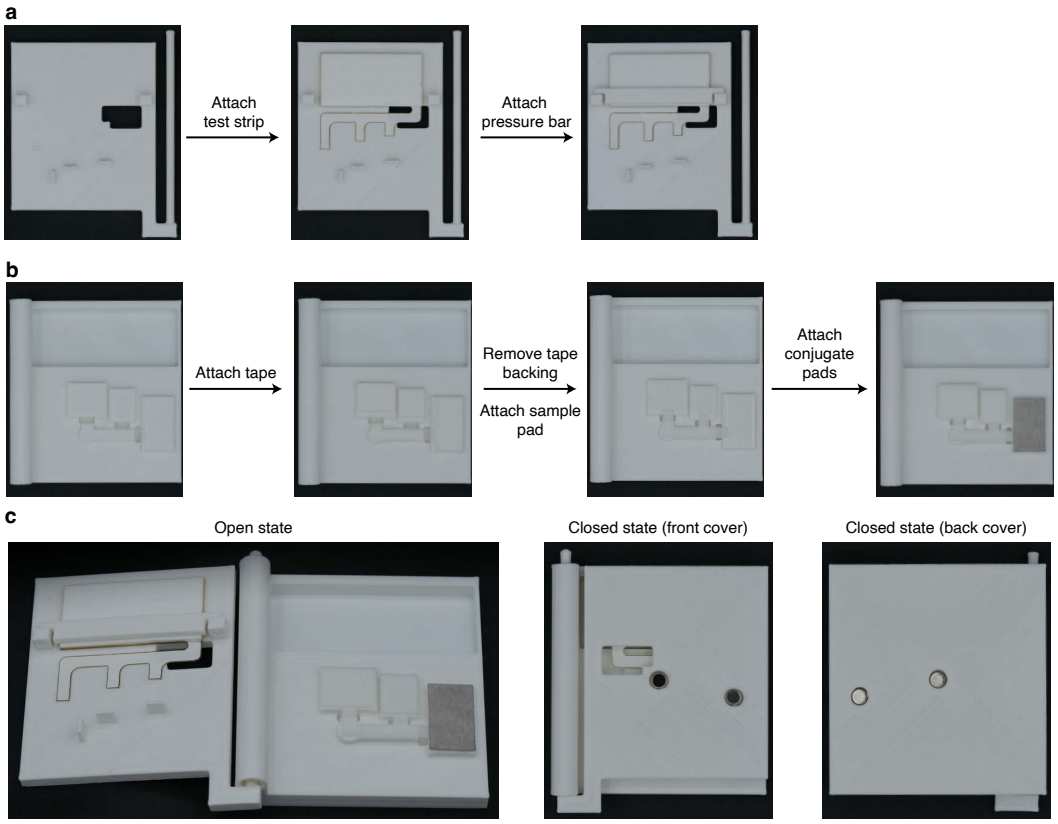

Figure C.6: Steps for assembling the folding card device for viral protein detection. (a) Assembling the left page. The adherent backing on the nitrocellulose membrane and wicking pad is removed, and the bottoms of the three nitrocellulose membrane channels are aligned with the thin markers on the device before adhering the nitrocellulose membrane and wicking pad in place. The pressure bar is added by pushing its two cylindrical prongs into the holes on either side of the wicking pad. (b) Assembling the right page. Double-sided tape is applied to the sample pad and conjugate pad pedestals. The adherent backing is removed from the double sided tape, and the sample pad is affixed to the sample pad pedestal. The conjugate pads are then applied to the conjugate pad pedestals, with their leading edges overlapping with the sample pad by 2 mm. (c) The left and right pages of the folding card device are assembled at the hinge. Images depict the device in the open state (left) and in the closed state viewing either the front cover (middle) or back cover (right).

Polystreptavidin R (Biotez, 10120030) was diluted to 0.94 mg/mL with 1× PBS. At the test region on the nitrocellulose membrane, 0.55 μL diluted polystreptavidin R was gently spotted with a P2 pipette. The nitrocellulose membrane was allowed to dry at room temperature for 30 min. Then, the adhesive backing was removed from the nitrocellulose and wicking pad, and the nitrocellulose and wicking pad were adhered to the left page of the folding card device. The pressure bar was then put in place on the left page of the device to apply pressure to the junction of the wicking pad and nitrocellulose membrane. The left and right pages of the folding card device were then assembled at the hinge (see Figure C.6).

C.1.5 Performing a viral protein detection test

Pooled human saliva collected before November 2019 (Lee Biosolutions, 991-05-P-PreC) was thawed at room temperature. Gamma-irradiated SARS-CoV-2 (BEI Resources, NR-52287), recombinant OC43 N protein (Sino Biological, 40643-V07E), or recombinant Influenza A H3N2 nucleoprotein (Sino Biological, 40499-V08B), was diluted in 1× PBS as needed, and 1 μL of the diluted solution was added to 299 μL of a solution of 2/3 saliva and 1/3 extraction buffer (5× SSC with 0.1% Tween-20). Gamma-irradiated SARS-CoV-2 was quantified by BEI Resources via droplet digital PCR. Then, 300 μL was slowly applied to the circular region of the sample pad pedestal with a pipette, and the top of the folding card device was closed to start the test. After 60 min, the device was placed in a 17-inch light tent (Angler, CT-DSLEDII) at maximum light intensity with a black background and photographed with a camera (Panasonic GH4) equipped with a 60 mm macro lens (Olympus, V312010BU000) with the following settings: 1/2000 sec shutter speed, 200 ISO, f/2.8 aperture, and neutral white balance.

C.1.6 Testing commercial SARS-CoV-2 lateral flow assays

Gamma-irradiated SARS-CoV-2 (BEI Resources, NR-52287) was diluted in 1× PBS as needed, and 1 μL of the diluted virus solution was added directly to the extraction buffer provided by the manufacturer to create a test sample at the target concentration; the volume of test sample specified by the manufacturer was then added to the commercial lateral flow device to start the test. After the minimum manufacture-recommended test time had elapsed, the device was photographed as described above.

C.1.7 Measurement of HCR polymer length using Alexa647-labeled HCR hairpins

To measure the average HCR polymer length, we do $N = 3$ replicate lateral flow assays for each of two types of experiment:

- Amplified experiment (h1 and h2): using both HCR hairpins (Alexa647-labeled h1 and Alexa647-labeled h2) in Channel 2 so that each HCR initiator labeling an anti-N antibody captured at the test region can trigger polymerization of a tethered Alexa647-decorated amplification polymer.
- Unamplified experiment (h1 only): use only HCR hairpin h1 (Alexa647-labeled h1) so that HCR polymerization cannot proceed and each HCR initiator labeling an anti-N antibody captured at the test region can bind only one Alexa647-labeled h1 hairpin.

To avoid interference with the fluorescent hairpin signal, the CB-labeled anti-DIG reporter antibody was omitted from the Channel 3 conjugate pad solution. Gamma-irradiated SARS-CoV-2 was spiked into a mixture of saliva and extraction buffer to a final concentration of 20,000 copies/μL for all tests. After 1 h, the test strip was removed from the folding card device, and fluorescence from the Alexa647-labeled hairpins was imaged with an FLA-5100 fluorescent scanner (Fujifilm Life Science) via a 635 nm laser and 665 nm long-pass filter. The mean HCR polymer length was then calculated as the ratio of amplified to unamplified intensities as described in Section C.1.9.

C.1.8 Measurement of HCR signal gain using DIG-labeled HCR hairpins and CB-labeled anti-DIG reporter antibodies

To calculate the HCR amplification gain, we do $N = 3$ replicate lateral flow assays for each of two types of experiment:

- Amplified experiment (h1 and h2): using both HCR hairpins (DIG-labeled h1 and DIG-labeled h2) in Channel 2 so that each HCR initiator labeling an anti-N antibody captured at the test region can trigger polymerization of a tethered DIG-decorated amplification polymer, which can then be bound by multiple CB-labeled anti-DIG reporter antibodies from Channel 3.
- Unamplified experiment (h1 only): use only HCR hairpin h1 (DIG-labeled h1) so that HCR polymerization cannot proceed and each HCR initiator labeling an anti-N antibody captured at the test region can bind only one DIG-labeled h1

hairpin, which can then be bound by one CB-labeled anti-DIG reporter antibody from Channel 3.

For viral protein detection tests, gamma-irradiated SARS-CoV-2 was spiked into a mixture of saliva and extraction buffer to a final concentration of 5,000 copies/μL and the test was run and photographed according to Section C.1.5. Images were converted to grayscale and the HCR amplification gain was then calculated as the ratio of amplified to unamplified intensities as described in Section C.1.9. Ideally, the amplification gain would match the mean polymer length, corresponding to a situation in which a reporter antibody is binding to each hairpin within an amplification polymer.

C.1.9 Quantitative image analysis

For each replicate of an amplified or unamplified experiment, the background-subtracted signal is calculated by taking the mean intensity in a signal box surrounding the test region and subtracting the mean intensity over one or two adjacent background boxes containing the same total number of pixels as the signal box. Let $\bar{x}_{\mathrm{h1+h2}}$ and $s_{\mathrm{h1+h2}}$ denote the sample mean and standard error of the mean for the background-subtracted amplified replicates, and let $\bar{x}_{\mathrm{h1}}$ and s_{h1} denote the sample mean and standard error of the mean for the background-subtracted unamplified replicates. The ratio of amplified to unamplified performance is then calculated as:

$$\bar{x}_{\mathrm{ratio}} = \bar{x}_{\mathrm{h1+h2}} / \bar{x}_{\mathrm{h1}} \tag{C.1}$$

with standard error estimated via uncertainty propagation as

$$s_{\mathrm{ratio}} \leq \frac{\bar{x}_{\mathrm{h1+h2}}}{\bar{x}_{\mathrm{h1}}} \sqrt{\left(\frac{s_{\mathrm{h1+h2}}}{\bar{x}_{\mathrm{h1+h2}}}\right)^2 + \left(\frac{s_{\mathrm{h1}}}{\bar{x}_{\mathrm{h1}}}\right)^2}. \tag{C.2}$$

This upper bound on estimated standard error holds under the assumption that the correlation between amplified and unamplified intensity is non-negative.

C.2 Replicates for lateral flow assays

C.2.1 Replicates for viral protein detection: amplified HCR lateral flow assay

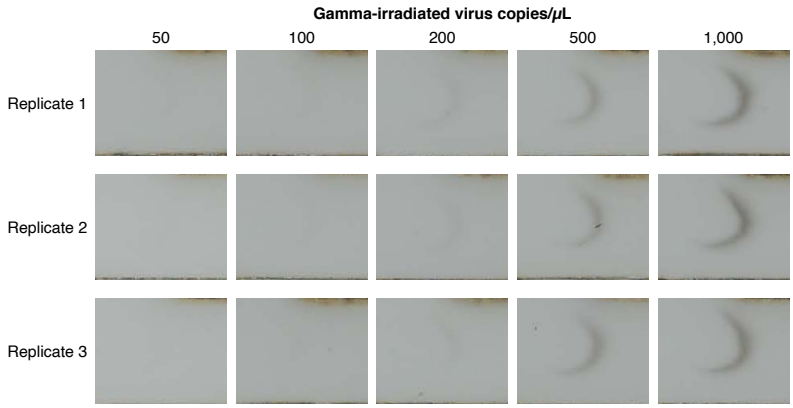

Figure C.7: Viral protein detection: sensitivity of amplified HCR lateral flow assay. Following the methods of Section C.1.5, gamma-irradiated SARS-CoV-2 was spiked into a mixture of saliva and extraction buffer at the target concentration and loaded onto the sample pad before closing the folding card device to start the test. The test region was photographed after 60 minutes. $N = 3$ replicate assays at each target concentration. The test region is visible in all three replicates down to a limit of detection of 200 copies/μL.

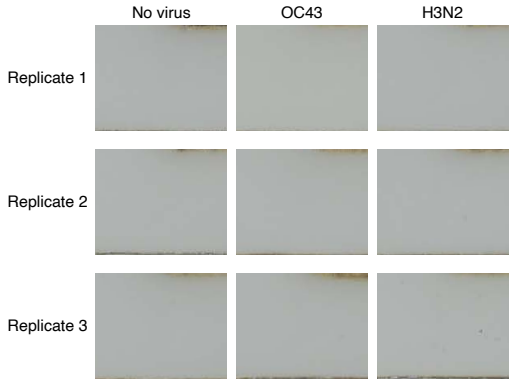

Figure C.8: Viral protein detection: background and cross-reactivity of amplified HCR lateral flow assay. Following the methods of Section C.1.5, no virus (to measure background) or off-target recombinant viral OC43 N protein (83.74 ng/mL) or Influenza A (H3N2) (50.43 ng/mL) nucleoprotein (to test cross-reactivity) were spiked into a mixture of saliva and extraction buffer and loaded onto the sample pad before closing the folding card device to start the test. For the cross-reactivity tests, the off-target viral proteins were spiked in at high concentrations equivalent to $\approx 10^6$ virions/μL (*110*, *115*). The test region was photographed after 60 min. $N = 3$ replicate assays at each target concentration. For each target type, no staining was visible at the test region for all three replicates, indicating that there is no visible background when SARS-CoV-2 is absent, and no visible cross-reactivity with off-target OC43 or H3N2 proteins.

C.2.2 Replicates for commercial SARS-CoV-2 rapid antigen tests: unamplified lateral flow assays

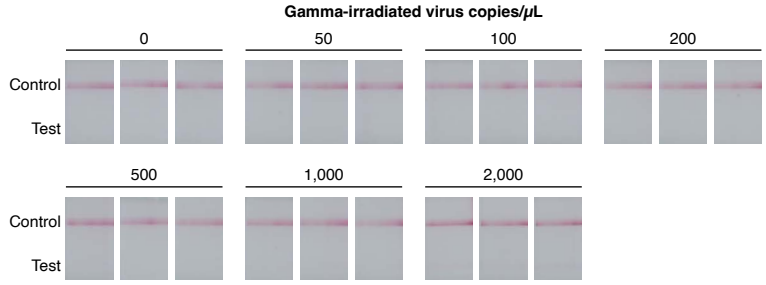

Figure C.9: BinaxNOW™ SARS-CoV-2 rapid antigen test: sensitivity of unamplified lateral flow assay. Following the methods of Section C.1.6, gamma-irradiated SARS-CoV-2 was spiked into the extraction buffer provided by the test manufacturer to create a test sample at the target concentration; the volume of test sample specified by the manufacturer was then loaded onto the device (130 μL was added to the swab well [equivalent to 6 drops with the provided dropper], a swab was added to the card device and rotated per the manufacturer's instructions, and the card device was closed). The test region was photographed after 15 min. $N = 3$ replicate assays at each target concentration. The test region is visible in all three replicates down to a limit of detection of 2000 copies/μL.

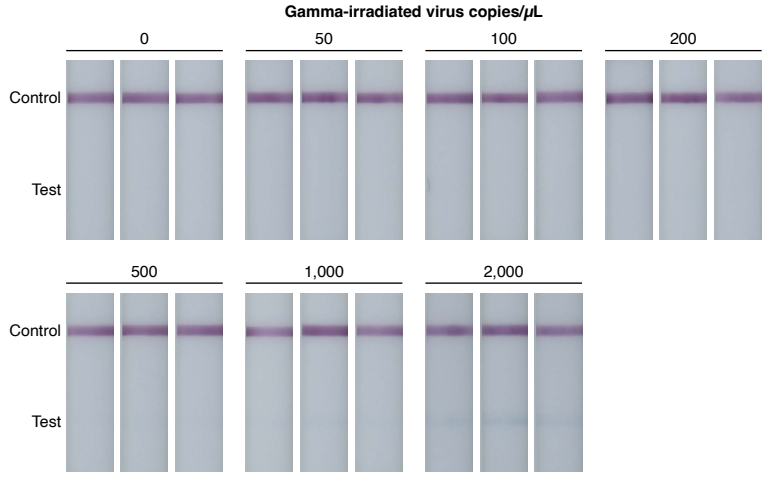

Figure C.10: CareStart™ SARS-CoV-2 rapid antigen test: sensitivity of unamplified lateral flow assay. Following the methods of Section C.1.6, gamma-irradiated SARS-CoV-2 was spiked into the extraction buffer provided by the test manufacturer to create a test sample at the target concentration; the volume of test sample specified by the manufacturer was then loaded onto the device (3 drops added to the sample region using the provided dropper). The test region was photographed after 10 min. $N = 3$ replicate assays at each target concentration. The test region is visible in all three replicates down to a limit of detection of 2000 copies/μL.

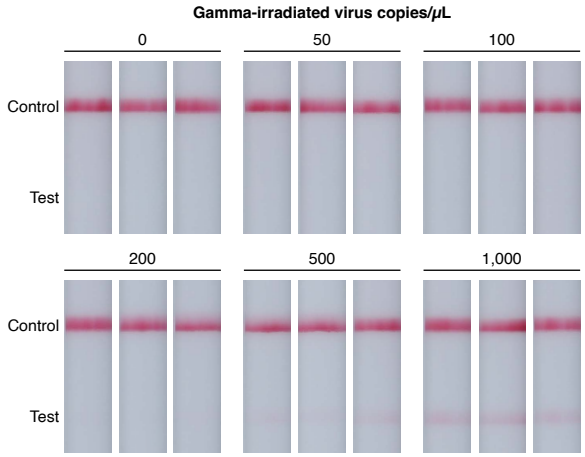

Figure C.11: Flowflex® SARS-CoV-2 rapid antigen test: sensitivity of unamplified lateral flow assay. Following the methods of Section C.1.6, gamma-irradiated SARS-CoV-2 was spiked into the extraction buffer provided by the test manufacturer to create a test sample at the target concentration; the volume of test sample specified by the manufacturer was then loaded onto the device (4 drops added to the sample region using the provided dropper). The test region was photographed after 15 min. $N = 3$ replicate assays at each target concentration. The test region is visible in all three replicates down to a limit of detection of 500 copies/μL.

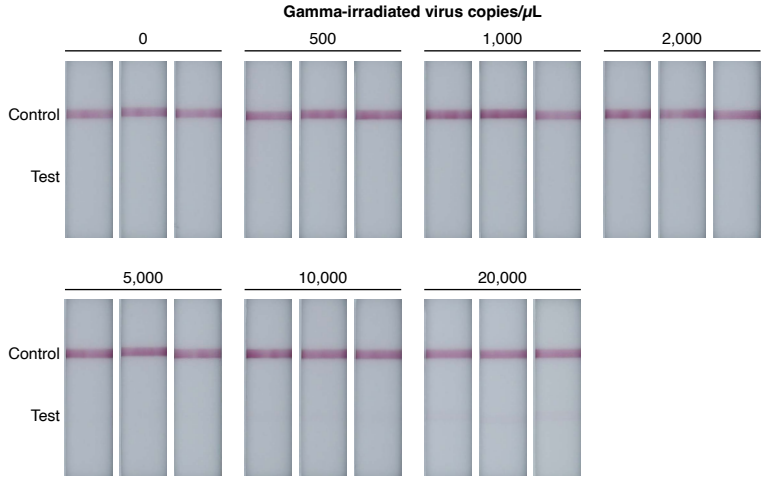

Figure C.12: GenBody SARS-CoV-2 rapid antigen test: sensitivity of unamplified lateral flow assay. Following the methods of Section C.1.6, gamma-irradiated SARS-CoV-2 was spiked into the extraction buffer provided by the test manufacturer to create a test sample at the target concentration; the volume of test sample specified by the manufacturer was then loaded onto the device (4 drops added to the sample region using the provided dropper). The test region was photographed after 15 min. $N = 3$ replicate assays at each target concentration. The test region is visible in all three replicates down to a limit of detection of 20,000 copies/μL.

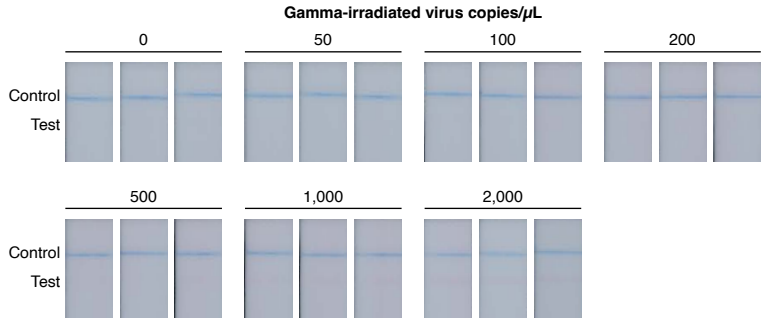

Figure C.13: QuickVue® SARS-CoV-2 rapid antigen test: sensitivity of unamplified lateral flow assay. Following the methods of Section C.1.6, gamma-irradiated SARS-CoV-2 was spiked into the extraction buffer provided by the test manufacturer to create a test sample at the target concentration; the end of the test strip was then placed into the test sample per the manufacturer's instructions. The test region was photographed after 10 min. $N = 3$ replicate assays at each target concentration. The test region is visible in all three replicates down to a limit of detection of 1000 copies/μL.

C.3 Additional studies

C.3.1 Gel study of HCR polymerization at short time scales

The gel study of Figure C.14 demonstrates that an HCR initiator can trigger self-assembly of HCR polymers in excess of ≈20,000 bp (> 500 HCR hairpins) in 10 minutes with HCR hairpins at 0.5 μM, suggesting the potential for achieving signal amplification of up to two orders of magnitude using HCR in the context of rapid lateral flow assays.

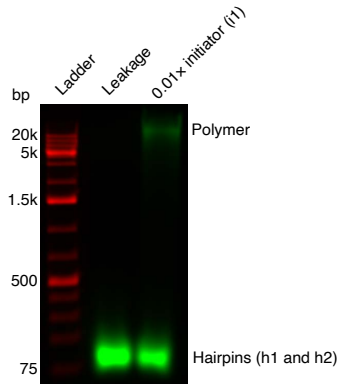

Figure C.14: Characterization of HCR polymerization at short time scales via agarose gel electrophoresis. Following the methods of Section C.1.2, HCR initiator (i1) triggers the self-assembly of HCR hairpins (h1 and h2) into amplification polymers. Each HCR hairpin (h1 and h2) at 0.5 μM with initiator i1 at 0.01×. Polymerization time: 10 min. Initiator i1 is omitted from the leakage lane to demonstrate that HCR hairpins are kinetically trapped and do not polymerize in the absence of initiator. Green channel: fluorescence from Alexa647-labeled HCR hairpins h1 and h2 (displayed with 1% of pixels saturated). Red channel: GeneRuler 1 kb Plus DNA Ladder pre-stained with SYBR Gold.

C.3.2 Measurement of HCR polymer length and amplification gain in the context of lateral flow assays

Following the methods of Section C.1.9, here we characterize HCR polymer length and amplification gain in the context of lateral flow assays as follows:

- HCR polymer length: Using Alexa647-labeled HCR hairpins, we compare fluorescent signal using both h1 and h2 (permitting growth of HCR amplification polymers) vs with h1 only (permitting only a single h1 binding event with no polymerization due to the absence of h2). The ratio of these two signal intensities provides a measurement of HCR polymer length in the context of the lateral flow assay format (in this case, for viral protein detection). The estimated HCR polymer length is ≈ 40 (Table C.1).
- HCR amplification gain: Using DIG-labeled HCR hairpins and CB-labeled anti-DIG reporter antibodies, we compare the CB signal using both h1 and h2 (permitting growth of HCR amplification polymers) vs with h1 only (permitting only a single h1 binding event with no polymerization due to the absence of h2). The ratio of these two signal intensities provides a measurement of HCR amplification gain in the context of the lateral flow assay format for viral protein detection (Figure C.16). The measured HCR amplification gain is $\approx$14 in the viral protein assay (Table C.2).

The fact that the amplification gain using CB-labeled anti-DIG reporter antibodies is lower than the HCR polymer length measured without using reporter antibodies suggests that there is room for improvement in optimizing the interaction between reporter antibodies and amplification polymers (e.g., to alleviate potential molecular crowding caused by bulky CB labels). Ideally, the amplification gain would match the mean polymer length, corresponding to a situation in which a reporter antibody is binding to each hairpin within an amplification polymer. With further optimization, it is plausible that the mean polymer length and amplification gain could be increased to two orders of magnitude within the constraints of the lateral flow assay format and a 1 hour overall assay duration.

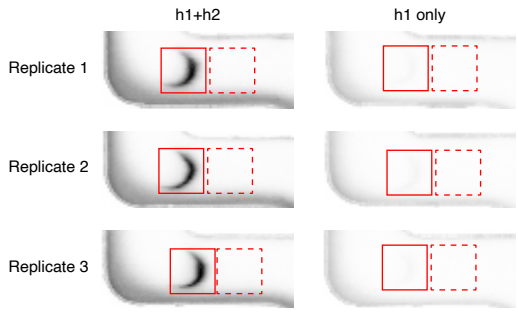

Figure C.15: Measurement of HCR polymer length in the context of a lateral flow assay for viral protein detection. Following the methods of Section C.1.7, two types of experiment are compared: amplified assays (using both h1 and h2, so that HCR polymerization can proceed) vs unamplified assays (using h1 only, permitting only a single h1 binding event with no polymerization due to the absence of h2). Gamma-irradiated virus was spiked into a mixture of saliva and extraction buffer at 20,000 copies/μL for all tests. $N = 3$ replicate assays for each condition. Quantitative image analysis following the methods of Section C.1.9 using the depicted signal boxes (solid boundary) and background boxes (dashed boundary).

	$\text{Signal}_{\text{h1+}h2}$	$\text{Signal}_{\text{h1}}$	Polymer length
Viral protein detection assay	1070 ± 16	26 ± 5	41 ± 8

Table C.1: Estimated HCR polymer length in the context of a lateral flow assay for viral protein detection. Quantitative image analysis of the amplified (h1 and h2) and unamplified (h1 only) assays of Figure C.15 following the methods of Section C.1.9. Mean ± estimated standard error of the mean via uncertainty propagation for $N = 3$ replicate assays for each experiment type.

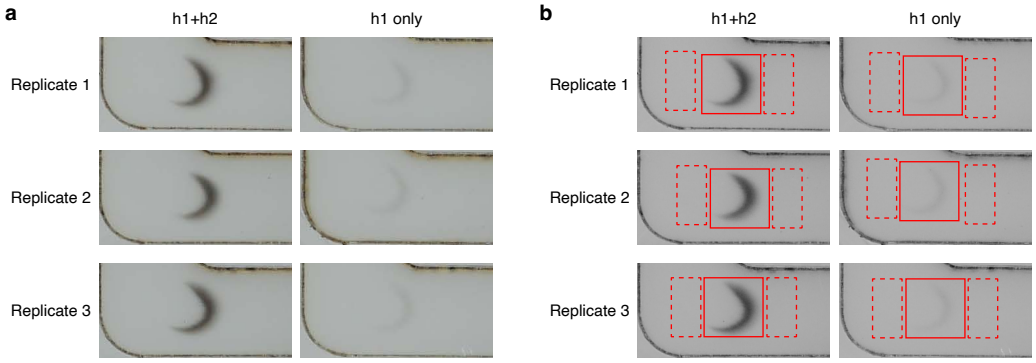

Figure C.16: Measurement of HCR amplification gain in the context of a lateral flow assay for viral protein detection. Following the methods of Section C.1.8, two types of experiment are compared: amplified assays (using both h1 and h2, so that HCR polymerization can proceed) vs unamplified assays (using h1 only, permitting only a single h1 binding event with no polymerization due to the absence of h2). Gamma-irradiated virus was spiked into a mixture of saliva and extraction buffer at 5000 copies/μL for all tests. $N = 3$ replicate assays for each condition. (a) Raw images. (b) Images after conversion to grayscale. Quantitative image analysis following the methods of Section C.1.9 using the depicted signal boxes (solid boundary) and background boxes (dashed boundary).

	$\text{Signal}_{\text{h1+h2}}$	$\text{Signal}_{\text{h1}}$	Amplification gain
Viral protein detection assay	19.6 ± 0.8	1.43 ± 0.05	13.7 ± 0.8

Table C.2: Estimated amplification gain in the context of lateral flow assays for viral protein detection. Quantitative image analysis of the amplified (h1 and h2) and unamplified (h1 only) assaysof Figure C.16 following the methods of Section C.1.9. Mean ± estimated standard error of the mean via uncertainty propagation for $N = 3$ replicate assays for each experiment type.

C.3.3 Visualization of automated reagent delivery using a 3-channel lateral flow assay with food coloring

Food coloring was used to validate that the 3-channel nitrocellulose membrane for the viral protein assay leads to successive delivery from Channels 1, 2, and 3 to the test region. Green, blue, and red food coloring was diluted 1:30 in 5× SSC and 0.1% Tween-20. Diluted food coloring was added to unblocked conjugate pads. Diluted green food coloring (90 μL) was added to the Channel 1 conjugate pad, diluted blue food coloring (60 μL) was added to the Channel 2 conjugate pad, and diluted red food coloring (120 μL) was added to the Channel 3 conjugate pad. The conjugate pads were dried in a 37 °C oven for 1 h before mounting to the folding card device. Lastly, 300 μL 5× SSC with 0.1% Tween-20 was added to the sample pad before closing the folding card device, initiating the flow of liquid from the three conjugate pads onto the nitrocellulose membrane (Supplementary Movie 2). Successive flow of the three colors demonstrates that liquid from each of the three channels reaches the test region in the correct order.